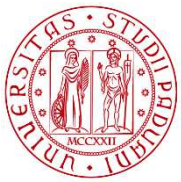

UNIVERSITÀ
DEGLI STUDI
DI PADOVA

Sede Amministrativa: Università degli Studi di Padova

Dipartimento di Tecnica e Gestione dei Sistemi Industriali

DOTTORATO DI RICERCA IN:
INGEGNERIA MECCATRONICA E DELL'INNOVAZIONE MECCANICA DEL PRODOTTO
CICLO XXIX

INFLUENCE OF MANUFACTURING-INDUCED DEFECTS ON THE MULTIAXIAL FATIGUE BEHAVIOUR OF COMPOSITE MATERIALS

Coordinatore : Ch.mo Prof. Roberto Caracciolo
Supervisore : Ch.mo Prof. Marino Quaresimin

Dottorando : Lucio Maragoni

List of Contents

Sommario

Grazie ad elevate proprietà meccaniche, bassa densità, e la possibilità di progettare il materiale stesso in funzione dello specifico componente, i materiali compositi sono stati ampiamente utilizzati negli ultimi decenni nel settore aerospaziale, automotive, e nella produzione di energia eolica, ambiti in cui elevate prestazioni e leggerezza ricoprono un ruolo di primaria importanza. Nonostante il loro già ampio impiego, l'ulteriore diffusione e il massimo sfruttamento di questi materiali sono tuttora ostacolati dal costo dei processi produttivi e dalla mancanza di criteri di progettazione affidabili e di validità generale, che costringe a condurre estese campagne sperimentali.

Un fattore rilevante che contribuisce all'esistenza di queste problematiche è la presenza in un componente in composito di difetti indotti dal processo produttivo, con particolare riguardo alla porosità. I vuoti infatti hanno un effetto notevolmente deleterio sulle proprietà meccaniche del materiale, e per tenerne basso il contenuto è necessario utilizzare parametri di processo che rendono la produzione più costosa. All'interno di questo quadro generale, il presente lavoro ha l'obiettivo di studiare l'influenza della porosità sul comportamento a fatica multiassiale di materiali compositi, attraverso attività sperimentali e di modellazione, allo scopo di fornire strumenti utili per una progettazione avanzata di componenti in composito.

Come primo step, sono stati condotti dei test per osservare i primi stadi del danneggiamento a fatica in lamine off-axis, che precedono la formazione di una cricca visibile (Capitolo 2). Nelle regioni di resina compresa tra fibre sono state rilevate micro-cricche, inclinate rispetto alle fibre, la cui orientazione è risultata in buon accordo con il *Local Nucleation Plane* predetto da Carraro e Quaresimin nella loro formulazione di un criterio basato sul meccanismo di danneggiamento per prevedere l'innesco di cricche a fatica, fornendo così solide osservazioni a sostegno di tale modello.

Lo stesso meccanismo di danneggiamento è stato poi osservato anche in presenza di vuoti nel laminato (Capitolo 3), mostrando quindi che lo stesso criterio *damage-based* può essere utilizzato anche in presenza di porosità. Tuttavia, si è notato che i vuoti causano una evoluzione più rapida del danneggiamento a livello micro, e di conseguenza un innesco di cricche visibili a numero di cicli inferiore rispetto al materiale *void-free*. Di conseguenza, è necessario quantificare l'effetto dei vuoti sullo stato di tensione locale nella matrice per estendere il modello *damage-based* proposto da Carraro e Quaresimin in modo da includere anche la presenza di porosità.

A seguito dei risultati preliminari relativi all'innesco di cricche a fatica in laminati porosi, è stata condotta una estesa campagna sperimentale per quantificare l'effetto dei vuoti sulle prestazioni a lungo termine di materiali compositi (Capitolo 4). Si è osservato un notevole effetto deleterio della porosità in termini di vita spesa per l'innesco delle prime cricche, velocità di propagazione delle cricche, evoluzione della densità di cricche e conseguente calo di rigidezza, evidenziando così la necessità di tenere debitamente conto della presenza di porosità nella progettazione di un componente in composito.

Passando dall'attività sperimentale alla modellazione, è stata innanzitutto realizzata ed implementata una procedura per la generazione di Elementi Volumetrici Rappresentativi (RVEs) (Capitolo 5). La procedura è stata validata confrontando i RVEs con microstrutture reali, e rappresenta uno strumento essenziale per analizzare le tensioni locali nella matrice, responsabili della formazione di una cricca.

È stata poi sviluppata una generalizzazione del criterio *damage-based* proposto da Carraro e Quaresimin che possa includere l'effetto della reale microstruttura del materiale, ed in particolare della presenza di vuoti (Capitolo 6). Lo stato tensionale in una zona di processo della matrice, calcolata mediante analisi agli Elementi Finiti su RVEs, è stata proposta come *driving force* per l'innesco di una cricca. Si è osservato che le curve S-N di laminati

contenenti e non contenenti vuoti entrano all'interno di un'unica banda se rappresentate in termini della *driving force* proposta, ad indicare che la vita a innesco delle prime cricche in presenza di porosità può essere predetto a partire dal comportamento del materiale *void-free*.

Infine è stata sviluppata una procedura per predire l'evoluzione della densità di cricche in laminati multidirezionali soggetti a carichi ciclici (Capitolo 7). La procedura si basa su simulazioni di tipo Monte Carlo, tiene conto della redistribuzione di tensioni dovuta alla presenza di cricche ed è in grado di includere anche la presenza di vuoti. Le previsioni degli andamenti della densità di cricche sono risultati in ottimo accordo con i dati sperimentali, sia per materiali senza vuoti che porosi.

In Appendice A si è osservata sperimentalmente l'influenza di vuoti di grandi dimensioni e forma irregolare sull'evoluzione della densità di cricche sotto carico statico, evidenziando la necessità di tener conto della loro reale geometria per prevedere l'innesco di cricche. Da test DCB statici, inoltre, è emerso che la presenza di vuoti di grandi dimensioni porta ad una maggiore tenacità a frattura interlaminare, a causa di un aumento di fenomeni di *fibre-bridging* e *ply-bridging*. Lo stesso effetto non è stato riscontrato in presenza di sollecitazioni cicliche.

In Appendice B viene proposto un nuovo metodo per prevedere l'innesco di cricche trasversali in lamine unidirezionali sottoposte a carico statico, sviluppato in collaborazione con la Texas A&M University. Il modello si basa su un concetto di percolazione, ed è stato utilizzato anche per analizzare l'effetto di un gradiente di temperatura, della frazione volumetrica di fibre e del tipo di fibra sul processo di formazione di una cricca. Seppur sviluppato per carichi statici, lo stesso principio potrebbe essere utilizzato per definire una *driving force* per la formazione di cricche a fatica in alternativa a quella proposta nel Capitolo 6.

Summary

Offering elevated mechanical properties, low density, and the possibility to design the material itself, composite materials have been widely used in the last decades in fields where high performances and lightweight are paramount, such as aerospace, automotive and wind power production. Nonetheless, the achievement of the full potential of such materials and their larger diffusion are prevented by the expensive manufacturing processes and the lack of design criteria of general applicability, that implies extensive experimental campaigns.

One important factor that contributes to both these issues is the presence of manufacturing-induced defects, and in particular porosity, in a composite part. Voids negatively affect the performances and require costly process conditions to keep their content to a minimum. Within this scenario, the present work aims at studying the influence of porosity on the multiaxial fatigue behaviour of composite materials, both under the experimental and modelling points of views, to provide helpful tools for the advanced design of composite structures.

As a first step in this direction, an investigation was carried out to experimentally observe the early stages of fatigue damage evolution in off-axis plies before the formation of a visible crack (Chapter 2). Micro-cracks were found in the inter-fibre regions, inclined with respect to the fibre direction, and their orientation was in good agreement with the Local Nucleation Plane predicted by Carraro and Quaresimin in their formulation of a damage-based criterion to predict life to crack initiation, thus providing a strong support to that model.

The same micro-damage scenario was observed also in porous specimens (Chapter 3), indicating that the same damage-based model could be used also in the presence of porosity. Voids, however, lead to a faster micro-damage evolution, resulting in earlier visible crack

formation. Therefore, their influence on the local stress state has to be accounted for to extend the same model to include the presence of porosity.

An extensive experimental campaign was then carried out to study the influence of porosity on the fatigue performances of composite laminates (Chapter 4). Voids were found to be highly detrimental in terms of life to crack initiation, crack growth rate, crack density evolution and stiffness drop, highlighting the need to properly account for the presence of porosity in the design of a composite part.

Moving from experimental to modelling activities, a procedure to build Representative Volume Elements (RVEs) was developed, and validated against real microstructures (Chapter 5). Such a tool is essential to analyse the local stresses in the matrix that are responsible for fatigue crack formation.

An extension of Carraro and Quaresimin's criterion was then developed to account for the actual material microstructure, proposing as the driving force to fatigue crack initiation the stress state in a process zone of the matrix, calculated by means Finite Element analyses on RVEs (Chapter 6). S-N curves for void-free and porous laminates were found to fall into the same scatter band when plotted in terms of the proposed driving forces, meaning that life to first cracks initiation in porous plies could be predicted from the behaviour of the void-free material.

Finally, a novel procedure was developed to predict crack density evolution in multidirectional laminates under cyclic loadings, based on Monte Carlo simulations and also capable of including the presence of voids in the laminate (Chapter 7). The procedure accounts for the stress redistributions cause by the presence of off-axis cracks, and the crack density predictions were found to be in good agreement with the experimental data both for void-free and porous laminates.

In Appendix A, the influence of large and irregularly shaped voids on static crack density evolution was observed experimentally, and the need to account for the actual void shape to predict crack initiation was shown. From static DCB tests it was possible to observe that macro voids lead to a higher interlaminar fracture toughness, as they increase fibre and ply bridging phenomena. The same effect was instead not detected under fatigue loading.

In Appendix B, a novel method is proposed to predict transverse crack initiation in unidirectional composite plies subjected to static load, developed in collaboration with Texas A&M University. The model is based on a percolation concept, and was used also to analyse the influence of temperature gradient, fibre volume fraction, and fibre material on the crack formation process. Even though this model was developed for static loads, the same concepts could be used to define a driving force to fatigue crack initiation in alternative to the one proposed in Chapter 6.

1

Introduction: motivations, problems and methodology

1.1 Composite materials for structural applications

Composite materials, often referred to as just *composites*, are a class of materials in which two or more distinct constituents are combined together to obtain properties that differ from the ones of the individual components.

Although composite materials offer desirable properties in many fields, they are experiencing a remarkable growth in structural design thanks to the possibility to combine high mechanical properties with low weight. Composite materials for structural applications usually consist of two constituents: a reinforcement, that carries the load, and a matrix, that gives the shape to the component, embeds the reinforcement and transfers the load to it. The reinforcement type greatly influences the behaviour of the overall material, and ranges from particles of various shape to short, long or continuous fibres, that can be also arranged in different ways. Among those, continuous fibres are the ones that offer the best mechanical properties. Since fibres introduce anisotropy in the mechanical response, plies with different fibre orientations can be combined to tailor the material for specific components, offering a further design advantage.

Many fibrous composites can be found in nature: for instance, wood is made of cellulose fibres embedded in a lignin matrix to better withstand the own weight of the branches and the bending of the trunk due to the wind. Although the first man-made fibre-reinforced composites date back to ancient Egyptians (papyrus paper, bricks made of straw and

mud…), the production of modern composites began in the 20th century, with the manufacturing of glass fibres first, followed by boron, carbon and aramid, developed in the late 1950s and early 1960s [1]. Extremely high stiffness-to weight and strength-to-weight ratios are achieved when such fibres are embedded in polymeric resins, making the resulting composite appealing for structural applications where lightweight is of crucial importance. In the following, if not specified otherwise, the terms *composites* and *composite materials* will refer to continuous fibre-reinforced polymers, on which the present work is focused.

Given the high potential of composite materials for structural applications, a large amount of interest arose around them since the 1950s, leading over the last decades to great technological developments and advances in the understanding of their mechanical behaviour. Examples of such achievements can be found in the Boeing 787 (Figure 1.1a), the Airbus A350 (Figure 1.1b), and the 88-metres long LM 88.4 P wind turbine blade (Figure 1.1c).

Despite what has been done so far, composites remain a relatively new class of materials, and their response to generic loads, made complex by the presence of multiple constituents, is yet to be fully clarified. Since the full potential of such materials could be achieved only when a sound knowledge of their behaviour is reached, efforts must be put into this research direction.

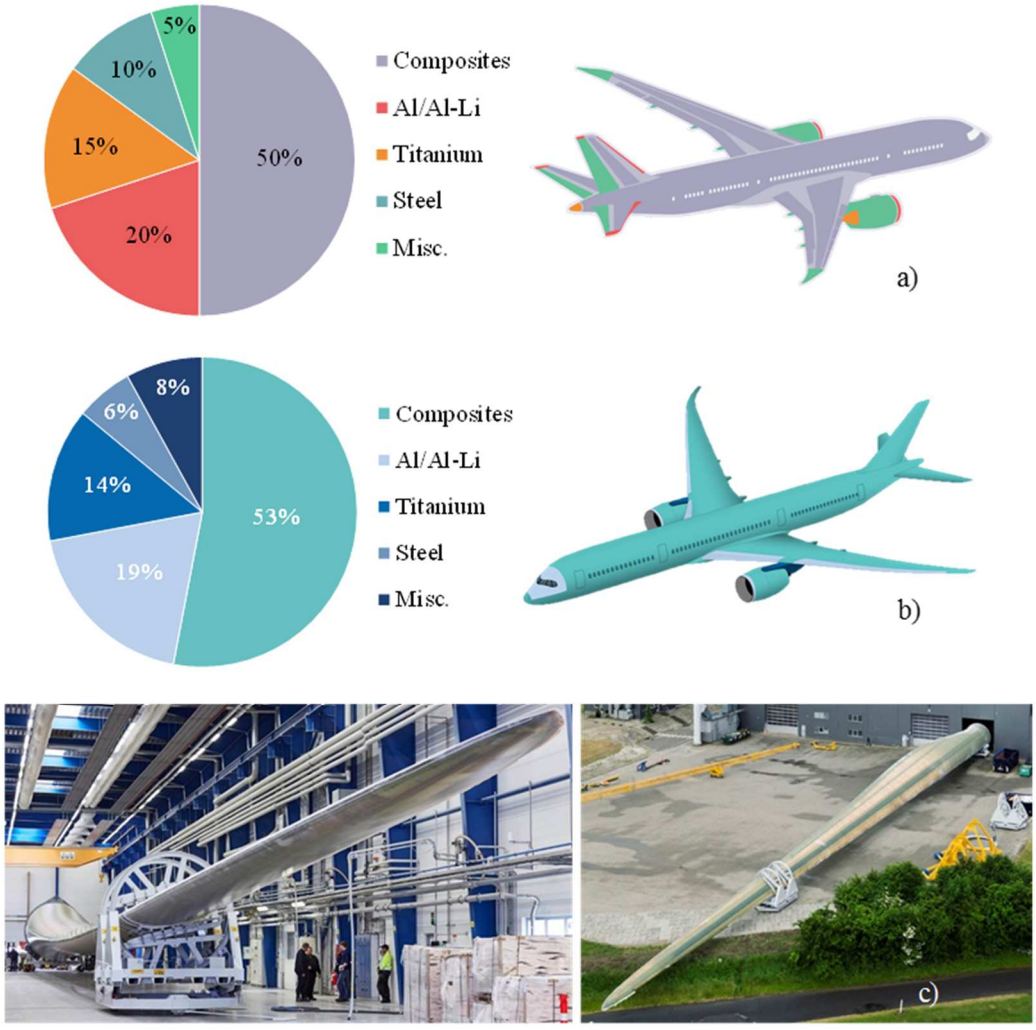

Figure 1.1 – Examples of structural use of composites: a) Boeing 787, b) Airbus A350, c) LM 88.4 P wind turbine blade.

1.2. A light world is a green world

Before devoting efforts into a research line, a question must be risen concerning the social impact that the research may potentially have. In our specific case, the question is the following: how does the society benefit from the deepening the knowledge on the mechanical behaviour of composites?

To evaluate the impact of the research on composite materials, two things must be kept in mind. First, despite their wide current use, composites are still a class of relatively new

materials and their behaviour under loadings, made complex by the presence of multiple constituents, is yet to be fully understood. Second, the main features of composite materials are their high mechanical properties combined with low weight, and the possibility to tailor the material for a specific component. Hence, the major benefits of a better understanding of the mechanical response of composites consists of a more optimised design of a structure, which means higher performances and less weight.

Given the advantages offered by composites, they are widely utilized in fields where lightweight and tailoring are of primary importance, in the specific: aerospace, automotive, wind energy production, and sports and leisure (Figure 1.2). Although Figure 1.2 refers to carbon-reinforced composites, it is safe to assume that continuous glass fibre-reinforced composites are used in the same fields, even if with different percentages.

Let us now exclude from the current analysis the sport and leisure sector, from which the society as a whole may have less to gain, and focus on the impact of lighter structures in the remaining applications.

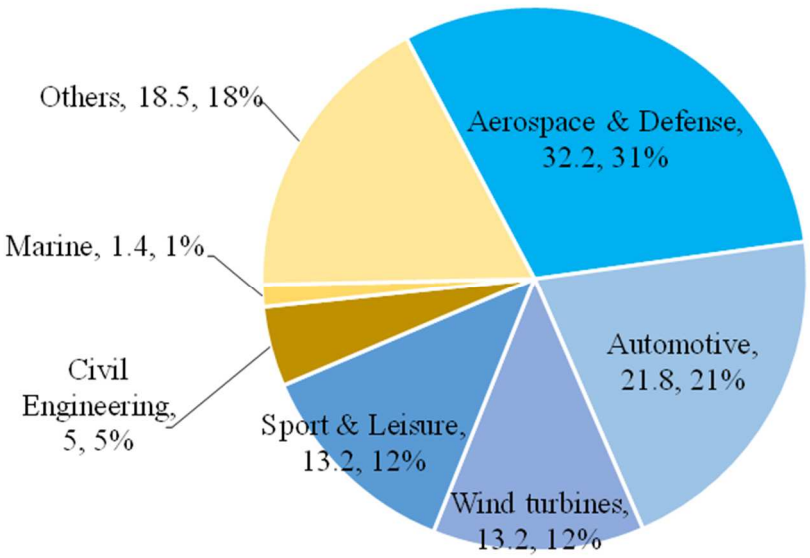

Figure 1.2 – Global carbon-reinforced composites demand in 1000 tons by field of application, adapted from [2].

Wind turbine blades are almost entirely made of composite materials. In the production of wind energy, the power that can be generated by a turbine is proportional to the area swept by the rotor. For this reason, the size of wind turbines has increased over the last decades, as shown in Figure 1.3. The trend and the future projections of Figure 1.3 were made possible by the development of lighter and lighter blades, which reduce the forces acting on the hub, shaft and themselves while rotating [4]. Of course, lighter structures could also increase the power generated by turbines of current size, also reducing transport and assembly costs.

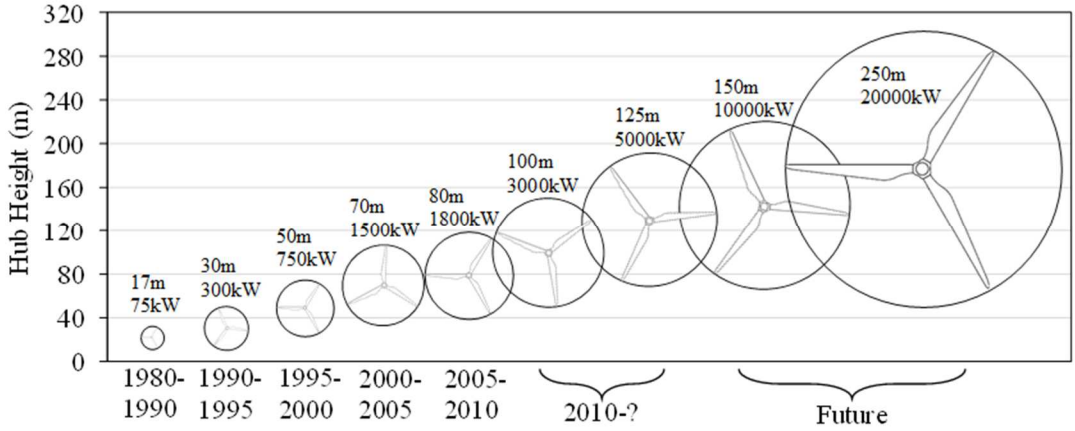

Figure 1.3 – Growth in size and power of typical commercial wind turbines, adapted from [3].

The aerospace field is the one in which the convenience of lighter structures may be the most obvious. A lighter plane means smaller fuel consumption, implying cost savings ($3000 of fuel per kilogram saved according to Ref. [5]), and less greenhouse gas emissions (1 kg of kerosene is estimated to produce 3.15 kg of CO_2 [6]). The contribution of planes to the global greenhouse effect as quantified by the *radiative forcing* is estimated to be around 3.5%, and growing as air traffic is increasing [6]. Therefore, although not striking,

a reduction in fuel consumption would be sensibly beneficial against climate change. Given the advantages offered by composite materials in the weight reduction, their use in commercial airplanes has been exponentially increasing in the last decades, as shown in Figure 1.4.

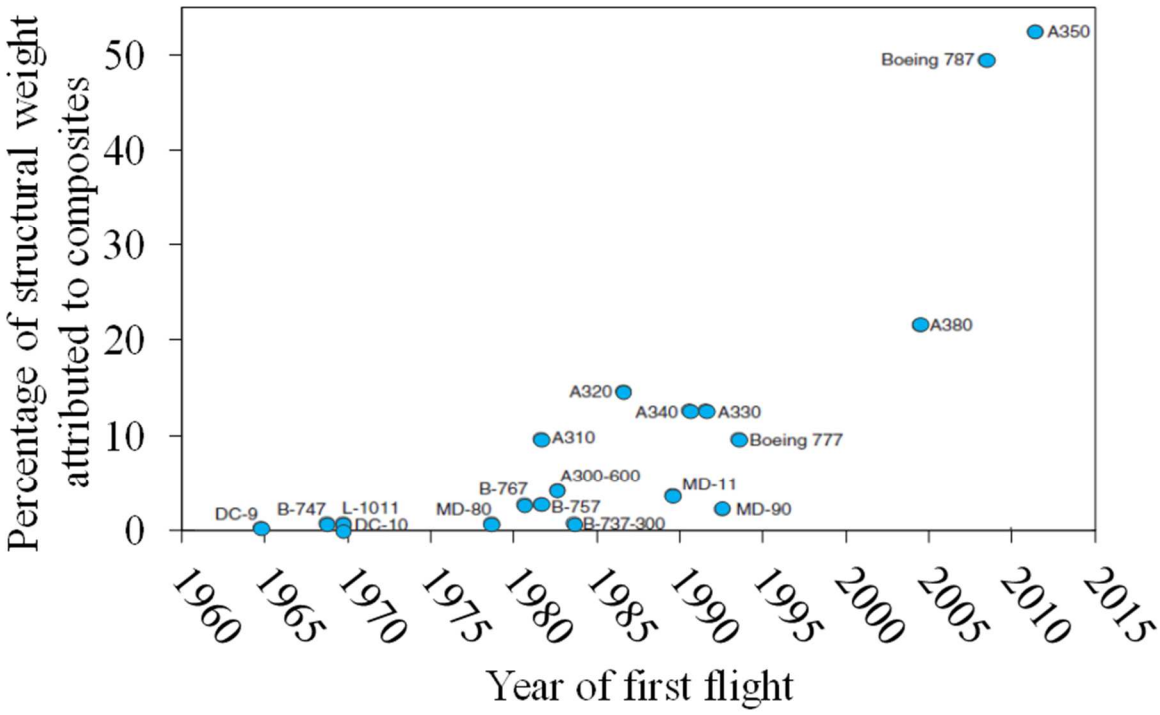

Figure 1.4 – Percentage of structural composites in commercial airplanes, adapted from [7].

Moving from the aerospace to the automotive field, the reason to design lighter structure stays the same: reduction of fuel consumption and therefore less greenhouse gas emission. Both in and in the United States the transport sector is the second largest source of greenhouse gases after the electricity sector, accounting for approximately a quarter of the total Europe (data from the European Commission and the US Environmental Protection Agency). Ground transportation contributes to such amount by 80% and 84%, respectively for the EU and the US. According to Ref. [8], there is a 0.08 g/km reduction per kilogram

saved in a vehicle. Even though eventually a shift towards electric powertrains will be needed to meet the progressive restrictions imposed by the EU on greenhouse gas emissions [8], the passage will be gradual and the use of lightweight material will be of great help in the transition, while combustion engines are still in use. Car making companies will also benefit from lighter cars under an economical point of view, given the high fines imposed by the EU if the emission limits are not respected. Moreover, once the transition to electric vehicles is complete, lightweight systems will still be desirable to extend the car autonomy and to improve driving dynamics due to the weight of the batteries [8].

From this analysis, it appears clear that lighter structures are extremely useful to increase the production of renewable energy and at the same time to reduce the emission of greenhouse gasses of the transport sector, which accounts for a large part of the world total. Of course, lighter structures are not the only mean to work in this direction. Indeed, in addition to the aforementioned electrical powertrains in the automotive case, the efficiency of wind turbines and planes can be improved by working, for example, on the engines and the aerodynamic. However, there is a high probability that improvements in such directions would be hard to transfer from one field to another, given their specificity. Instead, since structures are involved in so many different fields, improvements in structural design, and in particular towards lighter structures, are of benefit to all of those fields at once.

Moreover, if weight reduction can be achieved by a more advanced design with traditional materials, the intrinsic advantage of composite materials, consisting of very high specific properties and the possibility to design the material itself for a specific component, is what can really push the design of lightweight structures to the next level. And since many aspects of the mechanical behaviour of composites are far from clear, it is worth to carry out research in this direction to exploit their full potential.

1.3 Economic considerations

In today's world, beneficial effects for the society, such as reduction of greenhouse gas emissions and increase in green energy production, may not be enough to justify the efforts of research if they are not accompanied by economic advantages. Although some indications on the good economic impact of lighter structures on the various fields of application have been given in the previous Paragraph, it is worth to analyse the trend of the composites market. As shown in Figure 1.5 (that refers to the quantities reported in Figure 1.2), carbon composites are a multibillion-dollar market. As considered above, data for continuous glass-fibre reinforced polymers may be added to those of Figure 1.5 since they are used in the same fields. Not only the composite material market is large as of today, but, following the trend of the last years, the demand of composite components is predicted to grow annually by 11% in the next years (Figures 1.6 and 1.7) [2].

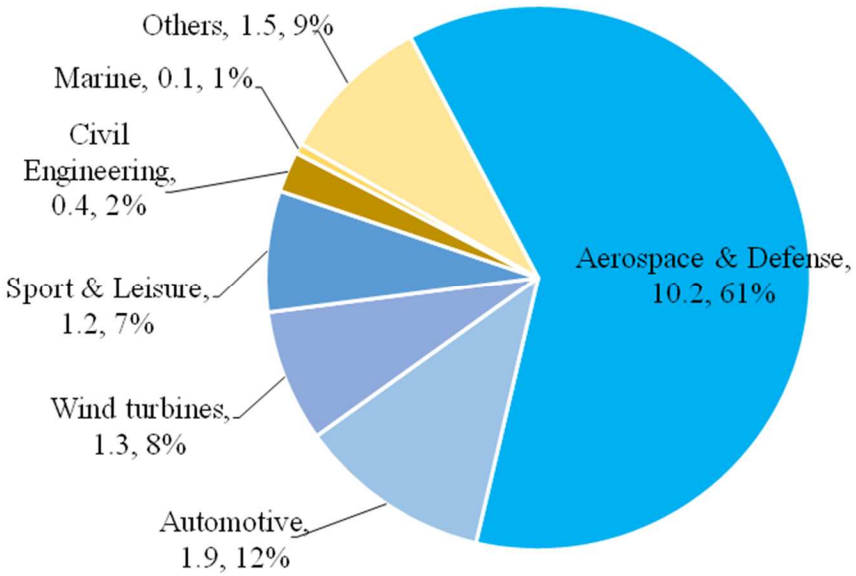

Figure 1.5 – Global carbon composite demand in US$ billion by application (2014), adapted from [2].

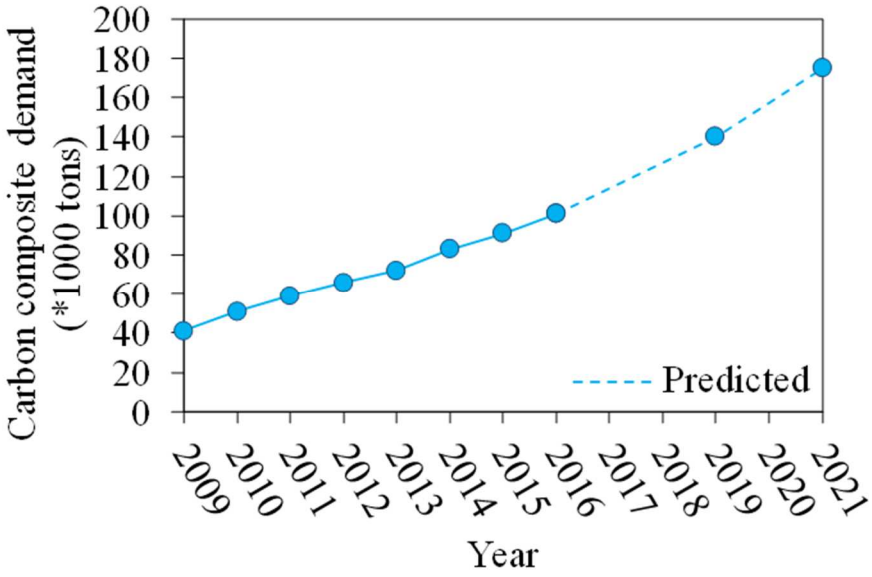

Figure 1.6 – Growth of global carbon components demand, adapted from [2].

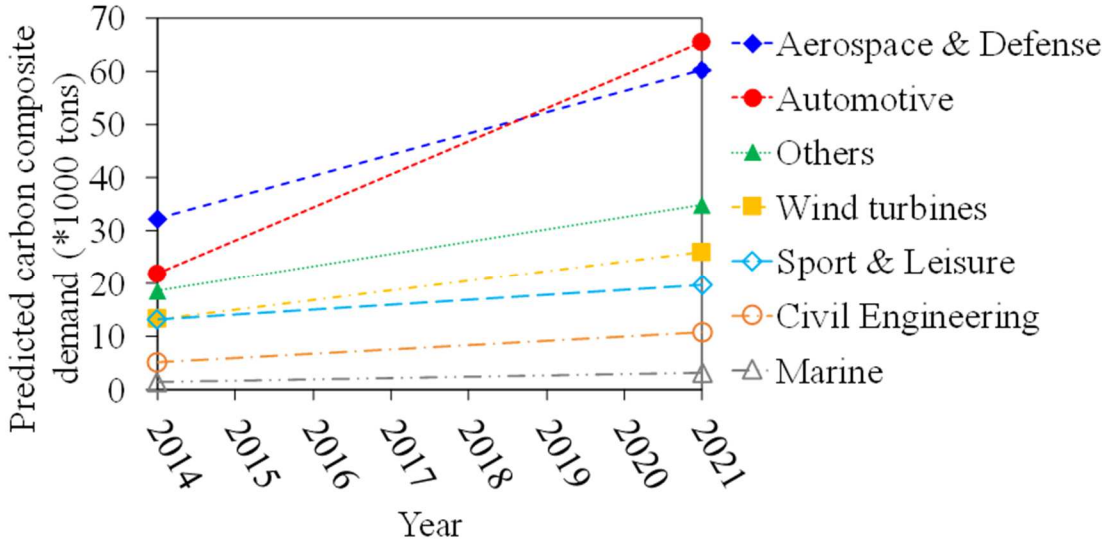

Figure 1.7 – Predicted growth of carbon components demand by application field, adapted from [2].

Given the increase in the demand of composite materials and the economic potential they bring, a proper design of composite components can be extremely appealing for companies that want to emerge in this market. To do so, more performing and less expensive composite

components have to be produced. The cost of a composite component may be lowered by reducing the cost of raw materials and by developing less labour-intensive manufacturing processes. To achieve at the same time costs reduction and better performances, we need to clearly understand the behaviour of such materials under loads and propose new design criteria accordingly. Only in this way composite components can be properly designed, increasing their performances, and the large cost of expensive and time-consuming experimental campaigns can be cut drastically.

In conclusion, deepening the knowledge on the mechanical behaviour of composite materials can be greatly beneficial for both the society and the economy, hence research lines that point in this direction are worth the efforts.

1.4. Fatigue behaviour of composite materials

In the fields in which composites are mostly employed (Figure 1.2), they are subjected to dynamic rather than static loadings, and they are required to work over a long period of time (wind turbines, for instance, are designed to last 20 years). In addition, the loading conditions are usually complex. Consequently, understanding the multiaxial fatigue behaviour of composites is crucial to achieve the best performance they can offer.

As reported by Reifsneider and co-authors [9], the damage scenario in composite laminates subjected to fatigue loading is progressive and complex (Figure 1.8). The first damage event that can be macroscopically observed is the initiation of multiple matrix cracks in the least-favorable oriented plies with respect to the loading directions (*off-axis* cracks). The multiple cracking phenomenon is due to the fact that after the first crack initiate, the cracked ply still carries load in regions sufficiently far from the crack, thanks to the load transfer due to the neighbouring plies. In most of the cases, cracks do not run along all the component as they initiate, but rather they have a finite initial length and propagate along

the fibre direction as the number of cycles increases. Cracks initiation and propagation continue until cracks are so close that the load transfer is not sufficient to initiate a new crack and to further propagate the already existing ones (condition of *crack saturation*). When saturation is approached, delaminations (i.e.: separations between plies) initiate from the cracks, and propagate along the inter-ply interface with the number of cycles. Finally, in the most-favorably oriented plies the fibres start to break, also helped by the stress concentrations caused by the matrix cracks and delaminations, until the amount of broken fibres brings to the final failure (separation) of the laminate. Even if such damage events have been reported as separated, they actually overlap in the time scale.

Off-axis cracks and delaminations are matrix-dominated phenomena, and they are usually referred to as *secondary damages*, while the term *primary damage* is often used for fibre breakage.

The presence of matrix-dominated secondary damages not only influence the occurrence of the final separation, but also causes a sensible reduction in the stiffness of the laminate (Figure 1.8). Therefore, understanding the mechanisms that govern them is of essential to design a composite component against fatigue, regardless of how *failure* is defined. Indeed, given the complex damage scenario, a component could be designed not to have damage during its whole life, to tolerate some damage provided that its stiffness does not drop below a certain level, or to avoid the final separation regardless of the amount of secondary damages.

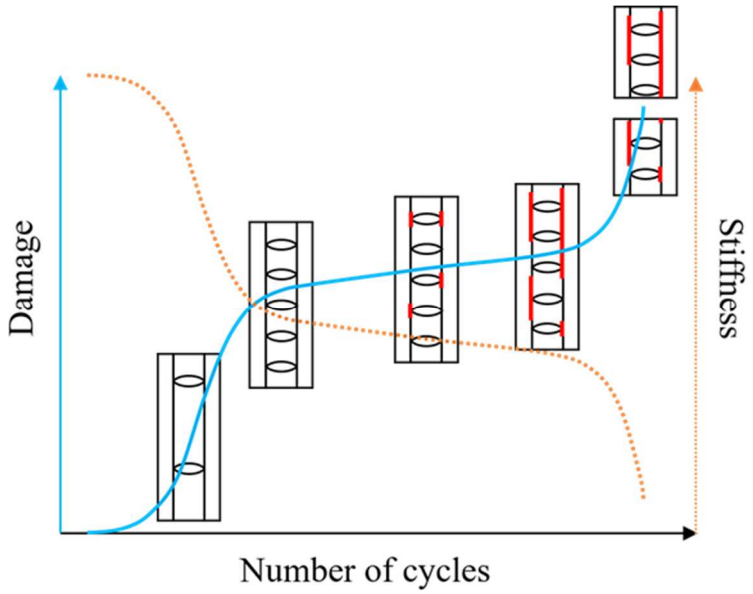

Figure 1.8 – Qualitative damage evolution and stiffness drop of a composite laminate subjected to fatigue loadings.

An extensive review on the multiaxial fatigue behaviour of composites was recently carried out by Quaresimin and co-authors [10]. They examined more than a thousand experimental data taken from the literature, denoting the main factors that influence the fatigue behaviour, namely the amount of shear to normal stress ratio, the load ratio, the phase angle between stress components and the presence of stress concentrators such as notches. Concerns were also risen about the equivalence between *external* and *internal* multiaxiality, where the former refers to the application of external loads in multiple directions, and the latter is due to the anisotropy of the material and takes place even under uniaxial external loads. In addition, they applied to the same experimental data several models proposed in the literature to predict laminate failures. Although easy to use, the analysed models lead in some cases to largely non-conservative predicitons, casting uncertainties on their general validity and applicability. To develop a robust model, it was finally suggested to better understand the damage mechanisms that drive fatigue damage and to include them into the model formulation.

Carraro and Quaresimin's work [11] followed the directions in which Quaresimin and co-authors' work pointed in. In particular, both experimental and modelling activities were carried out in his work, focusing on the matrix-dominated behaviour of composites under multiaxial fatigue loading, which, as stated earlier, is of fundamental importance to understand and predict composites damage evolution. Among the results of that work, the following are the most relevant:

1) The equivalence between *external* and *internal* multiaxiality was shown.
2) A change in damage mechanisms was observed in the final fracture surface when sufficiently high shear stress was applied compared to pure transverse tension.
3) Following the findings of point 2, a model was developed to predict crack initiation in an off-axis ply under fatigue loading, taking the Local Hydrostatic Stress (LHS) or the Local Maximum Principal Stress (LMPS) as driving forces to fatigue crack initiation, depending on the stresses acting on a ply (Figure 1.9).
4) An analytical model was developed to predict crack density evolution in symmetric multidirectional laminates, accounting for the stress redistribution between cracked plies.
5) A *shear lag* analysis was used to link the crack density to the stiffness of symmetric multidirectional laminates.

Although Quaresimin and Carraro's models for crack density predictions can be remarkably useful in the design of composites against fatigue, to account for local microstructural variations in the material, such as the one given by the presence of manufacturing-induced defects, they would require a new calibration curve for any possible defect content, provided that defects do not modify the damage mechanisms. Since manufacturing-induced defects are extremely common in composite materials, it would be of great interest to predict the behaviour of composites in their presence to reduce the

experimental efforts and the cost of designing composite components. To do so, further investigations are required, that are the focus of the present work.

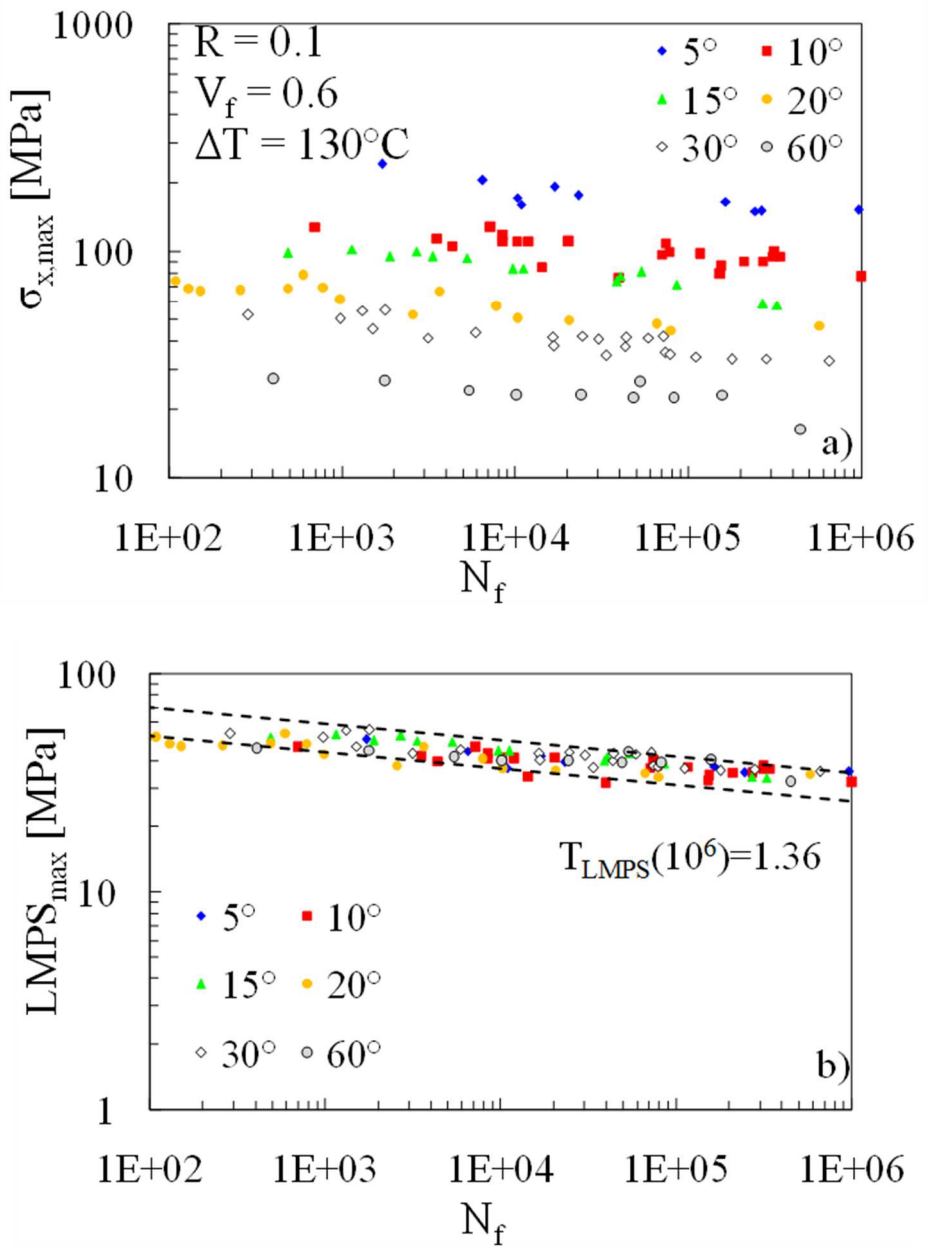

Figure 1.9 – Example of application of Carraro and Quaresimin's model to predict crack initiation under multiaxial fatigue loadings, adapted from [11].

1.5. Objective and contents

Due to the materials and the processes involved, composite components often contain manufacturing-induced defects. They may concern ply misalignment, error in the stacking sequence, fibre waviness, fibre distribution, matrix cure, presence of voids, presence of inclusions, moisture absorption [12].

Since such defects can sensibly affect the local material properties or the local stress state, it is fundamental to understand how they influence damage initiation and evolution to correctly design composite components and reduce their cost. If the relations between manufacturing-induced defects and mechanical properties are known, it would be possible to account for their presence in the design phase to allow a certain global or local amount of defects that is expected to occur during the manufacturing process. Less restrictive standards on quality control could also be achieved: if non-destructive tests detect a certain amount of defects once the manufacturing process is complete, it would be possible to assess with higher degree of accuracy if the component will still be able to properly carry out its function without failing. Finally, if also the relations between manufacturing process parameters and defects content and distribution are known, it would be possible to achieve a *cost-effective* production of composite materials, maximizing the performance/cost ratio (Figure 1.10).

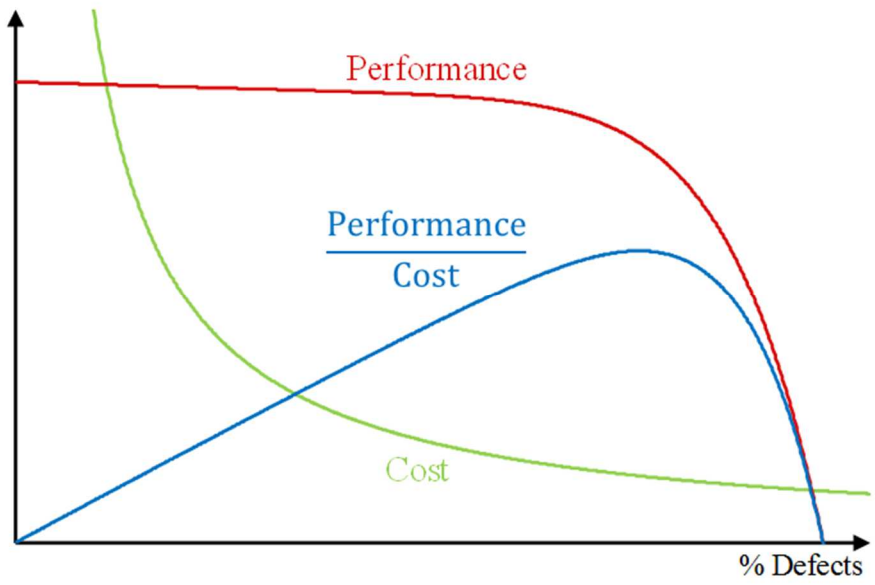

Figure 1.10 – Qualitative trends for a cost-effective production of composite components.

Among the possible manufacturing-induced defects in composite materials, the most common and most difficult to avoid is the presence of voids in the laminate. Voids may form for different reasons: when pre-pregs are used, air is entrapped between plies during the stacking operations, and volatile components can form as secondary products of the resin curing. If liquid resin is involved, as in vacuum infusion or RTM processes, air intake can take place when resin and hardener are mixed, and the degassing operation may not completely remove it. In addition, voids can form during the impregnation of dry fibres due to the different velocity of the resin in the fibre tows and in the channels between them (Figure 1.11). Moreover, both with autoclave and liquid resin processes, air can also enter the laminate due to a leakage in the vacuum bag.

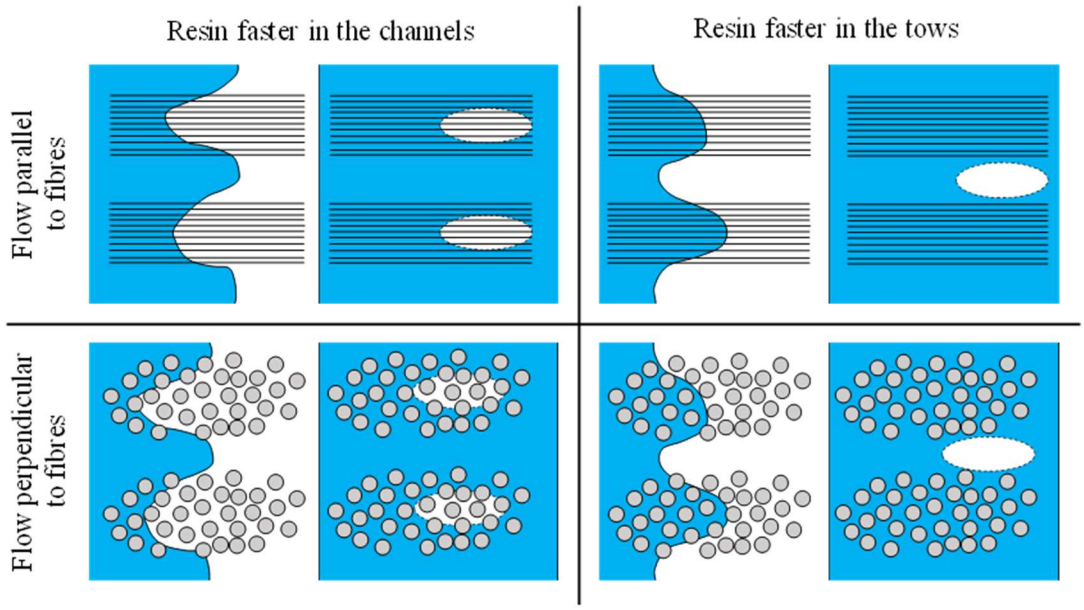

Figure 1.11 – Void formation during dry fibre impregnation in processes that use liquid resin.

Since in most of their applications composite materials are subjected to multiaxial fatigue loadings (see previous Paragraph), it is of great importance to assess the influence of manufacturing-induced voids under these loading conditions, which has not been extensively documented in the scientific literature.

Proceeding along the path traced by Carraro and Quaresimin [11], the present works aims at extending the developed models to account for the presence of manufactured-induced voids both for fatigue crack initiation and multiplication phenomena, which decrease the stiffness of the laminate and influence the occurrence of the final failure. The results may then be suitably generalized to other microstructural variations that alter the local stress state in the material. Both experimental (1-3) and modelling (4-6) activities were carried out to this aim, and are summerised as follows:

1) To strongly support the damage-based model for fatigue crack initiation proposed by Carraro and Quaresimin [11], a careful specimen design and preparation was

developed to observe damage events before the formation of an off-axis fatigue crack (Chapter 2).

2) By using the same specimen configuration developed in point 1, the influence of porosity on the micro-damage mechanisms was investigated, to understand if the same damage-based model could be used even in the presence of voids (Chapter 3).
3) An extensive experimental campaign was carried out on void-free and porous laminates made by vacuum assisted resin transfer moulding (VARTM) to observe the effect of manufacturing-induced voids on the fatigue performances. Crack initiation, crack growth rate, crack density evolution and consequent stiffness drop were analysed under both LHS-dominated and LMPS-dominated loading conditions (Chapter 4).
4) To observe the influence of voids on the local stresses in the matrix, responsible for crack initiation, a tool was developed to build Representative Volume Elements (RVEs) of the composite microstructure. RVEs were validated against real microstructures in terms of morphological indexes and stress distribution, and the stress distributions were studied under different loading conditions (Chapter 5).
5) A model based on the local stress distributions obtained from RVE was proposed to predict the life to crack initiation, by taking the average values of the LHS or the LMPS in a control volume of the matrix as the driving force (Chapter 6).
6) A procedure based on Monte Carlo simulations was developed to predict crack density evolution in composite laminates, accounting for the stress redistributions between plies due to the presence of cracks, and also capable of including the presence of voids (Chapter 7).

References of Chapter 1

[1] Herakovitch CT. Mechanics of composites: A historical review. Mechanics Research Communications 2012; 41: 1-20.

[2] Witten E, Kraus T, Kuhnel M. Composites Market Report 2015, Carbon Composites.

[3] IPCC, 2011: Summary for Policymakers. In: IPCC Special Report on Renewable Energy Sources and Climate Change Mitigation [O. Edenhofer, R. Pichs-Madruga, Y. Sokona, K. Seyboth, P. Matschoss, S. Kadner, T. Zwickel, P. Eickemeier, G. Hansen, S. Schlömer, C. von Stechow (eds)], Cambridge University Press, Cambridge, United Kingdom and New York, NY, USA.

[4] Marsh G, Composites – prime enabler for wind energy. Reinforced plastics 2003; 47: 29-45.

[5] The Economist, 2011. The printed world. The Economist 12 Feb 2011, 398 (8720), 69-71.

[6] Winther M, Rypdal K, Sorensen L, Kalivoda M, Bukovnik M, Kilde N, De Lauretis R, Falk R, Romano D, Deransy R, Whiteley M, Aviation. In EMEP/EEA air pollutant emission inventory guidebook, 2013, updated August 2014.

[7] United States Government Accountability Office (GAO), Aviation Safety – Status of FAA's Actions to Oversee the Safety of Composite Airplanes, September 2011.

[8] Heuss R, Muller N, van Sintern W, Starke A, Tschiesner A, Lighweight, heavy impact. McKinsey&Company, February 2012.

[9] Reifsneider KL, Henneke FG, Stinchcomb WW, Duke JC. Damage mechanics and NDE of composite materials. In: Hashin Z, Herakovich CT, editors. Mechanics of composite materials. Recent advances. New York: Pergamon Press, 1983. pp 399-420.

[10] Quaresimin M, Susmel L, Talreja R, Fatigue behaviour and life assessment of composite laminates under multiaxial loadings. International Journal of Fatigue 2010; 32: 2-16.

[11] Carraro PA. Multiaxial fatigue behaviour of composite materials: characterization and modelling. PhD Thesis, University of Padova, 2014.

[12] Summerscales J. Manufacturing defects in fibre reinforced plastic composites. Insight, Non-Destructive Testing and Condition Monitoring 1994; 36: 936-942

2

Early stage damage in off-axis plies under fatigue loading

Motivation

According to a damage-based model proposed by Carraro and Quaresimin to predict fatigue crack initiation under multiaxial loading conditions, micro-cracks in the matrix, normal to the local maximum principal stress, should form before the initiation of a visible crack. To further validate the predictive model, specimens were designed and prepared to observe such micro-damage events.

Abstract

The very early stages of damage evolution under fatigue loadings were investigated by testing [45/-45/0]$_s$ glass/epoxy specimens. Microscope observations revealed that the first damage event was the initiation of micro-cracks in the 45° plies within the inter-fibre region. Off-axis cracks then formed by the coalescence of these micro-cracks and propagated along the fibres direction with the same mechanism. The orientation of the micro-cracks was proven to be normal to the direction of the local maximum principal stress in the matrix. The results presented here are the first evidences of fatigue damage initiation at the inter-fibre scale and represent a further validation of the fatigue crack initiation criterion recently presented by the Carraro and Quaresimin.

2.1. Introduction

Multidirectional laminates made of unidirectional (UD) plies are frequently adopted in many structural applications as they offer optimal specific strength and stiffness, combined with the possibility to select and design material properties according to specific needs. Very often the in-service conditions are characterised by cyclic loads, which can lead to a progressive degradation of the laminate stiffness, mainly due to the damage evolution in the form of multiple off-axis cracks [1-9]. This behaviour is reported in several works in the literature for multidirectional laminates under uniaxial [1-7] or multiaxial loads [8,9].

Within this scenario, predicting the initiation of off-axis cracks is, first, necessary to define a procedure for describing the progressive damage evolution and stiffness degradation of laminates. Since the stress state in the off-axis plies of a laminate is in general multiaxial, even in the presence of uniaxial loads [7, 10, 11], a criterion for predicting the crack initiation must be capable of accounting for multiaxial stress states.

In addition, in the writer's view, a reliable initiation criterion should be based on evidences and observations derived from an extensive experimental activity, aimed not only at characterising the global material response, but also the damage mechanisms at the microscopic scale responsible for the damage onset.

The matrix-dominated fatigue behaviour of UD plies was characterised by testing flat unidirectional off-axis laminates under uniaxial loadings [12-16] and tubular specimens under combined tension-torsion loadings [11]. In these situations, damage evolution was confined to the very end of the life of the samples without significant stiffness reduction and visible crack formation during the fatigue life. This clearly indicates the absence of a progressive damage evolution at least at the macroscopic scale.

However, at the microscopic scale, i.e. the length scale of the inter-fibre distance, damage evolves from the early stages of fatigue life due to irreversible processes leading to a critical

condition for the initiation of an off-axis crack. In UD laminates the onset of an off-axis crack corresponds to the final separation, whereas in constrained plies the initiated off-axis cracks can propagate steadily in the fibre direction [1-4, 6, 7, 17-19]. Accordingly, the sensitivity of off-axis plies and laminates to fatigue loadings can only be justified by assuming the presence of a damage evolution at the micro-scale [20].

Notwithstanding this, in the writer's best knowledge, no experimental evidences are available in the in the literature allowing the fatigue damage initiation and evolution at the microscopic scale in off-axis UD plies to be understood. Only post-mortem observations of fatigued specimens are reported.

Carraro and Quaresimin presented SEM analyses of the fracture surfaces of glass/epoxy tubes with three 90° layers constrained by an external and internal thin fabric ply subjected to combined tension-torsion cyclic loadings [17]. The stress state in the 90° plies was characterised by the presence of the in-plane shear stress σ_6 and transverse stress σ_2, combined in four different values of their ratio $\lambda_{12} = \sigma_6/\sigma_2 = 0, 0.5, 1, 2$. Fracture surfaces were rather smooth when the shear stress component was null or very low ($\lambda_{12} = 0, 0.5$), whereas a significant presence of shear cusps in the matrix was observed in the case of higher shear stress contributions ($\lambda_{12} = 1, 2$).

A similar morphology was reported by Shiino and co-authors [21] for $[45/0/-45/90]_{2s}$ carbon/epoxy laminates brought to fatigue failure under a uniaxial load. These authors took in-plane images of the external 45° ply, showing the presence of shear cusps in the matrix.

Damage evidences identified on the fracture surfaces of samples under combined transverse and shear stresses were considered by Carraro and Quaresimin in the development of a fatigue crack initiation criterion recently presented in Ref. [22].

The main bases of the criterion are the following:

i) in the presence of combined transverse and shear stresses (with shear component high enough, i.e $\lambda_{12} > 0.5$) damage evolves at the micro-scale by means of the initiation and subsequent coalescence of micro-cracks in the matrix (producing the above mentioned shear cusps);

ii) the initiation of these micro-cracks is controlled by the Local Maximum Principal Stress (LMPS) in the matrix, calculated at the fiber-matrix scale;

iii) in the presence of a near transverse stress state, initiation of micro-cracks is controlled by the Local Hydrostatic Stress (LHS) in the matrix, extending to cyclic loads the approach proposed by Asp and co-authors for static loadings [23].

This Chapter focuses on the damage onset in the off-axis plies where the crack initiation is usually controlled by the LMPS (case ii). In this situation the initiation criterion was already validated, at least at a macroscopic level, by re-analysing multiaxial fatigue data at crack initiation coming from different sources in terms of this local stress parameter. The use of the LMPS produced a single, narrow scatter band capable to contain all the data analysed. This result represents indeed an implicit validation of the approach proposed, since it was directly applied on the last stage of the damage evolution at the micro-scale, i.e. the onset of an off-axis crack.

Something that is still missing, instead, is the direct observations of the damage mechanisms taking place at the microscopic scale (assumed to be micro-cracks between the fibres) before the formation of an off-axis crack. This would provide physical, experimental evidences to support the criterion. According to the writer's best knowledge the only evidence in the literature showing such micro-cracks in a specimen before its final separation was presented by Cox and co-authors [24] for a [±45] laminate under quasi-static loadings. To completely validate the initiation criterion it remains also to show that

the plane of nucleation of these micro-cracks is normal to the orientation of the LMPS in the matrix.

Within this context, the aim of the present Chapter is to identify by direct observations the damage mechanisms responsible for the damage onset at the micro-scale. A dedicated specimen with lay-up $[45/-45/0]_s$ was designed and tested under a uniaxial fatigue load. The surface of the external 45° ply was accurately polished to make the fibres and the matrix clearly observable. The specimen was removed from the testing machine at regular cycles intervals and observed under an optical microscope, revealing the presence of micro-cracks between the fibres, before the initiation of off-axis cracks. In addition, the orientation of the plane where micro-cracks nucleate was proved to be normal to the direction of the Local Maximum Principal Stress.

2.2. The damage-based criterion for crack initiation in composite laminates

To better motivate the damage investigation aim of this Chapter, in this paragraph the crack initiation criterion recently proposed by the Carraro and Quaresimin [22] is briefly presented. As already mentioned, it is based on the assumption that when the in-plane shear stress is high enough, damage at the microscopic scale occurs in the form of micro-cracks in the matrix and their initiation is driven by the Local Maximum Principal Stress. In particular it was assumed that these micro-cracks start to grow in a plane, named the *local nucleation plane*, which is normal to the direction of the Local Maximum Principal Stress. The LMPS is therefore representative of the driving force for this damage evolution, leading to the initiation of an off-axis crack, as schematically shown in Figure 2.1a.

As discussed in Ref. [22], this holds valid for stress states involving a reasonably high amount of shear. If the shear stress component is null, or very low, the damage initiation is

instead driven by the Local Hydrostatic Stress (LHS) in the matrix, as already proved by Asp and co-authors [23] in the case of static loadings.

The criterion proposed in [22] is applicable when the fibre-matrix adhesion is strong enough to prevent the initiation of damage in the form of fibre-matrix debonding. An extensive discussion of this issue can be found in [25].

Provided that this condition is verified, it was shown that crack initiation data can be collected into two scatter bands relating the number of cycles for the off-axis crack initiation to the LHS or LMPS, depending on the amount of the shear stress [22]. In the present Chapter, the attention is focused only on the LMPS-driven mechanism, which indeed characterises most of loading conditions of practical interest.

To calculate the LMPS resulting from a general in-plane stress state (σ_1, σ_2 and σ_6), Carraro and Quaresimin proposed to carry out Finite Element (FE) analyses on a fibre-matrix unit cell subjected to periodic boundary conditions as shown in Figure 2.1b [22]. For a square or hexagonal fibre array the highest value of the LMPS is located at point A, where the LMPS value and the orientation of the local nucleation plane, β_c, can be evaluated as

$$LMPS = \frac{1}{2}\left[\sigma_{rr} + \sigma_{zz} + \sqrt{\sigma_{rr}^2 + 4\sigma_{rz}^2 - 2\sigma_{rr}\sigma_{zz} + \sigma_{zz}^2} \right] \tag{2.1}$$

$$\beta_c = \pi - \frac{1}{2} ArcTan\left[\frac{2\sigma_{rz}}{\sigma_{rr} - \sigma_{zz}} \right] \tag{2.2}$$

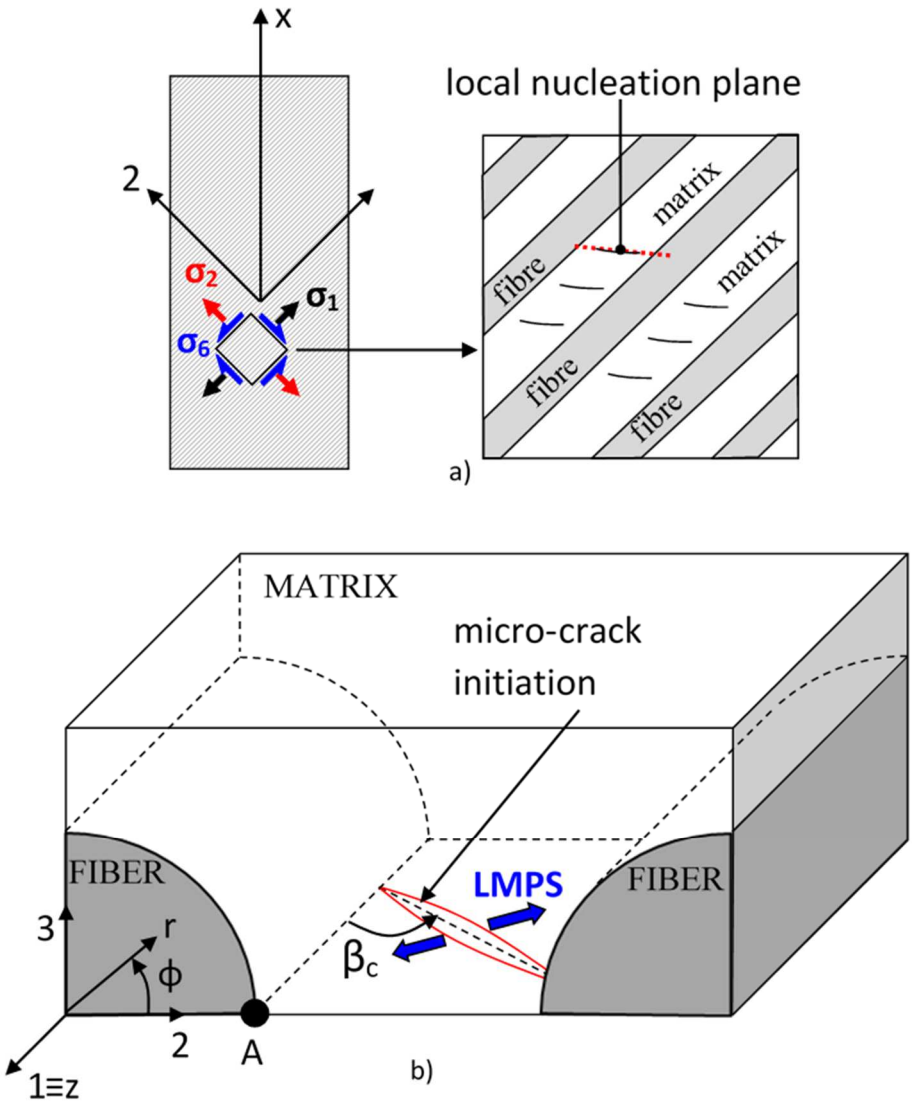

Figure 2.1 – a) Schematic of *local nucleation plane* and b) local reference system.

The orientation of the *local nucleation plane* is a paramater of fundamental importance as it quantifies the degree of local multiaxiality in the matrix. The capability of the LMPS-based criterion of collecting data for different multiaxial conditions lies, indeed, in the correct identification of the plane in which micro-cracks initiate, i.e. the *local nucleation plane*, as extensively discussed in the appendix of Ref. [22].

The assumption of a regular fibre array for computing the *local nucleation plane* orientation may be seen as too simplicistic and a potential limitation of the range of validity of the proposed approach.

However, it was already proved that the orientation β_c of the *local nucleation plane* does not depend on the unit cell type, orientation and volume fraction [22]. In addition, in Appendix 2.A it is proved that a random distribution of fibres, which is more likely to occur in actual laminates, results in the same β_c as evaluated by a regular fibre array, thus justifying the use of the LMPS and β_c calculated from unit cells even in the case of real laminates with non-regular fibre distributions.

2.3. Specimen design and testing procedure

As a first attempt to observe the initiation of micro-cracks in the matrix, $[45]_6$ laminates where produced using UD glass/epoxy pre-pregs (UE400-REM produced by Saati SpA, Italy) cured in an autoclave at the maximum temperature of 140 °C and the pressure of 6 bars for one hour. With this lay-up the stress state under an external tensile loading was such that the biaxiality ratio λ_{12} was equal to 1, which leads to a LMPS-driven damage evolution, according to the results presented in Ref. [22].

The specimens were tested under load control with a MTS 858 hydraulic machine under a uniaxial cyclic tensile load with a minimum to maximum load ratio R equal to 0.05. The specimens were removed at short regular intervals from the machine and their surface was observed under an optical microscope at high magnification.

With this configuration it was indeed not possible to observe micro-cracks initiating in the matrix before the final failure of the specimens occurring, as one may expect, by the initiation and sudden propagation of an off-axis crack parallel to the fibres direction (Figure 2.2). This is probably because micro-cracks initiated in the most critical location and then

coalesced immediately, bringing the specimen to the complete separation and a sudden failure, as it is typical for unconstrained off-axis UD laminates [11-16]. After the final failure no micro-cracks were observed elsewhere on the specimen surface, as the number of cycles was probably not enough to initiate detectable damage in other locations.

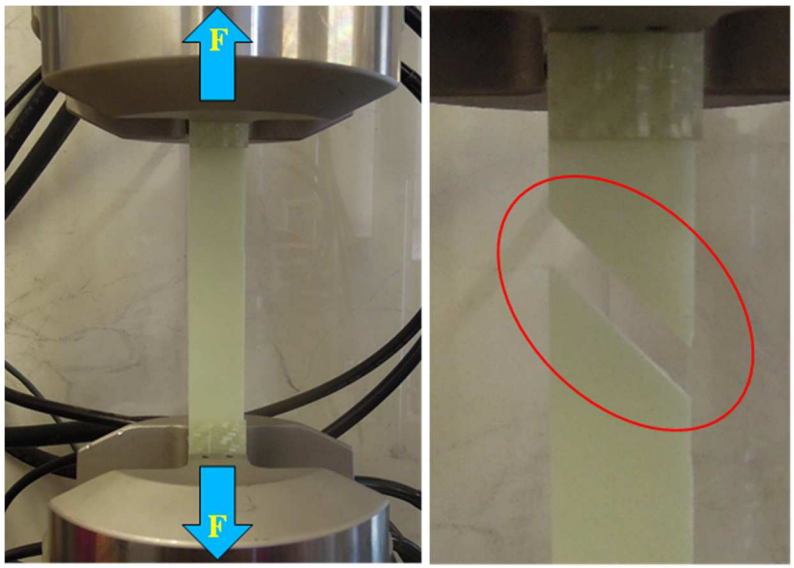

Figure 2.2 – Unstable crack propagation in UD specimens.

Another specimen configuration was therefore designed with s lay-up $[45/-45/0]_s$, as schematically shown in Figure 2.3.

These specimens were produced by means of the liquid resin infusion process. The materials used were dry unidirectional glass fibres UT-E500 (500 g/m^2, by Gurit) and an epoxy system EC157-W152LR (by Elantas). A fibre volume fraction around 0.56 was obtained. The material elastic and strength properties were measured by means of static tests on 0°, 90° and 45° UD laminates and are reported in Table 2.1.

Table 2.1 – Material properties of the infused UD laminates.

	E_1 [MPa]	E_2 [MPa]	ν_{12}	G_{12} [MPa]	$\sigma_{1,U}$ [MPa]	$\sigma_{2,U}$ [MPa]
average	48830	14070	0.308	5200	776	43
c.o.v.	0.19%	1.49%	1.20%	-	5.23%	7.50%

23 mm wide, 190 mm long and 2 mm thick specimens were cut from the 230x300 mm produced panel. The specimens were polished on the edges and on the entire top surface of the external +45° ply in order to make fibres and matrix clearly visible under a microscope. Tabs were then bonded at the ends of the specimens, obtaining a calibrated length of 100 mm. The observation zone was however restricted to 80 mm centred in the specimen mid-section.

The attention was focused on the external 45° plies, where a biaxiality ratio $\lambda_{12} = 1.65$. The biaxiality ratio $\lambda_1 = \sigma_2/\sigma_1$ was instead equal to 0.34, so that the longitudinal stress is comparable with the transverse and shear stresses. In this condition a matrix-dominated behaviour is expected and damage evolution at the microscopic scale is indeed driven by the LMPS.

Three specimens were tested under load control with R = 0.05 and a frequency of 3 Hz to avoid the temperature to increase more than 5°C. The remote applied stress in the loading direction was 150 MPa (about one third of the ultimate laminate stress in tension), corresponding to a transverse stress of 26 MPa in the external 45° ply. The specimens were removed from the tensile machine with intervals of 500 cycles until reaching 6500 cycles and the top 45° surface was observed under an optical microscope. The entire observation area, wide as the specimen and 80 mm long, was scanned.

Thanks to the specific layup chosen for the specimens, the initiation of the first off-axis crack (visible crack propagating in the fibres direction) did not lead to the separation of the

laminate, because of the presence of the neighbouring -45° and, most of all, of the load-bearing 0° plies. This specimen configuration is therefore expected to be the most suitable to observe the potential presence of damage at the microscopic level even before the initiation of off-axis cracks. Indeed, micro-cracks were observed throughout the fatigue tests, leading then to the formation, by coalescence, of multiple off-axis cracks. In addition, thanks to the fact that the off-axis cracks propagated steadily in the fibres direction it was also possible to analyse the subsequent propagation phase and the associated mechanisms. Another advantage of the new specimen configuration is that the stress state in the 45° ply is more uniform with respect to that achieved with the $[45]_n$ off axis unidirectional samples. This is well documented by the stress contour plots shown in Figure 2.4 for the 45° plies, as obtained from FE analyses carried out within the ANSYS 13® code using 8 nodes layered shell elements. A higher value of the biaxiality ratio λ_{12} is also achieved.

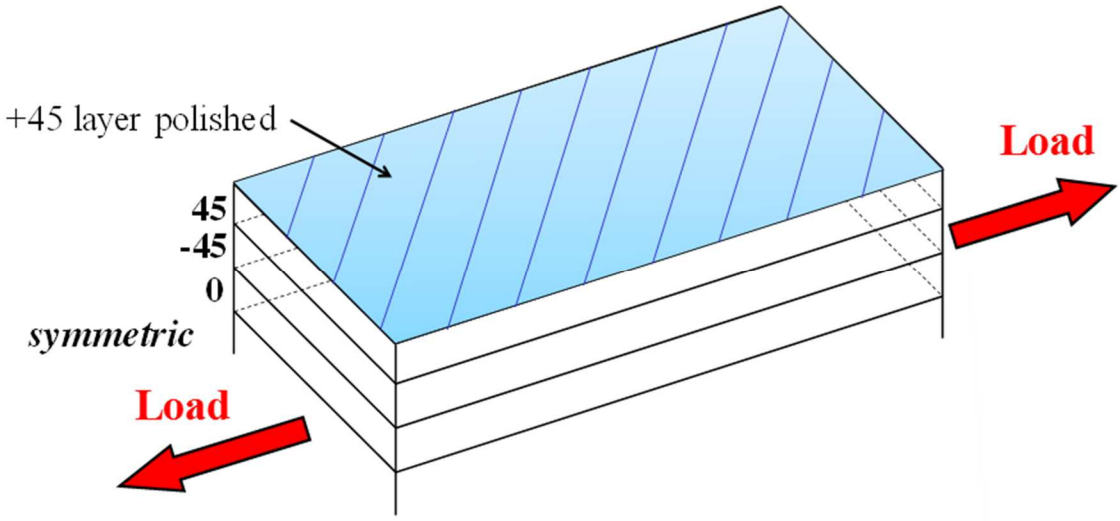

Figure 2.3 – Specimen configuration used in the experimental activity.

$[45]_6$ **$[45/-45/0]_S$**

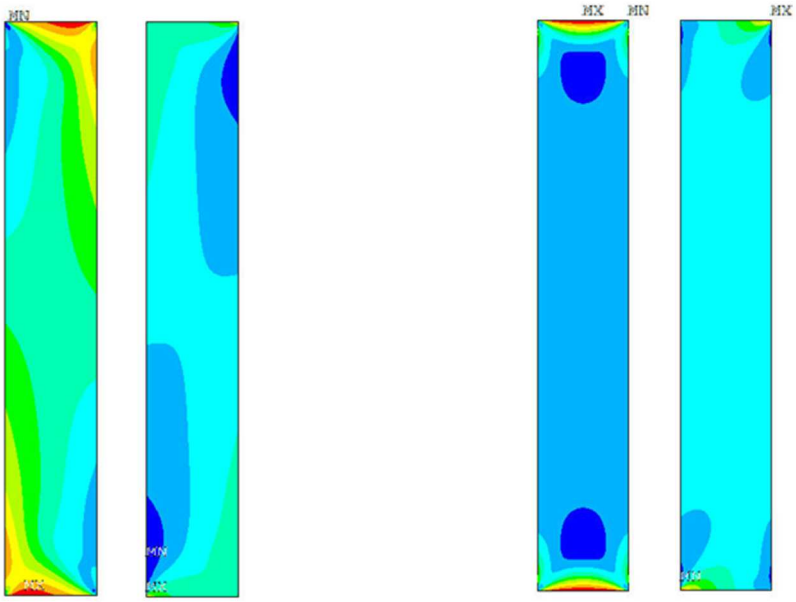

σ_6 σ_2 σ_6 σ_2

$$\lambda_1 = \frac{\sigma_2}{\sigma_1} = 1 \qquad \lambda_1 = \frac{\sigma_2}{\sigma_1} = 0.34$$

$$\lambda_{12} = \frac{\sigma_6}{\sigma_2} = 1 \qquad \lambda_{12} = \frac{\sigma_6}{\sigma_2} = 1.65$$

Figure 2.4 – Stress contour plots and biaxiality ratios in UD off-axis specimens (left) and in the 45° ply of $[45/-45/0]_s$ laminates (right).

2.4. Damage analysis

2.4.1. Micro-cracks initiation

Some representative examples of the onset of micro-cracks in the matrix, inclined with respect to the fibres on the polished top surface of the 45° ply, are reported in Figure 2.5. Micro-cracks were uniformly distributed along the specimen length and width and not only at the edges, without any preferential site of initiation. This scenario was observed in all the three tested specimens. These micro-cracks represented the first event of damage in the off-axis layer, anticipating the initiation of off-axis cracks. As a proof of the local nature of

this damage, in Figure 2.6a the top view and the related edge view of an off-axis crack are compared. The top view shows that an off-axis crack is starting to form on the top surface by coalescence of inclined micro-cracks, as one can derive from the shape of the crack profile, which is not straight but exhibits the typical hackles due to the phenomenon mentioned above. Conversely, in the edge view the crack is still not visible, meaning that the initiating off-axis crack has not propagated through the 45° ply thickness yet, and therefore damage is still confined at a local level near the surface.

Differently, in Figure 2.6b micro-cracks have already coalesced into an off-axis crack which has propagated throughout the entire thickness of the 45° ply and keeps on propagating in the fibre direction.

These observations corroborate and confirm the assumptions made by Carraro and Quaresimin [22] that under shear-dominated cyclic loading conditions there is a progressive damage evolution at the microscopic scale characterised by the initiation of multiple micro-cracks in the matrix. Their accumulation and coalescence lead to the formation of an off-axis crack involving the entire ply thickness and propagating in the fibre direction.

The evolution of these micro-cracks is also analysed in the following paragraph.

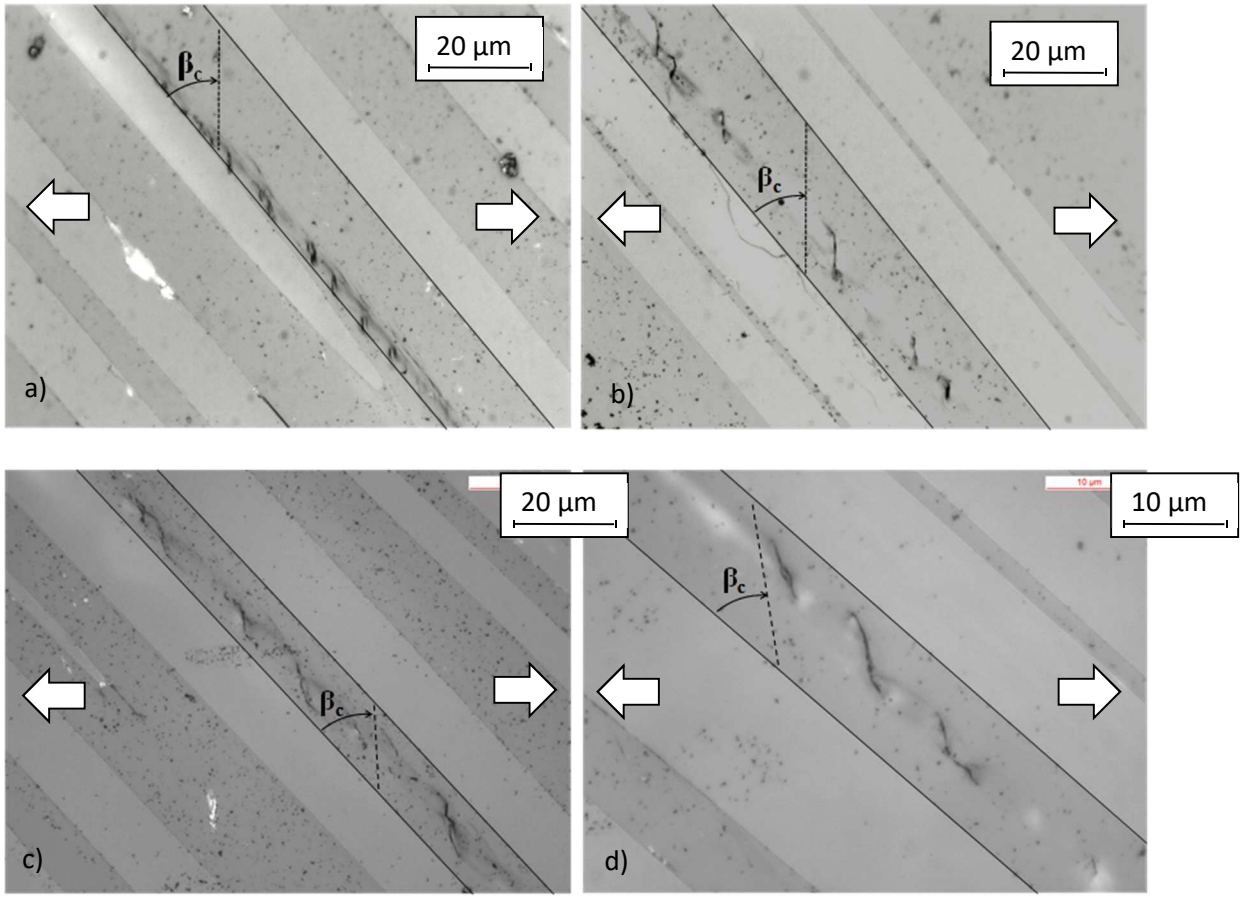

Figure 2.5 – Series of micro-cracks in the matrix, inclined with respect to the fibre direction; the arrows indicate the load application direction. The orientation of the local nucleation plane is also included for comparison.

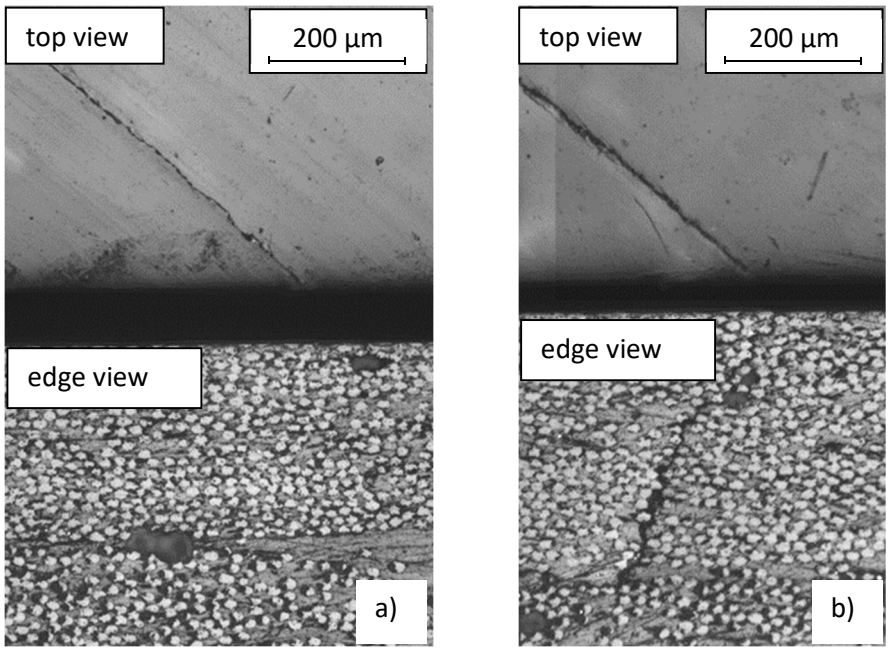

Figure 2.6 – a) Micro-crack initiated but not propagated through the thickness and b) off-axis crack propagated through the 45° ply thickness.

2.4.2. Micro-cracks coalescence and off-axis crack propagation

After an off-axis crack formed by coalescence of micro-cracks, the supporting effect of the neighbouring plies made its propagation in the fibres direction stable.

Micrographs taken on the top surface revealed that the micro-scale mechanism of crack propagation is similar to that for crack initiation. In fact, in front of the tip of off-axis cracks a process zone was observed characterised by the initiation of multiple micro-cracks in the matrix, again inclined with respect to the fibres, as shown in Figure 2.7.

This reminds the scenario observed by Carraro and co-authors concerning fatigue propagation of bondline cracks in composite bonded joints under mixed mode I + II loading [26]. Also in that case, when the mode II contribution was dominant, the same authors proved that the maximum principal stress averaged within a process zone in the adhesive layer was the driving force for this propagation mechanism [27].

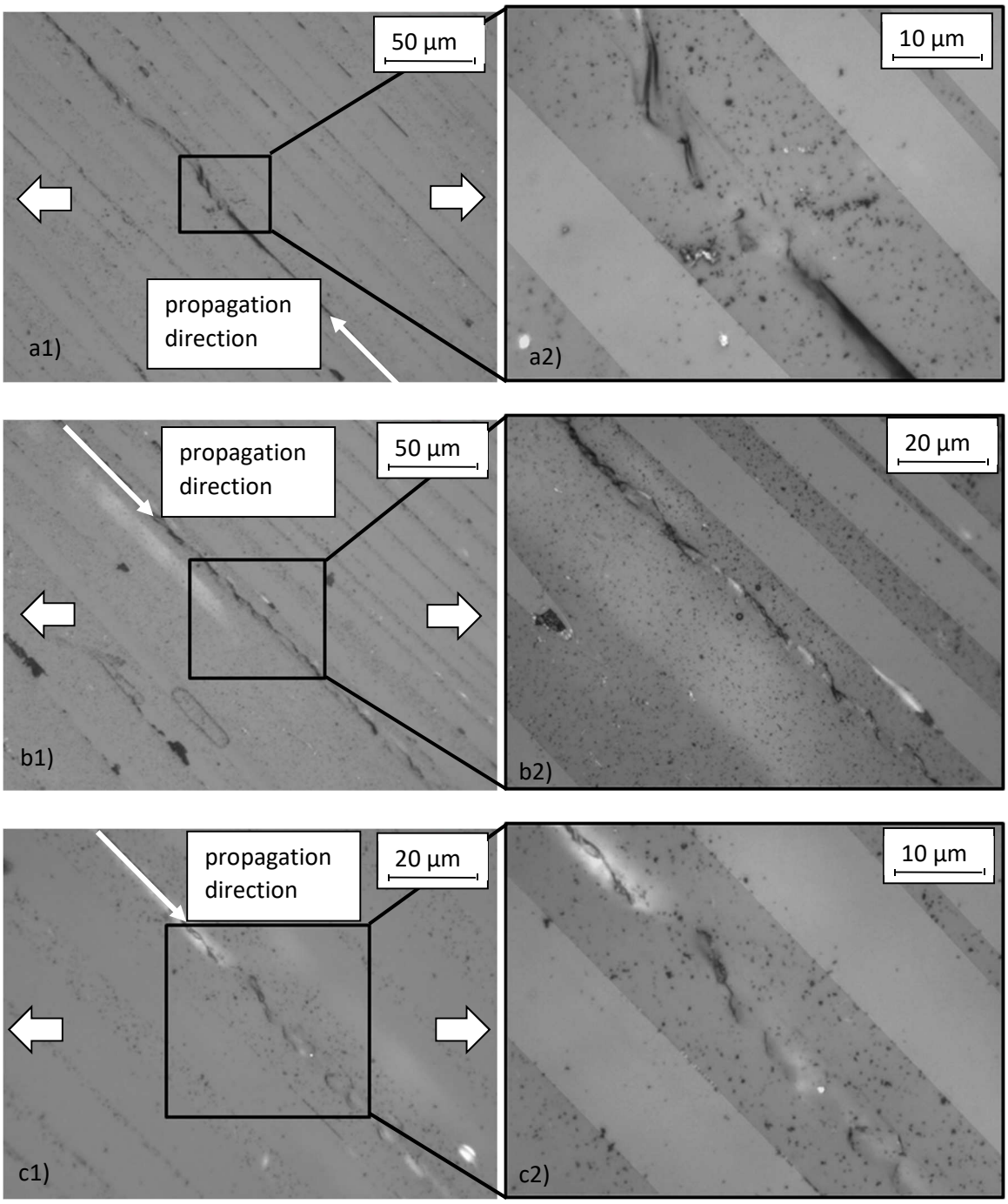

Figure 2.7 – Off-axis crack propagation by means of micro-cracks initiation in a process zone; the arrows indicate the load application direction.

2.5. Orientation of the local nucleation plane

The orientation of the observed micro-cracks was compared with the angle β_c of the *local nucleation plane*, calculated by means of Eq. (2), to confirm the assumption that the *local*

nucleation plane is normal to the Local Maximum Principal Stress in the matrix. It is worth reminding that the value of β_c calculated considering a simple periodical fibre-matrix unit cell [22] is also valid for a random fibre distribution, as shown in the Appendix 2.A.

Considering the stress state in the 45° ply β_c resulted equal to 41.3°. The *local nucleation plane*, oriented of an angle β_c with respect to the fibres, is also plotted in Figure 2.5 where it can be compared with the direction of the micro-cracks.

It is clear that there is a very good agreement between the predictions and the experimental evidences. This proves that the micro-cracks in the matrix are normal to the Local Maximum Principal Stress, which can be thus considered, within reason, the driving force for their initiation.

Moreover, being an off-axis crack the result of the accumulation and coalescence of micro-cracks, these observations provide a further solid support for the criterion based on the use of the LMPS to predict the initiation of an off-axis crack in UD plies in the presence of a significant contribution of the shear stress [22]. In fact, the higher the LMPSs is, the higher will be the rate of micro-cracks formation and coalescence, bringing to the initiation of an off-axis crack.

2.6. Conclusions

With the aim of observing the very early stages of fatigue damage evolution at the microscopic scale in off-axis loaded unidirectional plies a dedicated specimen configuration with lay-up $[45/-45/0]_s$ was defined and tested.

It was found that the first event of damage was the initiation of multiple micro-cracks in the inter-fiber region of the 45° ply, inclined of a certain angle with respect to the fibres. The subsequent coalescence of these cracks led to the formation of off-axis cracks involving the entire 45° ply thickness and propagating in the fibres direction with the same

mechanism. In fact, in front of the tips of propagating off-axis cracks a process zone was observed, characterised, again, by the presence of inclined micro-cracks in the matrix. The direction of these micro-cracks was seen to be very well consistent with the orientation of the so called *local nucleation plane*, calculated as the plane normal to the local maximum principal stress in the matrix.

Appendix 2.A

In this appendix it will be proved that the angle β_c calculated assuming a regular square fibres arrays (Eq. 2) is representative also of the *local nucleation plane* in a more realistic condition, where the fibres are randomly distributed. To this end a Volume Element (VE) containing 36 randomly distributed fibres was analysed and the angle β_c at each node in the matrix was computed (see Figure 2.A1). The algorithm used to generate the VE is that proposed by Pontefisso et al. [28] for creating representative volume elements with randomly distributed particles, suitably adapted for the case of long fibres.

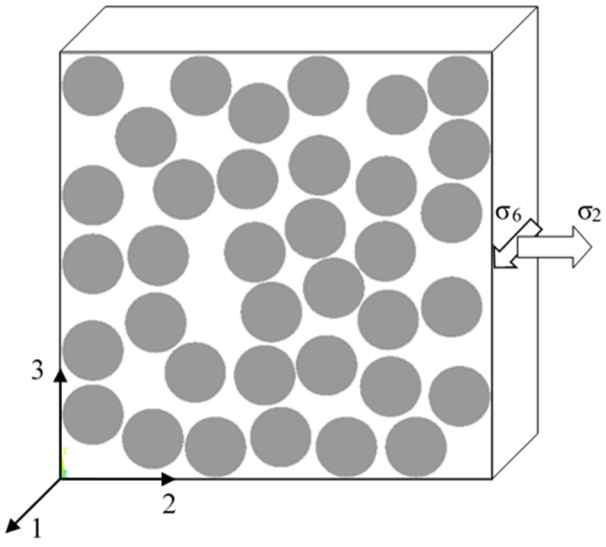

Figure 2.A1 – Volume element with random fibres distribution.

FE analyses were carried out on the VE under transverse and in-plane shear stresses with a biaxiality ratio $\lambda_{12} = 2$ using the Ansys13® FE code. 20 nodes 3D brick elements were adopted with an average size such to guarantee 144 divisions along the fibre circumference, enough to assure the convergence of local stresses. The local maximum principal stress and the orientation β_c of the local nucleation were computed on every node within the matrix and plotted in Figure 2.A2. The LMPS is normalised by the applied transverse stress whereas the angle β_c is normalised by its value computed with a square array under the same stress state ($\lambda_{12} = 2$). It is interesting to note that in the nodes where the LMPS has its maximum values (LMPS/σ_2 = 5 ÷ 20), i.e. the locations in which damage is expected to initiate, the angle β_c is very close to that predicted with a square unit cell.

This means that the orientation of the local nucleation plane, β_c, calculated for a simple regular fibre array, is a robust parameter, representative of the local multiaxial stress state in the matrix. This result justifies the use of the LMPS calculated from unit cells even in the case of real laminates with non-regular fibre distributions.

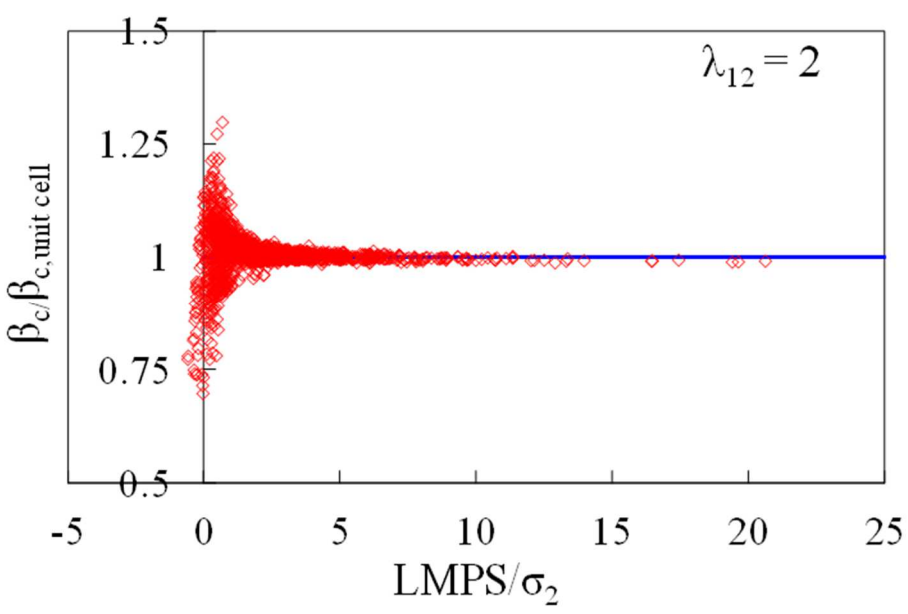

Figure 2.A2 – Normalised orientation β_c of the local nucleation plane plotted against the normalised LMPS for a VE with random fibre distribution.

References of Chapter 2

[1] Lafarie-Frenot MC, Hénaff-Gardin C. Formation and Growth of 90° Ply Fatigue Cracks in Carbon/Epoxy Laminates. Composites Science and Technology 1991; 40: 307-324.

[2] Tong J, Guild FJ, Ogin SL, Smith PA. Off-axis fatigue crack growth and the associated energy release rate in composite laminates. Applied Composite Materials 1997; 4: 349–359.

[3] Tong J. Three Stages of Fatigue Crack Growth in GFRP Composite Laminates. Journal of Engineering Materials and Technology 2001; 123: 139-143.

[4] Tong J. Characteristics of fatigue crack growth in GFRP laminates. International Journal of Fatigue 2002; 24: 291–297.

[5] Wharmby AW, Ellyin F. Damage growth in constrained angle-ply laminates under cyclic loading. Composites Science and Technology 2002; 62: 1239–1247.

[6] Yokozeki T, Aoki T, Ishikawa T. Fatigue growth of matrix cracks in the transverse direction of CFRP laminates. Composites Science and Technology 2002; 62: 1223–1229.

[7] Quaresimin M, Carraro PA, Pilgaard Mikkelsen L, Lucato N, Vivian L, Brøndsted P, Sørensen BF, Varna J, Talreja R. Damage evolution under internal and external multiaxial cyclic stress state: a comparative analysis. Composites Part B - Engineering 2014; 61: 282–290.

[8] Adden S, Horst P. Damage propagation in non-crimp fabrics under bi-axial static and fatigue loading. Composites Science and Technology 2006; 66: 626–633.

[9] Adden S, Horst P. Stiffness degradation under fatigue in multiaxially loaded non-crimped-fabrics, International Journal of Fatigue 2010; 32: 108–122.

[10] Quaresimin M, Susmel L, Talreja R. Fatigue behaviour and life assessment of composite laminates under multiaxial loadings. International Journal of Fatigue 2010; 32: 2-16.

[11] Quaresimin M, Carraro PA. On the investigation of the biaxial fatigue behaviour of unidirectional composites. Composites Part B - Engineering 2013; 54: 200-208.

[12] Hashin Z, Rotem A. A fatigue failure criterion for fibre-reinforced materials. Journal of Composite Materials 1973; 7: 448-464.

[13] Awerbuch J, Hahn HT. Off-axis fatigue of graphite/epoxy composite. Fatigue of Fibrous Composite Materials, ASTM STP 723, American Society for Testing and Materials, 1981: 243-273.

[14] El-Kadi H, Ellyin F. Effect of stress ratio on the fatigue of unidirectional fibreglass-epoxy composite laminae. Composites 1994; 25(10): 917-924.

[15] Kawai M, Yajima S, Hachinohe A, Takano Y. Off-axis fatigue behaviour of unidirectional carbon fibre-reinforced composites at room and high temperatures. Journal of Composite Materials 2001; 35(7): 545-576

[16] Kawai M, Suda H. Effects of non-negative mean stress on the off-axis fatigue behaviour of unidirectional carbon/epoxy composites at room temperature. Journal of Composite Materials 2004; 38(10): 833-854.

[17] Quaresimin M, Carraro PA, Damage initiation and evolution in glass/epoxy tubes subjected to combined tension-torsion fatigue loading. International Journal of Fatigue 2014; 63: 25–35.

[18] Boniface L, Ogin SL. Application of the Paris Equation to the Fatigue Growth of Transverse Ply Cracks. Journal of Composite Materials 1989; 23: 735-752.

[19] Balhi N, Vrellos N, Drinkwater BW, Guild FJ, Ogin SL, Smith PA. Intra-laminar cracking in CFRP laminates: observations and modelling. Journal of Materials Science 2006; 41: 6599-6609.

[20] Talreja R. Fatigue of composite materials: damage mechanisms and fatigue-life diagrams. Royal Society of Londo, Proceedings A – Mathematical, Physical and Engineering Sciences 1981; 378: 461–75.

[21] Shiino MY, De Camargo LM, Cioffi MOH, Voorwald HCJ, Ortiz EC, Rezende MC, Correlation of microcrack fracture size with fatigue cycling on non-crimp fabric/RTM6 composite in the uniaxial fatigue test. Composites Part B – Engineering 2012; 43: 2244–2248.

[22] Carraro PA, Quaresimin M. A damage based model for crack initiation in unidirectional composites under multiaxial cyclic loading, Composites Science and Technology 2014; 99: 154–163.

[23] Asp LE, Berglund LA, Talreja R. Prediction of matrix initiated transverse failure in polymer composites. Composites Science and Technology 1996; 56: 1089-1097.

[24] Cox BN, Dadkhah MS, Morris WL, Flintoff JG. Failure mechanisms of 3d woven composites in tension, compression, and bending. Acta Metallurgica et Materialia 1994; 42(12): 3967 3984.

[25] Carraro PA, Zappalorto M, Quaresimin M. A comprehensive description of interfibre failure in fibre reinforced composites. Theoretical and Applied Fracture Mechanics 2015; 79: 91-97.

[26] Carraro PA, Meneghetti G, Quaresimin M, Ricotta M. Crack propagation analysis in composite bonded joints under mixed-mode (I+II) static and fatigue loading: a damage-based model. Journal of Adhesion Science and Technology 2013; 27: 1393-1406.

[27] Carraro PA, Meneghetti G, Quaresimin M, Ricotta M. Crack propagation analysis in composite bonded joints under mixed-mode (I+II) static and fatigue loading: experimental investigation and phenomenological modelling. Journal of Adhesion Science and Technology 2013; 27: 1179-1196.

[28] Pontefisso A, Zappalorto M, Quaresimin M. An efficient RVE formulation for the analysis of the elastic properties of spherical nanoparticle reinforced polymers, Computational Material Science 2015; 96: 319–326.

3

Effect of voids on the crack formation in off-axis plies under fatigue loading

Motivation

In Chapter 2, micro-cracks were observed in the matrix before the formation of a visible crack, strongly supporting Carraro and Quaresimin's damage-based criterion for fatigue crack initiation. To understand if the same criterion could be applied in the presence of porosity, in this Chapter the influence of voids on the micro-damage mechanisms is analysed.

Abstract

In the present Chapter, the influence of manufacturing induced voids on damage mechanisms at the microscopic scale was analysed on [45/-45/0]$_s$ laminates subjected to tension fatigue loading. Microscopic observations of the top surface of the 45° ply revealed that the first event of damage at the microscopic scale was the initiation of multiple micro-cracks in the matrix between the fibres, located preferentially in correspondence of the voids in that layer. The subsequent coalescence of these micro-cracks gave rise to the formation of a macro-crack propagating in the 45° fibres direction. This is qualitatively the same scenario observed in void-free specimens (Chapter 2), thus confirming that the same crack initiation criterion can be applied in the absence and presence of voids. In

addition, the micro-scale damage is shown to evolve faster and therefore macro-cracks to initiate earlier and in a larger quantity in the presence of voids.

3.1. Introduction

The high specific properties of polymeric composite materials can be strongly influenced by the presence of defects, such as voids, that originate during the manufacturing process (see Ref. [1-4] among the others). Voids can be generated due to inaccuracies in the manufacturing process but also due to the very nature of the materials involved. Indeed, voids might form due to the release of volatile compounds during the resin cure, and, in processes that involve liquid resin (infusion, RTM), to the different flow velocity inside and outside the fibres bundles. This makes it difficult and costly to manufacture defect-free composite components.

The detrimental effect of voids on the mechanical properties of composites has been investigated experimentally by several authors.

Under tensile loadings, voids were found to affect more the transverse (i.e. matrix-dominated) than the longitudinal behaviour [5]. In unidirectional (UD) specimens, a larger void content leads to earlier transverse crack initiation and to a larger strain to failure [6], and in multidirectional (MD) laminates the effect of voids depends on the stacking sequence [7]. Crack density was reported to evolve more rapidly [Appendix A,8,9] and delamination to initiate earlier [Appendix A,9] in cross-plies containing voids.

Under compression, voids have been shown to decrease the strength along the longitudinal direction of UD specimens [10,11] and the strength and stiffness of laminates [12-14].

Also the bending performances of composites were reported to be negatively influenced by the presence of voids in terms of flexural strength and stiffness [5,15-18].

Many authors [5,10,15,19-26] investigated the influence of voids on the inter-laminar shear strength (ILSS) of UD and MD laminates, showing a high sensitivity of this property to the void content and highlighting in some cases [15,19,21,25] a linear relation between ILSS and void volume fraction.

Concerning the inter-laminar fracture toughness, small void contents (~1%) were found to actually increase the critical Energy Release Rate (G_c) for propagation of delamination and to have a negligible effect on G_c for crack initiation on a 0°/5° interface under both Mode I and Mixed Mode loadings, whereas no effect was observed for Mode II [27]. The same result under Mode I was noted also in Appendix A [9] for 0°/0° and 45°/-45° interfaces. A larger void content (~5%) caused instead an evident decrease of G_c on a 0°/0° interface [20].

Moving to cyclic loadings, the fatigue behaviour of composites is largely affected by the presence of voids. The fatigue life of laminates was found to be much shorter and the S-N curves for fatigue failure to be steeper in presence of voids under tension-tension, compression-compression, and bending loads [16,25,28-33].

In most of the early works, the decrease of the mechanical properties was related to the global content of voids, so that the influence of voids was often found to depend on the materials used, the manufacturing process and the laminate lay-up. Accordingly, it was not possible to draw criteria of general validity to predict the performances of composite components containing voids. A first step to assess this issue could be to take into account not just the global void content but additional void features such as size, shape, and distribution. However, under some loading conditions this may still not be sufficient, because voids can affect the mechanism of damage initiation and propagation at the microscopic level. Hence, the study of damage mechanisms in the presence of voids is a

matter of primary importance to predict the mechanical properties of composite components with voids.

Within this context, in Appendix A [9] it is shown that global parameters such as the void area fraction and the void density may not be sufficient to predict transverse crack initiation under tensile load in the presence of inter-tow voids in NCF cross-ply laminates. Instead, the stress concentration given by the actual shape of the voids should be accounted for.

Studying the compression behaviour of non-crimp fabrics (NCF) with voids, Kosmann et al. [13] highlighted that different process parameters might lead to different void morphologies: from homogeneously distributed voids of cylindrical and spherical shape, inside and between fibre tows, to large irregular voids concentrated in the middle of the laminate. Those authors found a large reduction in the compressive Young's modulus that was attributed to earlier micro-buckling and matrix cracking due to the lower lateral support of the fibres and the stress concentrations caused by the voids. The sensitivity of the Young's modulus to the presence of large irregular voids was much smaller than the other cases even though the void global content was the highest.

An extensive characterization of void content (void shape, orientation and spatial distribution) was carried out by Hernandez et al. [14] through micro-CT, but voids features were not explicitly correlated to the decrease in compression strength measured from mechanical tests.

The importance of void shape and location under compression was highlighted by Hapke et al. [34], who carried out *in situ* SEM microanalyses on UD specimens, and noted that kink bands propagating close to a void tip changed their orientation during propagation. Differently, kink bands encountering a void did not propagate further.

Scott and co-authors [35] tested a composite tube containing voids under hydrostatic loading caused by an internal pressure, and analysed *ex situ* the damage mechanism with a

multi-scale computed tomography technique. They observed that matrix cracks in the longitudinally wound plies clearly intersected with voids, and found a distinct correlation between voids and nearest neighbouring fibre breaks in the circumferentially wound plies. The increase of G_c for inter-laminar crack propagation in the presence of relatively small void volume fraction observed in Appendix A and Refs. [9,20] is possibly due to a change of the crack propagation mechanism. Voids were in fact seen to cause a more complicated crack path, with larger fibre and ply bridging and the formation of several secondary cracks at crack tip, which require more energy to be provided for the main crack to propagate.

For what concerns the fatigue behaviour, Lambert and co-authors [32] observed the involvement of voids in damage evolution (especially matrix cracking and delamination) in wind turbine blade materials with the aid again of micro-CT. They also found a linear correlation between the number of cycles to final failure and the size of the largest void in the most critical plies, whereas no correlation seemed to hold valid between fatigue life and global void content.

Seon and co-authors [33] observed a similar correlation, between the presence of a single void in a critical position and the inter-laminar tensile fatigue life of UD specimens.

In spite of the observation reported in the literature and discussed above, the influence of voids on the damage mechanisms at the microscopic scale, responsible for the initiation of cracks under static and mainly fatigue loadings, has not been fully clarified.

Several authors devoted their efforts to develop predictive models for the mechanical properties of composites accounting for the effect of voids. The Finite Elements Method (FEM) was mainly used to predict strength [22,28,36,37] and elastic properties [38,39]. Analytical models, instead, were used to correlate the void content to the strain to failure under transverse tensile load [6], to predict flexural and inter-laminar shear strength [17,24] and to study the influence of voids on the inter-laminar fracture toughness [40]. A statistical

model was proposed in Ref. [8] to assess the transverse tensile strength distribution and predict crack density evolution in cross-plies. This model was applied to laminates manufactured with different process parameters, but the void features were not correlated to the predicted strength distributions.

Predictive models should be as general and reliable as possible. For what concerns failure criteria, both generality and reliability can be greatly enhanced by taking into account the dominant damage mechanisms taking place. Under cyclic loading, Carraro and Quaresimin recently proposed a criterion to predict fatigue crack initiation in UD plies, assuming the Local Maximum Principal Stress (LMPS) as the driving force in the presence of relatively high shear stress [41], based on the observation of *shear cusps* on the fracture surface of tubular specimens subjected to tension/torsion [42]. The presence of micro-cracks in the matrix, perpendicular to the direction of the LMPS, was also observed by the authors in the off-axis plies of void-free MD laminates even before the onset of a macroscopic (visible) crack [43], thus providing a strong and further validation to the new failure criterion. As voids are commonly found in composite components, it is of great importance to assess if the fatigue crack initiation criterion proposed in Ref. [41] can hold its validity even in the presence of voids, hence to observe if voids influence the damage mechanism at the micro-scale under multiaxial fatigue loadings.

In this scenario, the present Chapter aims at characterising the effect of voids on the damage mechanisms at the microscopic scale responsible for the initiation of a macro-crack under a multiaxial stress state characterised by a high shear stress contribution. This is a fundamental step towards the definition of a criterion for fatigue crack initiation accounting for the presence of voids. To this end, the following steps are taken:

1) MD laminates are manufactured with the same lay-up used in Chapter 2 [43], varying the process parameters to induce void formation in the laminate;

2) Voids geometrical features are characterised;
3) Laminates are tested under uniaxial fatigue loadings and analysed under an optical microscope at regular intervals to observe damage evolution at the micro-scale;
4) S-N curves for first macro-cracks initiation in void-free specimens and specimens with voids are compared.

3.2. Manufacturing process and experimental techniques

The same specimen configuration developed in Chapter 2 [43] is adopted here, namely $[45/-45/0]_S$ laminates, to analyse the influence of voids on the micro-scale fatigue damage evolution in the presence of shear stresses. In particular, the attention is focused on the initiation of damage in the 45° plies. Compared to off-axis UD specimens, the chosen lay-up prevents the initiation of the first macro-crack (visible crack propagating along the fibres direction) to cause the complete separation of the specimens, mainly thanks to the load-bearing 0° plies. This offers the advantage that damage initiation can occur in multiple locations, thus increasing the number of possible observation sites from one single specimen. In addition to this, the stress field in the 45° plies is more uniform compared to UD specimens and, according to Classical Laminate Theory, characterised by the biaxiality ratios $\lambda_{12} = \sigma_2/\sigma_6 = 1.65$ and $\lambda_1 = \sigma_2/\sigma_1 = 0.34$ (see Chapter 2 [43]). This configuration leads to a matrix-dominated behaviour where the damage initiation at the micro-scale, at least in the absence of voids, is LMPS-driven (see Chapter 2 [43]).

A 230x300 mm laminate was produced via liquid resin infusion. The low-viscosity epoxy system EC157-W152LR by Elantas was used as matrix, and the dry UD glass fibre UT-E500 (500 g/m^2) by Gurit as reinforcement.

Resin and hardener were mixed for 5 minutes at 300 rpm with a DISPERMAT TU shear blender from VMA-Getzman. 150 g of resin and 45 g of hardener were used, in accordance with the 100:30 weight ratio recommended by the manufacturer.

Different from Chapter 2 [43], where an extensive degassing (20 minutes at 0.05 mbar) was carried out to obtain void-free specimens, in the present work the resin was not degassed prior to infusion, with the aim to obtain voids in the final laminate

During the infusion process, the outlet pressure was kept constant at 0.05 mbar. The inlet pressure was instead constantly controlled and tuned to avoid the resin to run too fast in the distribution medium placed over the dry reinforcement and to guarantee, in turn, a complete filling of the reinforcement at a macroscopic level. The resin was allowed to bleed until no more resin was left in the starting pot. After the infusion, the laminate was cured for 3 days at room temperature, and no post-curing process was performed.

After de-moulding, specimens were cut with dimensions 190x23x2 mm (length x width x thickness). The 45° ply in contact with the mould, where the damage mechanism were then analysed, was carefully polished, starting from P600 sandpaper down to a silicon oxide solution with particles of size 0.1 μm. At the end of the polishing procedure, fibres and matrix of the 45° ply were clearly distinguishable under an optical microscope. To ensure that cracks do not initiate from edge defects due to the specimens cut, the edges of the specimens were polished as well, allowing the damage mechanism of the “bulk” material to be observed. Eventually, specimens were tabbed, leaving an observation length of 100 mm.

Fatigue tests were carried out by means of a MTS 858 hydraulic machine. The specimens were tested with a load ratio of R = 0.05 and a maximum stress in the load direction of 150 MPa, resulting in a transverse stress of 26 MPa in the 45° plies (calculated through CLT). A low frequency (3 Hz) was chosen to prevent specimen heating during the test, which

could alter the damage mechanics. To observe damage mechanisms, the specimens were removed from the testing machine every 500 cycles, and the tests were stopped after 6000 cycles. Due to the high transverse and shear stresses in the 45° plies, a few thousands cycles were found to be enough to trigger damage initiation at both micro and macro level, according to the findings in Chapter 2 [43].

3.3. Morphological characterization of voids

As expected, infusing non-degassed resin lead to the presence of voids in the manufactured specimens. Figures 3.1 and 3.2 clearly show the presence of the voids both from the edge-view and from the top-view of the specimens. The majority of the voids is characterised by a *cigar-like* shape, as they are elongated along the fibres direction and have an approximately circular section and rounded tips. A low number of spherical-shaped voids were noted in the matrix-rich regions in the vicinity of the polyester tows used to keep the dry glass fibres in place.

Via an image analysis tool, developed in-house with Matlab®, it was possible to calculate the global void content in the polished 45° ply in terms of void area fraction (A_v) and the geometrical features of the voids from micrographic images. Only the images taken from the top views were considered in this analysis, since in the edge views the void features are altered due to the angle between the edge surface and the fibre directions of the 45° plies.

As shown by Nikishkov et al. [44], the void content in general varies along the laminate thickness. To characterise this variation, the void content in the edge views was analysed, as explained later on.

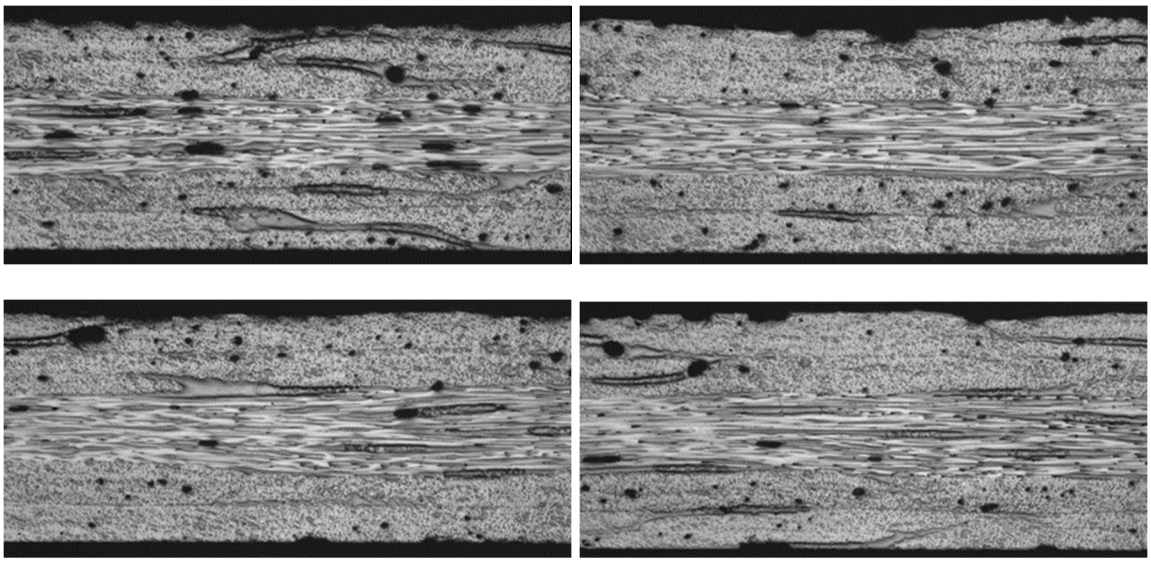

Figure 3.1 – Edge views of the samples.

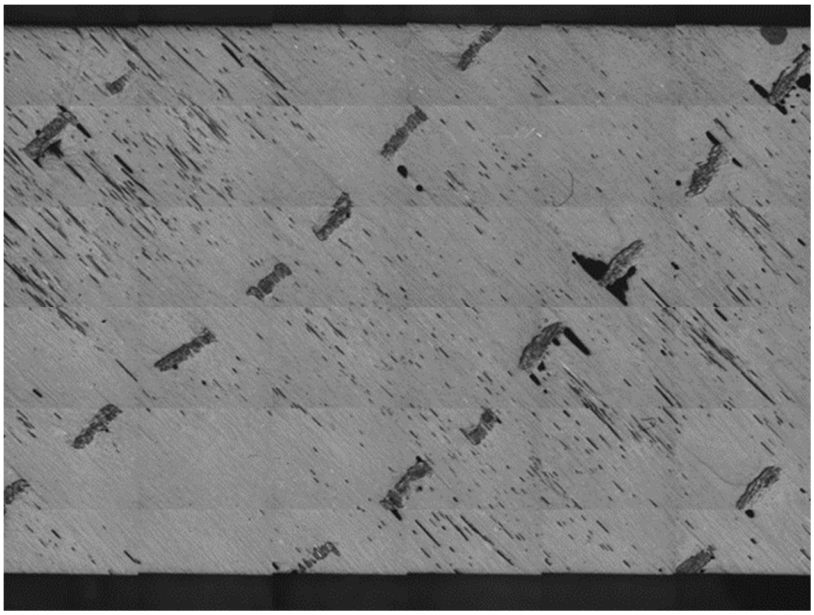

Figure 3.2 – Top view of a specimen (A_v = 3.8%).

The void content was characterized in three samples. The average void area fraction on the polished 45° layer resulted to be 3.15%. The *cigar-like* voids can be characterized, with the limitation given by a 2D top-view, by the following parameters: void orientation, void section diameter, void area, and void aspect ratio (Figure 3.3). As expected, the majority of the voids is confirmed to be oriented along the fibre direction (Figure 3.3a). Assuming a

circular section of the voids, the average void diameter is ~41 µm, and an asymmetrical void diameter distribution can be observed (Figure 3.3b). Though many voids are characterised by larger areas, half of them have an area under 400 µm^2 (Figure 3.3c). The elongated shape of the voids can be quantified with their aspect ratio (void diameter/void length), with an average value is of 5.5 (Figure 3.3d).

The void distribution along the thickness was analysed in terms of void area fraction in the off-axis plies taken from the edge views, compared with the one measured in the 45° ply on the mould side. As shown in Figure 3.4, the void content appears to slightly decrease moving from the distribution medium towards the mould. It can also be noted that the polished 45° is that with the lowest void content.

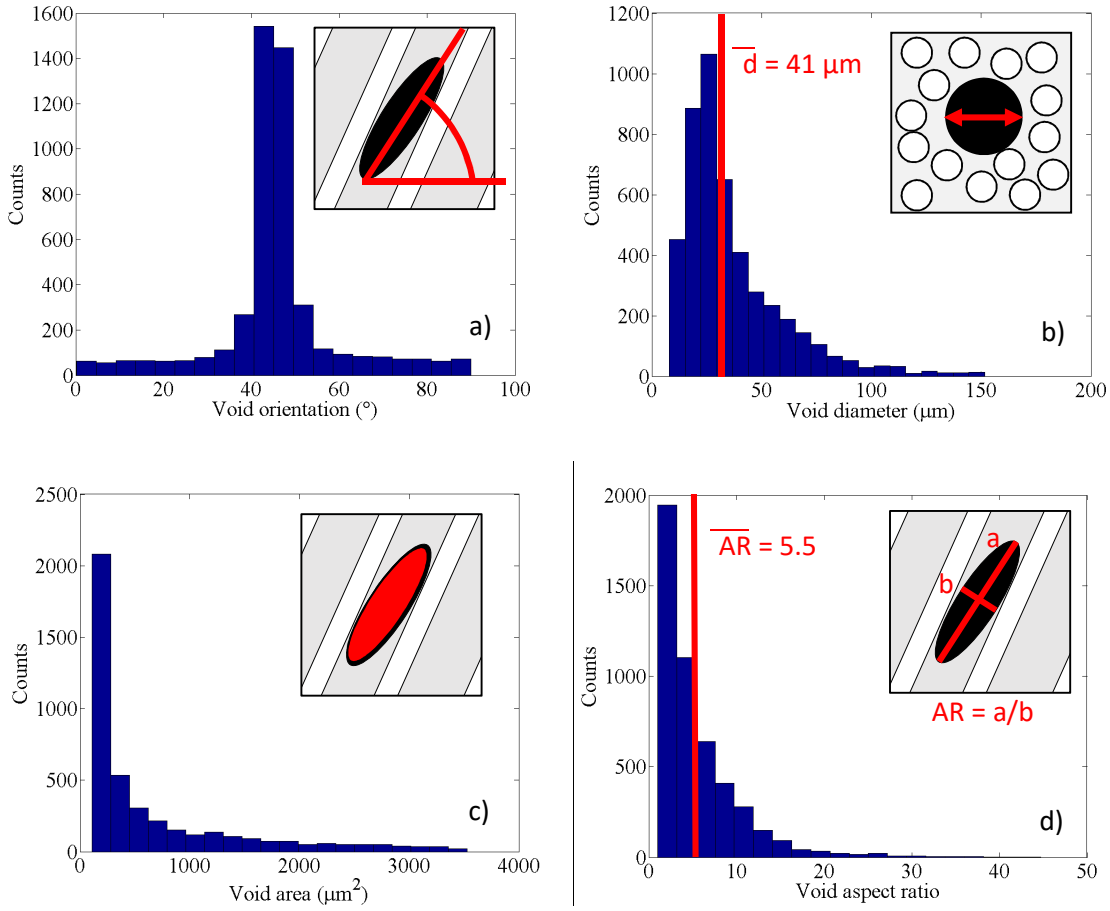

Figure 3.3 – Void geometrical features: a) orientation, b) diameter, c) area, d) aspect ratio.

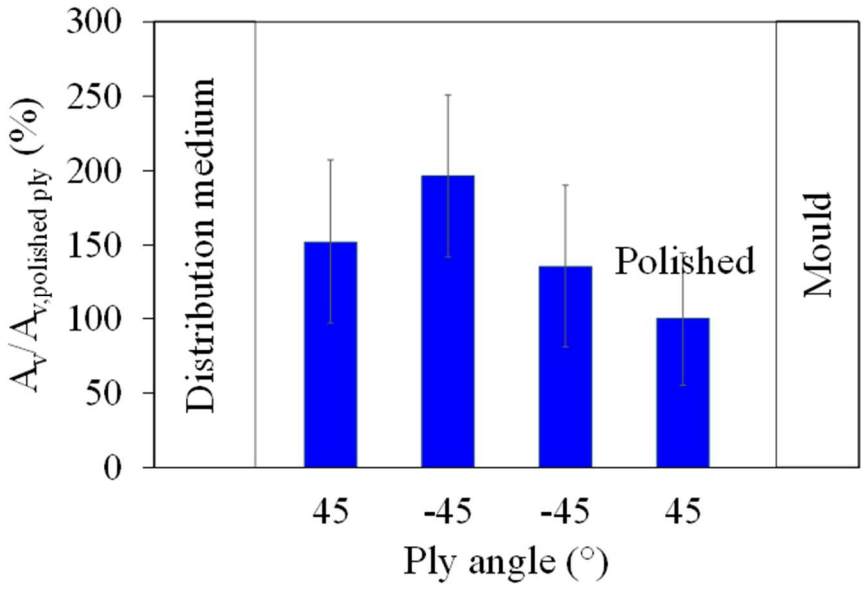

Figure 3.4 – Void distribution in the off-axis plies, calculated from the edge views.

3.4. Damage mechanisms at the micro-level

The presence of voids in a composite laminate induces stress concentrations. In particular, considering *cigar-like* 3D voids in the matrix between fibres, as those found in the manufactured specimens, the zones with higher stresses are expected in two different locations: at void tips (Figure 3.5a) and also above and below the void (Figure 3.5b). As a proof of this, a FE analysis was carried out, as reported in Appendix A, revealing peak values of the LMPS in the matrix between the fibres located immediately above and below a void. Damage initiation is therefore expected to occur at these preferential sites.

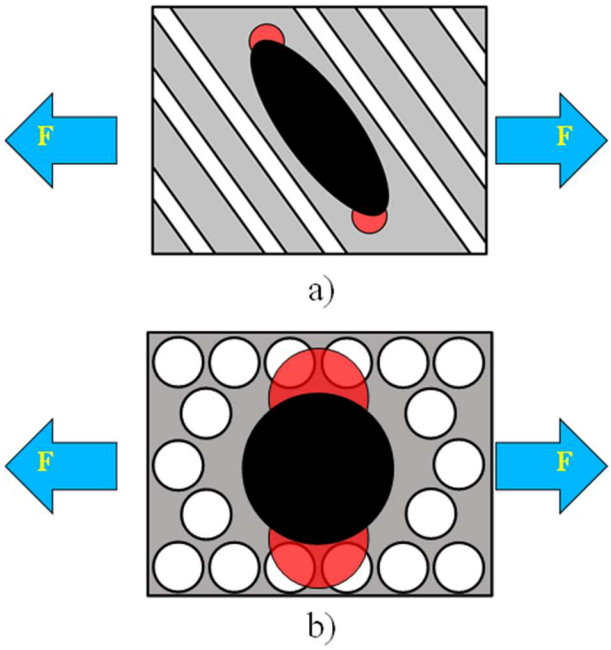

Figure 3.5 – Schematic of regions of stress concentrations (in red) in presence of 3D voids: (a) at void tips and (b) above and below the void.

Careful analyses carried out with an optical microscope spanning all the polished surface of the external 45° ply revealed that the first damage mechanism to occur at the micro-level is the initiation of micro-cracks in the matrix between fibres, inclined with respect to the fibres direction, in agreement with the scenario reported in the absence of voids in Chapter 2 [43]. As expected, considering the locations of stress concentration, such micro-cracks were detected at both void tips and above voids that lie right beneath the polished surface. Figures 3.6 and 3.7 show examples of such micro-cracks in the two mentioned cases. Micro-cracks above voids located under the polished surface were found to be the most common scenario, and micro cracks were found to be homogeneously distributed in all the observed surface.

A macro-crack, meant as an off-axis crack involving the entire ply thickness and propagating in the fibres direction, formed by means of the accumulation and coalescence of the mentioned micro-cracks, as shown also in Chapter 2 [43]. A similar scenario was

observed by O'Brien [46] concerning the formation of delaminations in composite laminates, occurring by initiation and then coalescence of inclined micro-cracks in the resin reach region between plies.

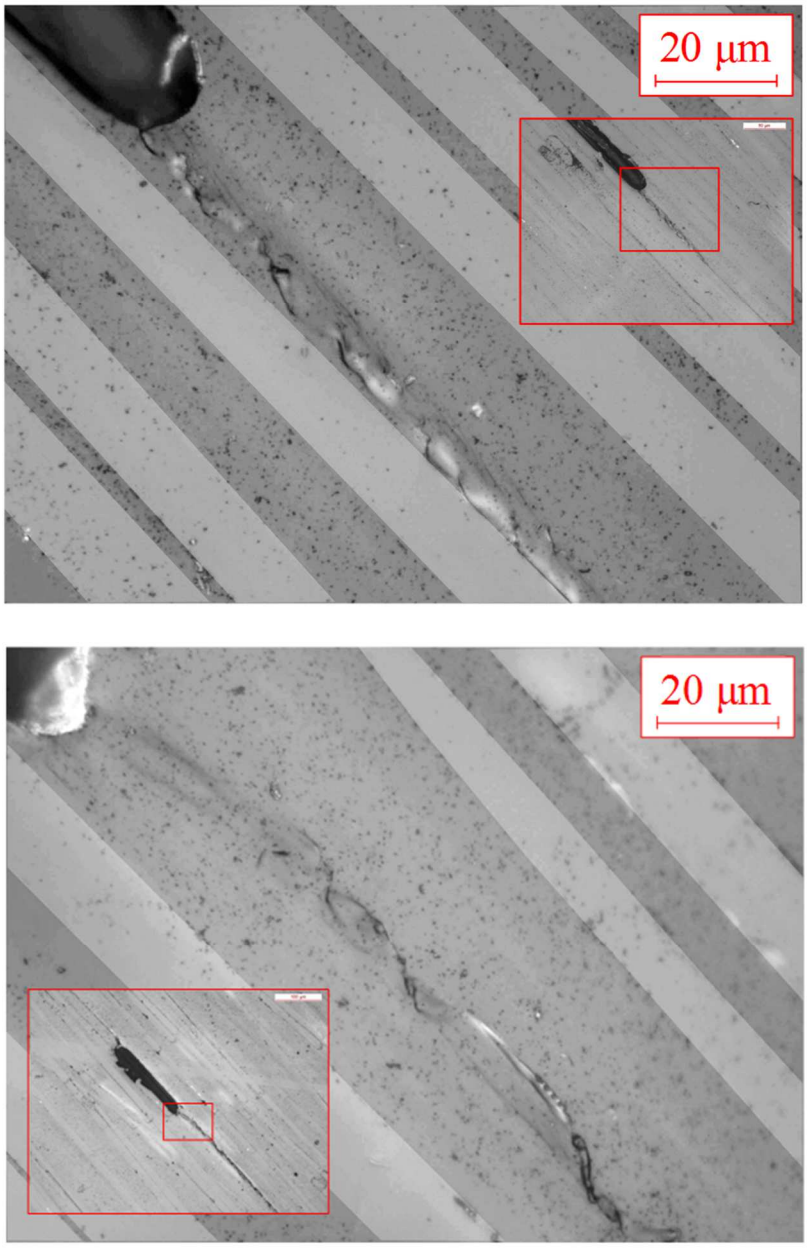

Figure 3.6 – Micro-cracks initiated at void tips.

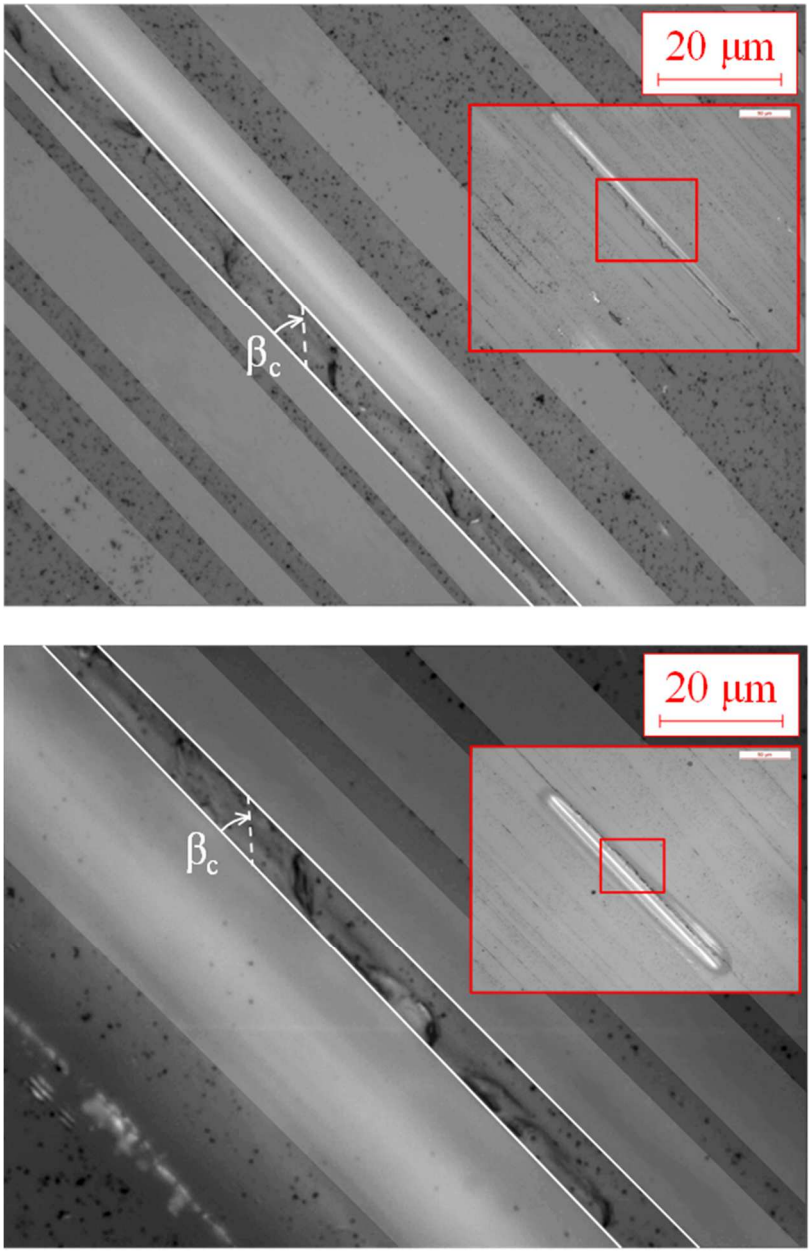

Figure 3.7 – Micro-cracks initiated above voids that lie beneath the polished surface.

The orientation of the *local nucleation plane* (i.e. the plane on which a micro-crack lies) with respect to the fibres direction was compared to the plane perpendicular to the Local Maximum Principal Stress (β_c) evaluated by means of Finite Element Analyses as reported in Appendix A. The FE model was built to reproduce a microstructure with a regular hexagonal fibres array and a void lying beneath the top surface, as in the scenarios shown in Figure 3.7. The angle β_c, resulting in a value of 40.83°, is plotted in Figure 3.7 for the

sake of comparison with the direction of the micro-cracks. The good agreement between the theoretically predicted and actual orientations of the *local nucleation plane* suggests that the initiation of the micro-cracks between the fibres is driven by the LMPS, when the shear stress is high enough, as observed in voids-free specimens in Chapter 2 [43]. As a consequence, it can be concluded that the mechanisms leading to the formation of an off-axis crack (initiation and coalescence of micro-cracks normal to the LMPS) are not affected, qualitatively, by the presence of voids. This allows one to adopt the same crack initiation criterion proposed by Carraro and Quaresimin [41], once the stress concentration at the micro-scale due to the presence of voids is suitably accounted for in the calculation of the LMPS.

Even if voids do not influence the damage mechanisms qualitatively, this does not imply that their presence is not detrimental for the fatigue response of composites. To show this from a quantitative point of view, it is possible to compare the number of zones showing micro-cracks, including also those which have already coalesced in macro-cracks, in a void-free specimen and in a specimen containing voids, as a function of the number of cycles. As reported in Figure 3.8 the number of these regions, counted under the optical microscope, is much larger in the non degassed specimen, highlighting a higher micro-scale damage evolution rate in the presence of voids.

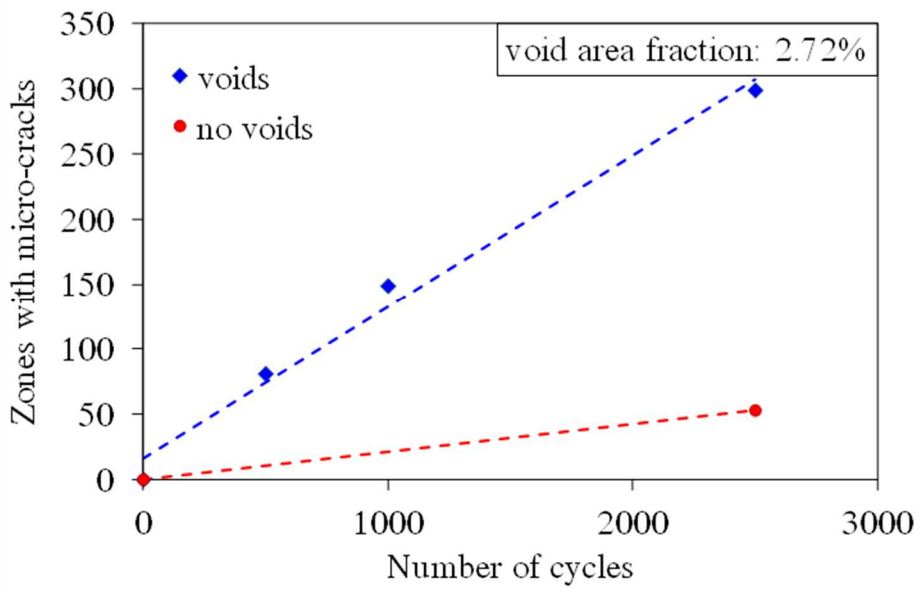

Figure 3.8 – Number of zones showing micro-cracks in a void-free specimen and in a specimen with A_v = 2.72% as a function of the number of cycles.

From a macroscopic point of view, this causes a lower number of cycles for the initiation of macro-cracks. In order to support this conclusion, three specimens without voids (the same specimens studied in Chapter 2 [43]) and three specimens containing voids were tested under three different load levels, corresponding to σ_x = 150, 118 and 82 MPa (σ_2 = 26, 20 and 14 MPa in the 45° plies, respectively).

Specimens were tested with a frequency of 3 Hz under load control. Exploiting the translucency of the glass/epoxy system it was possible to count the macro-cracks initiated during the fatigue tests, as shown in Figure 3.9.

In the early stages of the fatigue life, when the number of off-axis cracks is low and they are far enough from each other, the cycles spent for the initiation of each crack can be considered as an independent fatigue result, thus allowing the statistical distribution of fatigue strength to be accounted for [45]. A number of six cracks per specimen is assumed to be sufficiently high to have statistical validity and sufficiently low to treat the initiation of each crack as an independent event. The number of cycles for the initiation of the first

six macro-cracks in each specimen is shown in Figure 3.10, where a detrimental influence of voids can be observed.

As already mentioned, this is due to a faster evolution of damage at the micro-scale in the form of inclined micro-cracks in the presence of voids, which act as stress concentrators and are therefore preferential sites for the initiation and evolution of micro-scale damage.

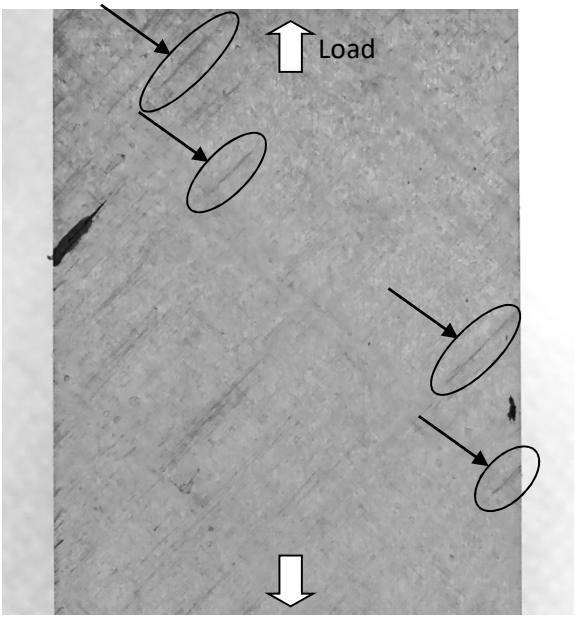

Figure 3.9 – Examples of 45° macro-cracks in the presence of voids (σ_x = 118 MPa, N = 2000 cycles).

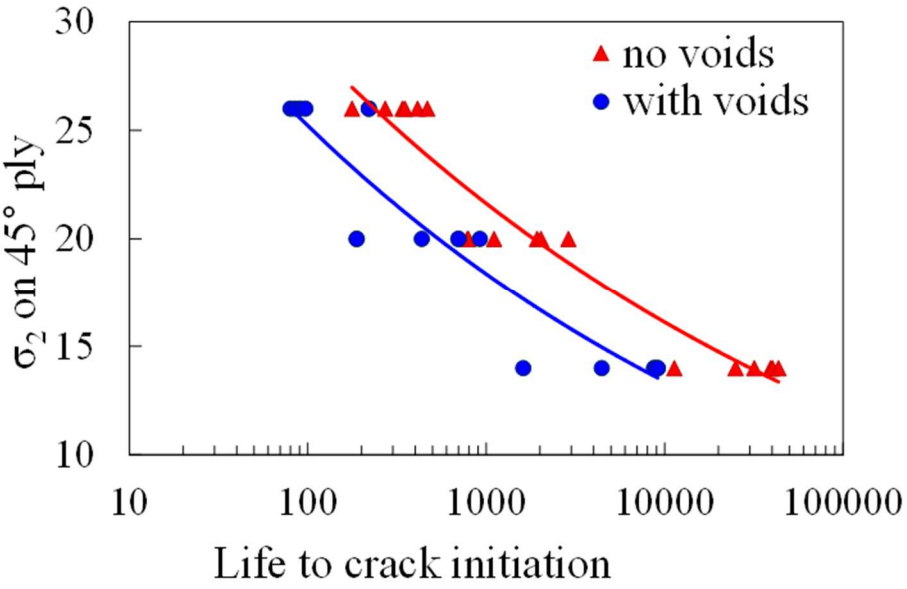

Figure 3.10 – Effect of voids on the initiation of the first cracks.

3.5. Conclusions

The main objective of the present Chapter was to observe the first damage mechanism at the micro-scale in the off-axis plies of a composite laminate containing voids subjected to fatigue load, and to compare it to the damage scenario found in void-free specimens.

To this aim, specimens with lay-up $[45/-45/0]_s$ were produced by infusion moulding without degassing the resin prior to infusion. The voids in the infused laminate were characterised by their global area fraction and by their geometrical features (orientation, diameter, length, aspect ratio).

Careful observations at the optical microscope carried out during fatigue tests revealed that the first damage mechanism at the micro-scale was the initiation of micro-cracks in the matrix between fibres, inclined with respect to the fibres direction. Such micro-cracks were found both close to void tips and above voids that lie beneath the observed surface, in the zones of highest stress concentration. This is the same mechanism previously observed in void-free specimens. It was shown that the orientation of the micro-cracks is normal to the Local Maximum Principal Stress (LMPS) in the matrix, which can therefore be considered

the driving force for damage initiation and evolution at the micro-scale, both in the absence and presence of voids.

These findings suggest that the criterion for fatigue crack initiation recently proposed by the authors based on the LMPS can be applied also to composite components containing voids. However, in the presence of voids the micro-scale damage evolves faster than in the absence of voids, leading to a lower number of cycles for the initiation of macro-cracks, as a result of the magnification of the local stresses due to the voids presence.

Appendix 3.A

With the aim of investigating the orientation of the *local nucleation plane* in the presence of a void, 3-D Finite Element analyses were carried out with Ansys 15.0 software adopting 20 nodes solid elements (SOLID 186). For simplicity, a regular (hexagonal) array of fiber was considered, with a fibre volume fraction of 0.55 (calculated as the ratio between the fibres and the matrix volumes). The geometry of the FE model is shown in Figure 3.A1a. It represents a void lying beneath the top surface, a scenario frequently observed in the tested specimens, leading to the initiation of micro-cracks between the fibres immediately above the void (see Figure 3.7).

Thanks to the elongated shape of the voids, it was possible to analyse a cross section normal to the void major axis, without reproducing the entire 3D geometry which would have needed a much higher computational effort.

A loading condition representative of the multiaxial stress state in the present specimens was simulated (σ_2 = 1 MPa, σ_6 = 1.65 MPa and σ_1 = 2.94 MPa). Periodicity conditions were adopted along the fibres direction. Both resin and glass fibres were treated as isotropic materials, with the following properties: E_{glass} = 74000 MPa, ν_{glass} = 0.25, E_{resin} = 3100 MPa, ν_{resin} = 0.38.

As it can be seen from figure 3.A1, where a contour plot of the LMPS is provided, the presence of the void causes a peak of the LMPS in the matrix between the two fibres positioned above the void. In particular, the highest Local Maximum Principal Stress was found in the matrix at the fibre-matrix interface, in points marked as "A" in Figure 3.A1b. In point A the angle normal to the Local Maximum Principal Stress, β_c, was found to be equal to 40.83° with respect to the fibre orientation.

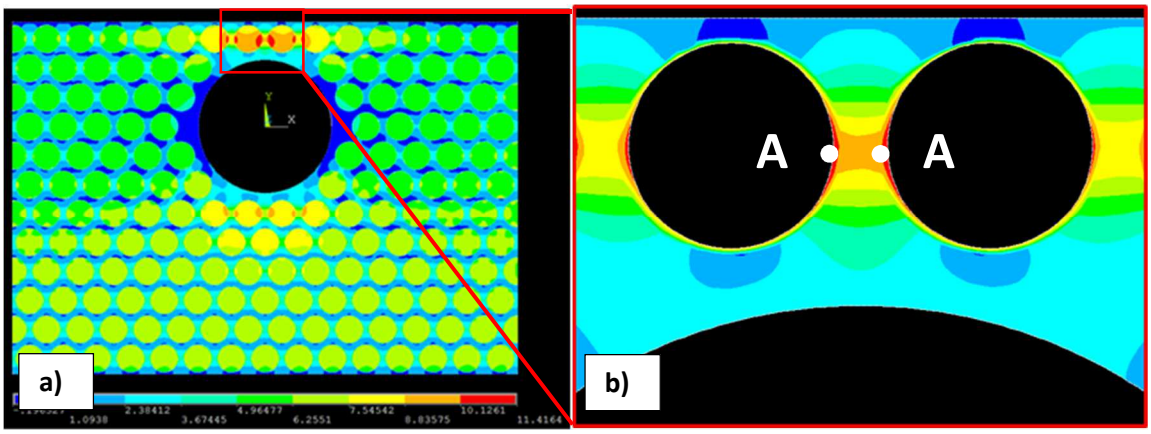

Figure 3.A1 – a) Geometry of the FE model and contour plot of the LMPS in the whole model and b) in the matrix above the void.

References of Chapter 3

[1] Rohatgi V, Patel N, Lee LJ. Experimental Investigation of flow-induced microvoids during impregnation of unidirectional stitched fiberglass mat. Polymer Composites 1996; 17: 161-170.

[2] Abraham D, McIlhagger R. Investigations into various methods of liquid injection to achieve mouldings with minimum void contents and full wet out. Composites Part A – Applied Science and Manufacturing 1998;29A:533-539.

[3] Afendi M, Banks WM, Kirkwood D. Bubble free resin for resin infusion process. Composites Part A – Applied Science and Manufacturing 2005; 36: 739-746.

[4] Kuentzer N, Simacek P, Advani SG, Walsh S. Correlation of void distribution to VARTM manufacturing techniques. Composites Part A – Applied Science and Manufacturing 2007; 38: 802-813.

[5] Olivier P, Cottu JP, Ferret B. Effects of cure cycle pressure and voids on some mechanical properties of carbon/epoxy laminates. Composites 1995; 26: 509-515.

[6] Varna J, Joffe R, Berglund LA, Lundstrom TS. Effect of voids on failure mechanisms in RTM laminates. Composites Science and Technology 1995; 53: 241-249.

[7] Zhu H, Wu B, Li D, Zhang D, Chen Y. Influence of voids on the tensile performance of carbon/epoxy fabric laminates. Journal of Material Science and Technology 2011; 27(1): 69-73.

[8] Huang Y, Varna J, Talreja R. Statistical methodology for assessing manufacturing quality related to transverse cracking in cross-ply laminates. Composites Science and Technology 2014; 95: 100-106.

[9] Carraro PA, Maragoni L, Quaresimin M. Influence of manufacturing-induced defects on damage initiation and propagation in carbon/epoxy NCF laminates. Advanced Manufacturing: Polymer and Composites Science 2015; 1: 44-53.

[10] Tang JM, Lee WI, Springer GS. Effects of Cure pressure on resin flow, voids, and mechanical properties. Journal of Composite Materials 1987; 21: 421-440.

[11] Suarez JC, Molleda F, Guemes A. Void content in carbon fiber/epoxy resin composites and its effects on compressive properties. In: Proceedings of ICCM9 Conference. Madrid, July 1993.

[12] Cinquin J, Triquenaux V, Rouesne Y. Porosity influence on organic composite material mechanical properties'. In: Proceedings of ICCM16 Conference. Kyoto, July, 2007.

[13] Kosmann N, Karsten JM, Schuett M, Schulte K, Fiedler B. Determining the effect of voids in GFRP on the damage behaviour under compression loading using acoustic emission. Composites Part B – Engineering 2015; 70: 184-188.

[14] Hernandez S, Sket F, Gonzales C, Llorca J. Optimization of curing cycle in carbon fiber-reinforced laminates: void distribution and mechanical properties. Advanced Manufacturing: Polymers and Composites Science 2013; 85: 73-82.

[15] Liu L, Zhang BM, Wang DF, Wu J. Effects of cure cycles on void content and mechanical properties of composite laminates. Composite Structures 2006; 73: 303-309.

[16] Chambers AR, Earl JS, Squires CA, Suhot MA. The effect of voids on the flexural fatigue performance of unidirectional carbon fibre composites developed for wind turbine applications. International Journal of Fatigue 2006; 28: 1389-1398.

[17] de Almeida SFM, Neto ZSN. Effect of void content on the strength of composite laminates. Composite Structures 1994; 28: 139-148.

[18] Hagstrand PO, Bonjour F, Manson JAE. The influence of void content on the structural flexural performance of unidirectional glass fibre reinforced polypropylene composites. Composites Part A – Applied Science and Manufacturing 2005; 36: 705-714.

[19] Yoshida H, Ogasa T, Hayashi R. Statistical approach to the relationship between ILSS and void content of CFRP. Composites Science and Technology 1986; 25: 3-18.

[20] Olivier PA, Mascaro B, Margueres P, Collombet F. CFRP with voids: ultrasonic characterization of localized porosity, acceptance criteria and mechanical characteristics. In: Proceedings of ICCM16 Conference. Kyoto, July, 2007.

[21] Thomason JL. The interface region in glass fibre-reinforced epoxy resin composites: 1. Sample preparation, void content and interfacial strength. Composites 1995; 26: 467-475.

[22] Wisnom MR, Reynolds T, Gwilliam N. Reduction in interlaminar shear strength by discrete and distributed voids. Composites Science and Technology 1996; 56: 93-101.

[23] Goodwin AA, Howe CA, Paton RJ. The role of voids in reducing the interlaminar shear strength of RTM laminates. In: Proceedings of ICCM11 Conference. Gold Coast, July, 1997.

[24] Costa ML, de Almeida SFM, Rezende MC. The influence of porosity on the interlaminar shear strength of carbon-epoxy and carbon-bismaleimide fabric laminates. Composites Science and Technology 2001; 61: 2101-2108.

[25] Bureau MN, Denault J. Fatigue resistance of continuous glass fiber-polypropylene composites consolidation dependence. Composites Science and Technology 2004; 64: 1785-1794.

[26] Zhu H, Li D, Zhang D, Wu B, Chen Y. Influence of voids on interlaminar shear strength of carbon/epoxy laminates. Transactions of Nonferrous Metals Society of China 2009; 19: 470-475.

[27] Asp LE, Brandt F. Effects of pores and voids on the interlaminar delamination toughness of a carbon/epoxy composite. In: Proceedings of ICCM11 Conference. Gold Coast, July, 1997.

[28] Dill CW, Tipton SM, Glaessge EH, Branscum KD. Fatigue strength reduction imposed by porosity in a fiberglass composite. In: Damage Detection in Composite Materials, ASTM STP 1128, J. E. Masters, Ed., American Society for Testing and Materials, Philadelphia, 1992, pp. 152-162.

[29] Schmidt F, Rheinfurt M, Horst P, Busse G. Multiaxial fatigue behaviour of GFRP with evenly distributed or accumulated voids monitored by various NDT methodologies. International Journal of Fatigue 2012; 43: 207-216.

[30] Gehrig F, Mannov E, Schulte K. Degradation of NCF-epoxy composites containing voids. In: Proceedings of ICCM 17 Conference. Edinburgh, July, 2009.

[31] Suhot MA, Chambers AR. The effect of voids on the flexural fatigue performance of unidirectional carbon fibre composites. In: Proceedings of ICCM16 Conference. Kyoto, July, 2007.

[32] Lambert J, Chambers AR, Sinclair I, Spearing SM. 3D damage characterization and the role of voids in the fatigue of wind turbine blade materials. Composites Science and Technology 2012; 72: 337-343.

[33] Seon G, Makeev A, Nikishkov Y, Lee E. Effects of defects on interlaminar tensile fatigue behavior of carbon/epoxy composites. Composites Science and Technology 2013; 89: 194-201.

[34] Hapke J, Gehrig F, Huber N, Schulte K, Lilleodden ET. Compressive failure of UD-CFRP containing void defects: In situ SEM microanalysis. Composites Science and Technology 2011; 71: 1242-1249.

[35] Scott AE, Sinclair I, Spearing SM, Mavrogordato MN, Hepples W. Influence of voids on damage mechanisms in carbon/epoxy composites determined via high resolution computed tomography. Composites Science and Technology 2014; 90: 147-153.

[36] McMillan AJ. Material strength knock-down resulting from multiple randomly positioned voids. Journal of Reinforced Plastics and Composites 2012; 32: 13-28.

[37] Huang H, Talreja R. Effects of void geometry on elastic properties of unidirectional fiber reinforced composites. Composites Science and Technology 2005; 65: 1964-1981.

[38] Van Den Broucke B, Hegemann J, Das R, Oster R, Hackl K, Stößel R. Modelling of textile composites using finite element tools and investigation of the influence of porosity on mechanical properties. In: Proceedings of Symposium 'Finite Element Modelling of Textiles and Textile Composites', St Petersburg, September 2007, 1–7.

[39] Vajari DA, Gonzalez C, Llorca J, Legarth BN. A numerical study of the influence of microvoids in the trensverse mechanical response of unidirectional composites. Composites Science and Technology 2014; 97: 46-54.

[40] Ricotta M, Quaresimin M, Talreja R. Mode I Strain Energy Release Rate in composite laminates in the presence of voids. Composites Science and Technology 2008; 68: 2616-2623.

[41] Carraro PA, Quaresimin M. A damage based model for crack initiation in unidirectional composites under multiaxial cyclic loading. Composites Science and Technology 2014; 99: 154-163.

[42] Quaresimin M, Carraro PA. Damage initiation and evolution in glass/epoxy tubes subjected to combined tension-torsion fatigue loading. International Journal of Fatigue 2014; 63: 25-35.

[43] Quaresimin M, Carraro PA, Maragoni L. Early stage damage in off-axis plies under fatigue loadings. Composites Science and Technology 2016; 128: 147-154.

[44] Nikishkov Y, Airoldi L, Makeev A. Measurement of voids in composites by X-ray Computed Tomography. Composites Science and Technology 2013; 89: 89–97.

[45] Quaresmin M, Carraro PA, Mikkelsen LP, Lucato N, Vivian L, Bronsted P, Sorensen BF, Varna J, Talreja R. Damage evolution under cyclic multiaxial stress state: a comparative analysis between glass/epoxy laminates and tubes. Composites Part B – Engineering 2014; 61: 282-290.

[46] O'Brien TK. Composite Interlaminar Shear Fracture Toughness, G_{IIC}: Shear Measurement or Sheer Myth?. ASTM STP 1330, Fatigue and Fracture, Ed. R.B.Bucinell, ASTM West Conshohocken, PA, 1998: 3-18

.

4

Fatigue behaviour of composite laminates in the presence of voids

Motivation

As shown in Chapter 3, although voids did not alter the micro-damage mechanisms that lead to fatigue crack formation, they induce damage in a larger number of regions, leading to earlier crack formation compared to a void-free scenario. To investigate more in depth the effect of voids on the fatigue performances, an extensive experimental campaign was carried out on both void-free and porous composite laminates.

Abstract

In the present Chapter, glass/epoxy panels with stacking sequence $[0/90_2]_S$ *and* $[0/45_2/0/-45_2]_S$ *were produced by vacuum resin infusion. Using different process parameters, which may lead to cost saving, also the presence of porosity was obtained in the laminates. Specimens were tested under uniaxial tensile fatigue loadings, monitoring the initiation and propagation of cracks in the off-axis plies. The performance of the material and the effect of porosity were evaluated in terms of life to crack initiation, crack growth rate, crack density evolution and stiffness degradation. A detrimental effect of the porosity was found even for a very low voids content, highlighting the importance of properly accounting for their presence in the design of composite parts.*

4.1. Introduction

In the recent years, the use of composite materials for structural components has been growing sensibly in many industrial fields, thanks to their specific mechanical properties. One of the factors that is still limiting the further employment of such materials is their cost, a large part of which is due to the manufacturing process. Expensive manufacturing processes are normally needed to maximize the mechanical properties, by means of increasing the fibre volume fraction and keeping the defects content low. To maximize the fibre volume fraction, adding an external pressure is beneficial thanks to the inherent compressibility of the fibre bundles. To decrease the defect content is a particularly difficult objective to accomplish, especially in terms of void content. Voids may form from air entrapped between pre-preg plies during the stacking operation, from the release of volatile molecules during the resin cure, and, in processes that use liquid resin, from a non-complete degassing operation and from different velocities of the resin in the fibre bundles and the channels between them.

The mechanical properties of composite laminates containing voids can be sensibly lower compared to the void-free condition.

Most of the work in the literature on this matter initially dealt with static loading conditions. Voids were shown to affect the tensile [Appendix A,1-5], compressive [6-10] and bending [1,11-15] behaviour of unidirectional, multidirectional and woven laminates, as well as the out-of-plane properties such as the inter-laminar shear strength [1,6,11,15-24] and fracture toughness [5,18,25]. As highlighted in [5,9,18,26-28], the decrease in mechanical performances was sometimes related to a change in the damage mechanism in the presence of voids. The reader is referred to Appendix A, Chapter 3 and Refs. [5,29,30] for more extended reviews on these subjects. With the exception of a few early works, the interest in the influence of manufacturing-induced voids on the fatigue behaviour of composite

materials has been growing only recently despite its wide importance. In many cases, in fact, composites are used in dynamic structures where lightweight materials are particularly desirable to increase efficiency (such as in wind turbine blades) and decrease energy consumption (aerospace, automotive). In those circumstances, components are subjected to variable rather than static loads.

Dill and co-authors [26] tested glass/epoxy pre-preg fabrics under tensile fatigue. Different void contents (0.11-2.66% in volume) were obtained using different vacuum and pressure in the autoclave. They observed a large reduction in the life to final failure and a higher experimental variability in the presence of voids.

De Almeida and Neto [13] intentionally induced the presence of voids (1-6%) in carbon/epoxy pre-preg fabric composites by specific modifications of the mould, and found a critical decrease in the life to final failure under flexural fatigue when the void content exceeded a certain threshold (~3%).

Bureau and Denault [23] produced woven glass/polypropylene laminates using different process parameters. Flexural fatigue tests showed a general decrease of the life to final failure and increase in the stiffness drop in the presence of porosity. However, a clear relationship between the performances and the void content (1-10%) could not be found, since the process parameters altered also the degree of crystallinity, the size of the crystals, and the fibre dispersion.

Chambers et al. [12] carried out flexural fatigue tests on 0° unidirectional SPRINT® carbon/epoxy specimens with different void levels (1.6-3.1%), achieved by varying the vacuum bag pressure. Shorter life to final failure and larger stiffness degradation were found for larger void contents. However, they suggested that the failure is driven by a large defect in a critical location rather than the average porosity content.

Gehrig and co-authors [31] performed axial fatigue tests on glass/epoxy NCF laminates, whose porosity level was varied (0-8.8%) by introducing air through a bypass during the infusion. Large voids were obtained, mainly the in resin-rich areas. The life to final failure was found to decrease in the presence of voids for tension-tension and compression-compression loadings, whereas a larger life to final failure was obtained for specimens with voids for fully reversed fatigue loads (R=-1). The reason for such a behaviour was not investigated in depth.

A detailed void characterization by means of μ-CT was done by Lambert et al. [32] on glass/epoxy pre-preg laminates with $[0/45/-45]_{3S}$ stacking sequence, with a ply of randomly oriented fibres between each group. μ-CT was also used to monitor damage evolution under fully reversed fatigue loads, showing the involvement of voids in the formation of cracks and delaminations. A correlation between the life to final failure and the largest void in a critical ply was highlighted.

Schmidt and co-authors [33] tested glass/epoxy tubes with $[0/45/90/-45]_S$ lay-up under tension/torsion loadings with a load ratio R = -1. Small distributed voids and large accumulated voids were obtained, respectively, by varying RTM process parameters and by simulating a leakage in the mould. The crack density evolution and the stiffness degradation were found not to be clearly dependent on the porosity. On the contrary, the final failure, which was observed to initiate from a local large damage, occurred earlier in the presence of voids.

Seon et al. [34] found that also the inter-laminar tensile fatigue strength appears to be related to the presence of a large void in a critical location in unidirectional carbon/epoxy specimens.

Protz and co-authors [35] found almost no influence of voids on the life to final failure of glass/epoxy NCF $[0/45/90/-45]_S$ laminates made with vacuum resin infusion (void contents: 0-4.5%).

A more detailed work on the effect of large, inter-tow voids on the damage evolution under tensile fatigue behaviour of $[0/-45/90/45]_{2S}$ carbon/epoxy NCF laminates was carried out by Sisodia et al. [36]. Laminates were manufactured by RTM and wet lay-up to obtain a wide range of void contents (0.8-20%) and tested with a maximum cyclic stress equal to 60% of the static strength. They found a very significant influence of the presence of voids in terms of the life to final failure compared to the reduction in static strength and stiffness, highlighting the limits of using static tests only as a means for quality control. For two void contents (0.8 and 3%), they analysed more in details the fatigue damage evolution, showing that voids appear to influence more the initiation of the first cracks than the crack density saturation. Moreover, a larger influence of voids on crack initiation was found in the 90° ply compared to the 45° one.

The importance of studying the influence of manufacturing-induced voids on the mechanical properties of composites is twofold. In fields where the highest mechanical properties are needed, such as aerospace, even if a low global void content is obtained, voids can be concentrated in some regions due to the geometrical shape of the component, and it is necessary to account for their presence in particular to predict, and therefore avoid, the initiation of damage. In other fields a compromise between mechanical performances and costs is to be sought. In these cases, the knowledge of the effect of voids on the long-term performances can be extremely useful in combination with the relations between manufacturing costs and void content, to find the process parameters that maximize the performance/cost ratio.

The performance of a structural component can be evaluated in different ways, depending on how the failure is defined. In composite laminates made of unidirectional (UD) plies the fatigue damage evolution involves, in general, different stages (see, for instance, Refs [37-44]). The first event of damage is usually represented by the initiation of cracks in the off-axis plies. Those cracks propagate and new ones initiate as the number of cycles increases, until the crack density saturates. During this stage, the stiffness of the laminate sensibly decreases. When the crack density is approaching the saturation condition, delaminations initiate and then grow. Eventually, the final separation of the laminate, involving fibre breakage, takes place.

In this complex damage scenario, failure can be variously defined as the occurrence of the first damage event (e.g.: the initiation of the first off-axis crack), as exceeding a certain stiffness drop, which means the presence of a specific crack density and/or delamination length, or as the occurrence of the final separation. Voids may influence differently the performances of a composite laminate depending on how failure is defined.

In the present Chapter, the attention is focused on the influence of some infusion process parameters on the presence of voids and their effect on the early stages of damage evolution in composite laminates made of UD plies. In Chapter 3 it was already reported how the life to crack initiation was reduced by the presence of voids in $[0/45/-45]_S$ laminates, as a consequence of a faster evolution of the micro-scale damage in the form of matrix micro-cracks [29]. In this Chapter, the analysis is extended to the crack propagation and multiplication phenomena, providing quantitative indications on the voids-performances relation.

Glass/epoxy laminates with $[0/90_2]_S$ and $[0/45_2/0/-45_2]_S$ stacking sequences were produced by vacuum resin infusion. Rather than introducing voids by purposely misleading the process (e.g.: by creating a leakage in the vacuum bag), different process parameters were

used to explore possible ways to reduce the manufacturing cost. Such less-expensive alternatives lead, on the other hand, to the presence of voids in the laminates. The influence of voids on the long-term performances of the laminates was evaluated in terms of life to fatigue crack initiation, crack growth rate, crack density evolution and stiffness drop.

4.2. Specimens manufacturing

As shown in Chapter2, Chapter 3, and Refs. [29,45,46], the damage mechanisms at the micro scale that lead to the formation an off-axis crack under cyclic loading appears to be different in the presence of sufficiently high shear compared to pure transverse tension [47]. To observe the influence of manufacturing induced voids on the fatigue performance in both these scenarios, laminates with two stacking sequences, namely $[0/90_2]_S$ and $[0/45_2/0/-45_2]_S$, were produced by vacuum resin infusion (VARTM). Three $[0/90_2]_S$ and two $[0/45_2/0/-45_2]_S$ laminates were manufactured varying some important process parameters, with the aim to obtain void contents that can result from possible ways to reduce manufacturing costs.

Unidirectional glass fibres UT-E500 by Gurit and epoxy resin RIMR-235 (hardener RIMH-235) by Momentive were used, respectively, as reinforcement and matrix materials. The dimensions of all the produced panels were 300x250 mm.

For the $[0/90_2]_S$ panels, 400 g of resin and 134 g of hardener were mixed for 3 minutes at 300 rpm with a DISPERMAT TU shear blender from VMA-Getzman. Then, for the first panel, an extensive degassing of the resin (at 15 mbar for 20 minutes) was carried out, to consistently reduce the amount of air entrapped by the resin during the mixing. The infusion was then carried out by keeping the outlet pressure (p_{out} = 15 mbar) constant, while the inlet pressure was continuously adjusted to control the resin speed and ensure the best impregnation of the dry fibres. A second laminate was manufactured as done for the first

one, but without degassing the resin after mixing, saving process time (20 minutes for a 6-plies 300x250 mm laminate). A third laminate was then produced without degassing the resin and keeping the inlet pressure constant (p_{in} = 1 bar) through all the infusion, saving process time and the cost of controlling the resin flow. All the panels were cured at room temperature for three days and then post-cured in an oven for 12 hours at 60°C. The $[0/45_2/0/-45_2]_S$ laminates were produced following the same processes used for the first and second $[0/90_2]_S$, using 600 g of resin and 201 g of hardener, mixed for 5 minutes at 300 rpm. Degassing was carried out only for the first panel, for 35 minutes at 15 mbar. The third processing conditions were not used for this stacking sequence due to the difficulties in monitoring damage evolution in such conditions, as shown later on in paragraph 4.5.

The fibre volume fraction V_f was measured by micrographic observations on more than 30 fields for each stacking sequence, and found to be around 55% for both the lay-ups. From the infused panels, 23 mm wide and 200 mm long specimens were cut, with their longitudinal direction parallel to the direction of the resin flow. The thickness of the laminates was 2 mm and 3.8 mm for the cross-ply and $[0/45_2/0/-45_2]_S$ laminates, respectively, without significant variations with the void content. The edges were polished starting with P180 sandpaper down to 0.1 μm SiO_2 solution, both to avoid crack initiation from edge defects due to the cut and to quantify the void content (see paragraph 4.3). 30 mm end tabs were bonded thus obtaining a gage length of 140 mm. However, damage was observed and quantified within a 60 mm long region positioned across the specimens mid-length.

The in-plane elastic properties of the UD plies were measured by means of static tests on five 0°, 45° and 90° specimens and are listed in Table 4.1. As reported later on in paragraph 4.5, the influence of porosity on the elastic modulus of the laminates was found to be negligible.

Table 4.1 – Material properties of the infused UD laminates.

	E_1 [MPa]	E_2 [MPa]	$E_{45°}$ [MPa]	ν_{12}	G_{12} [MPa]
Average	48830	14070	14750	0.308	5200
c.o.v.	0.19%	1.49%	0.72%	1.20%	-

4.3. Characterization of void content

As usually found in the presence of unidirectional reinforcements, the large majority of manufacturing-induced voids in the produced laminates had approximately circular section and was elongated along the fibres direction ("cigar-like" shape), as shown in Chapter 3 and Refs. [29,32,48]. Consequently, void content can be reasonably quantified from micrographs taken perpendicularly to fibres direction in the ply of interest. Micrographic images covering the whole length of the observation areas (60 mm) were taken on both edges of all the tested specimens. Void content measurements were carried out for the 90° ply in the $[0/90_2]_S$ laminates and in the -45° ply in the $[0/45_2/0/-45_2]_S$. The off-axis plies are indeed those of interest in the present work since fatigue cracks initiate and propagate within them. The porosity in the specimens was characterised by the void area fraction A_v and the average and maximum void size. Thanks to their shape, the size of each void could be quantified by its equivalent diameter D_v, defined as the diameter of a circle with the same area as the actual void section. Both the average $D_{v,av}$ and its highest values ($D_{v,max}$) were calculated. The information on void geometry from 2-D images is limited compared to μ-CT scans, but given the large number of images analysed is believed to be reliable.

No voids were detected in the panels produced with optimal process parameters for both the stacking sequences. $[0/90_2]_S$ specimens obtained without degassing the resin had A_v = 0.34% and $D_{v,av}$ = 43 μm (Figure 4.1), whereas a much larger void content was present when the inlet pressure was kept equal to 1 bar during all the infusion in addition to not

degassing the resin (A_v = 6.7% and $D_{v,av}$ = 45 µm, Figure 4.2). For the $[0/45_2/0/-45_2]_S$ panel manufactured without degassing the resin, A_v = 1.07% and $D_{v,av}$ = 49 µm were obtained in the -45° plies, whereas almost no voids were observed in the 45° ply on the mould side (which the side from which the specimens could be observed, thanks to its smooth surface). Voids were homogeneously distributed along the length of the $[0/90_2]_S$ specimens, whereas in the $[0/45_2/0/-45_2]_S$ panel they were found to be aggregated in regular locations, probably due to a sort of periodicity in the relative locations of the plies during the stacking operation. The elongated cigar-like shape of the voids can be deduced by those present in the 0° plies in Figures 4.2 and 4.3. The probability density function (PDF) of the voids diameter in the specimens tested is reported in Figure 4.4. It can be seen that, even though the specimens with A_v = 0.34% and 6.7% have a very similar value of the average diameter, larger voids were present in those with a higher voids content. As already mentioned, it can also be observed that a slightly higher average diameter is obtained for the voids in the -45° ply, but the larger voids are similar to those relevant to the cross-ply laminates with Av = 0.34%.

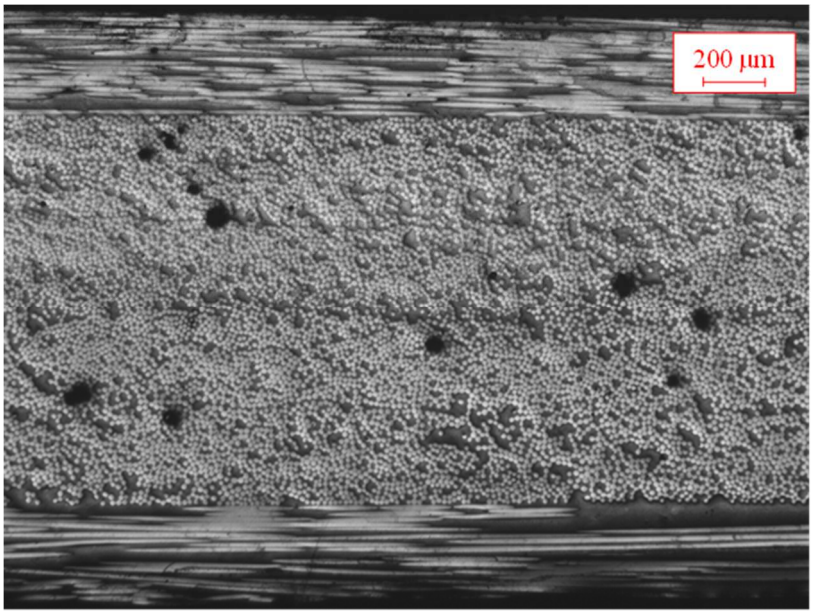

Figure 4.1 – Voids in the $[0/90_2]_S$ panel produced without resin degassing and controlled inlet pressure.

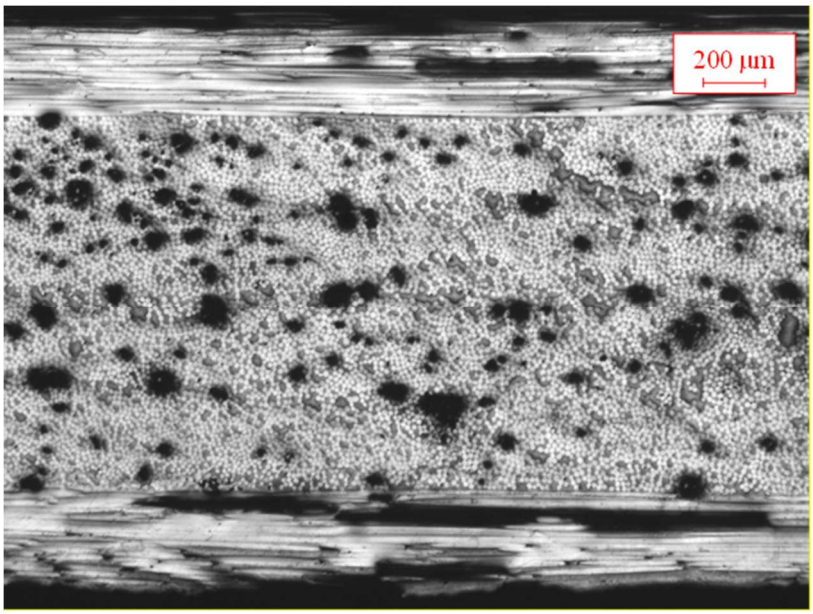

Figure 4.2 – Voids in the $[0/90_2]_S$ panel produced without resin degassing and with inlet pressure of 1 bar.

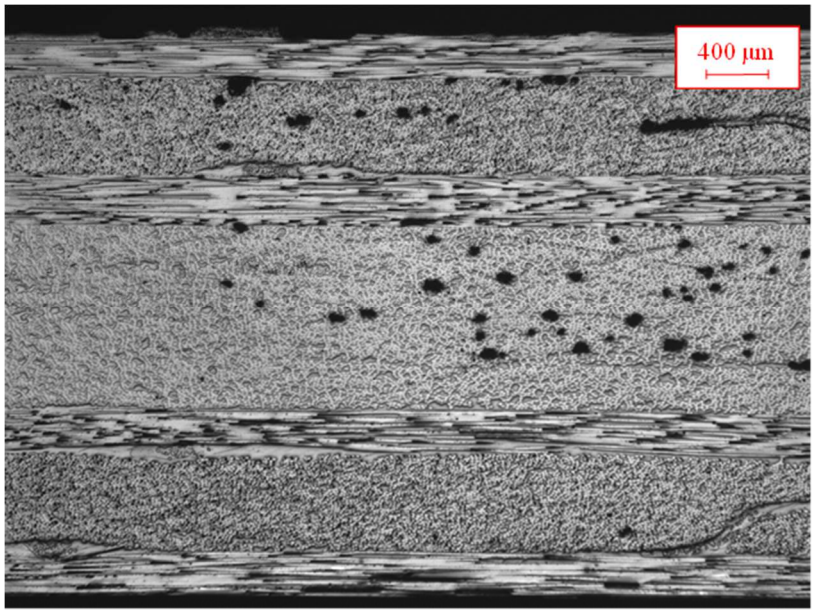

Figure 4.3 – Voids in the $[0/45_2/0/-45_2]_S$ panel produced without resin degassing and controlled inlet pressure.

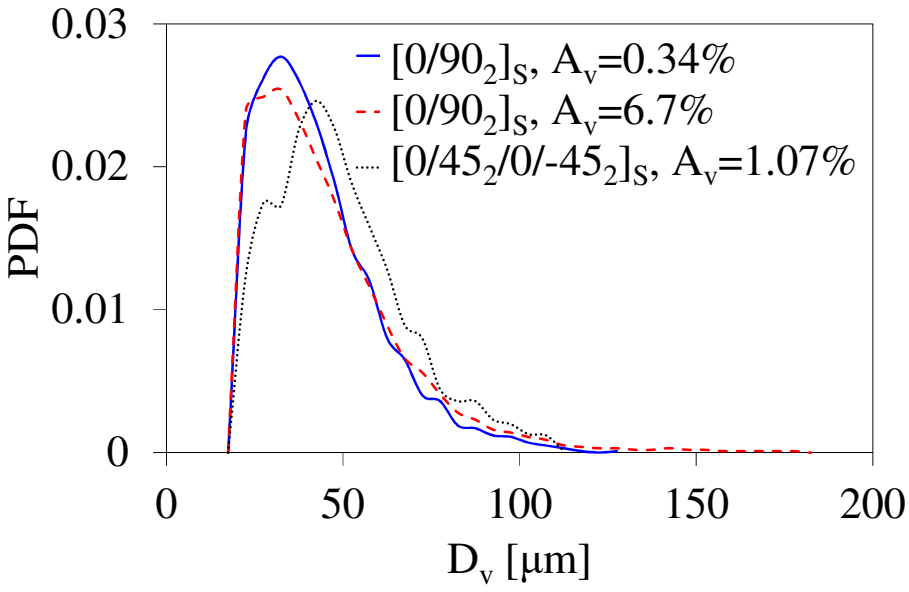

Figure 4.4 – Probability density function (PDF) of the voids diameter.

4.4. Experimental methods

The specimens were tested under a cyclic uniaxial tensile load by means of a MTS 858 hydraulic machine. Tests were carried out in load control, with a load ratio (minimum to maximum cyclic load) of 0.05. Frequencies of 10 Hz and 4 Hz were used, respectively, for $[0/90_2]_S$ and $[0/45_2/0/-45_2]_S$ specimens. A lower frequency was employed in the latter case to avoid heating up due to the presence of a large shear stress in the 45° plies. Loads corresponding to a global tensile stress σ_x of 50, 60, 70 and 80 MPa were applied to the $[0/90_2]_S$ specimens (tests at 80 MPa were not performed on the third panel), whereas $[0/45_2/0/-45_2]_S$ specimens were tested under global tensile stresses of 100, 110, 120, 130 MPa. An axial extensometer MTS632.29F-30 with a calibrated length of 25 mm was mounted on all the specimens to monitor their stiffness throughout the fatigue life.

To monitor damage evolution, consisting of the initiation and propagation of cracks in the off-axis plies, pictures were periodically taken to the specimens during the tests. The glass/epoxy system being transparent, cracks appear as dark lines. To automate the image acquisition, a system was developed in-house with LabView®, connecting the testing

machine to a linear camera (Basler raL4096-24gm) that runs on a rail mounted in front of the specimen (Figure 4.5). At regular intervals the fatigue test pauses, and the camera, which starts in a steady position, scans the specimen. Once the image is saved and the camera returns to its starting position, the fatigue test continues. To help the detection of the cracks, a light source was placed behind the specimens. All the specimens were placed on the machine with their mould-side facing the camera, since the opposite side was characterised by a rough surface due to the presence of the peel ply, which considerably reduces the detectability of the cracks from that side.

From the pictures, the crack initiation and growth could be analysed. To automate also this procedure, an image analysis tool, based on Gabor filter (as in [49]), was developed with Matlab®. An example of image processing is shown in Figure 4.6. The length of the observation area was 60 mm.

Tests for each load level were repeated twice, with the exception of σ_x = 50 MPa for the void-free cross-ply laminates, given the long duration of the test.

For the $[0/45_2/0/-45_2]_S$ laminates, the 45° close to the mould-side was void-free, as previously mentioned, and cracks in the 45° ply close to the peel-ply side were very hard to detect, in particular in the presence of voids. As the focus of the present Chapter is to investigate the effect of voids on the fatigue performances, only the cracks in the -45° ply will be reported for the $[0/45_2/0/-45_2]_S$ laminates.

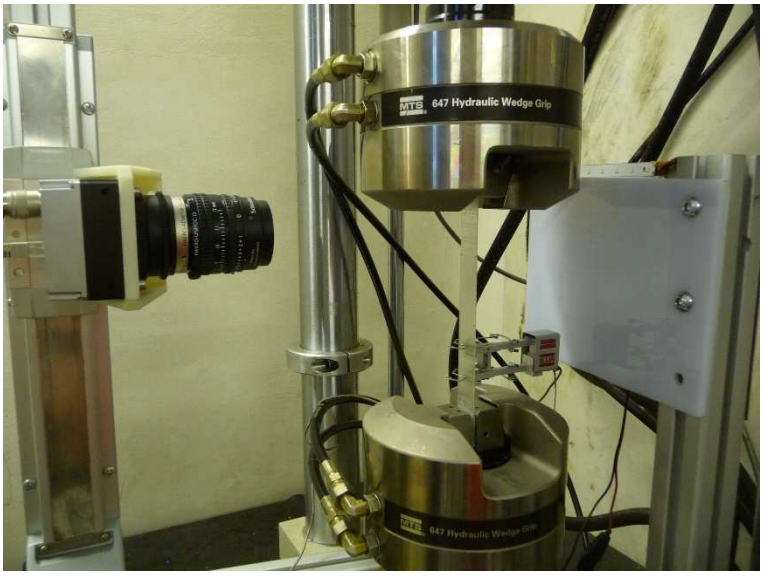

Figure 4.5 – Experimental setup.

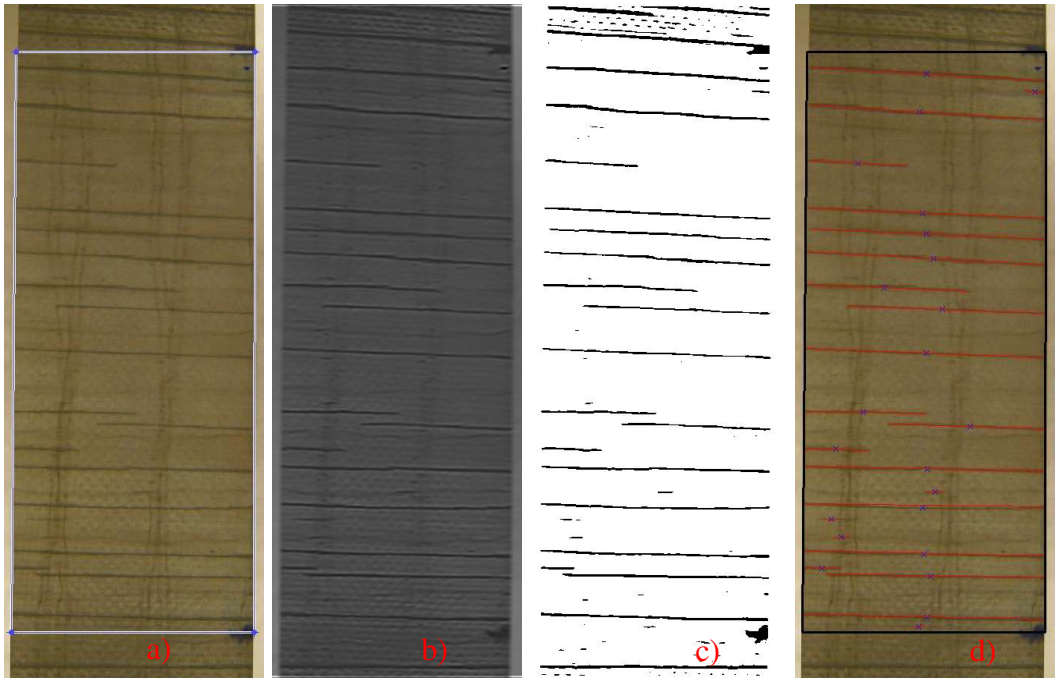

Figure 4.6 – Example of image processing to detect cracks and quantify crack density: a) observation area, b) Gabor filter, c) binarization, d) detected cracks.

4.5. Fatigue test results

As already mentioned, the first observable event of damage in multidirectional laminates

subjected to cyclic loading is the initiation of cracks in the off-axis plies. As the number of cycles increases, new cracks initiate and those already present propagate. For both $[0/90_2]_S$ and $[0/45_2/0/-45_2]_S$ stacking sequences, cracks were observed to initiate both at the edges and in the bulk regions of the specimens, and to stably propagate along the fibres direction. The influence of porosity on the fatigue performances of the laminates were evaluated in terms of the life to crack initiation, crack growth rate, crack density evolution and stiffness degradation. The $[0/90_2]_S$ specimens produced without degassing the resin and with p_{in} = 1 bar were characterised by a very high opacity, which made it particularly hard to detect crack propagation and multiplication. For this reason, only life to crack initiation data were recorded for those specimens.

S-N curves for the first cracks initiation are reported in Figures 4.7 and 4.8 in terms of global applied stress σ_x. The first six cracks for each specimen were taken into account, as they initiated far enough from each other to be considered as independent events [41,42].

It is possible to observe a dramatic effect of the presence of voids on the life to crack initiation, with an average life reduction of 80% for A_v = 0.34%, 98% for A_v = 6.7% ($[0/90_2]_S$), and 65% for A_v = 1.07% ($[0/45_2/0/-45_2]_S$). The influence of voids did not appear to sensibly depend on the load level for both the stacking sequences. The larger effect of voids for the $[0/90_2]_S$ lay-up compared to $[0/45_2/0/-45_2]_S$ is in line with the findings reported in [36].

The influence of voids on the first cracks initiation was documented by micrographs taken on the polished edges of the specimens in correspondence of locations where cracks were seen to initiate at or close to the edges. Figures 4.9a) and b) clearly show off-axis cracks initiated in a section in which one or more voids were present. In addition, some partial cracks, not propagated through the entire ply thickness, can be observed in correspondence of neighbouring voids, clearly highlighting the crucial role of the porosity in the crack

initiation process.

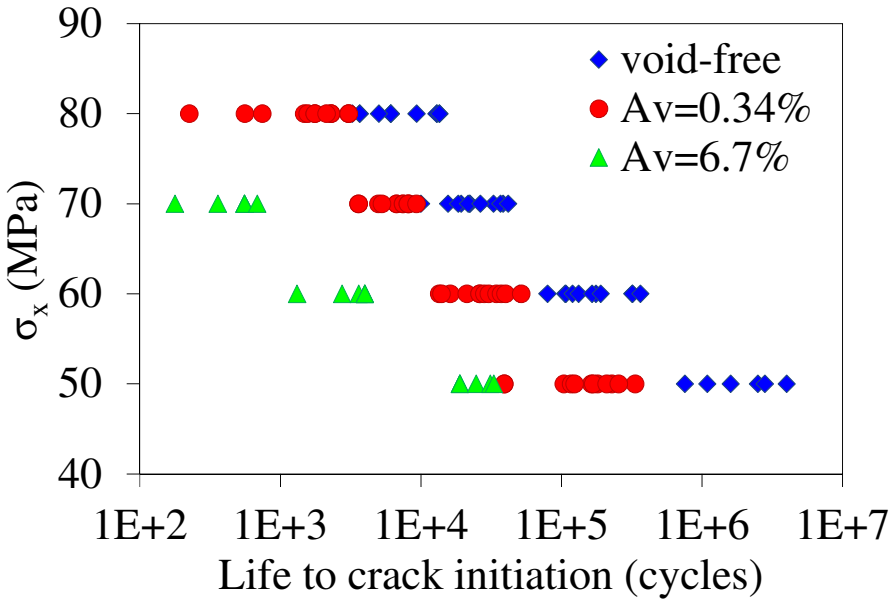

Figure 4.7 – Influence of voids on life to crack initiation for $[0/90_2]_S$ laminates.

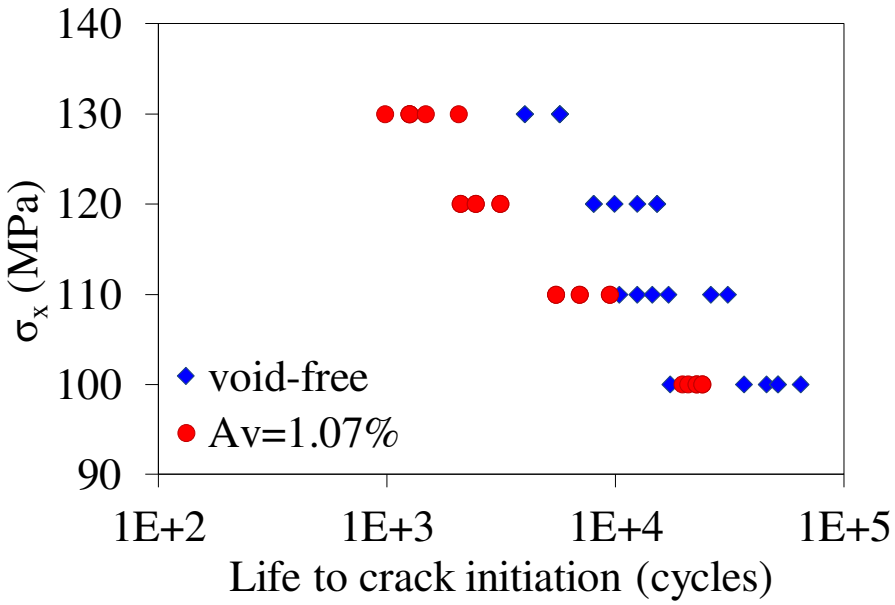

Figure 4.8 – Influence of voids on life to crack initiation for $[0/45_2/0/-45_2]_S$ laminates.

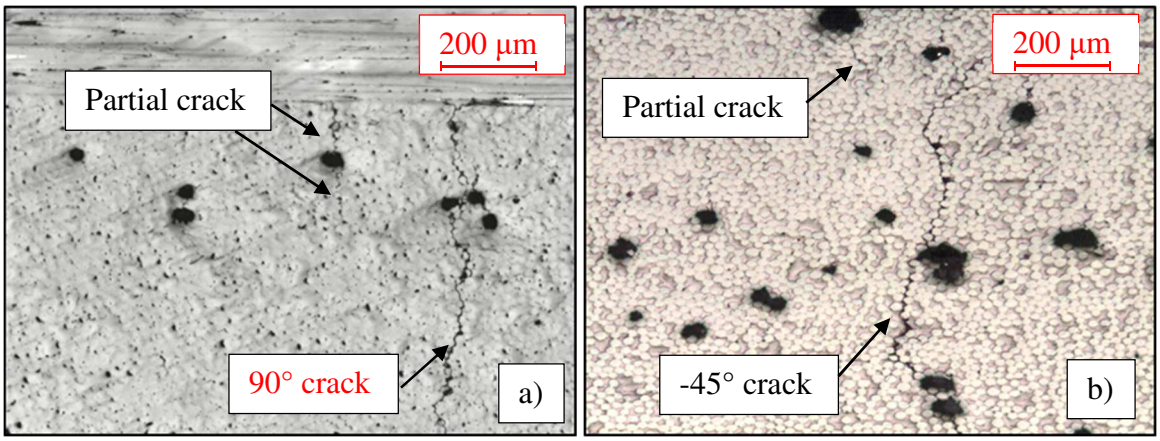

Figure 4.9 – Edge micrographs of a) $[0/90_2]_S$ and b) $[0/45_2/0/-45_2]_S$ laminates with off-axis cracks.

The first independent cracks in the off-axis plies were found to propagate with an approximately constant rate along the fibres direction, as shown in the crack propagation curves of Figures 4.10a) and b), where the slope of the straight lines represents the crack growth rate (CGR). This phenomenon, known as *steady state* propagation, is due to the fact that, as far as cracks are longer than approximately two times the layer thickness and the crack density is low, the Energy Release Rate (ERR) is independent of the crack length [43, 44, 50].

The mode I and II components of the ERR (G_I and G_{II}) were calculated with the approach proposed in [44], with the aid of linear elastic FE analyses. The commercial code ANSYS 15 was adopted for this purpose, using 20 nodes brick elements with 40 divisions along the off-axis plies thickness.

Figures 4.11 and 4.12 show the Paris-like charts for the propagating cracks. As cracks propagate in a steady state manner, each point in those diagrams represents one single crack.

The Paris-like diagrams are reported in terms of the total ERR $G_{tot}=G_I+G_{II}$. The 90° cracks in the cross-ply laminates propagate under a pure mode I condition (thus $G_{tot}=G_I$), whereas

the propagation of the -45° cracks occurs under mixed I+II mode, with a mode mixity $MM=G_{II}/G_{tot}=0.81$. Despite quite a large data scatter, the average value of the CGR increases, on average, by 75% for A_v = 0.34% ($[0/90_2]_S$) and by 60% for A_v = 1.07% ($[0/45_2/0/-45_2]_S$). These results are qualitatively in accordance with the findings of Ref. [51], in which an increment in mode I ERR was reported for a delamination propagating with voids ahead of crack tip.

As for the life to crack initiation, the effect of the porosity on the CGR does not seems to depend significantly on the load level.

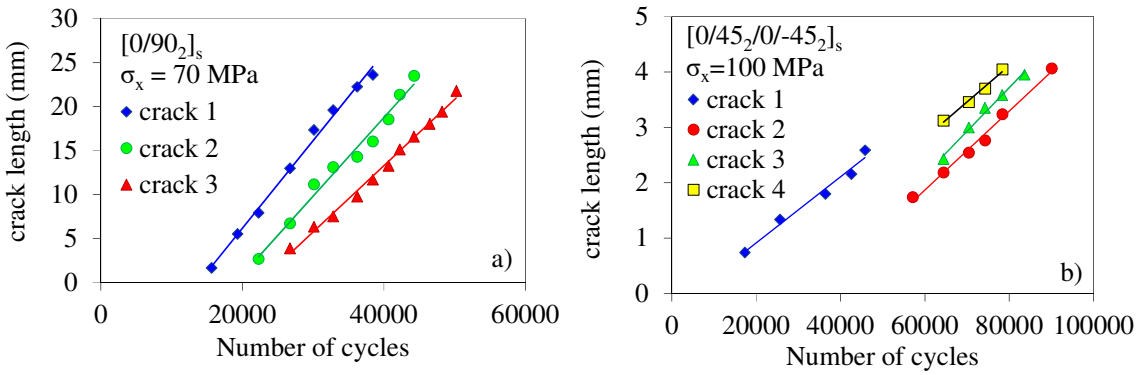

Figure 4.10 – Example of crack propagation curves for a) $[0/90_2]_S$ laminates with σ_x = 70 MPa and b) $[0/45_2/0/-45_2]_S$ laminates with σ_x = 100 MPa (the crack length represents the total length for edge cracks and the half-length for central cracks).

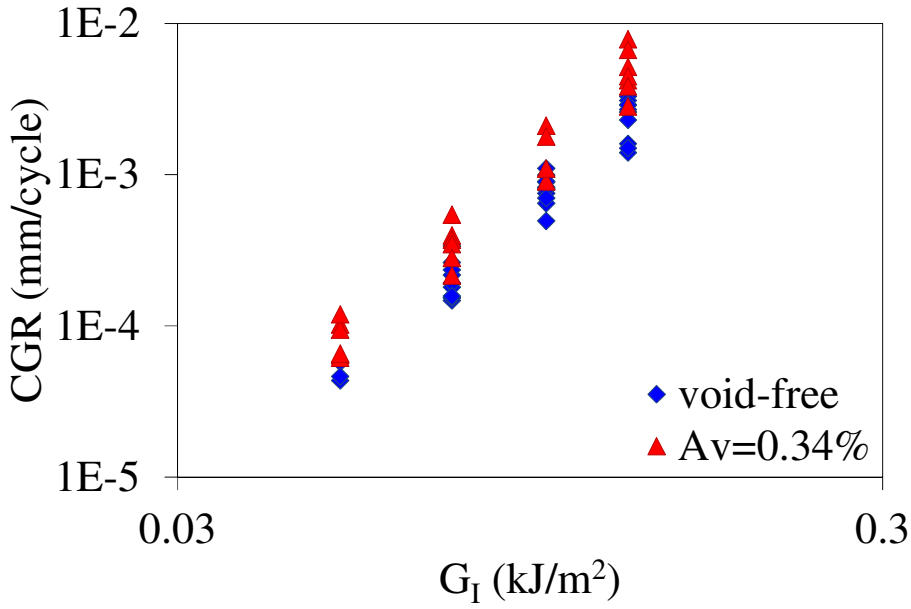

Figure 4.11 – Influence of voids on crack growth rate (CGR) for $[0/90_2]_S$ laminates.

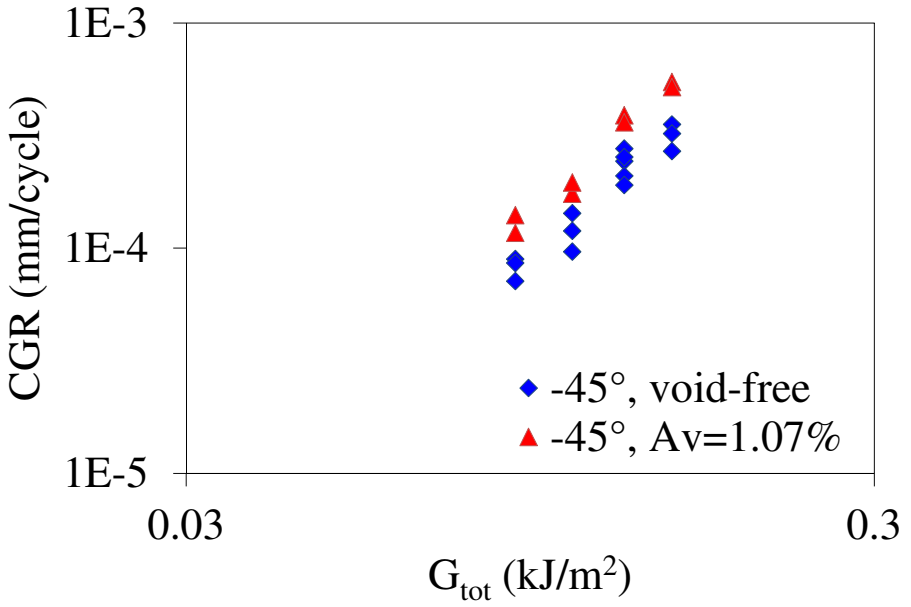

Figure 4.12 – Influence of voids on crack growth rate (CGR) for $[0/45_2/0/-45_2]_S$ laminates.

A meaningful quantification of the first stages of fatigue damage is represented by the crack density, which is related to the stiffness reduction of a laminate. The crack density can be defined in different ways, taking into account the total number of cracks or weighting each

crack by its length (*weighted* crack density [44]). The *weighted* crack density (ρ_w) is the parameter that better correlates with the stiffness drop in a laminate [44], and it is defined as:

$$\rho_w = \frac{\sum_{i=1}^{n} c_i}{w \cdot L} \tag{4.1}$$

where n is the number of cracks, L the length of the observation area, c_i the length of the i-th crack and w the specimen width. Figures 4.13 and 4.14 show the evolution of the *weighted* crack density for all the tested laminates. For the $[0/90_2]_S$ stacking sequence, the *weighted* crack density increases much faster and reaches saturation earlier in the presence of voids, as expected from the reduction in life to crack initiation and increase in crack growth rate. The saturation level appears not to vary sensibly in the absence and presence of voids, as highlighted also in Ref. [36]. For the $[0/45_2/0/-45_2]_S$ laminates, instead, the crack density seems to increase faster at the beginning but it soon follows the same trend as the void-free specimens. This behaviour can be explained by the fact that in those specimens voids were not homogeneously distributed but rather clustered in some regions. Therefore, they influence the initiation of the first cracks, but once those cracks initiated, most of the voids are in regions where the stress field is shielded by the crack itself. Therefore, most of the voids do not contribute to further damage development.

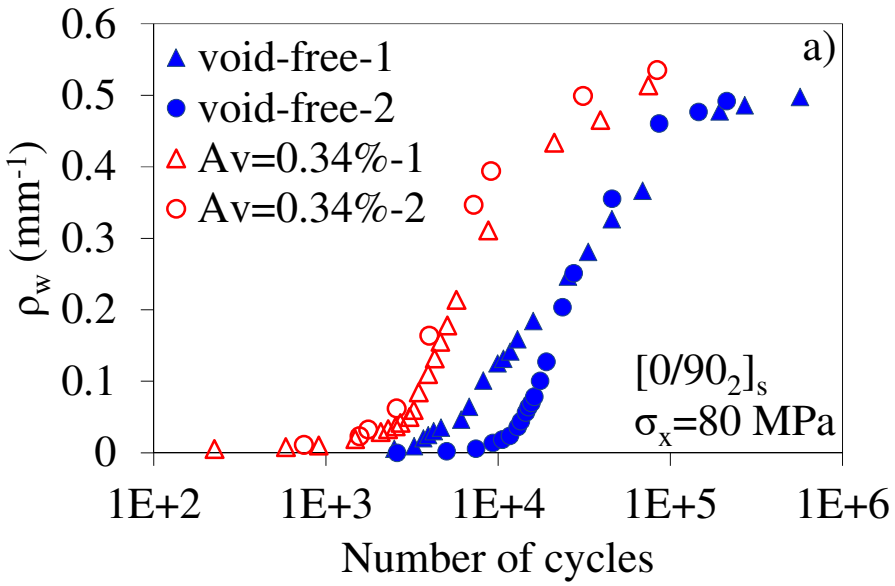
a)
void-free-1
void-free-2
Av=0.34%-1
Av=0.34%-2
[0/90$_2$]$_s$
σ_x=80 MPa
ρ_w (mm^{-1})
0.6
0.5
0.4
0.3
0.2
0.1
0
1E+2
1E+3
1E+4
1E+5
1E+6
Number of cycles

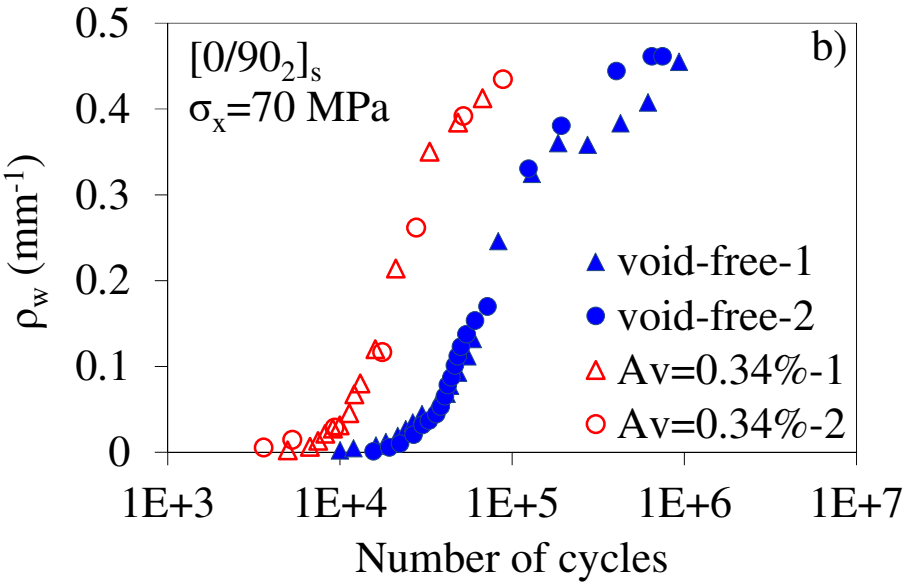
b)
[0/90$_2$]$_s$
σ_x=70 MPa
void-free-1
void-free-2
Av=0.34%-1
Av=0.34%-2
ρ_w (mm^{-1})
0.5
0.4
0.3
0.2
0.1
0
1E+3
1E+4
1E+5
1E+6
1E+7
Number of cycles

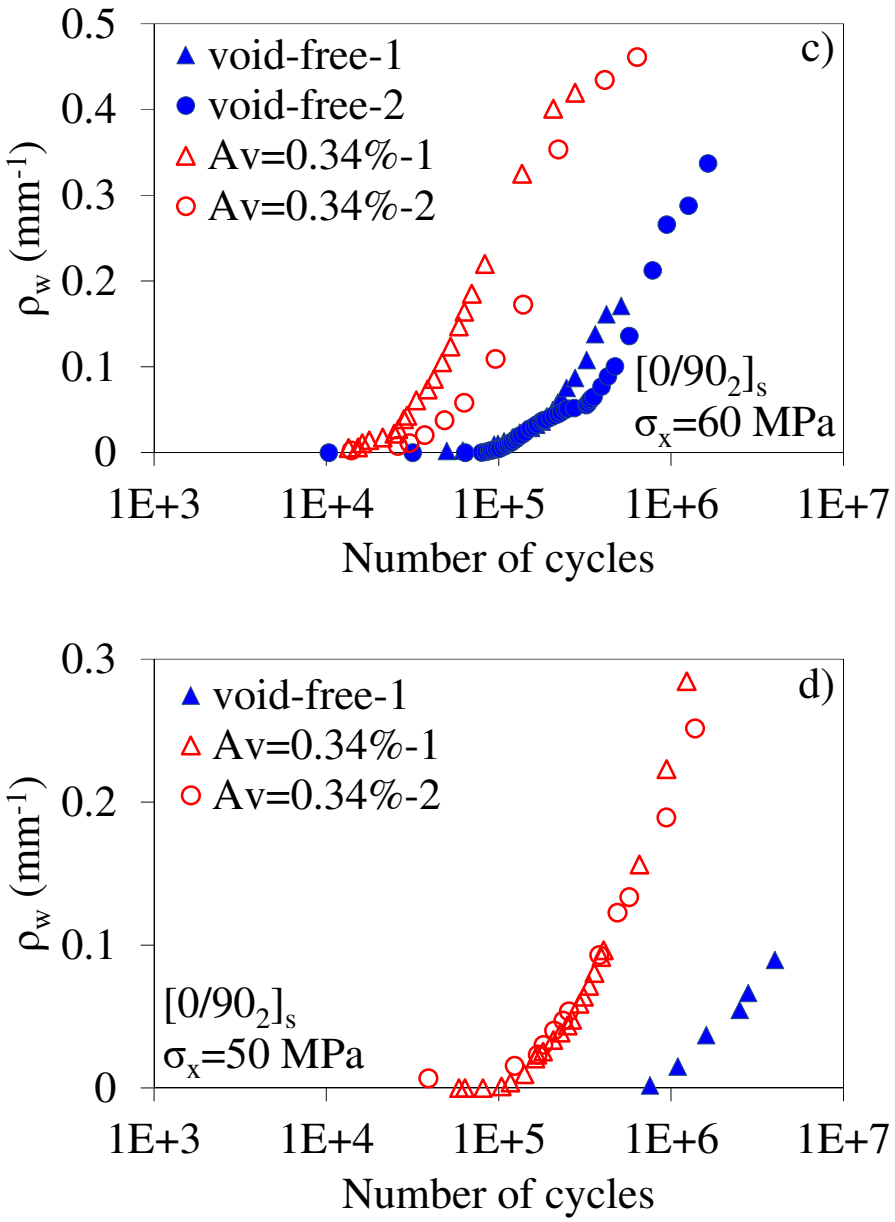

Figure 4.13 – Influence of voids on the *weighted* crack density evolution for $[0/90_2]_S$ laminates, a) σ_x = 80 MPa, b) σ_x = 70 MPa, b) σ_x = 60 MPa, d) σ_x = 50 MPa.

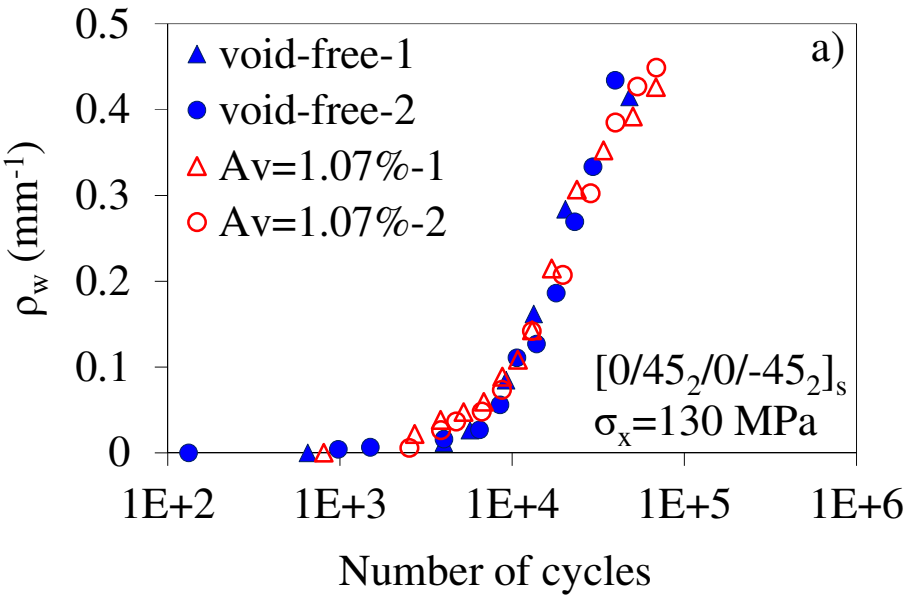
0.5
0.4
0.3
0.2
0.1
0
ρ_w (mm^{-1})
void-free-1
void-free-2
Av=1.07%-1
Av=1.07%-2
a)
[0/45$_2$/0/-45$_2$]$_s$
σ_x=130 MPa
1E+2
1E+3
1E+4
1E+5
1E+6
Number of cycles

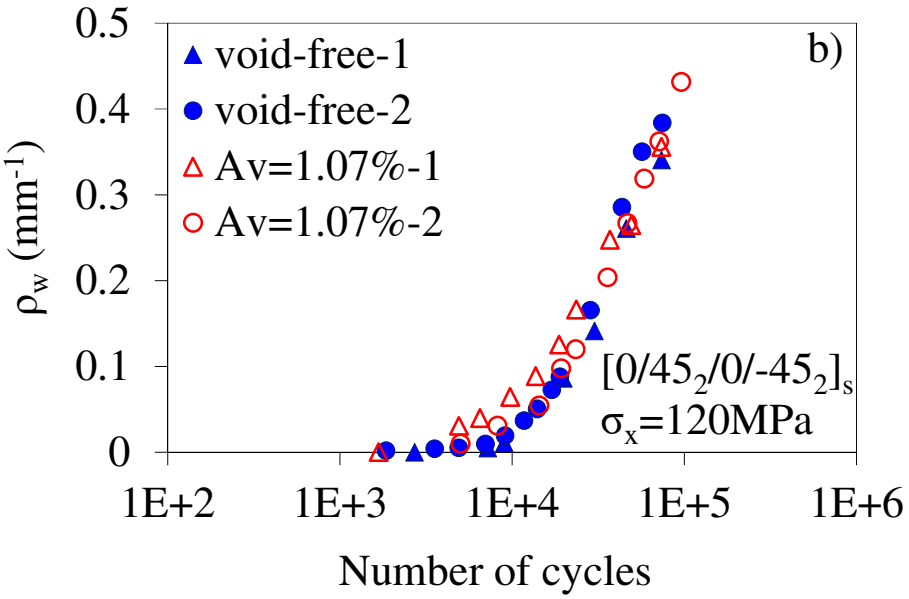
0.5
0.4
0.3
0.2
0.1
0
ρ_w (mm^{-1})
void-free-1
void-free-2
Av=1.07%-1
Av=1.07%-2
b)
[0/45$_2$/0/-45$_2$]$_s$
σ_x=120MPa
1E+2
1E+3
1E+4
1E+5
1E+6
Number of cycles

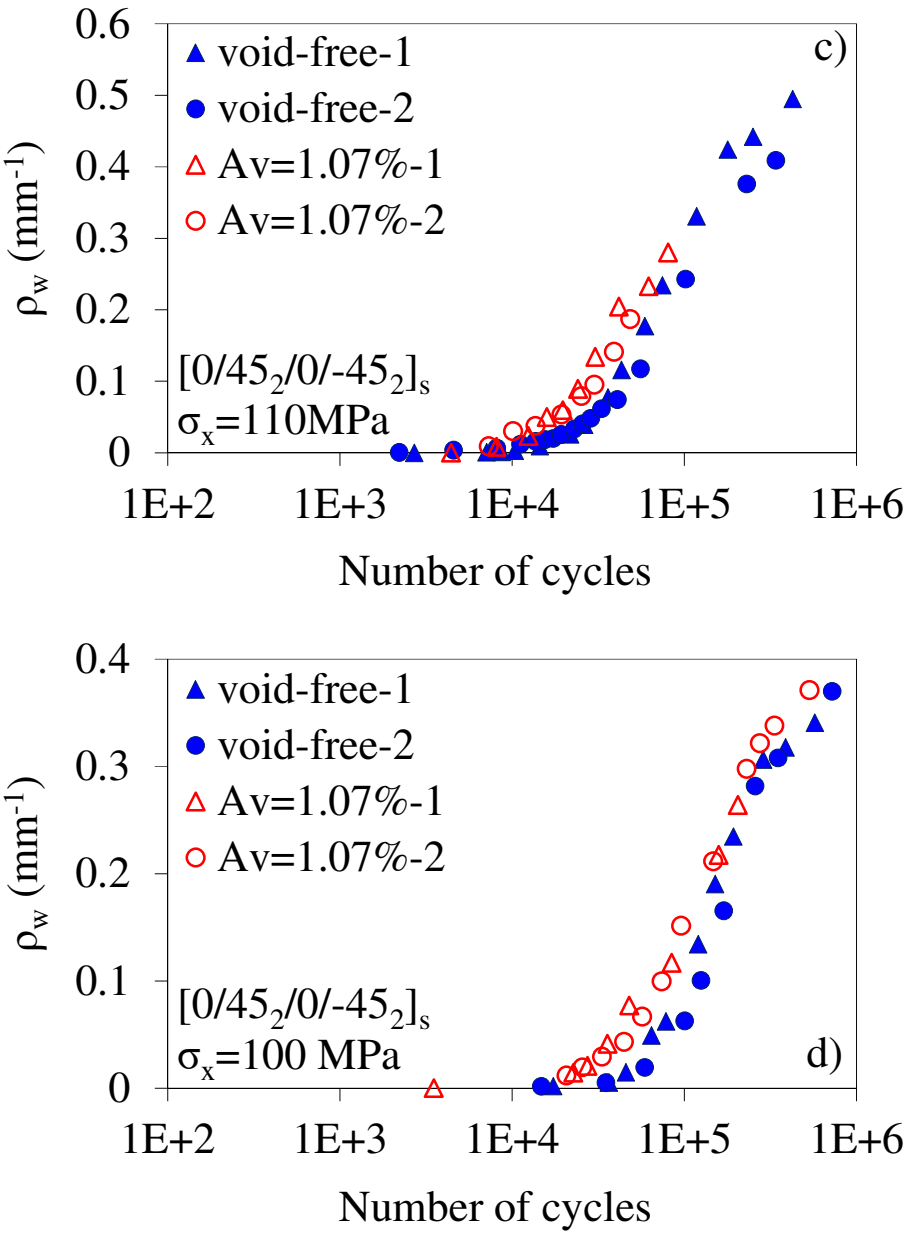

Figure 4.14 – Influence of voids on the *weighted* crack density evolution for $[0/45_2/0/-45_2]_S$ laminates, a) σ_x = 130 MPa, b) σ_x = 120 MPa, c) σ_x = 110 MPa, d) σ_x = 100 MPa.

Figures 4.15 and 4.16 show the stiffness degradation due to off-axis cracks in the absence and the presence of voids. The laminate Young modulus in the loading direction, E_x, is normalised with respect to its initial value E_{x0}. The presence of porosity was found not to sensibly affect the initial longitudinal modulus of the laminates, as reported in Table 4.2. As expected from the trends in the crack density evolution, the stiffness decreases much

faster in presence of voids for the $[0/90_2]_S$ specimens, whereas for the $[0/45_2/0/-45_2]_S$ lay-up the decrease rate is comparable for laminates with and without voids, in agreement with the small difference observed in the crack density trend.

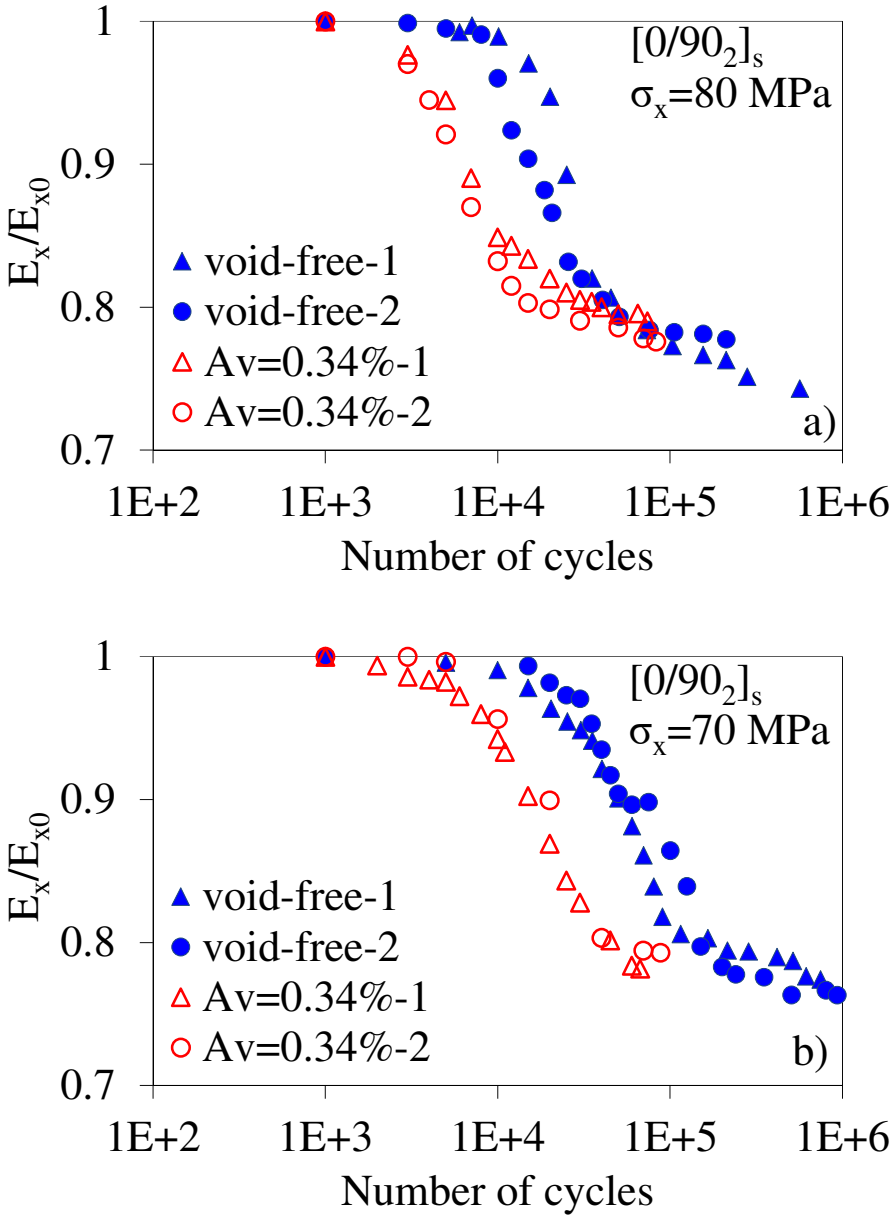

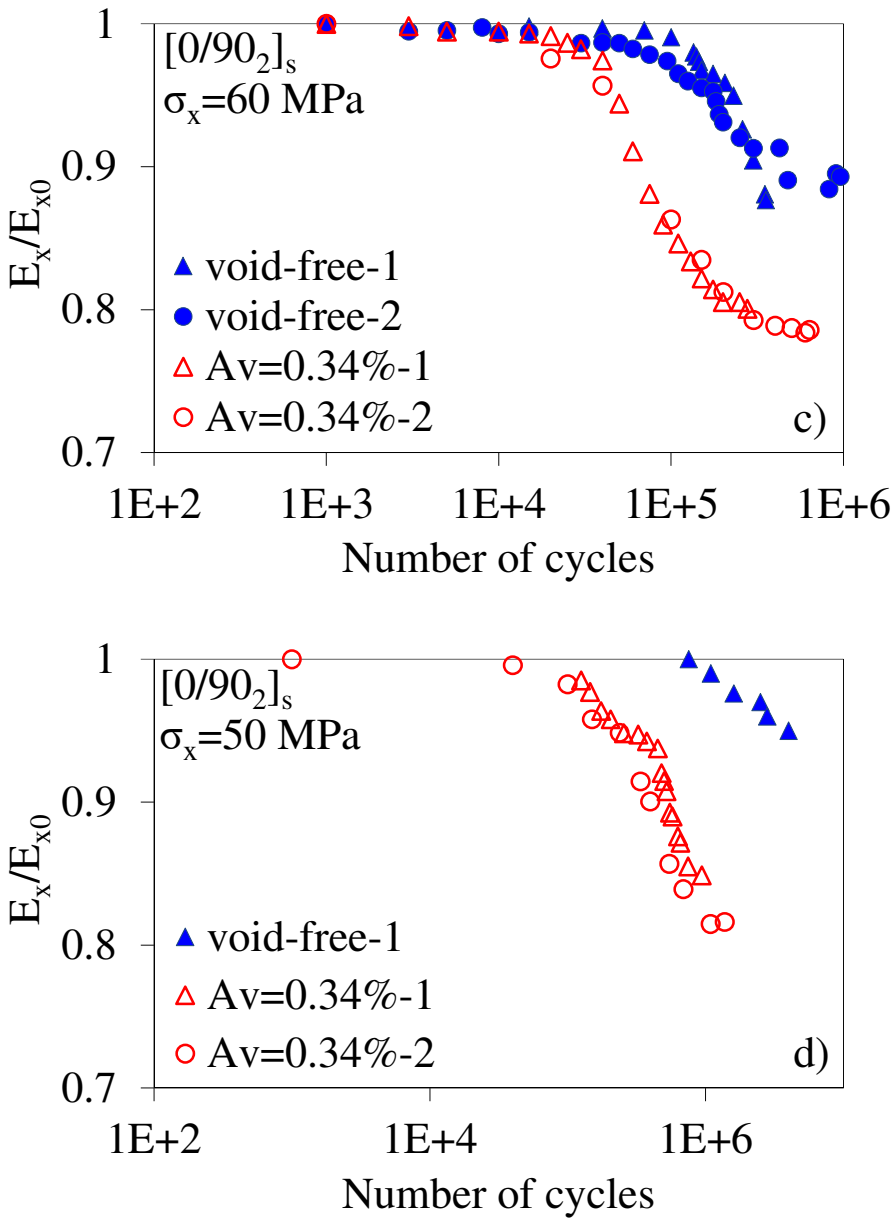

Figure 4.15 – Influence of voids on stiffness degradation for $[0/90_2]_S$ laminates, a) σ_x = 80 MPa, b) σ_x = 70 MPa, c) σ_x = 60 MPa, d) σ_x = 50 MPa.

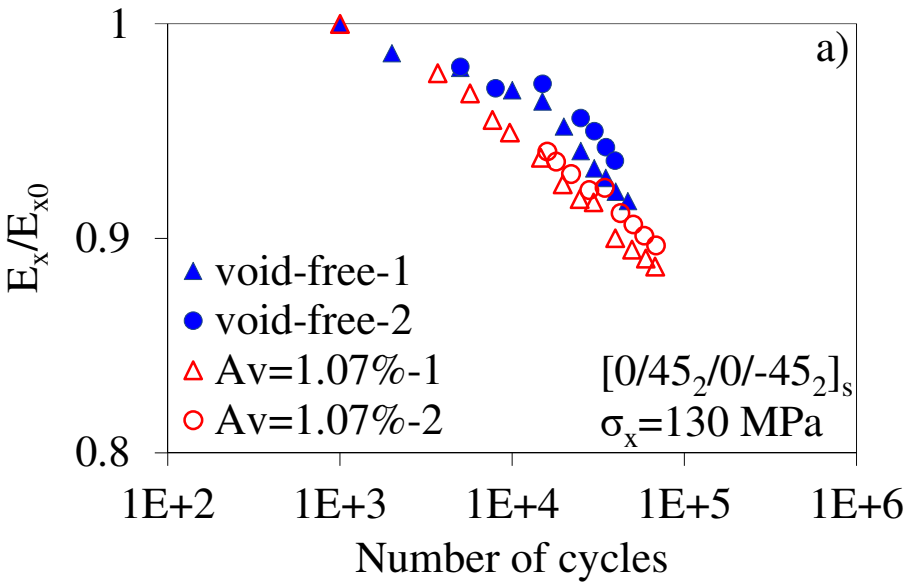
a)
1
0.9
0.8
E_x/E_{x0}
void-free-1
void-free-2
Av=1.07%-1
Av=1.07%-2
$[0/45_2/0/-45_2]_s$
σ_x=130 MPa
1E+2
1E+3
1E+4
1E+5
1E+6
Number of cycles

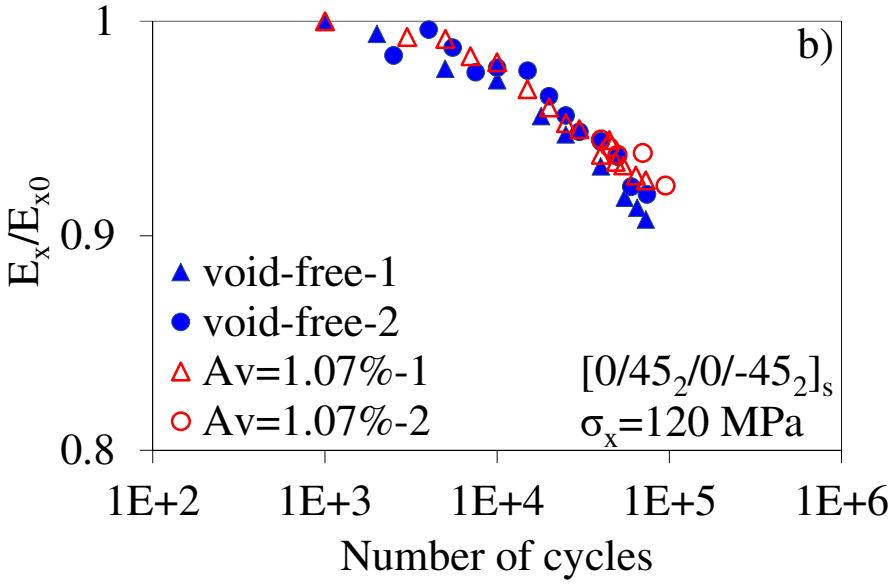
b)
1
0.9
0.8
E_x/E_{x0}
void-free-1
void-free-2
Av=1.07%-1
Av=1.07%-2
$[0/45_2/0/-45_2]_s$
σ_x=120 MPa
1E+2
1E+3
1E+4
1E+5
1E+6
Number of cycles

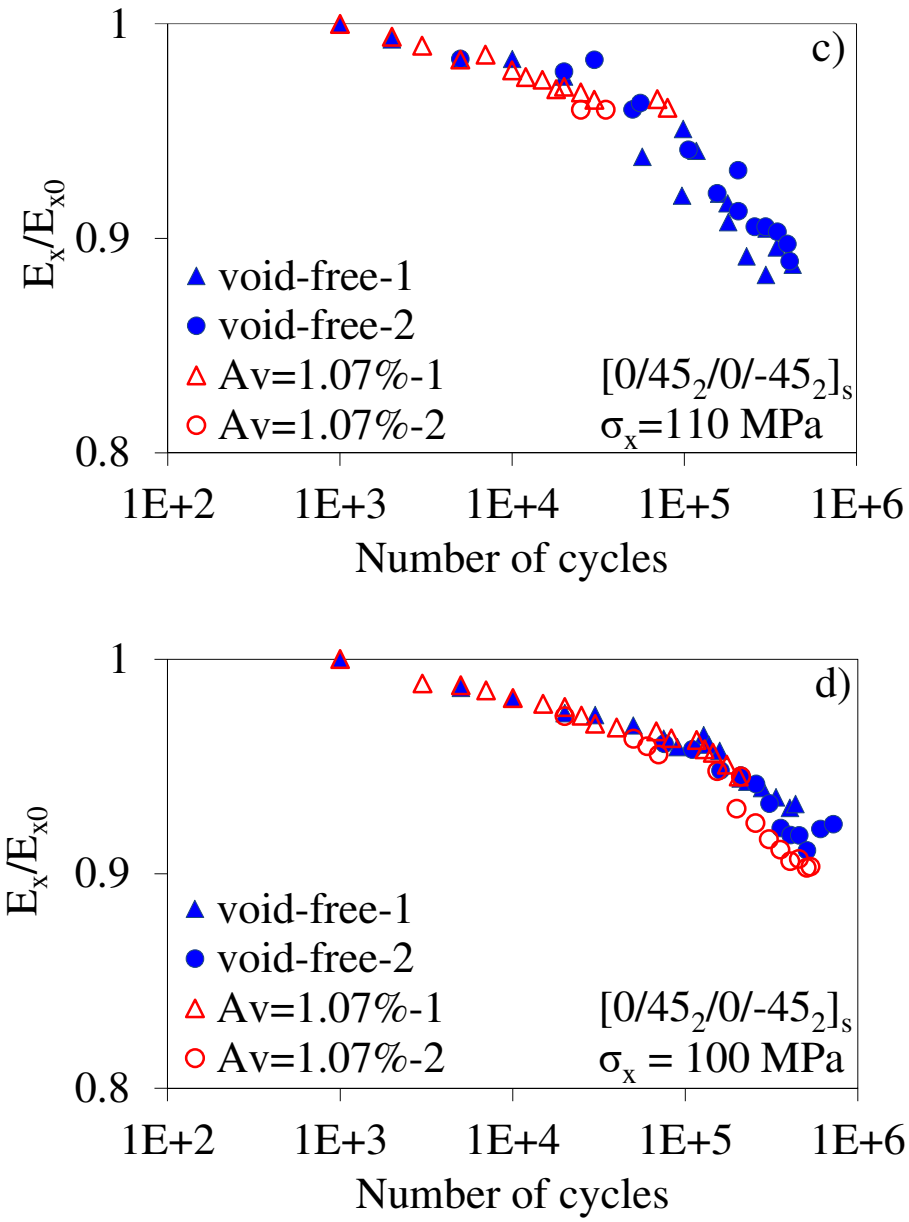

Figure 4.16 – Influence of voids on stiffness degradation for $[0/45_2/0/-45_2]_S$ laminates, a) σ_x = 130 MPa, b) σ_x = 120 MPa, c) σ_x = 110 MPa, d) σ_x = 100 MPa.

Table 4.2 – Longitudinal Young's modulus of the laminates.

	$[0/90_2]_S$		$[0/45_2/0/-45_2]_S$	
	Void-free	A_v=0.34%	Void-free	A_v=1.07%
E_{x0} – Average	24025	23837	25950	26010
E_{x0} – c.o.v.	2.4%	2.1%	2.1%	5.9%

4.6. Discussion

According to the results obtained from the present analysis, micro-sized voids have a non-negligible influence in the initiation and evolution of damage in the off-axis plies. For a safe and reliable design against fatigue, a model is needed to properly account for the presence of voids and their effect on the crack initiation, multiplication and the consequent stiffness degradation. However, the expression "effect of voids" is too general. In fact, the effect of voids can be attributed to one or more microstructural features as the void content, the void diameter (average diameter, PDF etc.), the void shape and the spatial distribution. As a first trial to obtain some guidelines in this direction, some correlations between the fatigue performances and some voids features are presented.

First, the life to the first cracks initiation is analysed in Figure 4.17 as a function of the void content (A_v), the average void diameter ($D_{v,av}$) and the void diameter corresponding to a cumulative probability of 95%. The average number of cycles for the initiation of the first six cracks at every load level for each specimen configuration is normalised to that for the void-free laminates. For the cross-ply laminates it can be observed that a strong correlation is found both with the void area fraction and the void diameter relevant to the 95% cumulative distribution. A slightly worse correlation is found for the average void diameter, for which a very small variation (from 43 to 45 μm) corresponds to a large degradation of the life to crack initiation. This is in agreement with the fact that the initiation of the first cracks is related to the worst scenarios, corresponding, presumably, to the larger voids, but also to regions with high void concentration.

It can also be observed that different trends are obtained for the 90° and -45° plies. This means that general conclusions, based only on this geometrical features, cannot be drawn independently of the ply orientation and the consequent stress state.

For the analysis of the further damage evolution, the life spent for a stiffness reduction of 5% is considered, always normalised with respect to that for the void-free laminates. The results are plotted in terms of the global void content and average diameter, as the later stage damage evolution does not depend only on the larger voids (Figure 4.18). As expected after the plots in Figure 4.16, there is no variation of the life to 5% stiffness loss for the $[0/45_2/0/-45_2]_S$ laminates. As already mentioned, this is due to the fact that voids are clustered in these specimens. This lead to a shorter life for the initiation of the first cracks but identical damage patterns in the later stages, as proved by the crack density trends in Figure 4.14. This means that, while for the damage initiation phase the void content and the larger diameters seem to synergistically play a crucial role, the damage evolution strongly depends on the voids spatial distribution also, which could be described by tessellation or fractal dimension [52]. As a conclusion, it can be said that the effect of voids depends on some geometrical features, whose synergistic effect must be quantified by means of a suitable model. In particular, the void content, size and distribution affect the local stress fields in the matrix and at the fibre-matrix interface. This increases the rate of the micro-scale damage evolution leading to the initiation of an off-axis crack (see Chapter 3 [29]). Therefore, any model to predict the effect of voids must be based on the local-stress perturbation caused by the presence of voids. Chapters 5 and 6 will be dedicated to the development of such a model, by extending the crack initiation criterion proposed by Carraro and Quaresimin [44] to account for the presence of voids in the microstructure.

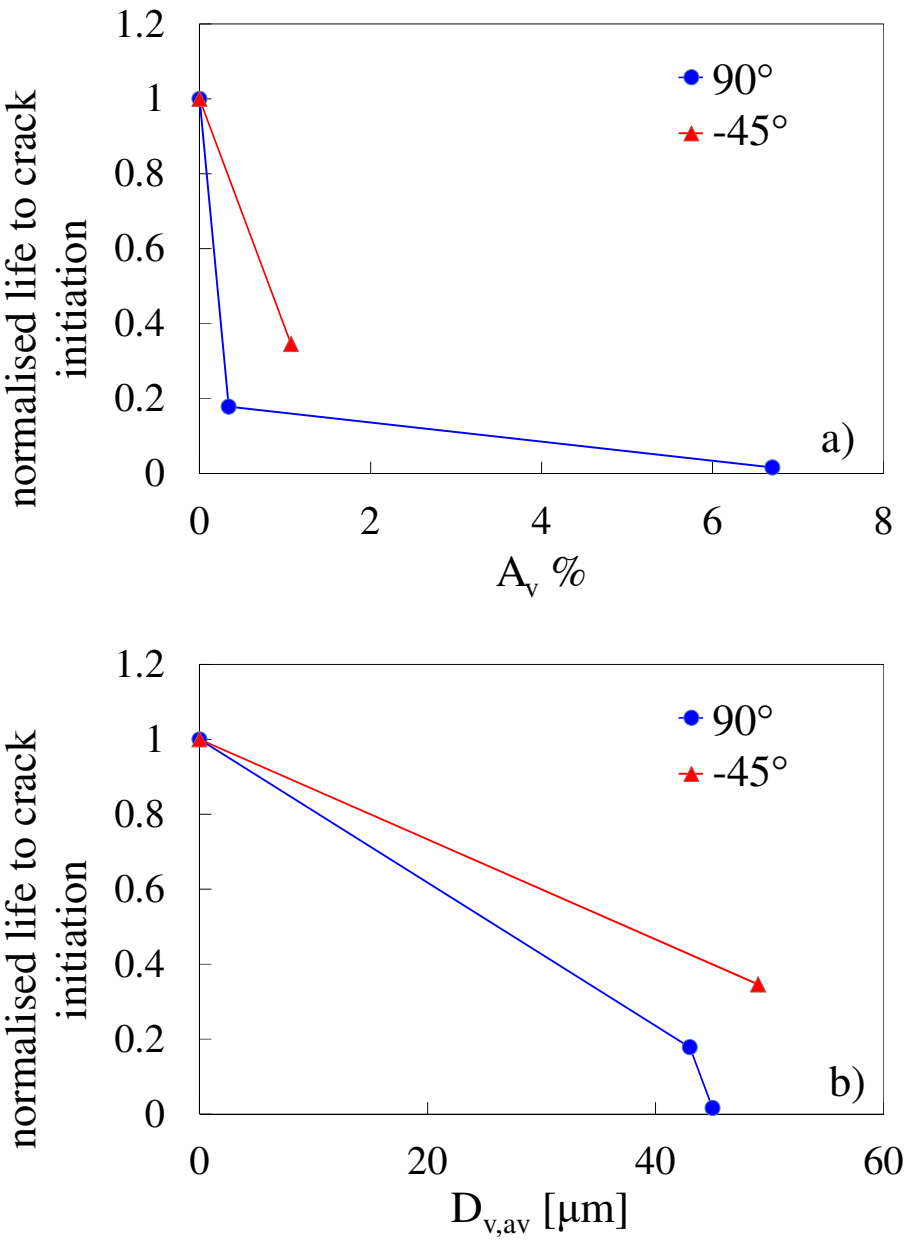
normalised life to crack initiation
1.2
1
0.8
0.6
0.4
0.2
0
0
2
4
6
8
A_v %
90°
-45°
a)
normalised life to crack initiation
1.2
1
0.8
0.6
0.4
0.2
0
0
20
40
60
$D_{v,av}$ [µm]
90°
-45°
b)

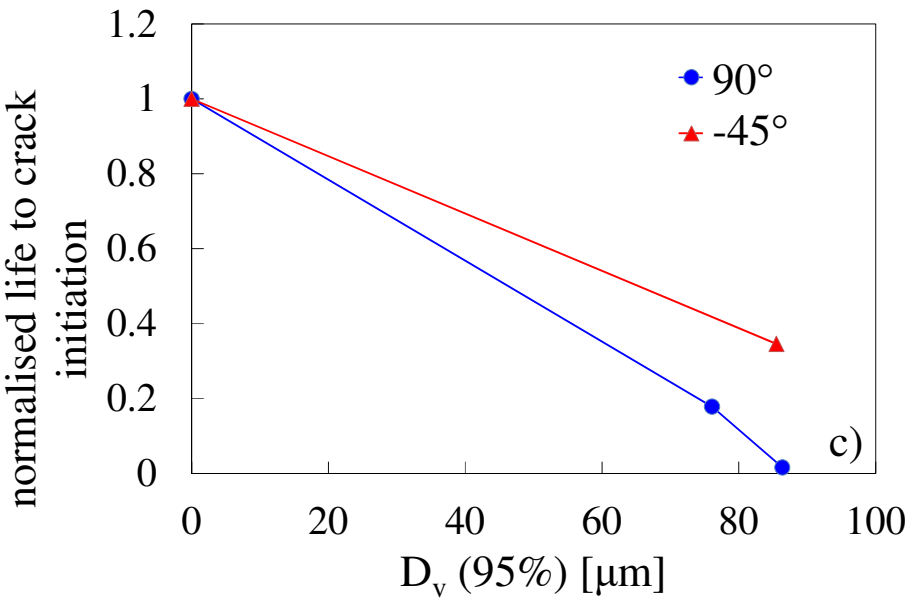

Figure 4.17 – Normalised life to crack initiation as a function of a) void area fraction, b) void average diameter and c) void diameter corresponding to a 95% cumulative probability.

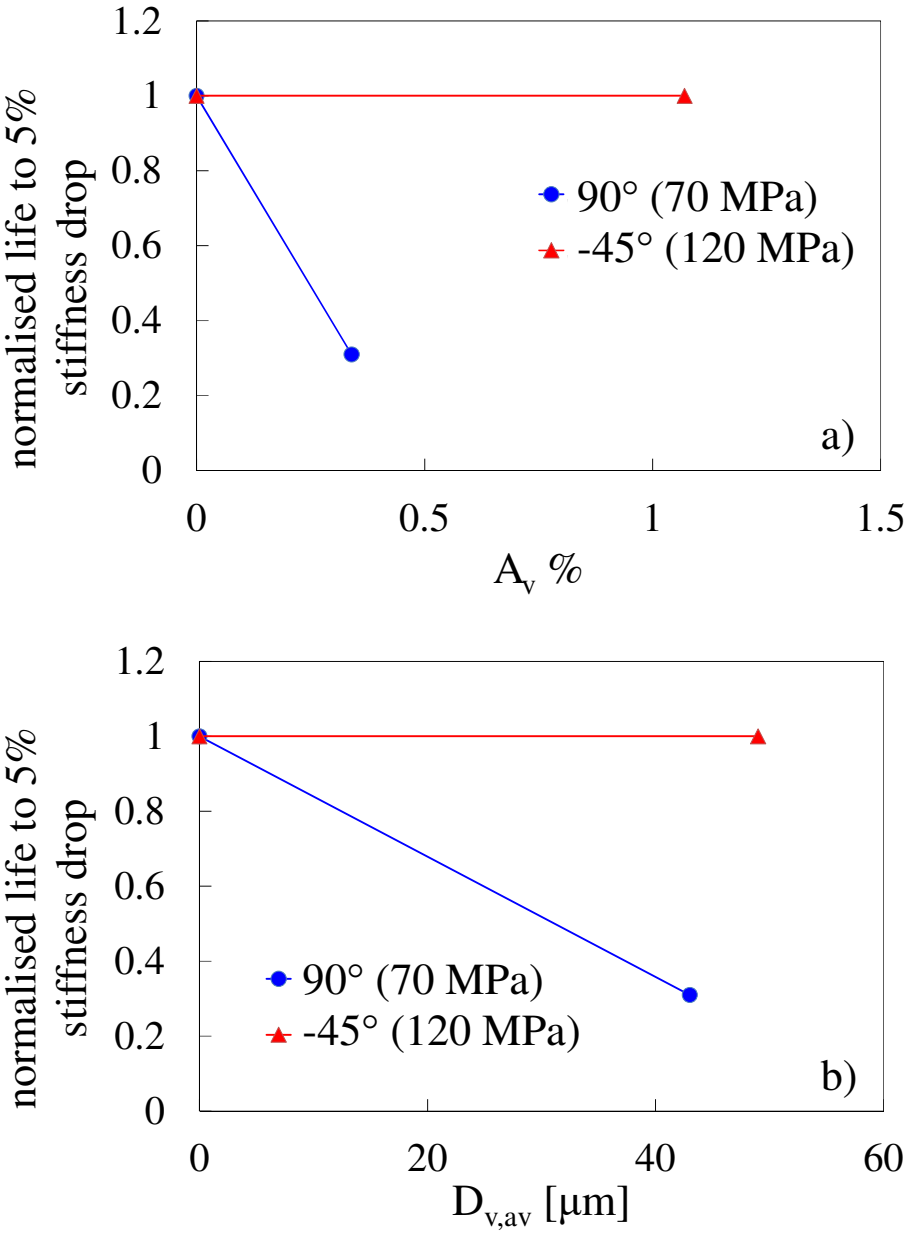

Figure 4.18 – Normalised life to the 5% stiffness loss as a function of a) void area fraction and b) void average diameter.

4.7. Conclusions

Glass/epoxy laminates with $[0/90_2]_S$ and $[0/45_2/0/-45_2]_S$ stacking sequences were produced by vacuum resin infusion using optimal process parameters and varying some of them in order to potentially decrease production costs obtaining, in turn, the presence of voids in the laminates. Void area fractions (A_v) of 0.34% and 1.07% were obtained, respectively,

for $[0/90_2]_S$ and $[0/45_2/0/-45_2]_S$ lay-ups if the resin was not degassed prior to infusion. A void area fraction of 6.7% was also obtained for $[0/90_2]_S$ lay-up when the resin was not degassed and the inlet pressure was kept constantly equal to 1 bar throughout the infusion. Controlling the resin flow seems therefore to influence the void content much more than ensuring a low air content in the resin before impregnating the preform.

Fatigue tests revealed a large detrimental influence of the presence of voids on the fatigue performances of both the stacking sequences. The life to crack initiation was reduced by 80% for A_v = 0.34%, by 98% for A_v = 6.7% ($[0/90_2]_S$), and by 65% for A_v = 1.07% ($[0/45_2/0/-45_2]_S$). Voids also increased the crack growth rate by 75% for $[0/90_2]_S$ and by 60% for $[0/45_2/0/-45_2]_S$.

In the $[0/90_2]_S$ laminates, voids were homogeneously distributed along the specimens length, and they largely influenced fatigue damage evolution, quantified by the crack density in the 90° ply, leading to a much faster stiffness degradation. In the $[0/45_2/0/-45_2]_S$ laminates, instead, voids were found to be aggregated at regular intervals, probably due to a periodicity in the position of the single plies during the stacking operation. As a consequence, voids influenced the crack density evolution and the stiffness drop only in the first stages of fatigue life, after which the trend was found to be the same as the void-free specimens.

As a final conclusion, to predict the effect of voids on the damage initiation and evolution in laminates, a suitable model has to be developed. It must be capable of accounting for the synergistic effect of several voids features (content, diameter, spatial distribution) on the local stresses in the matrix, which are responsible for the damage initiation and evolution at the micro-scale.

References of Chapter 4

[1] Olivier P, Cottu JP, Ferret B. Effects of cure cycle pressure and voids on some mechanical properties of carbon/epoxy laminates. Composites 1995; 26: 509-515.

[2] Varna J, Joffe R, Berglund LA, Lundstrom TS. Effect of voids on failure mechanisms in RTM laminates. Composites Science and Technology 1995; 53: 241-249.

[3] Zhu H, Wu B, Li D, Zhang D, Chen Y. Influence of voids on the tensile performance of carbon/epoxy fabric laminates. Journal of Materials Science Technology 2011; 27: 69-73.

[4] Huang Y, Varna J, Talreja R. Statistical methodology for assessing manufacturing quality related to transverse cracking in cross-ply laminates. Composites Science and Technology 2014; 95: 100-106.

[5] Carraro PA, Maragoni L, Quaresimin M. Influence of manufacturing-induced defects on damage initiation and propagation in carbon/epoxy NCF laminates. Advanced Manufacturing: Polymer and Composites Science 2015; 1: 44-53.

[6] Tang JM, Lee WI, Springer GS. Effects of Cure pressure on resin flow, voids, and mechanical properties. Journal of Composite Materials 1987; 21: 421-440.

[7] Suarez JC, Molleda F, Guemes A. Void content in carbon fiber/epoxy resin composites and its effects on compressive properties. In: Proceedings of ICCM9 Conference. Madrid, July 1993.

[8] Cinquin J, Triquenaux V, Rouesne Y. Porosity influence on organic composite material mechanical properties'. In: Proceedings of ICCM16 Conference. Kyoto, July, 2007.

[9] Kosmann N, Karsten JM, Schuett M, Schulte K, Fiedler B. Determining the effect of voids in GFRP on the damage behaviour under compression loading using acoustic emission. Composites: Part B – Engineering 2015; 70: 184-188.

[10] Hernandez S, Sket F, Gonzales C, Llorca J. Optimization of curing cycle in carbon fiber-reinforced laminates: void distribution and mechanical properties. Composites Science and Technology 2013; 85: 73-82.

[11] Liu L, Zhang BM, Wang DF, Wu J. Effects of cure cycles on void content and mechanical properties of composite laminates. Composite Structures 2006; 73: 303-309.

[12] Chambers AR, Earl JS, Squires CA, Suhot MA. The effect of voids on the flexural fatigue performance of unidirectional carbon fibre composites developed for wind turbine applications. International Journal of Fatigue 2006; 28: 1389-1398.

[13] de Almeida SFM, Neto ZSN. Effect of void content on the strength of composite laminates. Composite Structures 1994; 28: 139-148.

[14] Hagstrand PO, Bonjour F, Manson JAE. The influence of void content on the structural flexural performance of unidirectional glass fibre reinforced polypropylene composites. Composites Part A – Applied Science and Manufacturing 2005; 36: 705-714.

[15] Ghiorse SR. Effect of void content on the mechanical properties of carbon/epoxy laminates, SAMPE Q, 1993; 24: 54-59.

[16] Judd NCW, Wright WW. Voids and their effects on the mechanical properties of composites - an appraisal, SAMPE J, 1978; 14: 10-14.

[17] Yoshida H, Ogasa T, Hayashi R. Statistical approach to the relationship between ILSS and void content of CFRP. Composites Science and Technology 1986; 25: 3-18.

[18] Olivier PA, Mascaro B, Margueres P, Collombet F. CFRP with voids: ultrasonic characterization of localized porosity, acceptance criteria and mechanical characteristics. In: Proceedings of ICCM16 Conference. Kyoto, July, 2007.

[19] Thomason JL. The interface region in glass fibre-reinforced epoxy resin composites: 1. Sample preparation, void content and interfacial strength. Composites 1995; 26: 467-475.

[20] Wisnom MR, Reynolds T, Gwilliam N. Reduction in interlaminar shear strength by discrete and distributed voids. Composites Science and Technology 1996; 56: 93-101.

[21] Goodwin AA, Howe CA, Paton RJ. The role of voids in reducing the interlaminar shear strength of RTM laminates. In: Proceedings of ICCM11 Conference. Gold Coast, July, 1997.

[22] Costa ML, de Almeida SFM, Rezende MC. The influence of porosity on the interlaminar shear strength of carbon-epoxy and carbon-bismaleimide fabric laminates. Composites Science and Technology 2001; 61: 2101-2108.

[23] Bureau MN, Denault J. Fatigue resistance of continuous glass fiber-polypropylene composites consolidation dependence. Composites Science and Technology 2004; 64: 1785-1794.

[24] Zhu H, Li D, Zhang D, Wu B, Chen Y. Influence of voids on interlaminar shear strength of carbon/epoxy laminates. Transactions of Nonferrous Metals Society of China 2009; 19: 470-475.

[25] Asp LE, Brandt F. Effects of pores and voids on the interlaminar delamination toughness of a carbon/epoxy composite. In: Proceedings of ICCM11 Conference. Gold Coast, July, 1997.

[26] Dill CW, Tipton SM, Glaessge EH, Branscum KD. Fatigue strength reduction imposed by porosity in a fiberglass composite. In: Damage Detection in Composite Materials, ASTM STP 1128, J. E. Masters, Ed., American Society for Testing and Materials, Philadelphia, 1992, pp. 152-162.

[27] Hapke J, Gehrig F, Huber N, Schulte K, Lilleodden ET. Compressive failure of UD-CFRP containing void defects: In situ SEM microanalysis. Composites Science and Technology 2011; 71: 1242-1249.

[28] Scott AE, Sinclair I, Spearing SM, Mavrogordato MN, Hepples W. Influence of voids on damage mechanisms in carbon/epoxy composites determined via high resolution computed tomography. Composites Science and Technology 2014; 90: 147-153.

[29] Maragoni L, Carraro PA, Quaresimin M. Effect of voids on the crack formation in $[45/-45/0]_S$ laminate under cyclic axial tension. Composites Part A – Applied Science and Manufacturing 2016; doi: http://dx.doi.org/10.1016/j.compositesa.2016.02.018

[30] Baley C, Davies P, Cartié D. Porosity in ocean racing yacht composites: a review. Applied Composite Materials 2015; 22: 13-28.

[31] Gehrig F, Mannov E, Schulte K. Degradation of NCF-epoxy composites containing voids. In: Proceedings of ICCM 17 Conference. Edinburgh, July, 2009.

[32] Lambert J, Chambers AR, Sinclair I, Spearing SM. 3D damage characterization and the role of voids in the fatigue of wind turbine blade materials. Composites Science and Technology 2012; 72: 337-343.

[33] Schmidt F, Rheinfurt M, Horst P, Busse G. Multiaxial fatigue behaviour of GFRP with evenly distributed or accumulated voids monitored by various NDT methodologies. International Journal of Fatigue 2012; 43: 207-216.

[34] Seon G, Makeev A, Nikishkov Y, Lee E. Effects of defects on interlaminar tensile fatigue behavior of carbon/epoxy composites. Composites Science and Technology 2013; 89: 194-201.

[35] Protz R, Kosmann N, Gude M, Hufenbach W, Schulte K, Fiedler B. Voids and their effect on the strain rate dependent material properties and fatigue behaviour of non-

crimp fabric composites materials. Composites Part B – Engineering 2015; 83: 346:351.

[36] Sisodia SM, Gamstedt EK, Edgren F, Varna J. Effects of voids on quasi-static and tension fatigue behaviour of carbon-fibre composite laminates. Journal of Composite Materials 2015; 49: 2137-2148.

[37] Tong J, Guild FJ, Ogin SL, Smith PA. On matrix crack growth in quasi isotropic laminates - I. Experimental investigation. Composites Science and Technology 1997; 57: 1527-1535

[38] Tong J. Three Stages of Fatigue Crack Growth in GFRP Composite Laminates. Journal of Engineering Materials and Technology 2001; 123: 139-143

[39] Sun Z, Daniel IM, Luo JJ. Modeling of fatigue damage in a polymer matrix composite. Materials Science and Engineering 2003; A361: 302-311

[40] Wharmby AW, Ellyin F. Damage growth in constrained angle-ply laminates under cyclic loading. Composites Science and Technology 2002; 62: 1239–1247

[41] Tohgo K, Nakagawa S, Kageyama K. Fatigue behaviour of CFRP cross-ply laminates under on-axis and off-axis cyclic loading. International Journal of Fatigue 2006; 28: 1254-1262

[42] Adden S, Horst P. Damage propagation in non-crimp fabrics under bi-axial static and fatigue loading. Composites Science and Technology 2006; 66: 626–633

[43] Quaresimin M, Carraro PA. Damage initiation and evolution in glass/epoxy tubes subjected to combined tension-torsion fatigue loading. International Journal of Fatigue 2014; 63: 25-35

[44] Quaresimin M, Carraro PA, Pilgaard Mikkelsen L, Lucato N, Vivian L, Brøndsted P, Sørensen BF, Varna J, Talreja R. Damage evolution under internal and external

multiaxial cyclic stress state: a comparative analysis. Composites Part B – Engineering 2014; 61: 282–290

[45] Carraro PA, Quaresimin M. A damage based model for crack initiation in unidirectional composites under multiaxial cyclic loading. Composites Science and Technology 2014; 99: 154-163.

[46] Quaresimin M, Carraro PA, Maragoni L. Early stage damage in off-axis plies under fatigue loading. Composites Science and Technology 2016; 128: 147-154.

[47] Asp LE, Berglund LA, Talreja R. Prediction of matrix initiated transverse failure in polymer composites, Composites Science and Technology 1996; 56: 1089-1097.

[48] Huang H, Talreja R. Effects of void geometry on elastic properties of unidirectional fiber reinforced composites. Composites Science and Technology 2005; 65: 1964-1981.

[49] Glud JA, Dulieu-Barton JM, Thomsen OT, Overgaard LCT. Automated counting of off- axis tunnelling cracks using digital image processing. Composites Science and Technology 2016; 125: 80-89

[50] Ho S, Suo Z. Tunneling cracks in constrained layers. Journal of Applied Mechanics 1993; 60: 890–4.

[51] Ricotta M, Quaresimin M, Talreja R. Mode I Strain Energy Release Rate in composite laminates in the presence of voids. Composites Science and Technology 2008; 68: 2616-2623.

[52] Summerscales J, Guild FJ, Pearce NRL, Russel PM. Voronoi cells, fractal dimensions and fibre composites. Journal of Microscopy 2001; 201: 153-162.

5

Development, validation and analysis of Representative Volume Elements for unidirectional composites

Motivation

In Chapter 4, the highly detrimental influence of porosity on the fatigue performances highlighted the need to account for the presence of voids in the design of composite parts. From the findings of Chapters 2 and 3 it was possible to conclude that the same damage-based criterion to predict fatigue crack initiation, proposed by Carraro and Quaresimin, could be used both in the absence and the presence of porosity once the effect the actual microstructure on the local stresses is properly accounted for. The first step towards this aim was to build, validate and analyse the stresses in Representative Volume Elements of the material.

Abstract

In this Chapter, a tool is developed to build Representative Volume Elements (RVEs) for unidirectional composites, by "shaking" an initially regular fibre distribution. The generated RVEs proved to be comparable to real microstructures in terms of morphological features and stress distributions, also considering both uniform and variable fibre diameter. As the present tool is intended to be used in the development of a model to predict fatigue crack initiation, the stress analysis was focused on the Local

Hyrostatic Stress (LHS) and the Local Maximum Principal Stress (LMPS), as they have been recently proposed as driving forces to fatigue crack initiation. The influence of the fibre volume fraction on the trends of such stresses was also investigated.

5.1. Introduction

Fibre-reinforced composites offer a unique combination of low density and high mechanical properties, which makes them appealing for structural applications. Among the available fibre architectures, long unidirectional (UD) fibres offer the highest strength and stiffness, at least in the fibres direction. Since mechanical components are often subjected to multi-axial loads, UD laminates are rarely employed, and UD plies are rather combined into multidirectional laminates.

Given the loading conditions, a composite component can be designed either not to have any damage, to tolerate damage as long as the stiffness remains above a critical level, or not to reach the final separation regardless of the amount of "sub-critical damage".

In multidirectional laminates, both under static and fatigue loadings, the first visible event of damage usually consists of the formation of multiple cracks in the off-axis plies. Off-axis cracks do not directly cause the final failure (i.e.: separation) of a laminate, but they reduce its stiffness and lead to the development of further damage mechanisms (delamination, fibre fracture) that are responsible for the final separation. Therefore, the formation of off-axis cracks should be taken into account in all the design criteria, and predicting the crack initiation becomes necessary to properly design composite components and better exploit the potential of composite materials.

If the elastic properties of fibres and matrix are kept constant, the formation of off-axis cracks, both in terms of initiation and propagation along the thickness of the ply, is driven by the stress state within the matrix at the micro level, i.e. between the fibres. To know this

stress state is then fundamental to predict the crack formation, alongside with a failure criterion.

A widely employed method to obtain the matrix stresses at the micro scale is through the Finite Element (FE) analysis of Representative Volume Elements (RVEs) of the material. A Volume Element (VE) can be defined as a finite region of a material, and it can be considered as Representative with respect to a certain property if the estimate value of that property is the one of the actual material and any larger VE gives the same estimate of that property. Focusing on a UD ply, to reduce the computational effort of building and analysing a RVE, fibres can be considered as perfectly aligned along their longitudinal direction, and a two-dimensional RVE can be defined, based only on the fibres distribution on a plane perpendicular to the fibres direction.

The simplest and less computationally expensive RVEs assume the fibres position to follow a perfectly regular pattern (such as square or hexagonal). However, in composite laminates the actual fibre distribution in the matrix is irregular, due to the materials and manufacturing processes involved. Pyrz [1] showed that the fibres distribution in a composite material lies between a perfectly regular pattern and a complete random (Poisson) distribution, and that the distribution is influenced by the manufacturing process. More complex RVEs, that better represent the real composite microstructure, were then developed, consisting of several fibres irregularly positioned in the matrix according to different procedures [2-16]. The presence of fibres induces stress concentrations in the matrix. RVEs based on perfectly regular fibre patterns were shown not to be reliable to correctly estimate stress distributions [2-6]. In particular, the maximum values of the stresses in the matrix, which are related to the first damage initiation and are primarily involved in the crack formation process, are underestimated. Therefore, RVEs with irregular fibre distributions are to be used to study matrix stress distributions in composite laminates.

Several authors in the literature analysed real fibre distributions and proposed methods to reproduce them. The simplest method is known as the *hard-core* process (also called *Random Sequential Adsorption*, RSA), that is a Poisson process with finite size particles that do not overlap [1,4-8]. This technique is simple to implement but it requires large computational times to obtain high fibre volume fractions due to the high percentage of rejections (jamming limit).

To overcome this issue, modifications of this method have been attempted. Before placing a new fibre in a random position, Melro et al. [9] moved the already placed fibres towards one of their closest neighbours and far from the RVE edges. A similar approach was proposed by Zangenberg and Bronsted [10], who moved the neighbours towards each fibre before placing a new one. Thomas et al. [11] accounted for the fibre diameter distribution, and switched from a *hard-core* process to a different algorithm when the fibre volume fraction reached a value around 0.55. According to this algorithm, the new fibre location was chosen from the available regions, and the value of its diameter was assigned not to generate any overlap.

A different approach, of more complicated implementation but without technical limitations in fibre volume fractions, involves the alteration of an initially regular fibres distribution. Gusev et al. [12] placed the fibres without overlap in a regular square grid, and then made use of variable-box Monte Carlo runs in which they attempted to change the coordinate of the fibres and to adjust the RVE size to obtain the desired fibre volume fraction. Wongsto and Li [13] started instead to build the fibre distribution from hexagonally packed fibres. Then they iterated a process in which every fibre was moved in a random direction by a random distance, whose maximum value was calculated at each step not to have overlaps.

Another kind of methods to build RVEs is based on some microstructural characteristics of the microstructure that has to be replicated. Bulsara et al. [2] placed a fibre at the centre of the RVE and distributed the other fibres around it following the radial distribution function [14] of the studied material. Vaughan and McCarthy [15] instead placed the fibres in the RVE based on the experimental distribution of the first and second nearest neighbours distance.

Finally, micrographic images could be taken as RVE too, as done by Thomas et al. [11] and by Trias et al. [16]. Although this method eliminates any computation and guarantees the best reliability for the material under study, care must be put into extending the obtained results to other systems.

To assess their validity, RVEs have been quantitatively compared to actual composite microstructures in terms of microstructural statistical indexes [1,4,10-12,15]. Both short-range and long-range morphological indexes have been studied. Short-range indexes include the distribution of the nearest neighbours distance and orientation, the local number of neighbours and the local fiber volume fraction, calculated through the use of Dirichlet tessellation (or Voronoi cells). The most used long-range indexes are instead the second-order intensity function (K, also known as Ripley's K-function) and the radial distribution function (g, also called two-point correlation function or pair distribution function), that describes the fibre distribution on longer distances and whose definitions can be found in [14].

The morphological representativeness may not suffice for design purposes, for which mechanical properties or stress distributions are of primary interest. Huang et al. [6] validated their RVE by comparing it with real microstructure in terms of interfacial stresses distribution. Other mechanical indexes that can be used to assess the validity of a RVE can be found in the work by Trias et al. [7] on the dertermination of the minimum RVE size.

They include effective properties, Hill condition, and mean, variance and probability density function of stress and strain field in the composite constituents.

When RVEs are employed to study the mechanical behaviour of composites, one last important feature is how the boundary conditions are applied when Finite Element analyses are carried out. Boundary conditions can be applied directly on the RVE, and they can be periodic [9,12,15] or not [2,4,13]. In alternative, an embedded cell approach (ECA) can be used [3,5,7,16], in which the microstructure is embedded in a homogeneous material whose properties can be determined from the microstructure itself.

In a large scientific background on the construction and analysis of RVEs, the present Chapter firstly aims to propose another procedure to build a RVE for UD composite plies. The randomness of the obtained RVEs will be checked through a newly developed model for the nearest neighbor distribution in a random hard-core process. In addition, the RVEs will be compared with the real microstructure of glass/epoxy laminates manufactured by vacuum resin infusion, in terms of morphological features and stress distribution, highlighting also the influence of non-uniform fibre diameter. Since the present tool is meant to be used in the prediction of fatigue crack initiation, the stress analysis will be focused on the Local Hydrostatic Stress (LHS) and Local Maximum Principal Stress (LMPS) in the matrix, recently proposed as driving forces to fatigue crack initiation (see Chapter 2, Chapter 3 and Refs. [17-19]). The stress distributions will be analysed under different loading conditions, namely transverse, shear, longitudinal and thermal stresses, highlighting also the influence of the fibre volume fraction.

5.2. RVE construction

The approach chosen to build the RVE is based on the principle of altering an initially regular fibre distribution. This prevents the jamming issue for high fibre volume fractions

that characterise *hard-core* models, and potentially has a more general validity than building the RVE based on experimental microstructural parameters.

Before building the RVE, two more choices have to be discussed. The first one regards if the fibres are allowed to cross an edge of the RVE. If this is prevented, the RVE construction is simpler, and boundary conditions will be applied to the same material (the matrix) on all the edges. However, as highlighted in [3], the local fibre volume fraction becomes smaller in the regions close to the edges. The data from such regions should then be excluded from the analysis.

The second additional choice that affects the procedure to build a RVE regards the boundary conditions to be applied for the stress analysis. Non-periodic boundary conditions applied directly on the RVE edges generate a different stress state in the regions close to a RVE edge than the one in the "bulk" region. Such a perturbation of the stress state is present also if an embedded cell approach is used, due to the interface between a homogeneised material and the region containing separate fibres and matrix. Also in such cases it could be possible not to account the regions close to the RVE edges in the stress analysis.

It is reasonable to expect that for sufficiently large RVEs, the exclusion of the regions close to the edges will not sensibly affect the analysis. In any case, a dedicated study should be carried out to establish the extension of the region to be excluded. To avoid this and to get as many data from a RVE as possible, which means keeping the RVE as small as possible, fibres are allowed to cross the RVE edges, and periodic boundary conditions are applied to the RVE edges. The latter condition implies that when a fibre crosses (or intersect) one edge, it (or part of it) is reported on the opposite side of the RVE.

The application of periodic boundary conditions to a RVE means that the same microstructure is repeating itself in all the directions of the plane. This is not true in real composites, where the morphology changes in each region. However, since the RVE is by

definition representative of the material, the presence of the same microstructure around the RVE is expected not to sensibly alter the morphological features and the stress state of the RVE itself.

The whole procedure to build the RVE is reported in Figure 5.1 and can be summarized in the following steps:

1) Fibre volume fraction (V_f), fibres diameter (D), RVE size (quantified by the edge length to fibre diameter ratio, $\delta = L / D$), and type of the initial array of fibres (square, diagonal square, hexagonal) are given as input.
2) The distance between fibre centres in the initial disposition is calculated so that the distribution of fibres in the RVE is as homogeneous as possible.
3) "Shaking": each fiber is moved in a random direction by a random distance. Since each fibre is intended to be moved only in its vicinity, the distance ranges from 0 to the distance between fibre centres in the initial disposition.
4) The "shaking" step is repeated until convergence is found in terms of the morphological indexes described in paragraph 5.3.

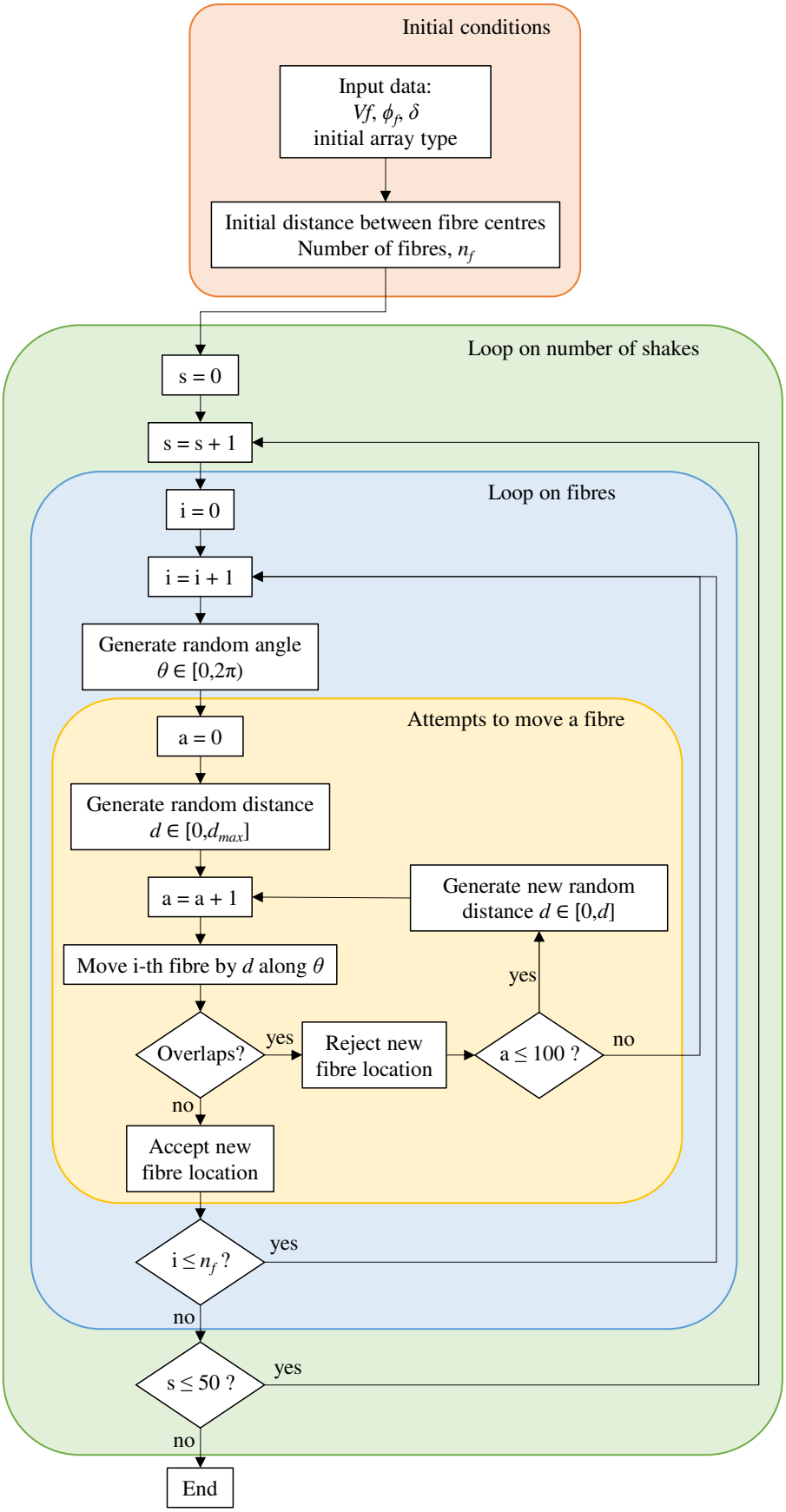

Figure 5.1 – Procedure to build the RVE.

In the procedure, both the maximum distance in step 3 and the number of shakes in step 4 can be arbitrary. To establish such parameters, dedicated analyses were carried out for different fibre volume fractions, namely V_f = 0.45, 0.55, 0.65.

A maximum traveling distance equal to the initial fibre distance was found to be well within the convergence region for a fixed number of shakes in terms of the morphological indexes described in paragraph 5.3 for all the values of V_f. A possible alternative to this approach is to set the maximum distance a fibre can move so as the fibre cannot overlap the nearest neighbor [13]. In this way, however, the fibre displacement may be excessively limited in directions different from the one of the nearest neighbor.

In step 4, a number of 50 "shakes" proved to be sufficient to reach convergence for V_f = 0.45, 0.55. After such a number of shakes, also, the initial fibre arrangement given in point 1 of the procedure does not influence the morphological indexes anymore. A different scenario was found for V_f = 0.65. Given the small mobility of the fibres due to the high packing level, convergence is reached only after several hundreds of shakes. A number of shake equal to 700 was chosen for such a high V_f.

Finally, to avoid touching fibres, which may lead to singular stresses in FE analyses (see paragraph 5.5), a minimum inter-fibre distance of 0.1 μm was imposed.

In Figure 5.2 is reported an example of a RVE construction for V_f = 0.55, D = 16 μm, δ = 30, showing the initial fibre array (Figure 5.2a), the fibre locations after one shake (Figure 5.2b) and the final configuration after 50 shakes (Figure 5.2c).

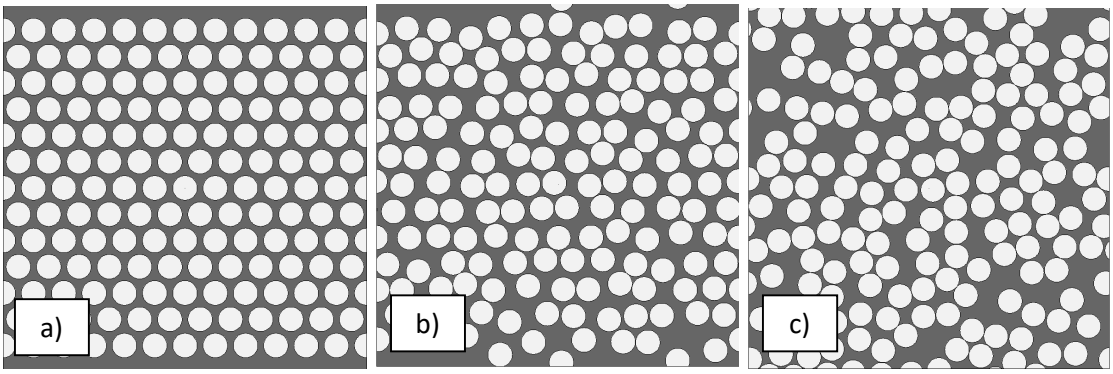

Figure 5.2 – Example of generated RVE with $V_f = 0.55$, $D = 16$ µm, $\delta = 30$: a) initial hexagonal array, b) after 1 shake, c) after 50 shakes.

5.3. Morphological indexes

To assess the validity of a RVE from a morphological point of view, several indexes were proposed in the literature. These indexes aims to quantitatively describe a microstructure and can be divided in short- and long-range descriptors.

On the short-range, the probability distribution of the distance and orientation of the nearest and second-nearest neighbours are often analysed. The centre-to-centre distance is usually considered. Additional information can be taken from Voronoi cells. Given a set of points on a plane (the fibre centres in our case), the region of the plane containing all the points of the plane that are closer to a certain point than to any other is defined as a "Voronoi cell". The ratio between the fibre area and its Voronoi cell area gives the local fibre volume fraction. Both the probability distribution of Voronoi cell areas and their location in the plane can be studied to quantitatively describe a microstructure.

On the long-range, the most frequently used descriptors are the second-order intensity function and the radial distribution function [14]. The second-order intensity function can be defined as the ratio between the number of events expected to lie within a circle of radius h centered in an arbitrary event and the density of events in the observation area. It can be expressed as

$$K(h) = \frac{A}{N_{tot}^2} \sum_{k=1}^{N_{tot}} I_k(h) \tag{5.1}$$

where A is the observation area, N_{tot} the total number of events within A, and $I_k(h)$ the number of events that lie within a circle of radius h having one event as centre, excluding the central event itself. In our case, A is the area of the RVE and an event is represented by the centre of a fibre. This function can be used to detect patterns and regularities in the fibre distribution. In particular, if K(h) is below the K(h) curve of random a Poisson process ($K_P(h) = \pi h^2$), then the fibre distribution has some level of regularity; if K(h) is instead above $K_P(h)$, then some clustering is present; if, finally, K(h) is stair-shaped, it means that the fibre distribution tends to follow a periodic pattern.

Since the RVE has a finite size, a correction of K(h) must be considered when the circle of radius h is intersecting the RVE edges. Several correction methods have been proposed and Yamada and Rogerson [20] showed that the most reliable ones are the use of a weight function w_k in the summation, and the toroidal correction. The weight function is defined as the ratio between the circle area within the observation area and the whole circle area πh^2; the toroidal correction assumes instead that the top and right edges of the observation area are connected, respectively, to the bottom and left ones. Since during the construction of the RVE fibres were allowed to pass from one edge to the opposite one, and periodic boundary conditions will be applied to the RVE for the Finite Element analyses, the toroidal correction was chosen for K(h).

The radial distribution function g(h) represents the probability of the presence of an event in a circular region of radius h and thickness dh, centred in an arbitrary event. It is related to the second-order intensity function by the following formula

$$g(h) = \frac{1}{2\pi h}\frac{dK(h)}{dh} \tag{5.2}$$

and provides information about the intensity of fibre centre-to-centre distances. The most and least frequent distances result, respectively, in local maxima and minima of g(h). For a completely random (Poisson) process, g(h) = 1.

5.4. Morphological validation

The proposed procedure to generate RVEs was compared in terms of the indexes reported in paragraph 5.3 to a *hard-core* process and then to an actual composite microstructure, to test its capability to represent real UD composites. Given the statistical nature of the RVE, its validity is analysed on multiple *realizations*.

5.4.1. Comparison with hard-core process

The procedure to generate a RVE is compared to a random hard-core process in terms of short-range morphological indexes. Davy and Guild [21] proposed an analytical model to predict the probability density function (PDF) of the equivalent radius of the Voronoi cell for a random hard-core process. The equivalent radius is meant as the radius of the circle having the same area of the Voronoi cell. Figure 5.3 shows a comparison between the theoretical PDF and the PDF obtained for 5 RVEs with a volume fraction V_f=0.55, with a uniform fibre diameter. The difference between the RVE results and the theoretical solution suggests that the process simulated with the realization algorithm is not representative of a theoretical hard-core process.

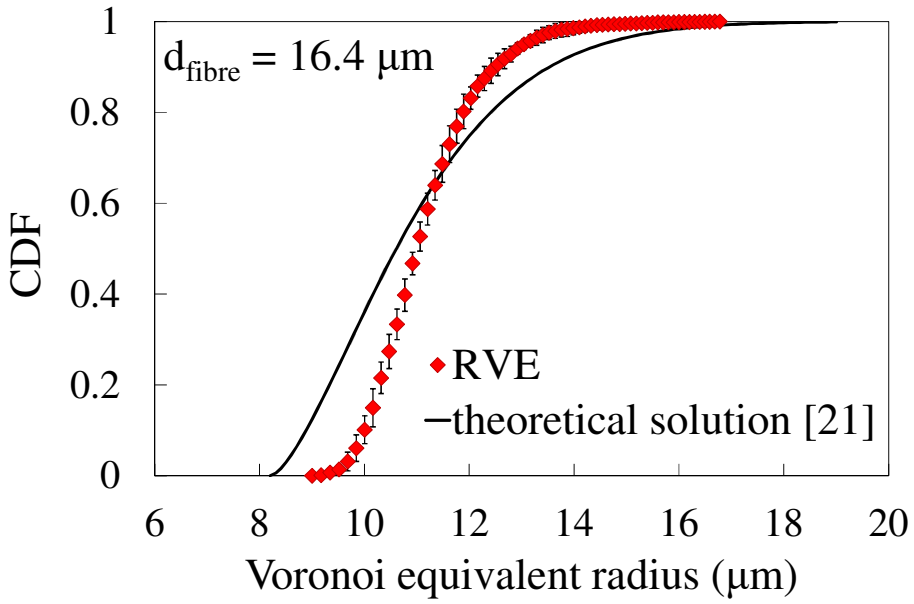

Figure 5.3 – Comparison between the current procedure to generate a RVE and a hard-core process in terms of Voronoi equivalent radius.

As a further proof of this statement, the nearest neighbor distance distribution is analysed. In particular, a model was developed and presented in Appendix 5.A, to predict the cumulative distribution function (CDF) of the nearest neighbor distance for a random hard-core process. In figure 5.4 the PDF trends obtained with the model and with five RVEs for V_f=0.55 and a uniform fibre diameter are compared, revealing, again, a sound agreement. This confirms that the microstructure obtained with the proposed algorithm using a uniform fibre diameter is not a random hard-core process. However, as it will be shown in the next paragraph, the generated microstructure is in a very good agreement with the experimental data for infused laminates. The reason for this may be searched, in the writer's view, in the way of generating the microstructure with the proposed algorithm. In fact, *shaking* the fibres previously placed in a regular hexagonal array is more consistent with what happens in an actual manufacturing process in which the fibres do not appear (as in a theoretical hard-core process) but are moved by the resin during the infusion.

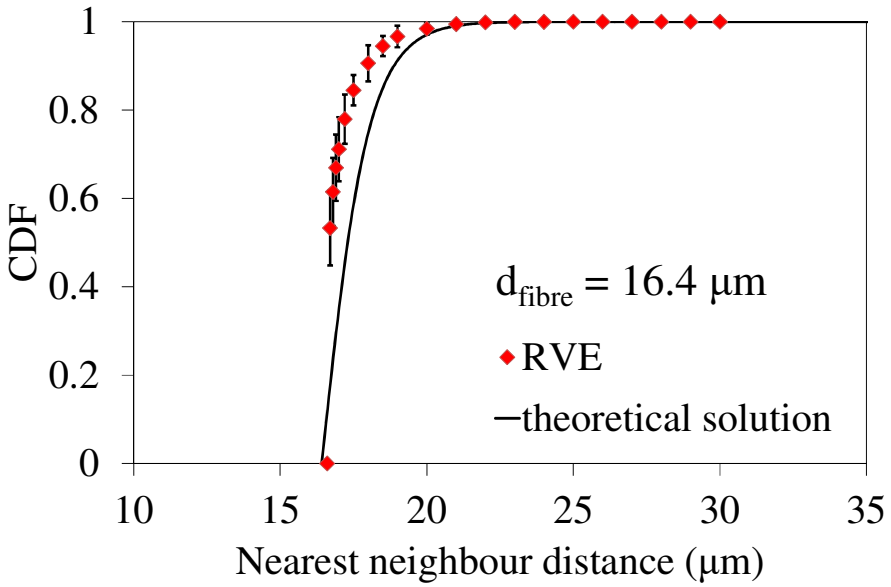

Figure 5.4 – Comparison between current procedure to generate a RVE and hard-core process in terms of the nearest neighbor distance.

5.4.2 – Comparison with experimental microstructures

To obtain a reference microstructure to compare the RVE with, void-free glass/epoxy samples were cut from the $[0/90_2]_S$ and $[0/45_2/0/-45_2]_S$ specimens manufactured and tested in Chapter 4 [22]. The specimens were produced by vacuum resin infusion, and no post-curing was carried out. The samples were cut, respectively, perpendicularly to the fibres in the 90° ply and in the -45° ply in the two laminates, and the faces to be observed were polished down to 0.1 μm SiO_2 solution.

The fibre locations can be obtained from micrographic image of the samples. To automatically distinguish the fibres from the matrix in a greyscale image with the aid of an image analysis tool, the two components must sufficiently differ in the grey level. As can be seen in Figure 5.5a, the glass/epoxy surface "as polished" presents a uniform level of grey. To overcome this issue, the surface was etched with concentrated sulphuric acid (98%) for 20 seconds, greatly enhancing the contrast between fibres and the matrix thanks

to the selective etching of the epoxy resin by the acid (Figure 5.5b). The depth of the etching is minimal and it is believed not to influence the fibre locations.

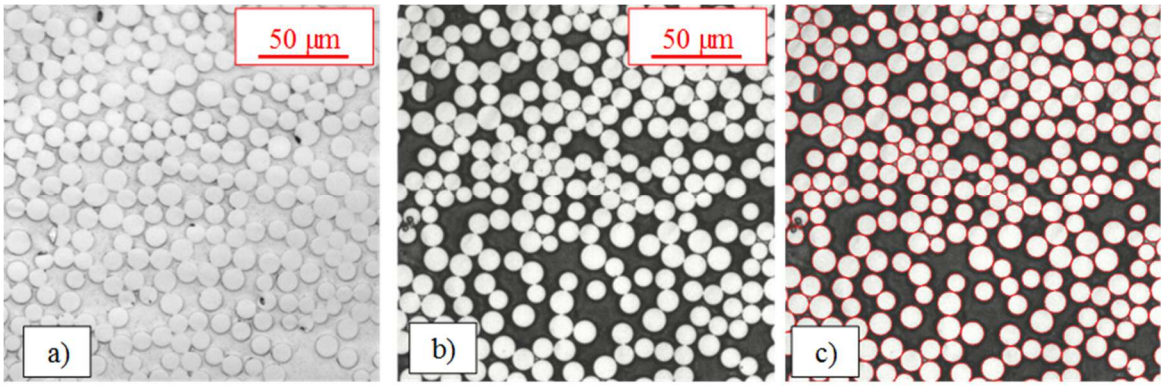

Figure 5.5 – Glass/epoxy sample: a) as polished, b) after chemical etching, c) fibres detection.

An image analysis tool was developed with Matlab® to obtain automatically the fibre diameters and locations from a micrographic image. The tool is based on an in-built function that makes use of the circular Hough transform to detect circles in an image, as also done in [11]. An example of fibre detection is shown in Figure 5.5c. Using Hough transform for fibres detection offers the advantages of having fibre diameter and centre location directly from the image analysis, and also spoiled or dirty fibres are detected as circles. Thirty-five images were analysed for both the laminate stacking sequences, detecting over 50000 fibres. The resulting average fibre volume fraction was $V_f = 0.55$ (Figure 5.6a), and the average fibre diameter 16.4 µm (Figure 5.6b). The distribution of the glass fibre diameter is comparable with the one reported in [10,12].

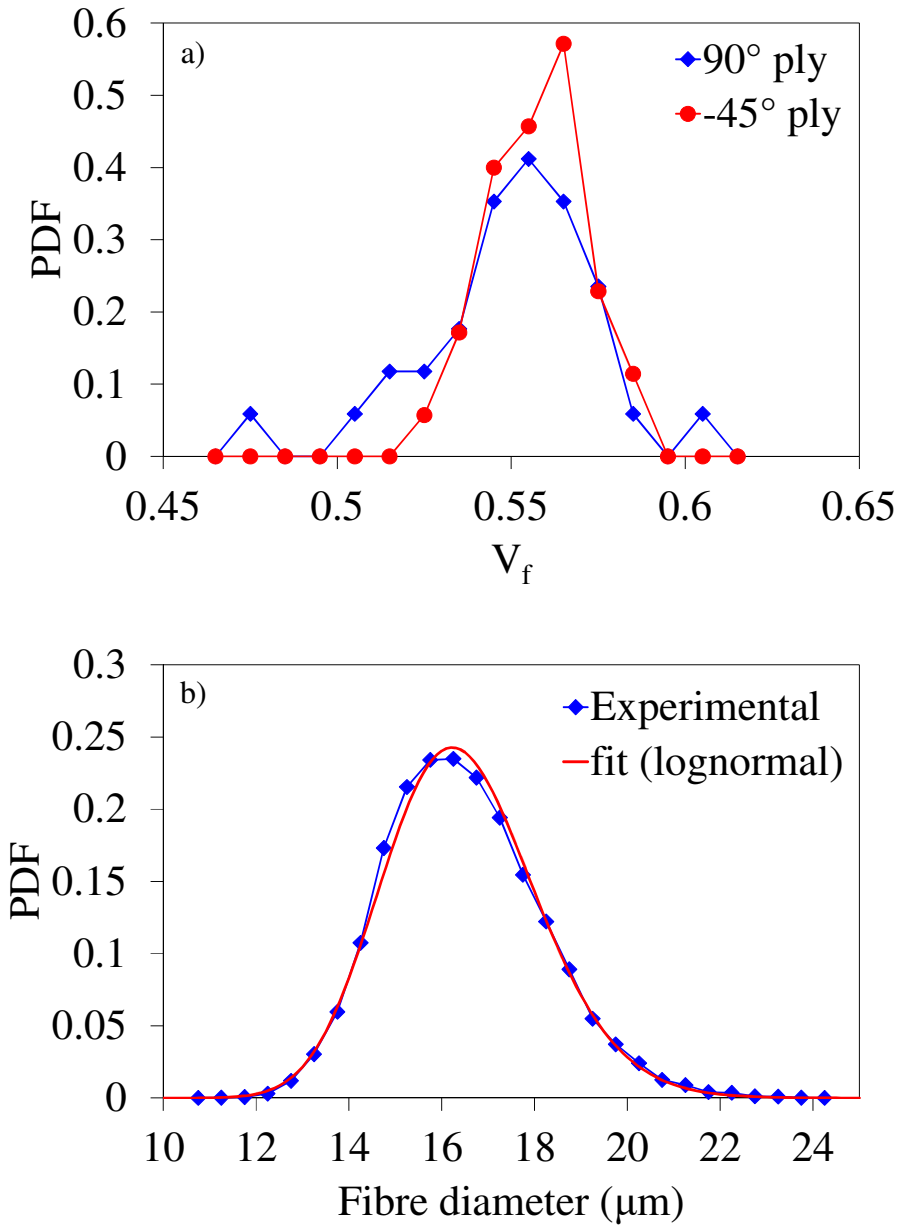

Figure 5.6 – Experimental distribution of (a) fibre volume fraction, and (b) fibre diameters.

The comparison between generated RVEs with uniform fibre diameter and real microstructures is reported in Figures 5.7 to 5.9 in terms of nearest neighbours distance and orientation, and radial distribution function g(h). Since K(h) and g(h) are directly related, the former is not reported.

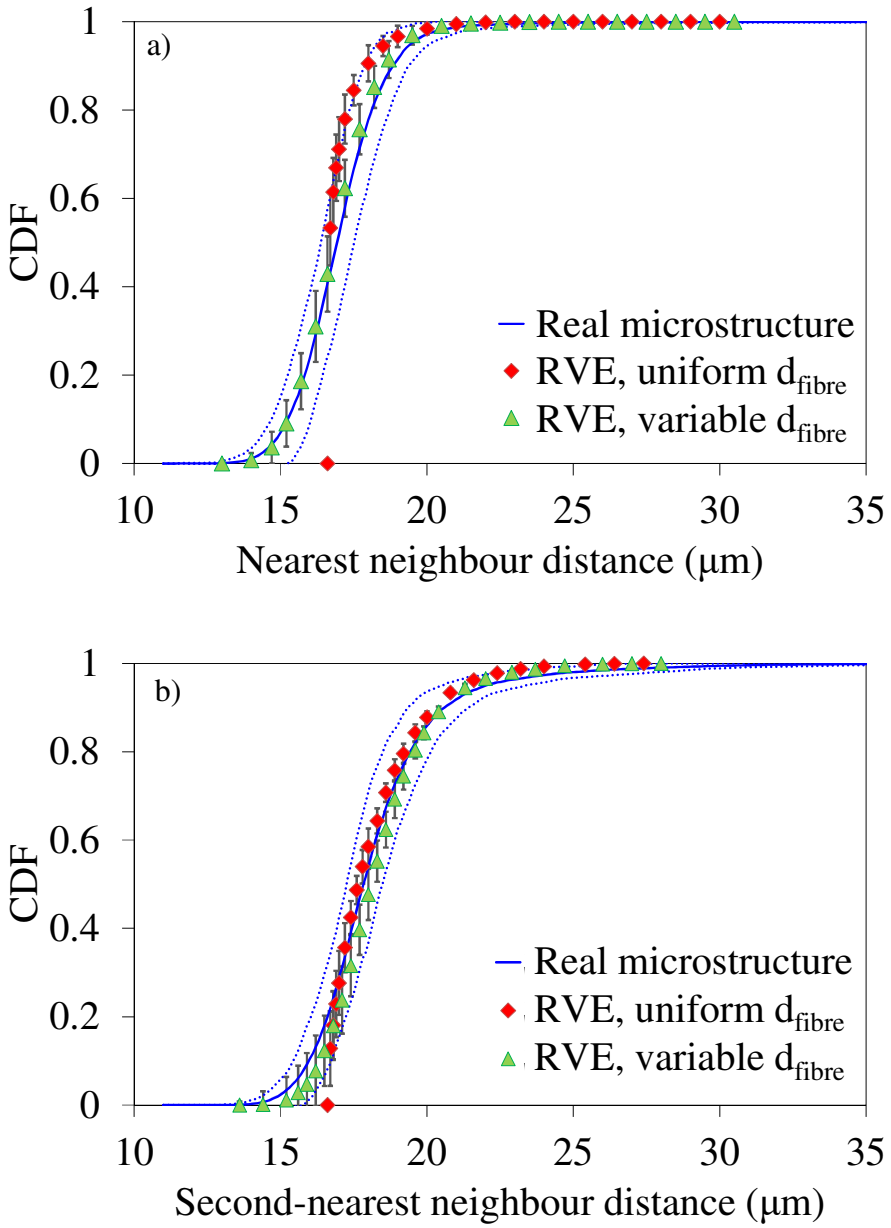

Figure 5.7 – Distribution of (a) nearest and (b) second-nearest neighbour distance. Dotted lines and error bars refer to ± two standard deviations.

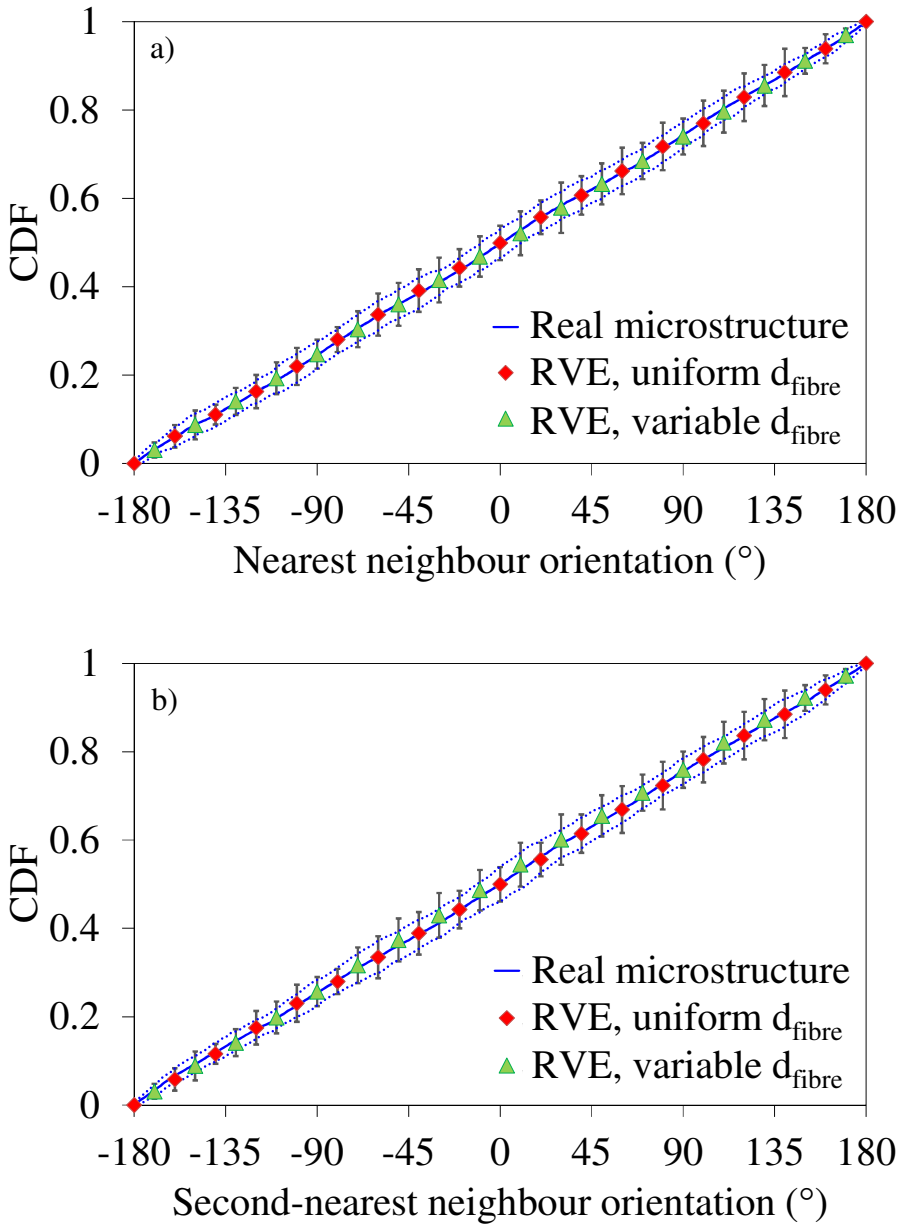

Figure 5.8 – Distribution of (b) nearest and (b) second-nearest neighbour orientation.

Dotted lines and error bars refer to ± two standard deviations.

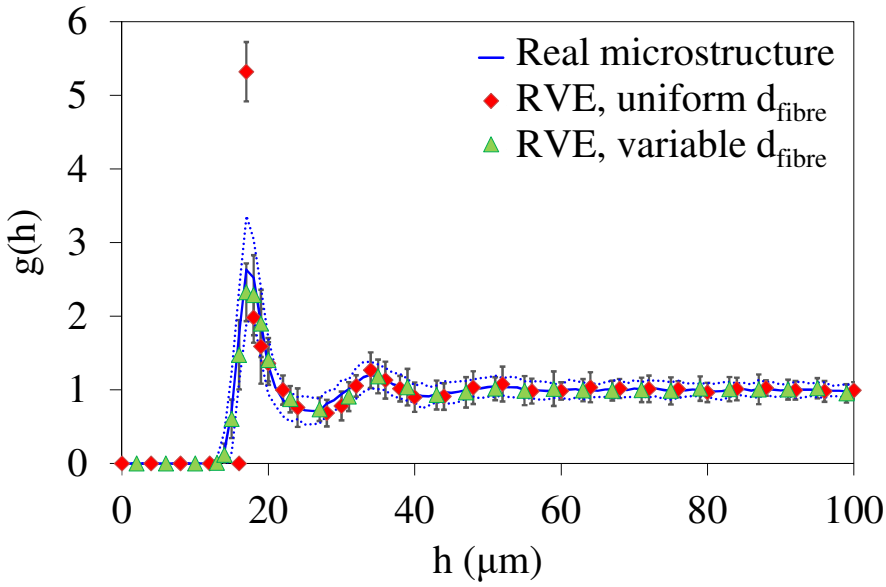

Figure 5.9 – Radial distribution function, g(h). Dotted lines and error bars refer to ± two standard deviations.

From Figures 5.7 to 5.9 it is possible to observe that building RVEs using uniform fibre diameters leads to inaccuracies in the lower part of the distributions of the nearest neighbours distance, and in the radial distribution function g(h) for values of h around the average fibre diameter. Such characteristics are caused by the fact that a uniform fibre diameter prevents distance between fibre centres smaller than the diameter itself, as also highlighted in [1].

As a consequence, an additional step was added to the building procedure: after the fibres are placed with the initial regular pattern, a diameter is assigned to them according to the experimental distribution, fitted with a lognormal distribution with average value 16.4 µm and standard deviation 1.106 µm (Figure 5.6b). This step may lead to initial overlapping between fibres. However, such overlappings are found to be always removed during step 4. Convergence is reached for the same number of shakes as with uniform diameter.

As shown in Figures 5.7-5.9, including the fibre diameter distribution leads to the construction of RVEs capable of better representing the experimental microstructure.

A dedicated study showed that a RVE size of $\delta = 40$ is sufficient to be representative in terms of morphological indexes, hence this size was used for the comparisons.

5.5. Mechanical validation

The purpose of a RVE of a UD composite ply can be limited to describe the actual microstructure. However, more useful information for design may come from its stress analysis.

The present RVE is intended to be used in the prediction of the fatigue crack initiation in multidirectional laminates. Therefore, to assess the validity of the RVE under a mechanical point of view, RVEs were compared to real microstructures in terms of the distribution of the Local Hydrostatic Stress (LHS) and Local Maximum Principal Stress (LMPS) in the matrix, which have been recently proposed by Carraro and Quaresimin as driving forces to the fatigue crack initiation (see Chapter 2, Chapter 3 and Refs. [17-19]). The stress distributions were analysed under different loading conditions, namely a transverse stress (σ_2), shear stress (σ_6), longitudinal stress (σ_1), and thermal gap (ΔT).

Stress analyses on the RVEs were carried out by means of Finite Element (FE) software ANSYS 15.0. To keep the same element type for all the loading conditions, 3-D geometry were used in all cases (20-nodes element SOLID186). A mesh sensitivity study lead to an element size of 0.5 μm. A perfect bond was assumed between fibres and matrix, whose mechanical properties are reported in Table 5.1. Periodic boundary conditions were applied in all the directions. To apply consistent periodic boundary conditions on real microstructures (see paragraph 5.4.2), the following steps were taken before the conduction of FE analyses:

1) a central square is taken from a micrographic image

2) for every fibre that intersects one edge of the square, the part of the fibre that lies outside the RVE is reported at the opposite edge;
3) fibres chosen randomly among the ones that during step 2 cause any overlap are eliminated.

This process is found not to affect the fibre volume fraction. Concerning the size of the central square, a square with $\delta = 40$ was sufficiently large to be representative in terms of stress distributions.

Table 5.1 – Mechanical properties used in Finite Element Analyses.

Property	Symbol	Unit	Matrix (epoxy resin)	Fibres (glass)
Young's Modulus	E	MPa	3100	74000
Poisson's ratio	ν	---	0.38	0.25
C.T.E.	α	---	$6.75 \cdot 10^{-5}$	$7 \cdot 10^{-6}$

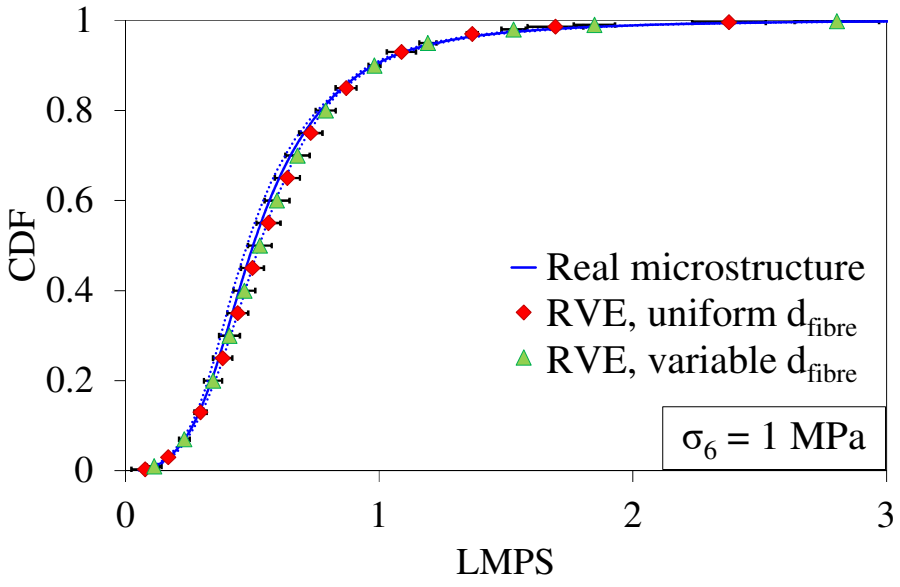

Figure 5.10 – Distribution of LMPS in the matrix under global shear stress (σ_6). Dotted lines and error bars refer to ± two standard deviations.

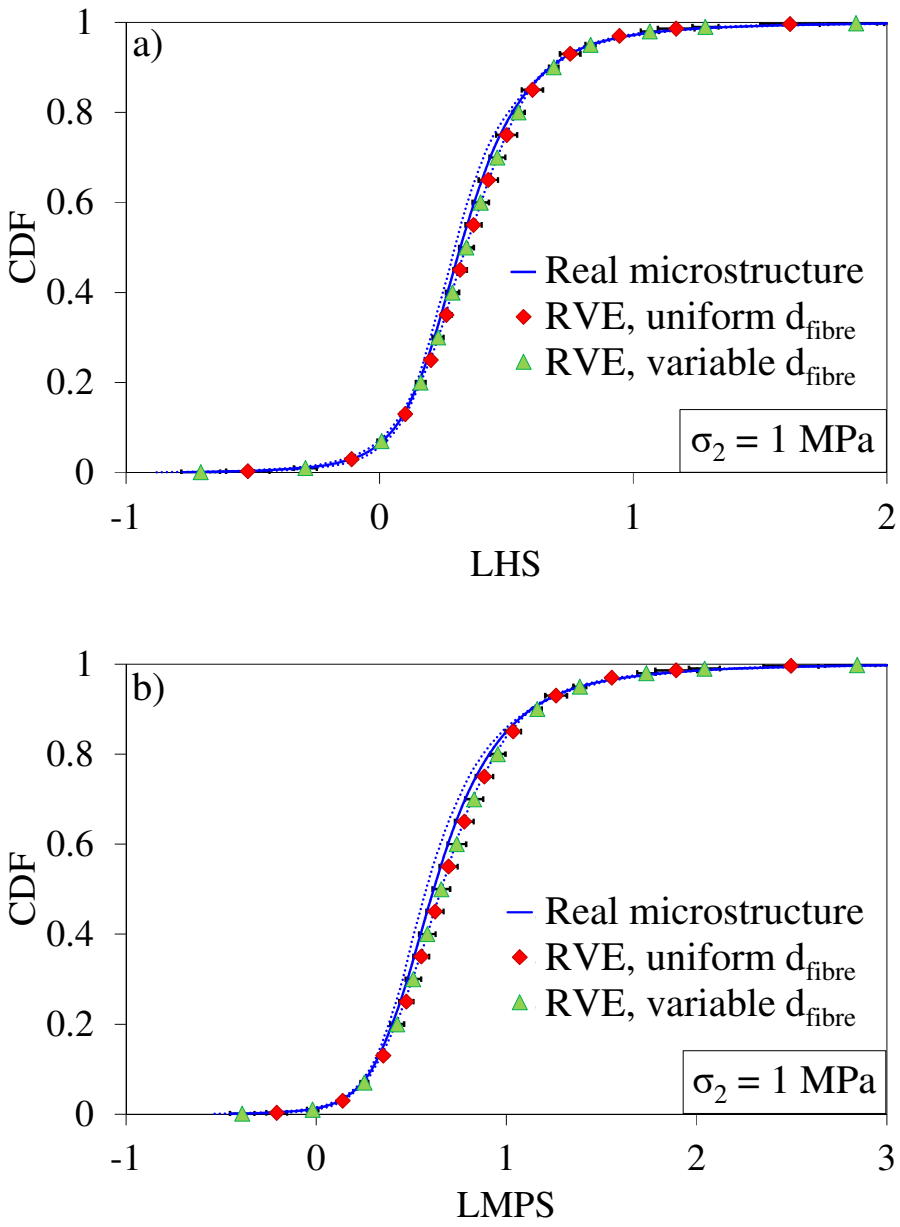

Figure 5.11 – Distribution of (b) LHS and (b) LMPS in the matrix under global transverse stress (σ_2). Dotted lines and error bars refer to ± two standard deviations.

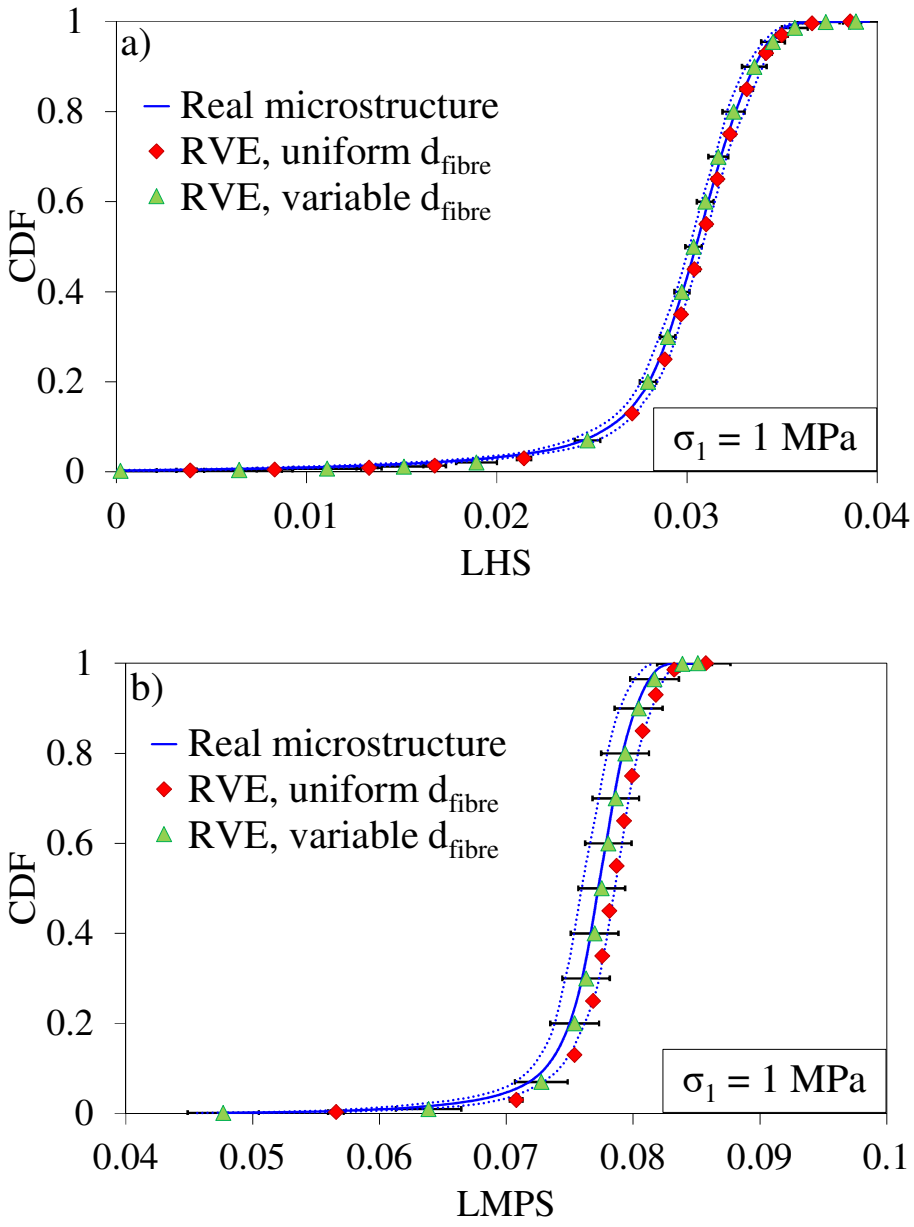

Figure 5.12 – Distribution of (b) LHS and (b) LMPS in the matrix under global longitudinal stress (σ_1). Dotted lines and error bars refer to ± two standard deviations.

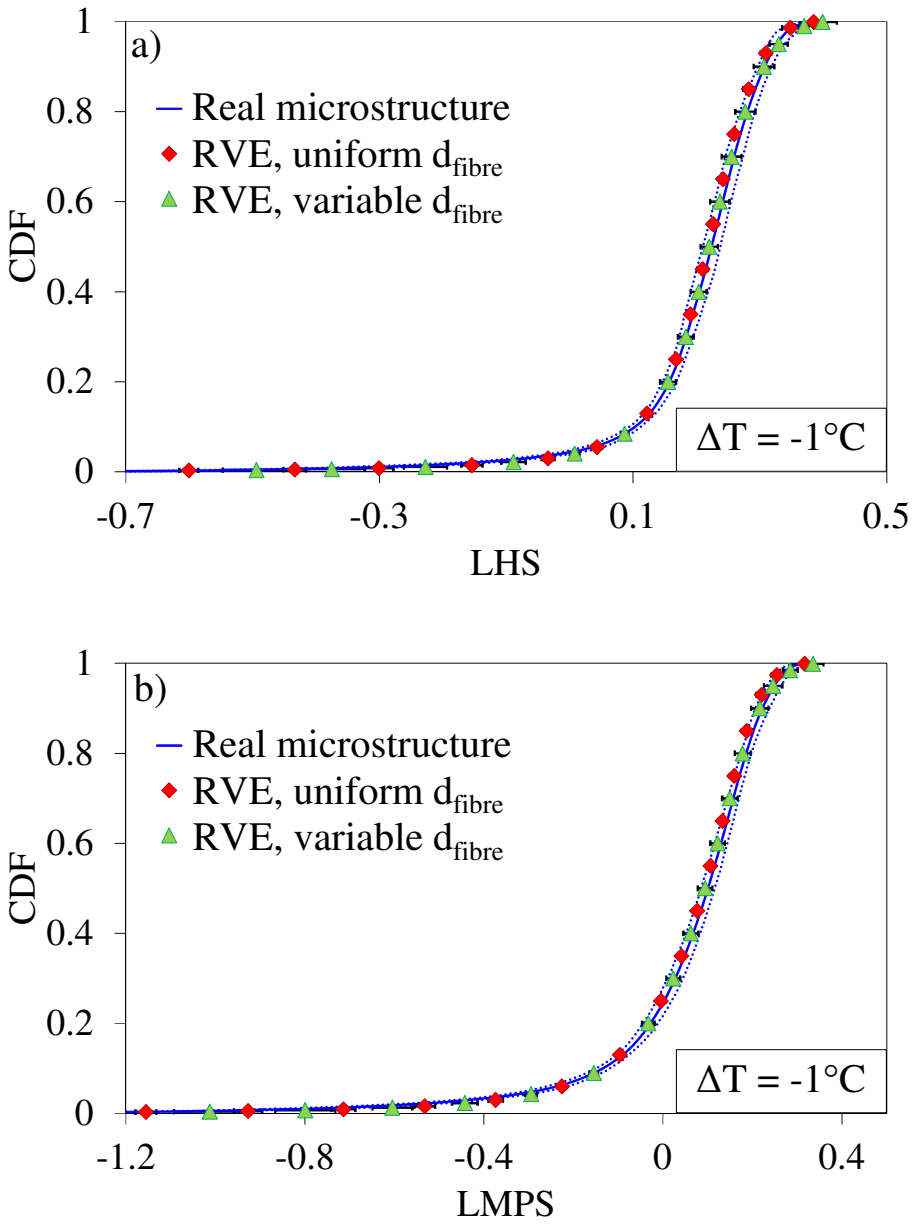

Figure 5.13 – Distribution of (b) LHS and (b) LMPS in the matrix under temperature gradient (ΔT). Dotted lines and error bars refer to ± two standard deviations.

Figures 5.10 to 5.13 show the cumulative distribution function (CDF) of LHS and LMPS for all the global loading conditions applied (in the case of shear stress, LHS is zero). It is possible to observe that the proposed RVE is capable of representing real microstructures also in terms of stress distribution, under all the loading conditions studied. RVEs were

characterized by $\delta = 40$, confirming that such a size is sufficient to achieve representativeness in terms of both stress distribution and morphological features.

It can be highlighted that not accounting for the distribution of fibre diameters does not seem to influence much the stress distribution, despite the differences in morphological indexes, with the exception of a smaller scatter in some cases. This can be explained by the fact that stresses are more influenced by the inter-fibre spacing than the distance between fibres (measured as the distance between fibre centres). Such inter-fibre distances may not vary much if the distribution of fibre diameter is taken into account or not.

5.6. Influence of fibre volume fraction on stress distributions

The morphological and mechanical validation of the RVEs was carried out only for fibre volume fractions around 0.55. Assuming that the procedure to build the RVE keeps its validity also at other fibre volume fractions, it is possible to study how the amount of reinforcement influences the distribution of the LHS and LMPS in the matrix under all the loading conditions previously considered. The results of the analysis are reported in Figures 5.14 to 5.17. Under transverse and shear stresses (Figures 5.14-5.15), a larger fibre volume fraction leads to a higher number of fibres carrying the load, therefore the average stress state in the matrix diminishes. However, the largest stress values, where the first damages are expected to occur, are comparable for all the V_f considered, if not slightly higher for the higher volume fractions. To explain this, it has to be considered that under transverse and shear stresses, the highest stress concentrations occur where fibres are very close to each other and aligned along the transverse direction. Fibres are more closely packed for larger V_f, which makes the presence of higher stress concentrations more likely to take place.

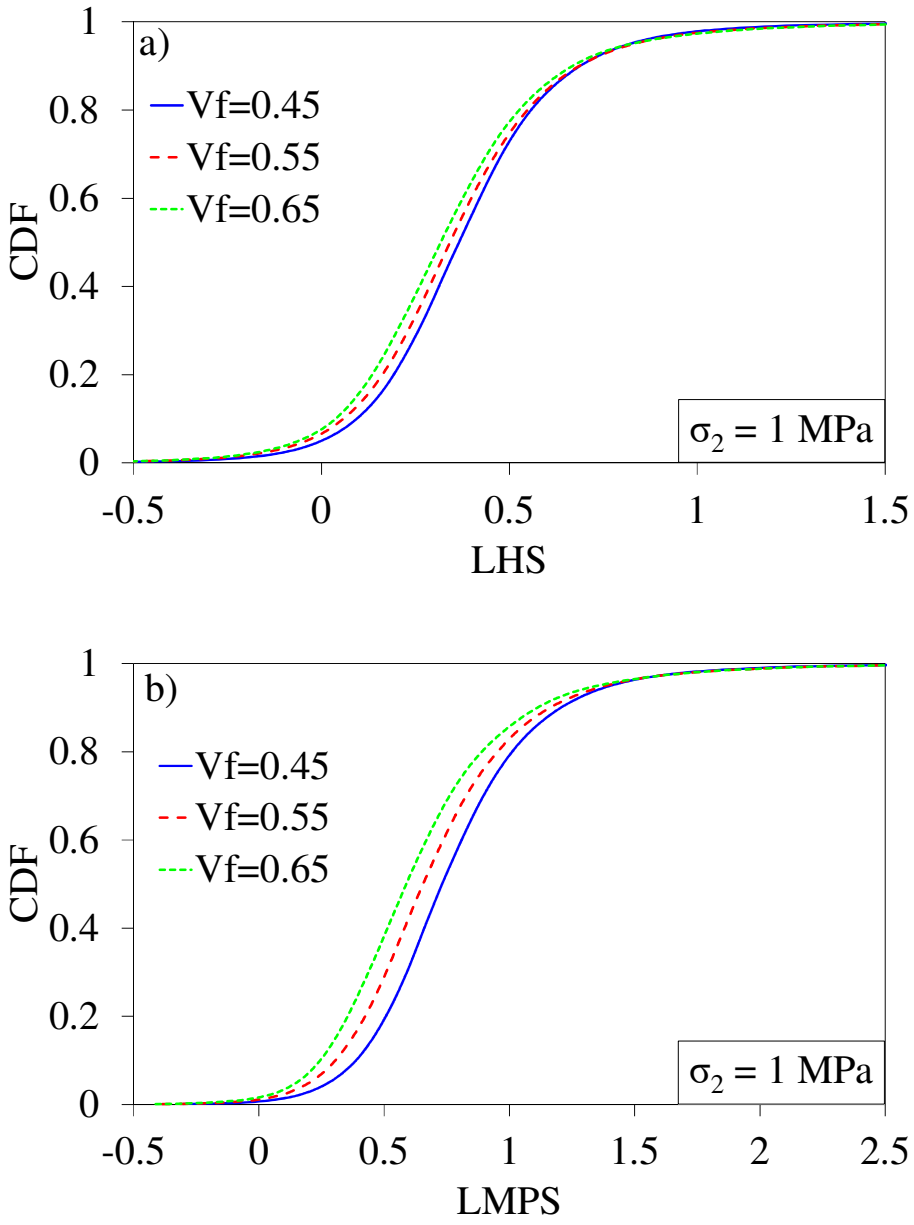

Figure 5.14 –Distribution of (a) LHS and (b) LMPS in the matrix under global transverse stress (σ_2) for different fibre volume fractions (V_f).

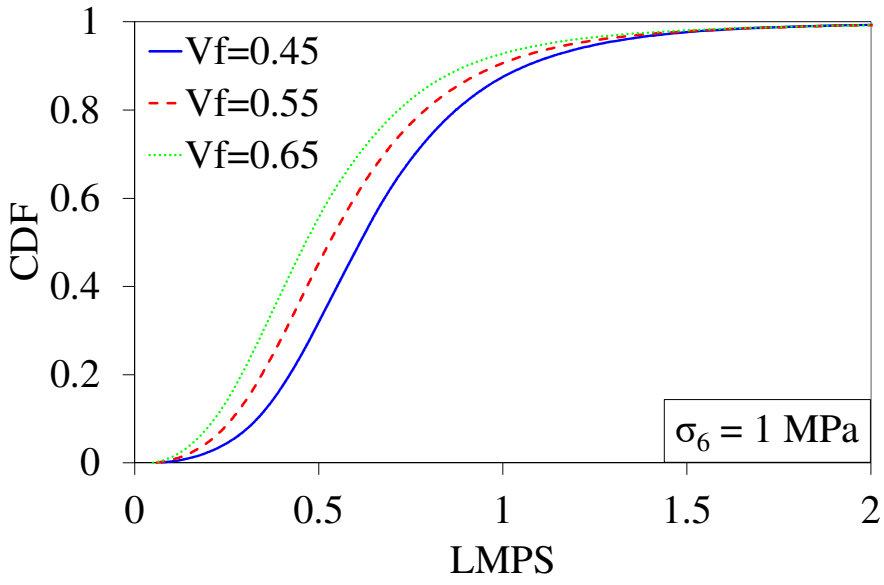

Figure 5.15 –Distribution of LMPS in the matrix under global shear stress (σ_6) for different fibre volume fractions (V_f).

Under global longitudinal stress (Figure 5.16), the average stress in the matrix is found again to be smaller for higher V_f, due to a larger number of load-carrying fibres. This trend holds also for the highest stresses, since in this case the matrix between fibres close to each other is in compression.

If the stress distributions are plotted for a unit strain (1%) instead that for a unit stress, the trends change as shown in Figures 5.17 to 5.19. In the presence of transverse and shear stresses, the larger global stress needed to reach the same strain at higher fibre volume fractions leads to higher stresses in the matrix. The same trend also holds when a longitudinal stress is applied, even if it is not so clear for the LMPS distribution.

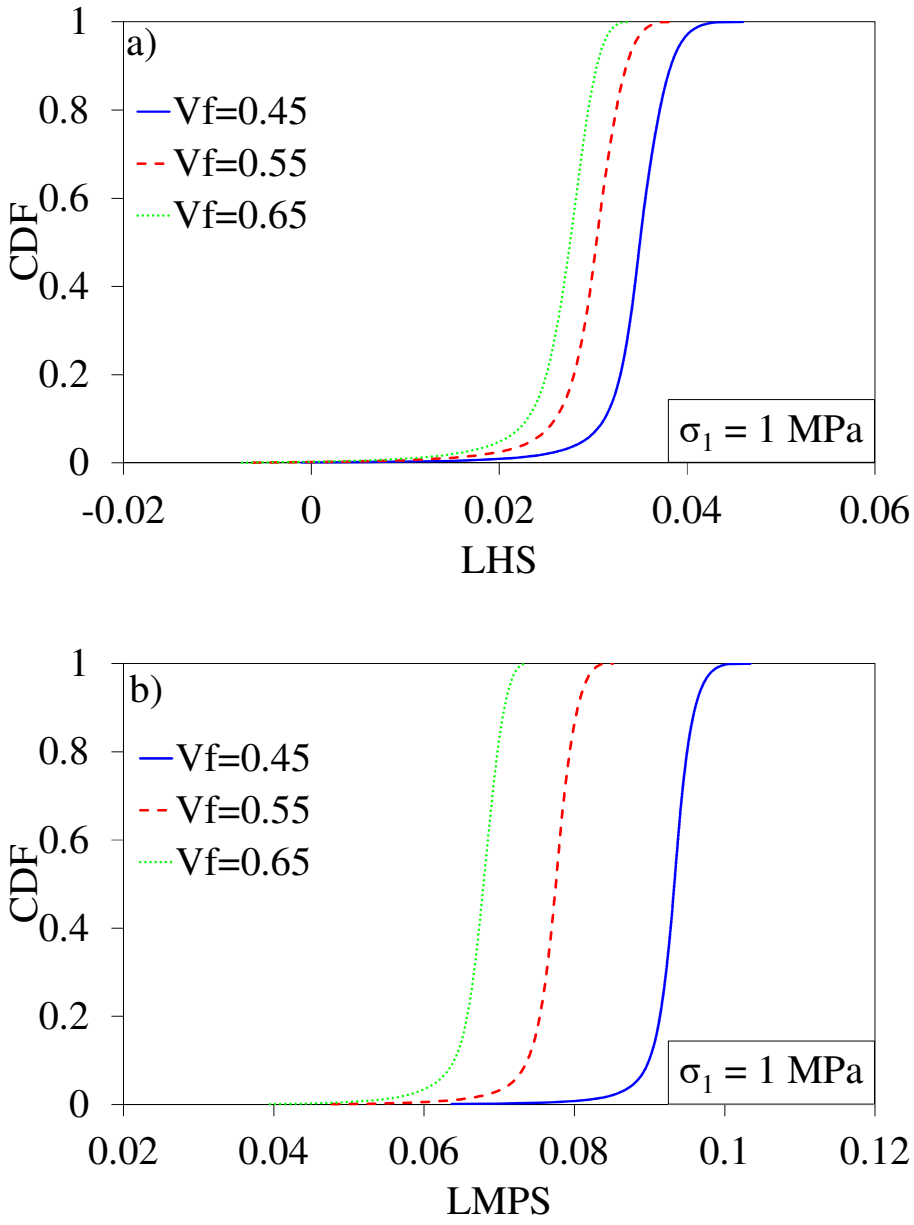

Figure 5.16 –Distribution of (a) LHS and (b) LMPS in the matrix under global longitudinal stress (σ_1) for different fibre volume fractions (V_f).

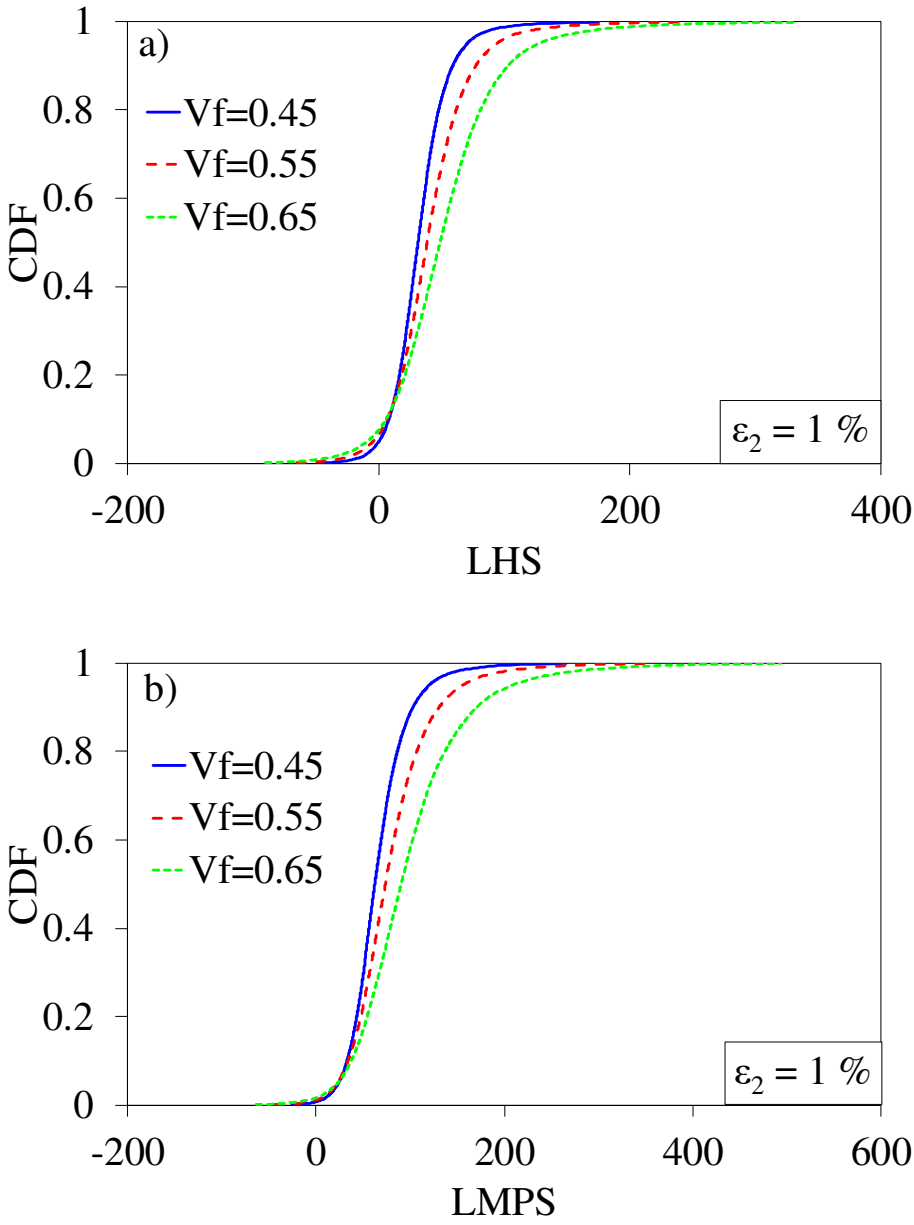

Figure 5.17 –Distribution of (a) LHS and (b) LMPS in the matrix under global transverse strain (ε_2) for different fibre volume fractions (V_f).

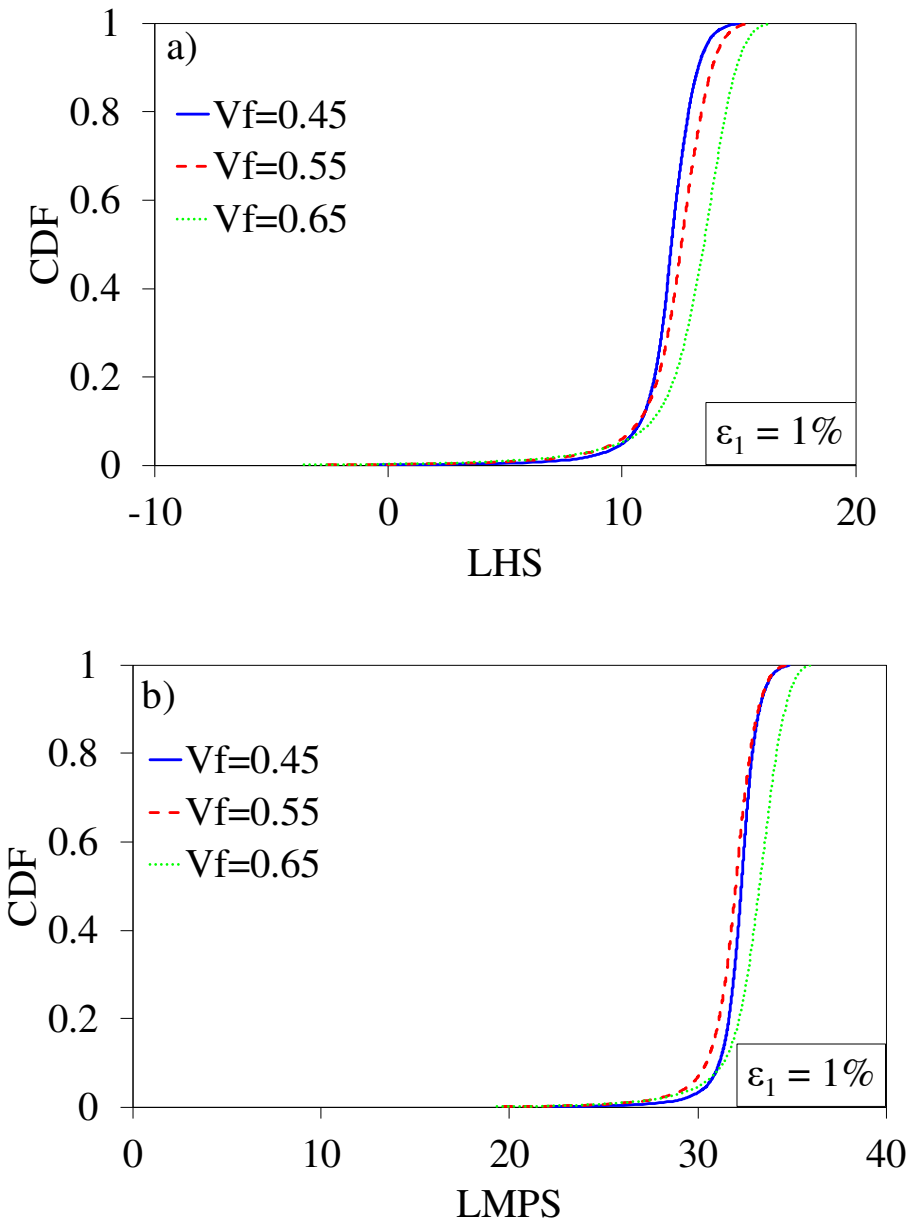

Figure 5.18 –Distribution of (a) LHS and (b) LMPS in the matrix under global longitudinal strain (ε_1) for different fibre volume fractions (V_f).

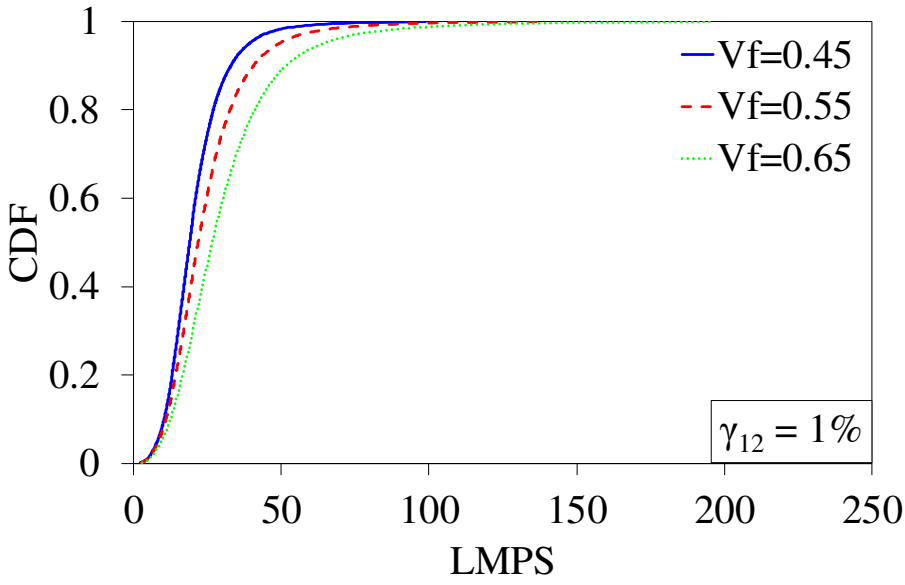

Figure 5.19 –Distribution of LMPS in the matrix under global shear strain (γ_{12}) for different fibre volume fractions (V_f).

If a negative temperature gradient is applied (Figure 5.20), the matrix between almost-touching fibres is again in compression, as under σ_1. Contrarily to the previous loading conditions, larger fibre volume fractions appear to lead to larger positive stresses also for the highest CDF values, indicating a more critical scenario.

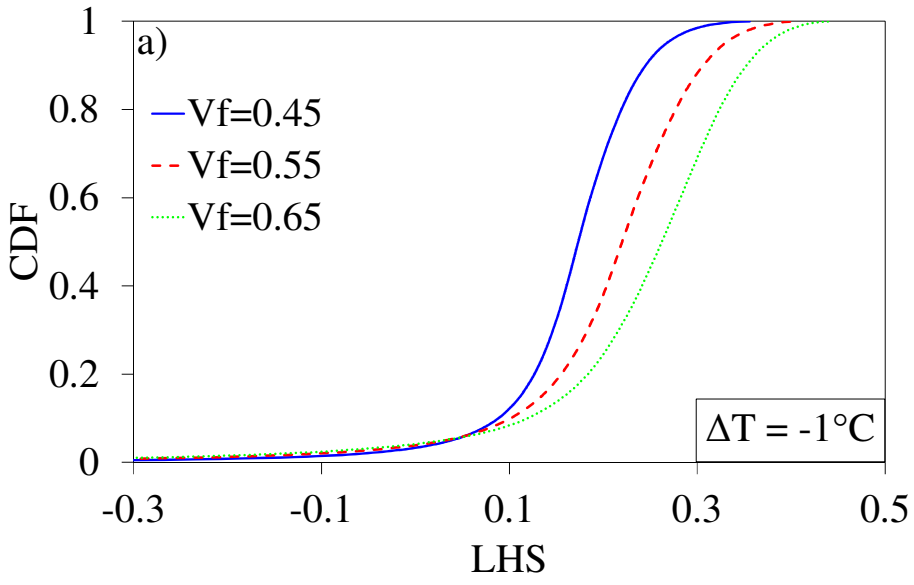

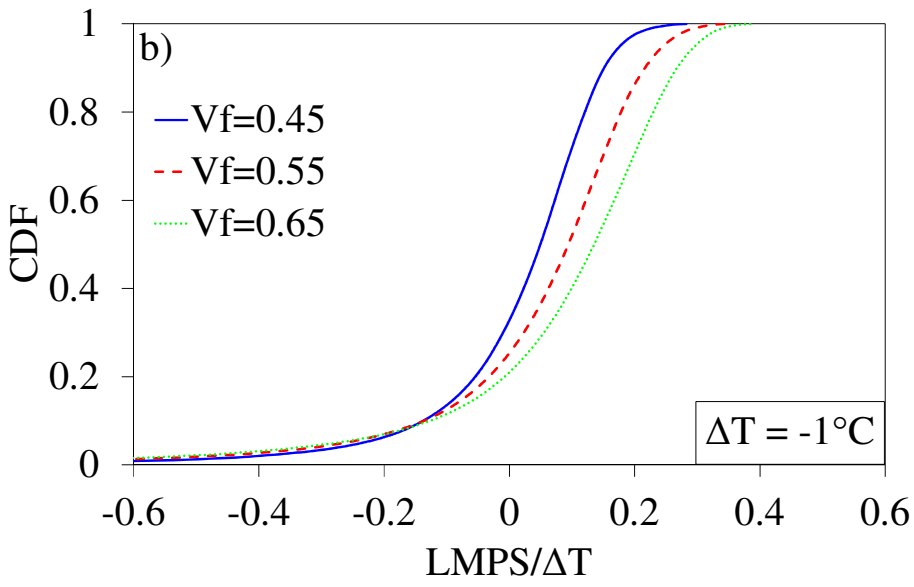

Figure 5.20 – Distribution of (a) LHS and (b) LMPS in the matrix under temperature gradient (ΔT) for different fibre volume fractions (V_f).

5.7. Conclusions

To study the stress distribution within the matrix in real composite microstructures, a new and efficient method to build RVEs of unidirectional composite plies was proposed, based on the alteration of an initially regular fibres distribution.

The obtained RVEs were validated in terms of morphological indexes and stress distributions with the microstructure of vacuum infused glass/epoxy laminates, both neglecting and accounting for the actual fibre diameter distribution. The stress analysis focused on the Local Hydrostatic Stress (LHS) and Local Maximum Principal Stress (LMPS), recently proposed as driving forces to fatigue crack initiation in multidirectional laminates, calculated by FEM under transverse, shear and longitudinal stresses, and thermal gradient. The RVEs showed a good agreement with the real microstructure for both the morphological indexes and the stress distributions.

If the distribution of the fibre diameter is neglected, some differences are encountered in the morphological indexes for small distances from a fibre centre. Despite such differences,

good agreement is achieved for the stress distribution also in this case, even if the scatter resulted smaller.

Finally, the influence of the fibre volume fraction on the distribution of LHS and LMPS has been studied. A small influence of this parameter was found on the highest values of such stresses under all the mechanical loading conditions, whereas larger volume fractions lead to larger stresses under a negative thermal gradient.

In the next Chapter, the present tool is used to propose a criterion to predict of fatigue crack initiation in composite laminates containing voids.

Appendix 5.A

In this appendix, a newly developed model is presented for the prediction of the nearest neighbor distance in a hard-core spatial Poisson process. This model is used in paragraph 5.4.1 to compare the morphology of the realized RVEs to that relevant to such a process, considering a uniform fibre diameter, for simplicity of treatise. An approximated solution for the nearest neighbor distribution was provided by Torquato [23]. The present model was developed to improve the existing solution, starting from geometrical considerations.

Let us consider a spatial distribution involving fibres with a diameter D and a volume fraction V_f. The present model is an iterative one. For the first iteration, the probability that the first neighbor distance is higher than a distance h_1, the subscript 1 indicating the first iteration, is equal to the probability that there are no fibre centres in the shaded area of Figure 5.A1. Differently from a Poisson point process, the considered area is deprived of the region occupied by the fibre, as well as the region in which any other fibre centre cannot be placed because of the non-interpenetrating condition. Therefore, the probability that the distance is higher than h_1 is

$$P_1(h_1) = 1 - \exp\left[-\lambda'\pi\left(h_1^2 - D^2\right)\right] \tag{5.A1}$$

where λ' is the process intensity, corrected as proposed by Davy and Guild [21] to account for a hard-core process. In particular, $\lambda' = k \cdot \lambda / V_f$, where k depends only on the fibre volume fraction and can be calculated numerically as explained in [21]. λ is the Poisson process intensity:

$$\lambda = \frac{4 \cdot V_f}{\pi D^2} \tag{5.A2}$$

By differentiating Eq. (5.A1) it is possible to obtain the probability density function for the nearest neighbor distance at the first iteration, which reads

$$f_1(h_1) = \frac{dP_1}{dh_1} = 2\pi\lambda' h_1 \cdot \exp\left[-\pi\lambda' \cdot \left(h_1^2 - D^2\right)\right] \tag{5.A3}$$

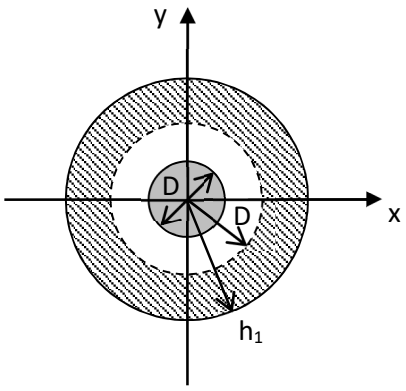

Figure 5.A1: Region which must contain no fibre centre at the first iteration.

The prediction of $P_1(h_1)$ obtained with the first iteration is expected to be overestimated. In fact, the shaded area in Figure 5.A1 should be deprived of the area corresponding to the

intersection between the shaded area itself and the circle of radius D, centered at a distance h_1 from the considered fibre (see Figure 5.A2). In fact, this intersection area cannot be occupied by any fibre centre thanks to the non-interpenetration condition. At the second iteration, therefore, the probability that the nearest neighbor distance is higher than h_2 corresponds to the probability of finding no fibre centre in an area $\pi(h_2^2 - D^2)$-A_i, where A_i is the intersection area which depends on h_1 and h_2 and reads (Figure 5.2):

$$\begin{aligned} A_i(h_1,h_2) &= h_1\left(\frac{1}{2}C - B\right) - 2D\cdot \mathrm{Arccot}\left(\frac{h_1}{C}\right) + \\ &+ D^2\cdot \mathrm{Arctan}\left(\frac{2Bh_1}{D^2+h_1^2-h_2^2}\right) + h_2^2\cdot \mathrm{Arctan}\left(\frac{2Bh_1}{h_1^2+h_2^2-D^2}\right), \text{if } D \le h_1 < 2D \\ A_i(h_1,h_2) &= -Bh_1 + h_2^2\cdot \mathrm{Arctan}\left(\frac{2Bh_1}{h_1^2+h_2^2-D^2}\right), \text{if } 2D \le h_1 < h_2 + D \\ A_i(h_1,h_2) &= 0, \text{if } h_1 \ge h_2 + D \end{aligned} \tag{5.A4}$$

Where

$$\begin{aligned} B &= \sqrt{h_2^2 - \frac{\left(h_1^2+h_2^2-D^2\right)^2}{4h_1^2}} \\ C &= \sqrt{4D^2 - h_1^2} \end{aligned} \tag{5.A5}$$

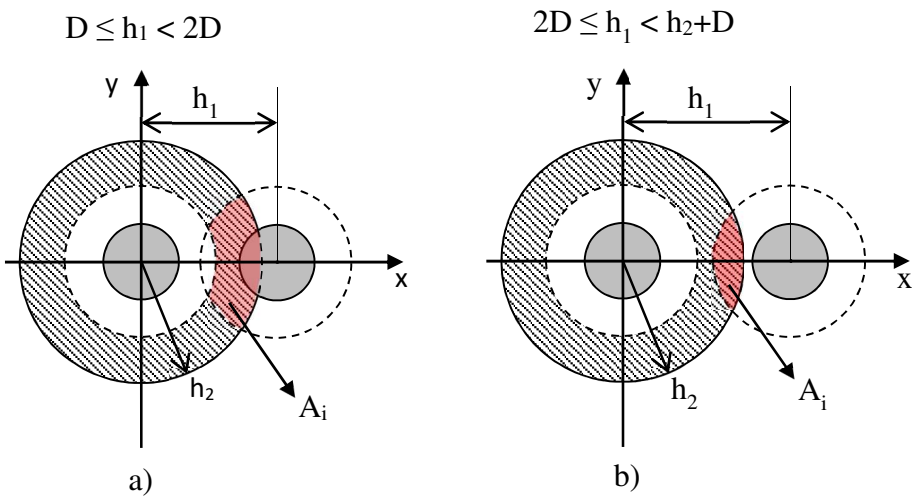

Figure 5.A2: Intersection area

Therefore, for a given value of the distance h_2 at the second iteration, an average intersection area $\bar{A}_i(h_2)$ must be eliminated from the shaded annulus in Figure 5.A1:

$$\bar{A}_i(h_2) = \int_{h_2}^{h_2+D} A_i(h_1, h_2) \cdot f(h_1)\, dh_1 \tag{5.A6}$$

As a consequence, the probability that, at the second iteration, the nearest neighbor distance is lower than a certain value h_2 is

$$P_2(h_2) = 1 - \exp\left[-\lambda' \pi \left(h_1^2 - D^2\right) - \bar{A}_i(h_2)\right] \tag{5.A7}$$

Again, the probability density function can be calculated differentiating Eq. (5.A7):

$$f_2(h_2) = \frac{dP_2}{dh_2} \tag{5.A8}$$

Given the complexity of the functions involved, the integral in Eq. (5.A6), and therefore the derivative in Eq. (5.A8), are calculated with a numerical approach.

Now, a third iteration can be performed with the same procedure, using the probability density function $f_2(h_2)$ for the calculation of the average intersection area as in Eq. (5.A6). The procedure should be iterated until convergence, which is observed to occur after a very limited number of iterations.

As an example, let us consider a volume fraction V_f of 0.6. The predicted trend for the CDF of the nearest neighbour distance h, normalized to the fibre diameter D, is shown in Figure 5.A3. It can be seen that at the third iteration the solution is already at convergence. In addition, the model proposed by Torquato [23] is shown to overestimate the cumulative probability, mainly in the region of low values of h/D, which are actually those of higher interest as the peak stresses occur where the fibres are closer, and also well oriented along the transverse direction.

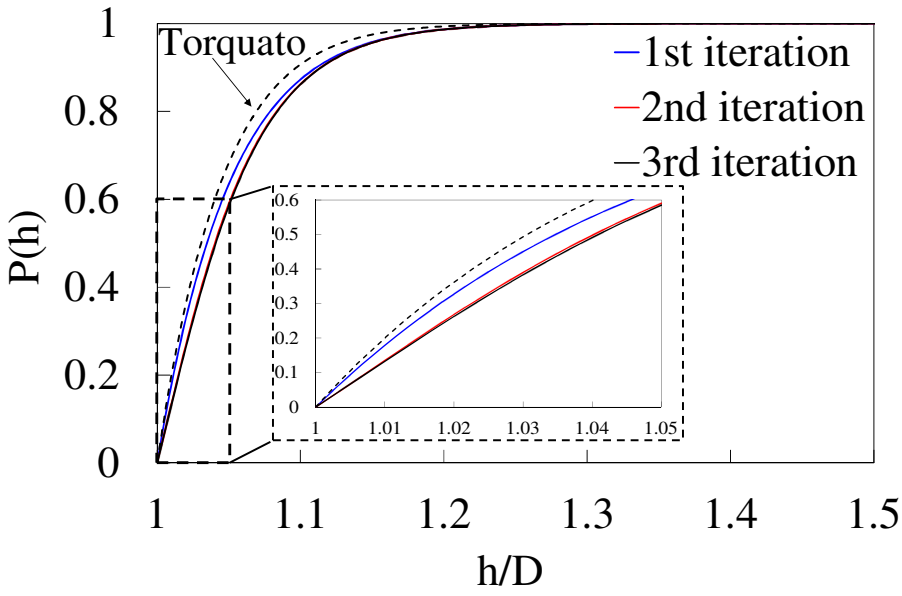

Figure 5.A3: Prediction of the cumulative probability of the first neighbor distance for V_f=0.6

References of Chapter 5

[1] Pyrz R. Quantitative description of the microstructure of composites. Part I: morphology of unidirectional composite systems. Composite Science and Technology 1994; 50: 197-208.

[2] Bulsara VN, Talreja R, Qu J, Damage initiation under transverse loading of unidirectional composites with arbitrarily distributed fibers. Composite Science and Technology 1999; 59: 673-682.

[3] Knight MG, Wrobel LC, Henshall JL, Micromechanical response of fibre-reinforced material using the boundary element technique. Composite Structures 2003; 62: 341-352.

[4] Oh JH, Jin KK, Ha SK. Interfacial strain distribution of a unidirectional composite with randomly distributed fibers under transverse loading. Journal of Composite Materials 2006; 40: 759-778.

[5] Trias D, Costa J, Mayugo JA, Hurtado JE. Random models versus periodic models for fibre reinforced composites. Computational Material Science 2006; 38: 316-324.

[6] Y. Huang Y, K. K. Jin KK, S. K. Ha SK, Effects of fiber arrangement on mechanical behavior of unidirectional composites, Journal of Composite Materials 2008; 42: 1851-1871.

[7] Trias D, Costa J, Turon A, Hurtado JE. Determination of the critical size of a statistical representative volume elements (SRVE) for carbon reinforced polymers. Acta Materialia 2006; 54: 3471-3484.

[8] Pontefisso A, Zappalorto M, Quaresimin M. An efficient RVE formulation for the analysis of the elastic properties of spherical nanoparticle reinforced polymers. Computational Materials Science 2015; 96: 319-326.

[9] Melro AR, Camanho PP, Pinho ST. Generation of random distribution of fibers in long-fibre reinforced composites. Composite Science and Technology 2008; 68: 2092-2102.

[10] Zangenberg J, Bronsted P. Quantitative study on the statistical properties of fibre architecture of genuine and numerical composite microstructures. Composites Part A – Applied Science and Manufacturing 2013; 47: 124-134.

[11] Thomas M, Boyard N, Perez L, Jarny Y, D. Delaunay D. Representative volume element of anisotropic unidirectional carbon-epoxy composite with high-fibre volume fraction. Composite Science and Technology 2008; 68: 3184-3192.

[12] Gusev AA, Hine PJ, Ward IM, Fiber packing and elastic properties of a transversely random unidirectional glass/epoxy composite. Composite Science and Technology 2000; 60: 535-541.

[13] Wongsto A, Li S, Micromechanical FE analysis of UD fibre-reinforced composites with fibres distributed at random over the transverse cross-section. Composites Part A – Applied Science and Manufacturing 2005; 36: 1246-1266.

[14] Ripley BD, Modelling spatial patterns. Journal of the Royal Statistical Society, Series B (Methodological) 1977; 39: 172-212.

[15] Vaughan TJ, McCarthy CT. A combined experimental-numerical approach for generating statistically equivalent fibre distributions for high strength laminated composite materials. Composite Science and Technology 2010; 70: 291-297.

[16] Trias D, Costa J, Fiedler B, T. Hobbiebrunken T, J. E. Hurtado JE. A two-scale method for matrix cracking probability in fibre-reinforced composites based on a statistical representative volume element. Composite Science and Technology 2006; 66: 1766-1777.

[17] Carraro PA, Quaresimin M. A damage based model for crack initiation in unidirectional composites under multiaxial cyclic loading. Composite Science and Technology 2014; 99: 154-163.

[18] Quaresimin M, Carraro PA, Maragoni L. Early stage damage in off-axis plies under fatigue loading. Composites Science and Technology 2016; 128: 147-154.

[19] Maragoni L, Carraro PA, Quaresimin M. Effect of voids on the crack formation in $[45/-45/0]_S$ laminate under cyclic axial tension. Composites Part A – Applied Science and Manufacturing 2016; doi: http://dx.doi.org/10.1016/j.compositesa.2016.02.018.

[20] Yamada I, Rogerson PA. An empirical comparison of edge effect correction methods applied to K-function analysis. Geographical Analysis 35 (2), 2003, 97-109.

[21] Davy PJ, Guild FJ. The distribution of interparticle distance and its application in finite-element modelling of composite materials. Proceedings of the Royal Society of London A: Mathematical, Physical and Engineering Sciences 1988; 418: 95-112.

[22] Maragoni L, Carraro PA, Peron M, Quaresimin M. Fatigue behaviour of glass/epoxy laminates in the presence of micro-sized voids. International Journal of Fatigue 2017; doi: http://dx.doi.org/10.1016/j.ijfatigue.2016.10.004.

[23] Torquato S. Nearest neighbor statistics for packing of hard spheres and disks. Physical Review E 1995; 51: 3170-3182.

6

Prediction of life to crack initiation in unidirectional plies containing voids

Motivation

The findings of Chapter 4 showed the importance of accounting for porosity in the design of a composite part. In the present Chapter, a damage-based model proposed by Carraro and Quaresimin to predict life to crack initiation is extended to include the influence of the actual microstructure and the presence of voids. The model is based on the local stress state in the matrix, calculated in Representative Volume Elements (RVEs) obtained according to the procedure developed and validated in Chapter 5.

Abstract

In the present Chapter, Carraro and Quaresimin's model to predict life to fatigue crack initiation in unidirectional plies is extended to take into account the presence of voids. The average values of the Local Maximum Principal Stress (LMPS) and Local Hydrostatic Stress (LHS) in a most critical percentage of the matrix, calculated by means of Representative Volume Elements (RVEs), is proposed to be the driving force to the formation of a fatigue crack in off-axis plies.

The model was developed for homogeneously distributed cigar-like voids and applied to experimental data, showing good predictions of the number of cycles to crack initiation in

the presence of voids, once the S-N curve of the void-free material is known. A parametric analysis was carried out to study the influence of the void content and average void size on the reduction of the life to crack initiation, and the possible extension of the model to other void distributions and shapes is discussed.

6.1. Introduction

The use of fibre-reinforced composites for load-bearing applications has sensibly grown in the last decades, pushed by the need of light structures to reduce fuel costs (automotive, aerospace) and increase the production of green energy (wind turbines). Despite the already wide use, the diffusion of composites is still limited by their high production costs and the lack of design criteria of general validity, in particular against fatigue loadings.

A fundamental role in both manufacturing costs and design is played by manufacturing-induced defects. Such defects involve, among others, ply misalignment, fibre waviness, and moisture absorption, but the most common and difficult to avoid is the presence of porosity, due to the materials and processes involved. Voids may form due to different velocities of the resin flow within and between fibre tows when liquid resin is used, while in pre-preg processing they may originate from air entrapped during the stacking operation, from absorbed moisture and from the release of volatile components during the cure. As shown in several works, voids have a detrimental effect on the mechanical response of composite laminates in the presence of both static and fatigue loadings (see Refs. [1-34], Appendix A, and Chapters 3 and 4). As a consequence, to achieve the best mechanical properties it is desirable to keep their content to a minimum, which means increasing the manufacturing costs, by including operations such as the degassing of liquid resin before infusion, careful resin flow control, the application of intermediate vacuum during pre-pregs lay-up, and the use of high pressures in autoclave. Unfortunately, even if all the

precautions are taken, voids may form anyway in specific locations due to the geometry of the part. The knowledge of the relations between porosity and mechanical behaviour is therefore of primary importance for the design of composite parts for two main reasons: first, in combination with the relations between process parameters and porosity content, they can lead to a *cost effective* production, that maximizes the performance/cost ratio. Second, they enable a more reliable design, in which the material properties can be globally or locally changed based on the expected or allowable void content.

The easiest way to draw void-performance relations is through extensive experimental campaigns. Apart from being expensive and time-consuming, their validity outside the specific lay-up and manufacturing process that have been analysed is not granted. To overcome these issues, models to predict the mechanical behaviour in the presence of voids Most of the models to predict the mechanical behaviour in composite laminates containing voids rely on Finite Element (FE) methods.

Dill and co-authors [24] calculated via FE analyses the stress concentration factor on internal voids of shape and size similar to those they found in their glass fabric/epoxy specimens. They did not find a good correlation between the stress concentration factor (1.85) and the experimental fatigue strength reduction (1.2-1.5), and proposed that the actual shape of individual voids should be included to reduce such difference.

Wisnom et al. [18] measured the Inter-Laminar Shear Strength (ILSS) of unidirectional (UD) laminates containing artificial holes produced with PTFE filaments. After observing that the local stress concentration factor and the linear elastic fracture mechanics were not suited to predict ILSS in the presence of such defects, they developed a non-linear interface modelling approach, assuming the yield to be localized to the interfaces between plies, which were modelled with non-linear spring elements. By including both a stress criterion

for yielding and an energy release rate criterion for failure, their predictions were in good agreement with the experimental results.

McMillan [35] studied the effects of multiple voids in matrix-rich regions on the maximum principal stress under global shear loadings, but he did not attempt to correlate those values to experimental data.

Through the use of a unit cell, Huang and Talreja [36] analysed the influence of the geometry of *cigar-like* voids on the elastic properties of unidirectional laminates, obtaining good agreement with experimental results. A parametric analysis showed that the in-plane properties are less affected by voids compared to the out-of-plane ones, and that the void shape does not influence in the same way the different moduli.

A unit cell approach was also used by Van den Broucke et al. [37] to study the effect of porosity on the elastic properties of textile composites, accounting also for an increase in thickness of the laminate with void content, but no comparisons with experimental data were reported. Since voids were generated by modifying the properties of a randomly selected a set of elements in the matrix, the influence of void shape, size and location was not analysed.

Linqi and Talreja [38] studied how voids affect the postbuckling delamination growth in unidirectional plies when located ahead of its tip. G_{II} was found to increase with larger voids and closer to the crack tip, whereas their influence on G_I was more complex, and also dependent on the elastic properties of the material and the thickness of the delaminated part.

Vajari and co-authors [39] analysed the influence of randomly positioned microvoids on the onset and propagation of transverse failure in UD plies by means of FE analyses carried out on RVEs. The void content was found to reduce the strength of the material under both

tensile and compressive loadings. The failure envelope was found to agree well with of the Puck's model.

In a few cases, models to predict the composite properties in the presence of voids were proposed without involving Finite Elements techniques.

Varna et al. [2] used a simple shear lag model to describe the larger strain to failure for larger void contents that they found experimentally in glass /vinyl ester cross-ply laminates. Such a model could qualitatively explain the experimental trend, but as the authors suggested, a more accurate stress analysis was needed for quantitative discussions.

After finding a linear relation between void content and the ultrasonic absorption coefficient of the laminate in carbon/epoxy fabrics, de Almeida and Neto [13] modified the Mar-Lin criterion assuming the static flexural resistance to be a function of the absorption coefficient, which could adequately fit their experimental results.

Ricotta [40] and co-authors developed an analytical model to study how the Mode I Strain Energy Release Rate (SERR) is affected by voids located ahead of the crack tip. They made use of the beam-on-elastic-foundation theory, suitably modified to include the shear compliance and material orthotropy, and modelled the presence of voids as unsupported zones. After validating their model by comparison with FEM results, they carried out a parametric analysis to analyse the influence of void shape, size, and location of single and multiple voids.

Huang et al. [4] proposed a statistical model to find the distribution of the transverse strength in cross-ply laminates obtained with different process parameters. Their model could predict well the crack density evolution during static tests, but the strength distribution was not explicitly correlated to the porosity content.

From the scientific literature emerges that not sufficient efforts were put into developing models that account for the presence of voids on the long-term behaviour of composite

materials, despite their large detrimental influence (see Refs. [12,13,21,24,28-34] and Chapters 3 and 4). By normalizing the flexural fatigue life to the static strength, De Almeida and Neto [13] found the S-N curves for different void content to collapse in the same scatter band for carbon/epoxy fabrics. Lambert and co-authors [29] observed a slightly linear correlation between the final failure under fully reversed fatigue loading and the largest void in a critical location for multidirectional glass-epoxy laminates. In their work, no clear trend could be detected between fatigue life and global void content, indicating the importance of accounting for voids shape and distribution.

Before final failure occurs in composite laminates under cyclic loadings, other damage events take place, such as initiation and propagation of multiple off-axis cracks and delaminations. If predicting the final failure is essential for strength-driven design, to predict crack initiation and evolution is needed in many applications that impose stiffness constraints to determine failure, and in conservative approaches that require no damage at all to initiate in the part. Therefore, the influence of voids on life to crack initiation should be suitably modelled for an advanced design of structural composite components.

As suggested by Quaresimin and co-authors [41], a predictive model should be based on the damage mechanisms actually occurring in the material to be applicable in the largest variety of cases. Following this direction, Carraro and Quaresimin [42] developed a damage-based criterion to predict life to crack initiation in multidirectional laminates obtaining good predictions of experimental data. As observed by the writer, the damage mechanisms that lead to fatigue crack formation have been observed to be similar in absence and presence of voids, even if crack density evolution is faster in the latter case (see Chapters 2-4 and Refs. [27,34,43]). This indicates that the same damage based criterion developed by Carraro and Quaresimin might be used in the presence of voids, once the perturbation of the microstructure and local stresses caused by the porosity is properly taken

into account. The aim of the present Chapter is to extend such criterion to predict fatigue crack initiation in composite plies containing voids. The model will be developed and validated for homogeneously distributed *cigar-like* voids in multi-directional laminates, but the results could be suitably generalised to different void shape and distribution and different fibre architectures.

6.2. Model development

Since the model here proposed to predict fatigue crack initiation in the presence of voids is based on the damage-based model developed by Carraro and Quaresimin [42] to predict life to crack initiation in UD plies, a brief recall of the latter follows. After careful observations on fracture surfaces, Carraro and Quaresimin proposed the Local Maximum Principal Stress (LMPS) in the matrix to be the driving force to fatigue crack formation when a UD ply is subjected to sufficiently large shear stress to normal stress ratios. When the stress state of a UD ply is close to pure transverse tension, instead, they proposed that the crack formation is driven by the Local Hydrostatic Stress (LHS) in the matrix, extending to fatigue loadings the findings of Asp and co-authors [44]. Carraro and Quaresimin succeeded in collapsing S-N curves for crack initiation obtained for different off-axis angles (hence different stress states) by plotting the curves in terms of LMPS or LHS, as shown in Figure 6.1 as an example. To predict fatigue crack initiation under any external stress state it is then sufficient to obtain experimentally only two S-N curves, applying one LMPS-dominated loading condition and one LHS-dominated loading condition.

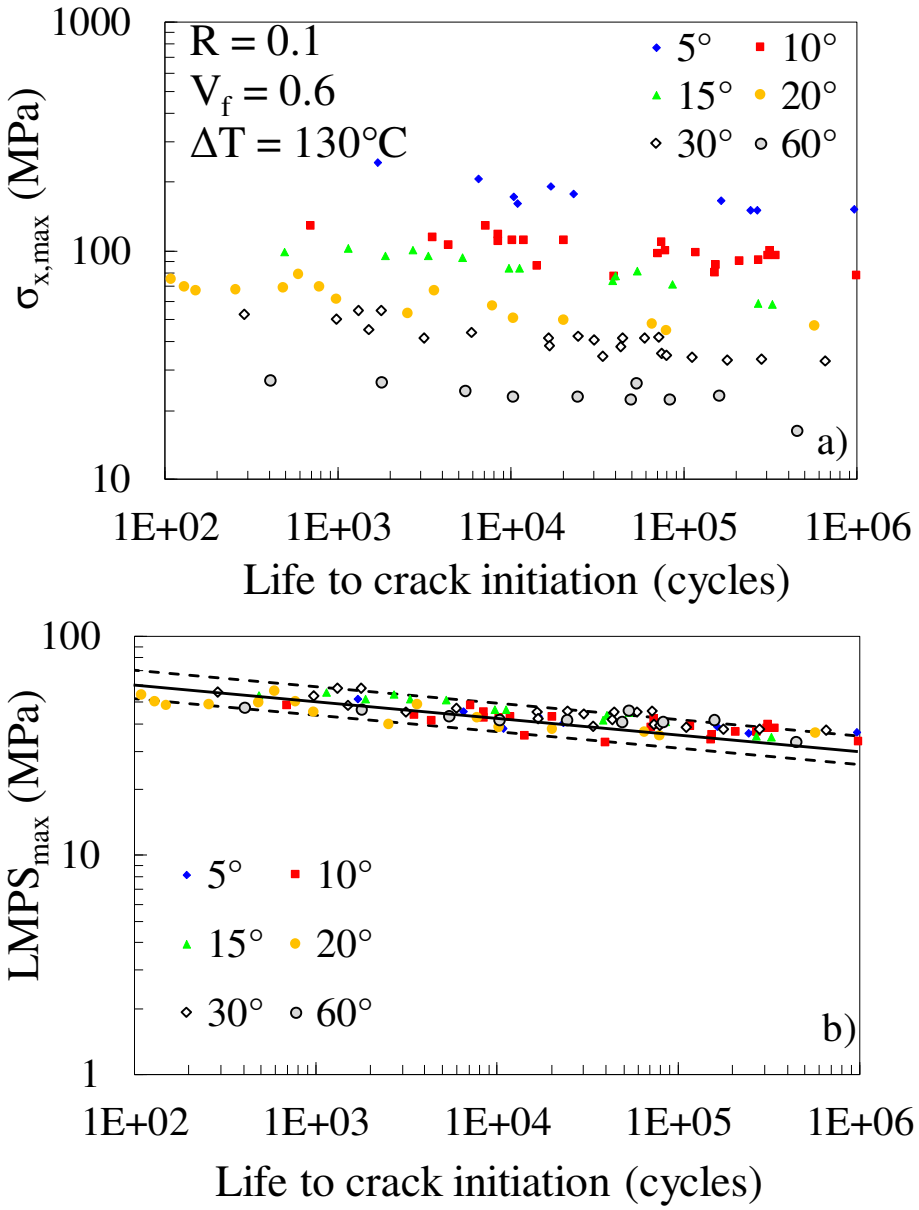

Figure 6.1 – Example of application of Carraro and Quaresmin's model, adapted from [42]: experimental data (a) before and (b) after the application of the model.

According to Carraro and Quaresimin's model, the LMPS and the LHS are calculated for a given material by means of FE analyses carried out on a unit cell. Therefore, a uniform distribution is assumed for the fibres in the matrix, which implies that the model, as formulated, does not allow to take directly into account the presence of microstructural variations in the material, and in the specific the presence of defects such as voids. The

model could actually be able to account for the presence of voids, but two S-N curves should be obtained experimentally for any void content, implying a large experimental effort.

To extend Carraro and Quaresimin's model so that the influence of voids and microstructural variations could be included, the average value of the LMPS or LHS in a control volume of the matrix is here proposed as the driving force to fatigue crack initiation. Such values of LMPS and LHS are from here on referred to as LMPS* and LHS*, and their calculation is explained in the following. To account for the actual microstructure, the stress state in the matrix has to be calculated by means of Representative Volume Elements (RVEs). A tool to build RVEs was already developed and validated in terms of both morphological features and stress distributions in Chapter 5, and was suitably modified to be capable of including a void at its centre (Figure 6.2). Since no variations of the microstructure are assumed along the fibres direction, voids are assumed to be cylindrical, which is a good approximation of elongated the cigar-like voids commonly found in UD plies (see Chapters 3 and 4 and Refs. [27,29,34,36]). Periodic boundary conditions are applied to the RVE, meaning that for the stress analysis in the presence of porosity an average void distribution is considered, characterised by regular (square) pattern and a uniform void size.

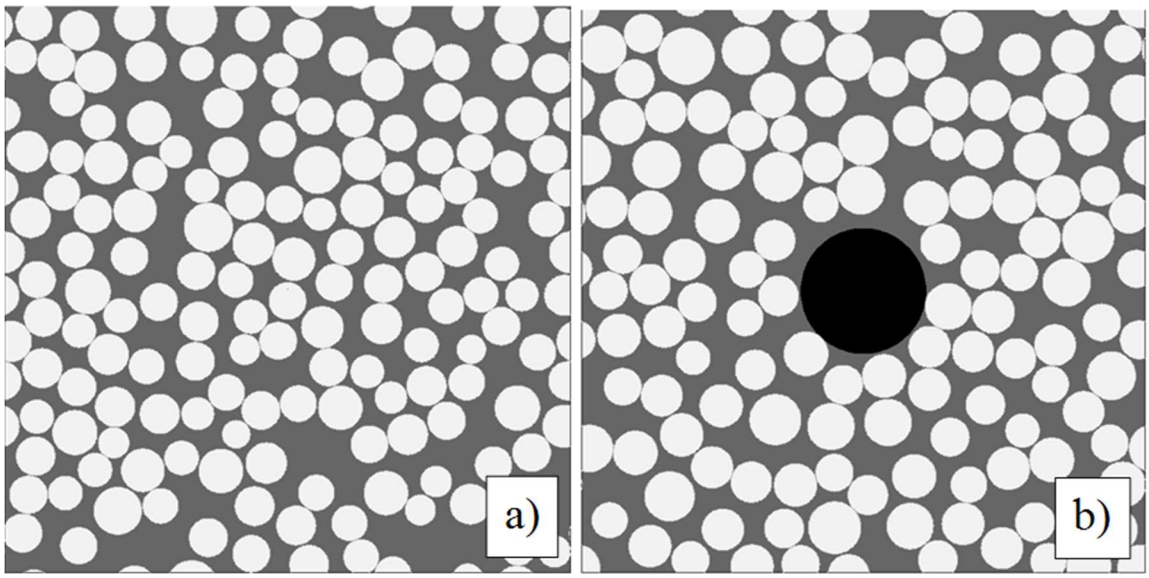

Figure 6.2 – Examples of RVEs in (a) absence and (b) presence of voids.

To calculate LMPS* and LHS*, two considerations are made. The first regards the width of material involved in the formation of a crack, which is the width across which a crack spans horizontally along the ply thickness. Two locally damaged areas will not contribute to the formation of the same crack if they are sufficiently far apart from each other. From experimental observations, a width of two times the fibre diameter seems to be a good approximation (Figure 6.3a). Therefore, once the stress analysis is carried out for the whole RVE, LMPS* and LHS* are calculated on "strips" of material having a width of two fibre diameters (Figure 6.3b). This is a simplifying assumption, since evidences have been reported in the literature of cracks not following such a straight path. In the presence of porosity, also, voids are often interconnected by a crack following an irregular pattern. Nonetheless, it happens rarely that a single point of the crack is connected to another point of the same crack in the immediate vicinity along the vertical direction and distant more than a couple of fibre diameters in the horizontal direction, which keeps the assumption reasonable also in such cases.

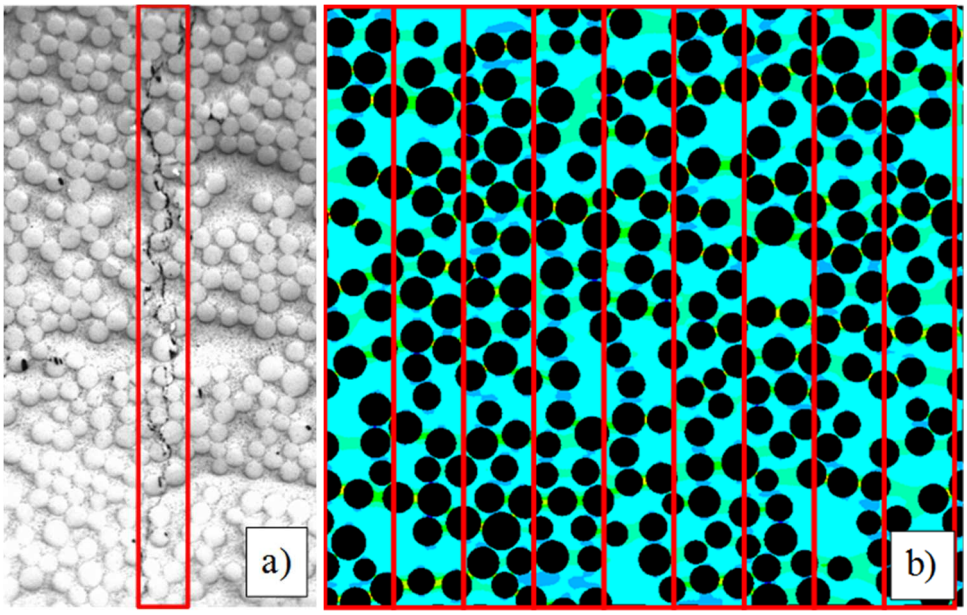

Figure 6.3 – Examples of (a) experimental fatigue crack in a 90° ply, and (b) "strips" where LMPS* and LHS* are calculated after a FE analysis of a RVE.

The second consideration concerns the definition of the control volume, over which the LMPS* and LHS* are calculated. In a composite ply, stress concentrations occur in the matrix due to the presence of fibres, and their intensity is influenced by the local fibre distribution. It is believed that the formation of a crack is mainly influenced by the regions characterised by larger stresses along the thickness of a ply. Therefore, the control volume has to involve a most critical percentage of the matrix volume, where the highest values of LHS and LMPS take place, and a maximum value to is imposed by keeping it limited to inter-fibre regions. As shown in Figure 6.4, the most critical 10% of the matrix volume can be considered as an upper limit to the control volume, since it already involves areas that are far from the inter-fibre regions. The specific value to be assigned to the control volume will be discussed in the next paragraph.

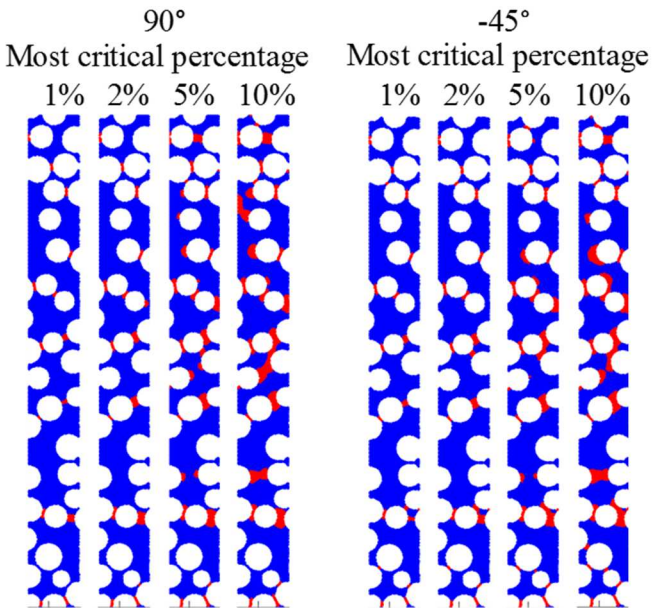

Figure 6.4 – Matrix regions (in red) in a strip characterised by the highest LHS in the 90° ply of a $[0/90_2]_S$ laminate and highest LMPS in the -45° ply of a $[0/45_2/0/-45_2]_S$ laminate.

The calculation of LMPS* and LHS* is repeated for several strips and their mean value across the strips is taken as the driving force to fatigue crack initiation. In the absence of voids, the size of the RVE, quantified by the ratio δ = fibre radius/RVE side, was found not to influence the mean value of LMPS* and LHS* for any value of the control volume V_c, but it affects only its standard deviation, which resulted to be smaller for larger RVEs, as reported in Figure 6.5. The number of strips evaluated for each RVE size was sufficient to reach convergence in terms of both mean values and standard deviations. When voids are present, the size of the RVE is a direct function of the void size and the global void content, and LMPS* and LHS* are calculated only in the strips involving the voids.

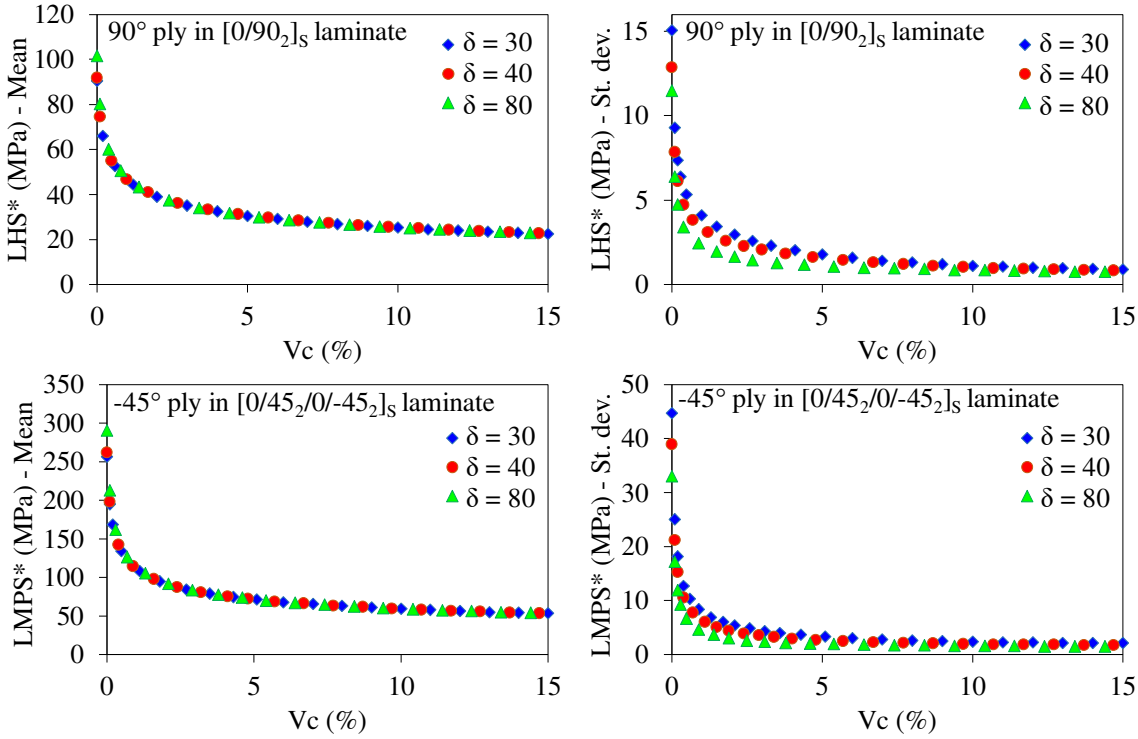

Figure 6.5 – Influence of RVE size (δ) on LHS* calculated in the 90° ply of a $[0/90_2]_S$ laminate subjected to σ_x=50 MPa, and LMPS* calculated in the -45° ply of a $[0/45_2/0/-45_2]_S$ laminate subjected to σ_x=100 MPa (glass/epoxy, V_f = 0.55).

To summarize the present extension of Carraro and Quaresimin's model, the initiation of a fatigue crack in a UD ply is proposed to be driven by the average value of the LMPS, or LHS depending on the stresses acting on the ply [42], calculated by means of RVEs in a most critical percentage of the matrix volume (V_c) confined to inter-fibre regions along a vertical "strips" of material. In the presence of voids, only the strips involving the voids are considered for each RVE. A schematic of the data processing flow is reported in Figure 6.6. As for the Carraro and Quaresimin's model [42], the relation between LMPS* or LHS* and the life to crack initiation is found by calibration on two experimental S-N curves of the void-free material, obtained respectively under a LMPS-dominated loading conditions and a LHS-dominated loading condition. Once this relation is found, it will be possible to predict the life to crack initiation in the presence of any combination of global void content

and average void size, at least for voids that are *cigar-like* and homogeneously distributed.

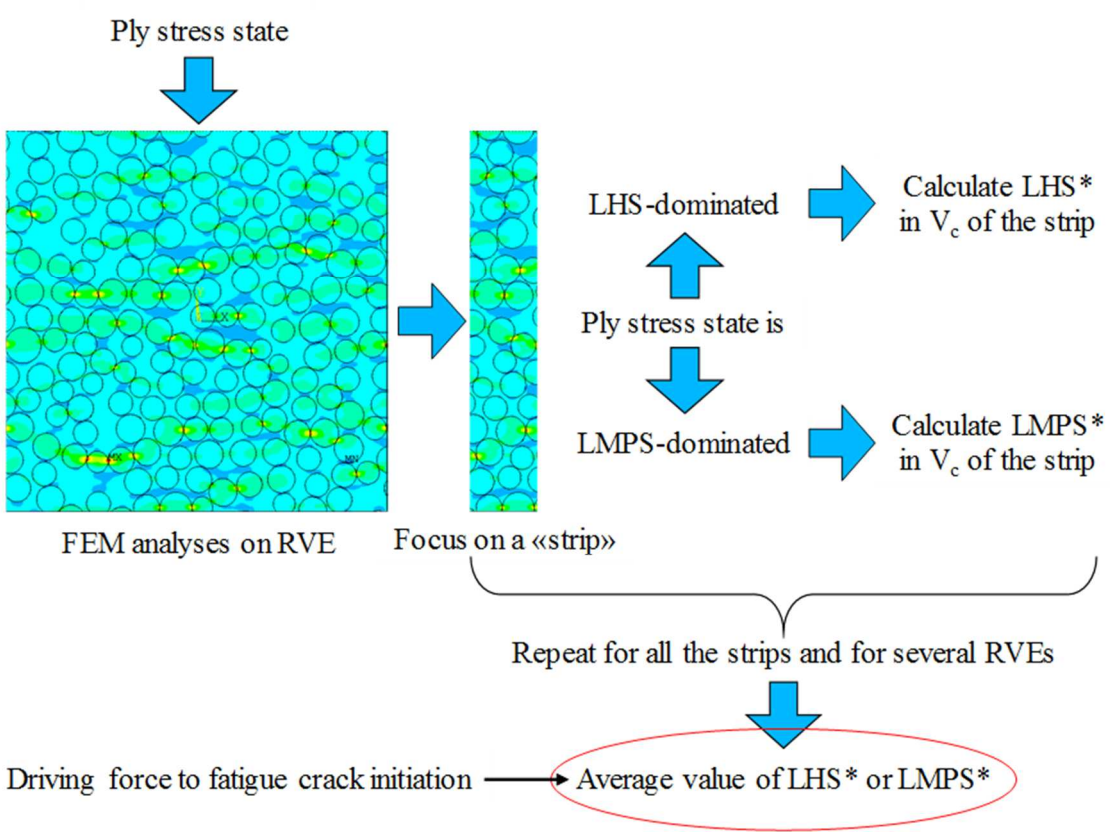

Figure 6.6 – Schematic of the data processing for the application of the model.

6.3 Experimental validation

The first step to validate the proposed model is to check its capability to predict the life to crack initiation for a given material subjected to different values of the *biaxiality ratio* $\lambda_{12}=\sigma_6/\sigma_2$ as the original model proposed by Carraro and Quaresimin [42]. To verify this, it is sufficient to prove that different combinations of σ_6 and σ_2 that lead to the same values of LMPS in the original model lead also to the same value of LMPS*. As shown in Figure 6.7, the equivalence of the proposed extension to the original model to predict life to crack initiation in the absence of porosity is proved. Moreover, this equivalency appears to hold

for any value of the control volume, indicating a low sensitivity of the proposed model to this parameter, as will be discussed also later on.

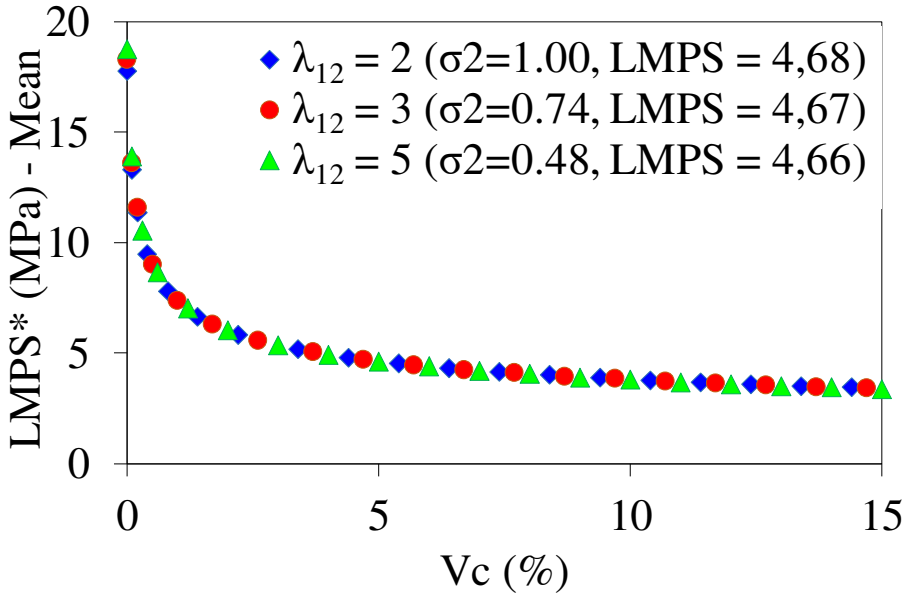

Figure 6.7 – Comparison between Carraro and Quaresimin's original model [42] and current extension. Same values of LMPS* are expected for different λ_{12} having the same LMPS.

As stated, the present generalization of Carraro and Quaresimin's model should be capable of accounting for microstructural variations such the presence of voids in the prediction of life to crack initiation. To validate this capability, a comparison with fatigue crack initiation data obtained for the same material in the absence and presence of voids is needed. In Chapter 4 [34], $[0/90_2]_S$ and $[0/45_2/0/-45_2]_S$ glass/epoxy laminates were produced by vacuum assisted resin transfer moulding (VARTM) by using different process parameters, obtaining both void-free and porous specimens. Tensile fatigue tests were carried out on the specimens, and damage evolution was monitored throughout the tests, observing the influence of voids on life to crack initiation, crack growth rate, and crack density evolution in the 90° ply and in the -45° ply. The void content was measured by micrographic images,

and quantified by the void area fraction A_v and the average void diameter D_v, whose values are reported in Table 6.1. For the $[0/90_2]_S$ lay-up, voids were found to be homogeneously distributed along the specimens. In the -45° ply of the $[0/45_2/0/-45_2]_S$ stacking sequence, voids were instead rather concentrated at regular intervals along the length of the specimens, and the values reported in Table 1 refer to the void-containing regions. Within such regions, voids could be considered as homogeneously distributed, so both for the 90° and the -45° plies the assumption of regular void pattern, discussed in the previous paragraph, may be applicable. Even if void size follows a statistical distribution, it is possible to assume that a crack on its path along the ply thickness involves smaller and larger voids, and its formation is therefore affected by an average void size. A fibre volume fraction of 0.55 was measured for all the laminates, both in absence and presence of porosity.

Table 6.1 – Void content in specimens manufactured in Chapter 4 [34].

	90°		-45°
A_v (%)	0.34	6.7	2.1
D_v (μm)	43	45	49

.

In Chapter 4 [34], the initiation of the first six cracks was considered for each specimen as data for life to crack initiation, as they were sufficiently far apart from each other to be considered as independent events. The two stacking sequences were respectively LHS-dominated ($[0/90_2]_S$) and LMPS-dominated ($[0/45_2/0/-45_2]_S$) [42]. As shown in Figures 6.8 and 6.9, the S-N curves for fatigue crack initiation obtained for different void content fall into the same scatter band when plotted in terms of LHS* and LMPS*, as confirmed by the high value of R^2 of the power-law fit.

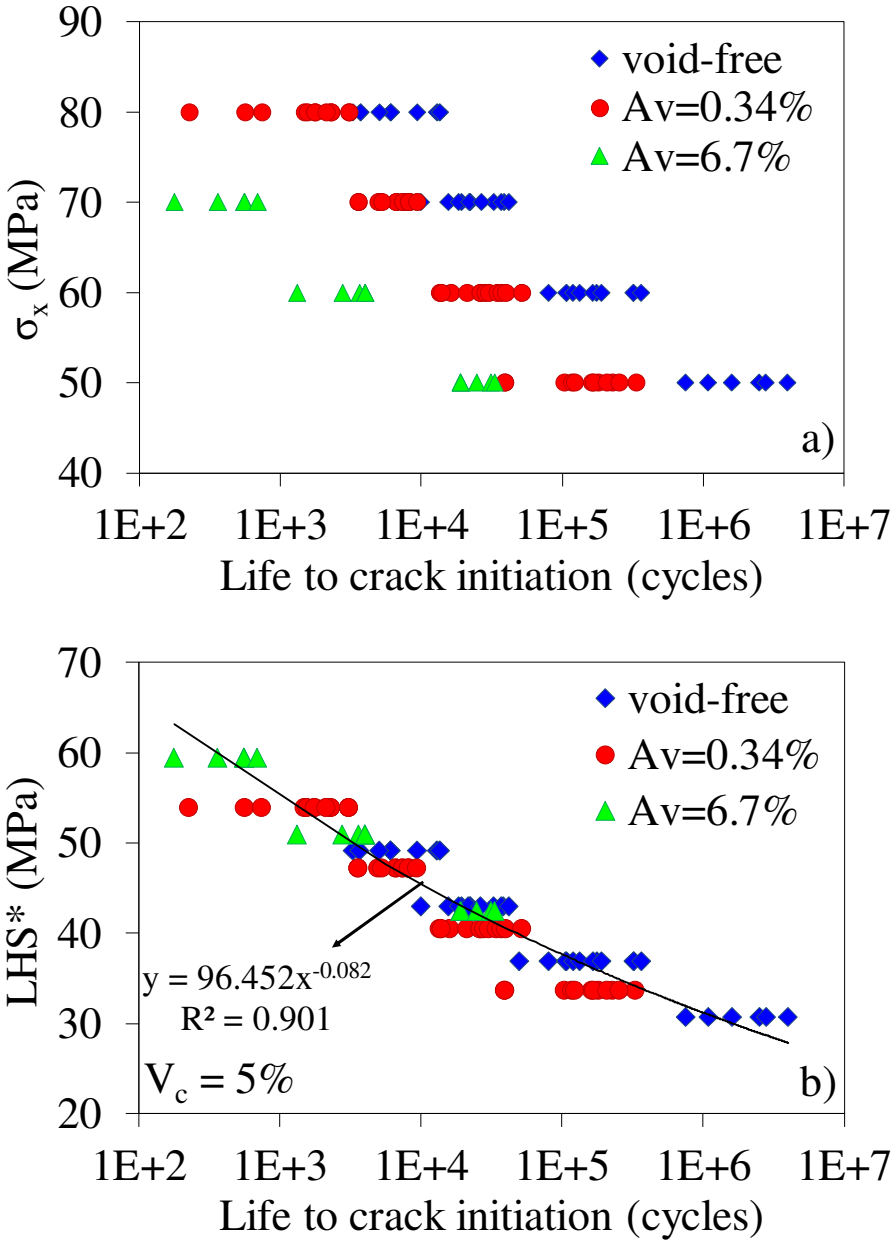

Figure 6.8 – (a) S-N curve of the 90° ply in $[0/90_2]_S$ specimens adapted from Chapter 4 [34], and (b) same data after the application of the model.

In Figures 6.8, and 6.9, a control volume of 5% was taken. Since this choice was arbitrary, a deeper investigation is needed on the influence of this parameter on the predictions of the model. As shown in Figure 6.10, the S-N curves for fatigue crack initiation in terms of LHS* and LMPS* calculated for V_c = 1%, 2%, 5%, 10%, when fitted with an exponential

law, have a very similar R^2, and also the same value of the exponent (same slope in a log-log scale). This indicates that the predictions of the model only marginally depend on the exact value of V_c, at least for values of V_c up to 10%, which was chosen as an upper limit as discussed in the previous paragraph.

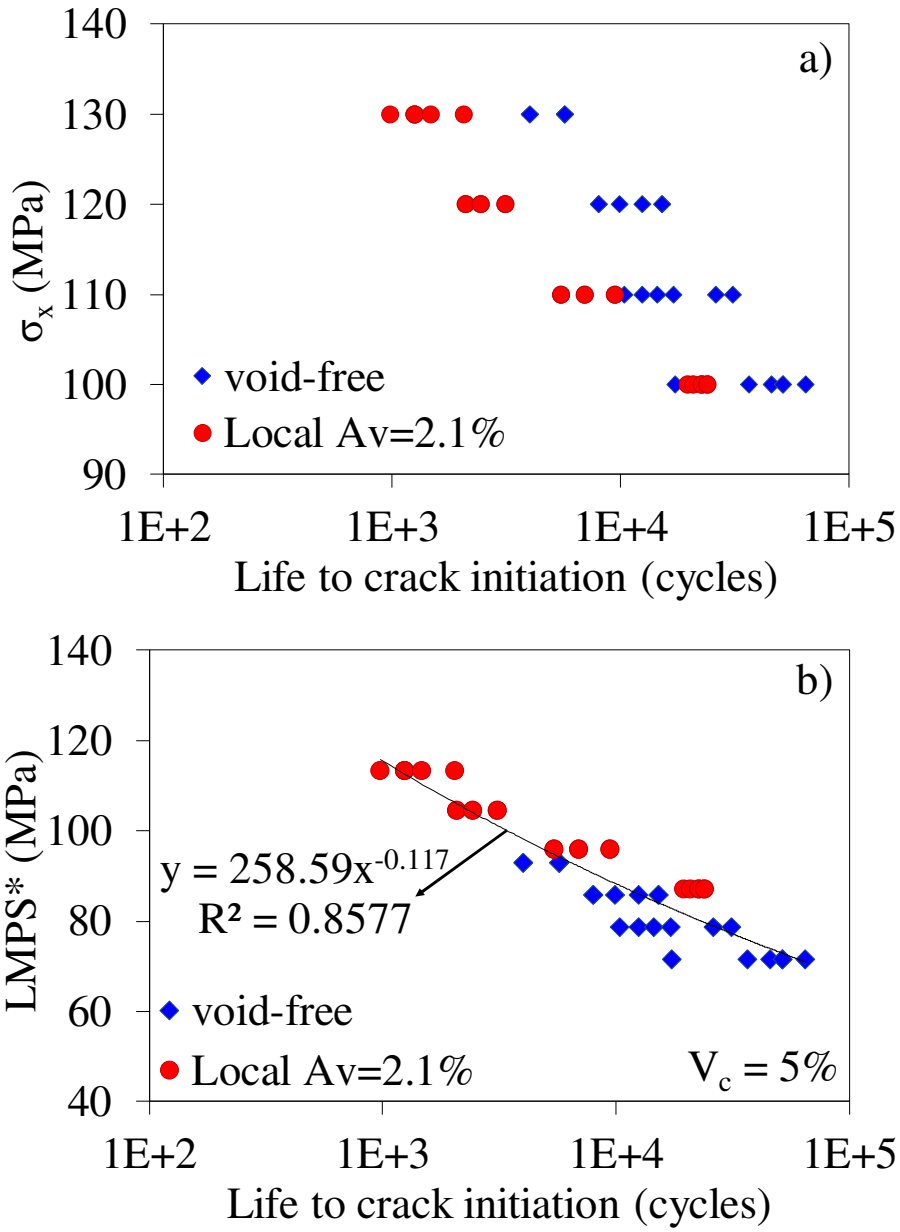

Figure 6.9 – (a) S-N curve of -45° ply in $[0/45_2/0/-45_2]_S$ specimens adapted from Chapter 4 [34], and (b) same data after the application of the model.

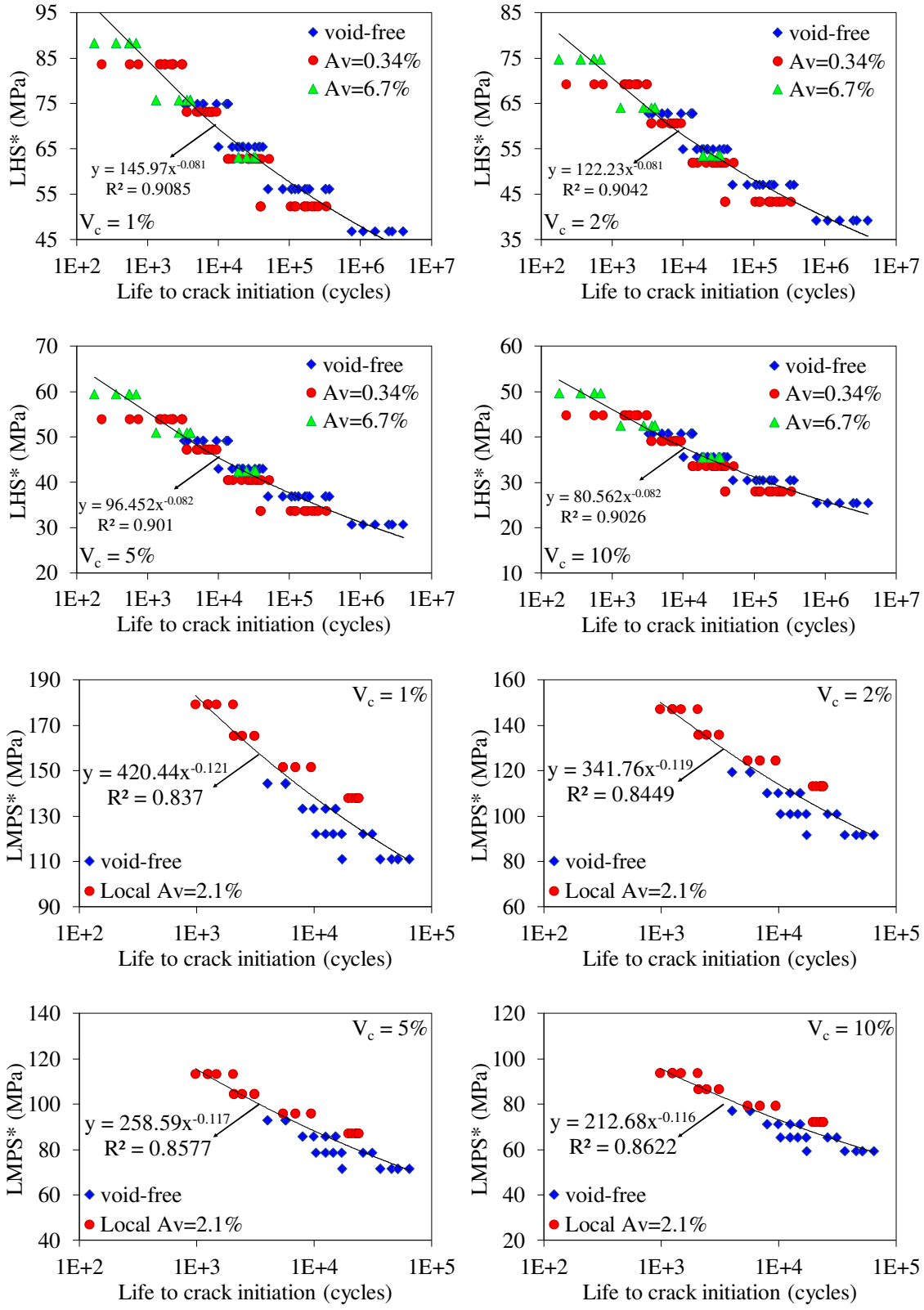

Figure 6.10 – Robustness of the model against the choice of V_c.

This result is in line with the comparison made above with the original Carraro and Quaresimin's model [42], and shows the robustness of the current model with respect to the choice of V_c.

6.4. Design use

Modelling the relations between void content and long term properties of composite materials can be of great help in both the advanced design and the definition of a *cost-effective* manufacturing of a composite part. In addition to being in good agreement with experimental data, the present model has the advantage of requiring a small experimental effort to be applied. It is indeed sufficient to have two S-N curves for the void-free material (one under LMPS-dominated loading condition and one under LHS-dominated loading conditions, as for Carraro and Quaresimin's model [42]) to be able to estimate fatigue crack initiation for any combination of global void content and average void size.

By comparing the predicted life to crack initiation in the presence of voids with the behaviour of the void-free material, design plots such as the ones reported in Figure 6.11 can be drawn, in which the predicted life reduction for the initiation of the first cracks ($N_i/N_{i,void\ free}$) is reported as a function of void content and void size, quantified by the void diameter (D_v) to fibre diameter (D_f) ratio. It is interesting to note that most of the decrease in the performance is predicted to be given by the "introduction" of the first voids in the ply even if in small amounts, and that the increase in the detrimental influence gets smaller with increasing global void content. Also, for the same global void content, a smaller number of larger voids tends to be more detrimental than a larger number of smaller voids, until a sort of plateau is reached, that appears to begin at smaller void size for higher void contents. Small irregularities in these trends can be attributed to the randomness of the

generated RVEs. Finally, as expected, the larger influence of voids on the 90° ply compared to the -45° ply, observed experimentally, appears to hold for all the analysed void contents. Plots as the ones reported in Figure 6.11 can be used as an easy-to-read reference in the design of parts where voids are expected to occur and be tolerated. They can also be useful in the development of manufacturing processes that maximize the performance/cost ratio. To this end, however, more information is needed linking the process parameters to the porosity in the material.

To have the most general validity, a predictive model concerning the influence of porosity should be capable of accounting for void shape, size and distribution. The proposed model was developed to predict fatigue crack initiation in UD plies containing homogeneously distributed *cigar-like* voids. However, it is believed to be applicable also in other cases: if cigar-like voids are concentrated in certain regions, the material properties can be changed just locally, as seen for the -45° ply in the previous paragraph. If the distribution of cigar-like voids could not be approximated to uniform, larger RVEs could be built accommodating multiple voids that are distributed following a desired spatial distribution, and the strips of those larger RVEs could be analysed, implying on the other hand a higher computational cost. In the same way, if a few large voids of irregular shape are present in the material, such as the ones found in Appendix A [5], they can be included in RVEs with their actual shape, and to reduce the computation effort fibres and matrix could be modelled only in the vicinity of the voids, where LMPS* and LHS* will be calculated, and homogenizing the other regions of material. Therefore, even if the current generalisation of Carraro and Quaresimin's model was conceived and validated for a specific void content case, it is potentially applicable to other microstructural conditions.

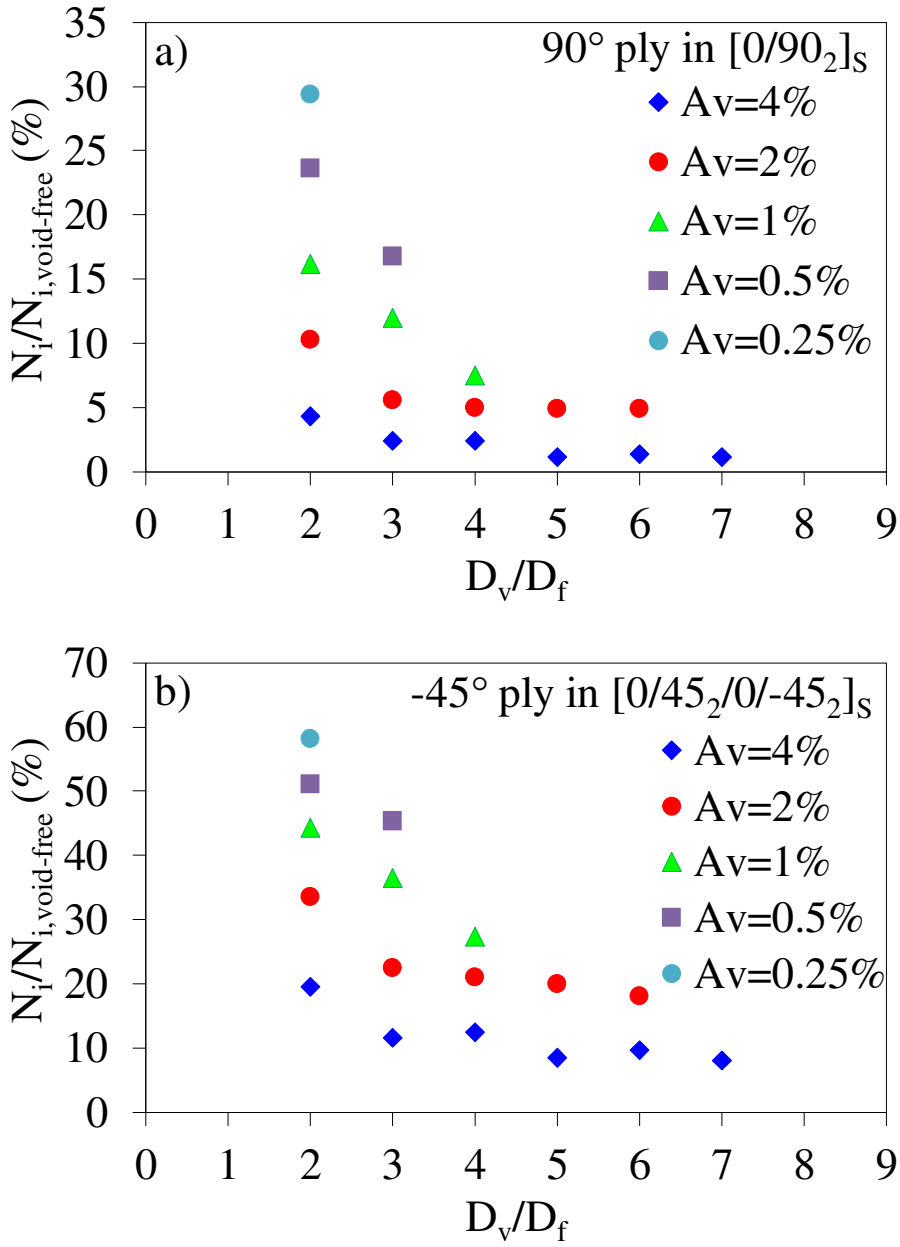

Figure 6.11 – Predicted reduction of life to crack initiation as a function of global void content and average void size for (a) 90° ply in $[0/90_2]_S$ laminate and (b) -45° ply in $[0/45_2/0/-45_2]_S$ laminate.

6.5 Conclusions

In the present Chapter, a model was developed to predict life to crack initiation in UD plies containing homogeneously distributed *cigar-like* voids. The model is an extension of Carraro and Quaresimin's criterion, and proposes as driving force to fatigue crack

formation the average values of the Local Maximum Principal Stress (LMPS) and Local Hydrostatic Stress (LHS) in a control volume of the matrix along vertical strips of materials, calculated by means of FE analyses of Representative Volume Elements (RVEs).

By assuming that voids are distributed following a regular pattern and by taking an average void size, the S-N curves for life to crack initiation of void-free and porous laminates with fall into the same scatter band when plotted in terms of the suggested driving forces. This indicates that the fatigue crack initiation can be predicted in the presence of voids once the behaviour of the void-free material is known, under both LHS- and LMPS-dominated loading conditions.

As shown by a parametric study, it appears that a few voids are sufficient to sensibly reduce the life to crack initiation, in accordance with experimental data, and for the same global void content, a smaller number of larger voids is more detrimental than a larger number of smaller voids. Even if the proposed model was developed for homogenously distributed voids, the same principles are potentially applicable to other void distributions and more complicated void shapes, once they have been suitably modelled in a RVE.

The proposed model requires only a small experimental data to be applied, namely one S-N curve under LHS-dominated loading condition and one S-N curve under LMPS-dominated loading condition (as for the original model proposed by Carraro and Quaresimin [42]), and can be useful in the advanced design of composite parts where voids are expected to be present and tolerated as well as a reference to achieve a *cost-effective* production.

References of Chapter 6

[1] Olivier P, Cottu JP, Ferret B. Effects of cure cycle pressure and voids on some mechanical properties of carbon/epoxy laminates. Composites 1995; 26: 509-515.

[2] Varna J, Joffe R, Berglund LA, Lundstrom TS. Effect of voids on failure mechanisms in RTM laminates. Composite Science and Technology 1995; 53: 241-249.

[3] Zhu H, Wu B, Li D, Zhang D, Chen Y. Influence of voids on the tensile performance of carbon/epoxy fabric laminates. Journal of Materials Science and Technology 2011; 27: 69-73.

[4] Huang Y, Varna J, Talreja R. Statistical methodology for assessing manufacturing quality related to transverse cracking in cross-ply laminates. Composite Science and Technology 2014; 95: 100-106.

[5] Carraro PA, Maragoni L, Quaresimin M. Influence of manufacturing-induced defects on damage initiation and propagation in carbon/epoxy NCF laminates. Advanced Manufacturing: Polymer and Composites Science 2015; 1: 44-53.

[6] Tang JM, Lee WI, Springer GS. Effects of Cure pressure on resin flow, voids, and mechanical properties. Journal of Composite Materials 1987; 21: 421-440.

[7] Suarez JC, Molleda F, Guemes A. Void content in carbon fiber/epoxy resin composites and its effects on compressive properties. In: Proceedings of ICCM9 Conference. Madrid, July 1993.

[8] Cinquin J, Triquenaux V, Rouesne Y. Porosity influence on organic composite material mechanical properties'. In: Proceedings of ICCM16 Conference. Kyoto, July, 2007.

[9] Kosmann N, Karsten JM, Schuett M, Schulte K, Fiedler B. Determining the effect of voids in GFRP on the damage behaviour under compression loading using acoustic emission. Composites Part B – Engineering 2015; 70: 184-188.

[10] Hernandez S, Sket F, Gonzales C, Llorca J. Optimization of curing cycle in carbon fiber-reinforced laminates: void distribution and mechanical properties. Composite Science and Technology 2013; 85: 73-82.

[11] Liu L, Zhang BM, Wang DF, Wu J. Effects of cure cycles on void content and mechanical properties of composite laminates. Composite Structures 2006;73:303-309.

[12] Chambers AR, Earl JS, Squires CA, Suhot MA. The effect of voids on the flexural fatigue performance of unidirectional carbon fibre composites developed for wind turbine applications. International Journal of Fatigue 2006; 28: 1389-1398.

[13] de Almeida SFM, Neto ZSN. Effect of void content on the strength of composite laminates. Composite Structures 1994; 28: 139-148.

[14] Hagstrand PO, Bonjour F, Manson JAE. The influence of void content on the structural flexural performance of unidirectional glass fibre reinforced polypropylene composites. Composites Part A – Applied Science and Manufacturing 2005; 36: 705-714.

[15] Yoshida H, Ogasa T, Hayashi R. Statistical approach to the relationship between ILSS and void content of CFRP. Composite Science and Technology 1986; 25: 3-18.

[16] Olivier PA, Mascaro B, Margueres P, Collombet F. CFRP with voids: ultrasonic characterization of localized porosity, acceptance criteria and mechanical characteristics. In: Proceedings of ICCM16 Conference. Kyoto, July, 2007.

[17] Thomason JL. The interface region in glass fibre-reinforced epoxy resin composites: 1. Sample preparation, void content and interfacial strength. Composites 1995; 26: 467-475.

[18] Wisnom MR, Reynolds T, Gwilliam N. Reduction in interlaminar shear strength by discrete and distributed voids. Composite Science and Technology 1996; 56: 93-101.

[19] Goodwin AA, Howe CA, Paton RJ. The role of voids in reducing the interlaminar shear strength of RTM laminates. In: Proceedings of ICCM11 Conference. Gold Coast, July, 1997.

[20] Costa ML, de Almeida SFM, Rezende MC. The influence of porosity on the interlaminar shear strength of carbon-epoxy and carbon-bismaleimide fabric laminates. Composite Science and Technology 2001; 61: 2101-2108.

[21] Bureau MN, Denault J. Fatigue resistance of continuous glass fiber-polypropylene composites consolidation dependence. Composite Science and Technology 2004; 64: 1785-1794.

[22] Zhu H, Li D, Zhang D, Wu B, Chen Y. Influence of voids on interlaminar shear strength of carbon/epoxy laminates. Transactions of Nonferrous Metals Society of China 2009; 19: 470-475.

[23] Asp LE, Brandt F. Effects of pores and voids on the interlaminar delamination toughness of a carbon/epoxy composite. In: Proceedings of ICCM11 Conference. Gold Coast, July, 1997.

[24] Dill CW, Tipton SM, Glaessge EH, Branscum KD. Fatigue strength reduction imposed by porosity in a fiberglass composite. In: Damage Detection in Composite Materials, ASTM STP 1128, J. E. Masters, Ed., American Society for Testing and Materials, Philadelphia, 1992, pp. 152-162.

[25] Hapke J, Gehrig F, Huber N, Schulte K, Lilleodden ET. Compressive failure of UD-CFRP containing void defects: In situ SEM microanalysis. Composite Science and Technology 2011; 71: 1242-1249.

[26] Scott AE, Sinclair I, Spearing SM, Mavrogordato MN, Hepples W. Influence of voids on damage mechanisms in carbon/epoxy composites determined via high resolution computed tomography. Composite Science and Technology 2014; 90: 147-153.

[27] Maragoni L, Carraro PA, Quaresimin M. Effect of voids on the crack formation in $[45/-45/0]_S$ laminate under cyclic axial tension. Composites Part A – Applied Science and Manufacturing 2016; doi: http://dx.doi.org/10.1016/j.compositesa.2016.02.018

[28] Gehrig F, Mannov E, Schulte K. Degradation of NCF-epoxy composites containing voids. In: Proceedings of ICCM 17 Conference. Edinburgh, July, 2009.

[29] Lambert J, Chambers AR, Sinclair I, Spearing SM. 3D damage characterization and the role of voids in the fatigue of wind turbine blade materials. Composite Science and Technology 2012; 72: 337-343.

[30] Schmidt F, Rheinfurt M, Horst P, Busse G. Multiaxial fatigue behaviour of GFRP with evenly distributed or accumulated voids monitored by various NDT methodologies. International Journal of Fatigue 2012; 43: 207-216.

[31] Seon G, Makeev A, Nikishkov Y, Lee E. Effects of defects on interlaminar tensile fatigue behavior of carbon/epoxy composites. Composite Science and Technology 2013; 89: 194-201.

[32] Protz R, Kosmann N, Gude M, Hufenbach W, Schulte K, Fiedler B. Voids and their effect on the strain rate dependent material properties and fatigue behaviour of non-crimp fabric composites materials. Composites Part B - Engineering 2015; 83: 346:351.

[33] Sisodia SM, Gamstedt EK, Edgren F, Varna J. Effects of voids on quasi-static and tension fatigue behaviour of carbon-fibre composite laminates. Journal of Composite Materials 2015; 49: 2137-2148.

[34] Maragoni L, Carraro PA, Peron M, Quaresimin M. Fatigue behaviour of glass/epoxy laminates in the presence of voids. International Journal of Fatigue 2017; 95: 18-28.

[35] A. J. McMillan: 'Material strength knock-down resulting from multiple randomly positioned voids', Journal of Reinforced Plastics and Composites 2012, 32, (1) 13-28.

[36] Huang H, Talreja R. Effects of void geometry on elastic properties of unidirectional fiber reinforced composites. Composite Science and Technology 2005;65: 1964-1981.

[37] B. Van Den Broucke, J. Hegemann, R. Das, R. Oster, K. Hackl, R. Stößel: 'Modelling of textile composites using finite element tools and investigation of the influence of porosity on mechanical properties'. In: Proceedings of Symposium 'Finite Element Modelling of Textiles and Textile Composites'. St Petersburg, September, 2007.

[38] Zhuang L, Talreja R. Effects of voids on postbuckling delamination growth in unidirectional composites. International Journal of Solids and Structures 2014, 51, 936-944.

[39] Vajari DA, Gonzalez C, Llorca J, Legarth BN. A numerical study of the influence of microvoids in the transverse mechanical response of unidirectional composites. Composite Science and Technology 2014; 97: 46-54.

[40] Ricotta M, Quaresimin M, Talreja R. Mode I Strain Energy Release Rate in composite laminates in the presence of voids. Composite Science and Technology 2008; 68: 2616-2623.

[41] Quaresimin M., Susmel L, Talreja R., Fatigue behaviour and life assessment of composite laminates under multiaxial loadings. International Journal of Fatigue 2010; 32: 2-16.

[42] Carraro PA, Quaresimin M. A damage based model for crack initiation in unidirectional composites under multiaxial cyclic loading. Composite Science and Technology 2014; 99: 154-163.

[43] Quaresimin M, Carraro PA, Maragoni L. Early stage damage in off-axis plies under fatigue loading. Composite Science and Technology 2016; 128: 147-154.

[44] Asp LE, Berglund LA, Talreja R. Prediction of matrix initiated transverse failure in polymer composites. Composite Science and Technology 1996; 56: 1089-1097.

7

Prediction of crack density evolution in multidirectional laminates under fatigue loadings

Motivation

In Chapter 6, a model was proposed to predict the initiation of the first cracks in the presence of porosity from the S-N curve of the void-free material, which can be of help when no damage at all is allowed in a composite part. The design of many composite structures, however, is stiffness-driven, which means that cracks could be tolerated as long as the stiffness does not drop below a critical limit. Since the stiffness of a composite laminate is linked to the crack density in its plies, in this Chapter a procedure is developed to predict the crack density evolution in multidirectional laminates subjected to cyclic loadings, capable also of including the presence of porosity.

Abstract

In the present Chapter, a procedure is proposed for the prediction of the crack density evolution in multidirectional laminates subjected to cyclic loading. The crack initiation and propagation phases are treated separately and described by means of S-N and Paris-like curves, respectively. A damage-based multiscale strategy is adopted for the prediction of multiple cracks initiation. The statistical distribution of fatigue strength and crack propagation resistance are accounted for. The procedure has been implemented in a

Matlab code for the simulation of the fatigue damage evolution in multi-directional symmetric laminates. Comparisons with experimental results show a very good agreement. Finally, the model developed in Chapter 6 is used to predict crack density evolution in the presence of voids from the behaviour of the void-free material, obtaining predictions of good accuracy.

7.1. Introduction

The fatigue behaviour of composite laminates is characterised by a progressive damage evolution from the beginning of fatigue life to the final failure. The main macroscopic evidence of the damage evolution is the degradation of the global elastic properties of a laminate. In several applications, the stiffness is a crucial parameter and this makes the prediction of its variation essential in the design process.

It is proved that the degradation of the elastic properties is due to damage mechanisms that are not directly responsible for the laminate failure and therefore they have been defined *sub-critical damage mechanisms* [1,2]. They are represented by the initiation and through-the-width propagation of multiple cracks in the off-axis layers, followed by the onset and propagation of delaminations [2-6]. In particular, the accumulation of matrix cracks can lead to a considerable stiffness loss much before the laminate failure. In addition, they act as 2stress concentrators, triggering delaminations and rising the stresses in the 0° plies promoting the failure of the fibres. Fibre failure brings to the complete separation of a laminate and it is therefore considered a *critical damage mechanism* [1,2].

Because of the importance of predicting the fatigue damage evolution, besides the final failure, this topic has been treated by several researchers in the last two decades. The main predictive models in the literature are based on two different approaches and can be divided as follows:

1) Models which do not directly correlate the damage evolution (stiffness and residual strength degradation) to the damage mechanisms (i.e. off-axis cracks initiation and propagation):

1.1. Analytical models based on a Continuum Damage Mechanics-like approach;

1.2. Finite Element (FE) methods where the element behaviour is characterised by progressive and/or sudden degradation rules;

2) Models based on the prediction of the off-axis crack density evolution:

2.1. Models based on crack density evolution, predicted by means of empirical laws;

2.2. Models based on crack density evolution predicted by means of stress fields and the statistical fatigue strength distribution.

In the following, some relevant examples to the above mentioned approaches are briefly presented and discussed. To follow a logical flow among the ideas at the basis of the models, the references are not reported in chronological order.

1.1. Based on the damage evolution pattern highlighted by Reifsneider and co-authors [7], Wu and Yao in 2010 [8] proposed a new versatile empirical rule for the degradation of a laminate stiffness in the loading direction. As two parameters must be calibrated by means of experimental data, and they depend on the stacking sequence, this model is not suitable to make predictions for different lay-ups without a dedicated experimental characterisation. However, the proposed law was shown to describe very well the stiffness trend once the parameters were suitably calibrated.

Much before, in 1997, Shokrieh and Lessard [9,10] proposed to model the fatigue damage evolution of a unidirectional (UD) lamina by means of empirical laws describing the gradual stiffness and residual strength degradation under fatigue loading. An extensive experimental campaign is needed for the calibration of such laws under several loading conditions leading to different damage mechanisms. The final failure of a ply is then

predicted by means of polynomial criteria where the stress components are normalised with respect to the residual strength expressed by means of the degradation rules mentioned above.

1.2. Later, Shokrieh and Lessard [11,12] applied Shokrieh and Lessard's model to multidirectional laminates by means of 3D FE analyses of laminates in which the elements of each ply behaved according to the degradation rules defined in [9]. After the failure of a ply was detected by means of the polynomial criteria proposed in Ref. [9], its properties were suddenly degraded to zero. The application of the model in Ref. [12] showed a very good capability in the prediction of the S-N curve for the complete failure of a laminate, but no considerations were done on the global stiffness trend.

In 2012 Naderi and Maligno [13] applied the same method proposed by Shokrieh and Lessard [11] with two important differences: they carried out 2D FE analyses and, most of all, they assigned to every element a strength, based on a Gaussian distribution. In this way it was possible to simulate the presence of defects due to the manufacturing process and the variability of the microstructure. They obtained sound predictions for the S-N curves related to the laminates complete failure, but, again, no comparisons were shown for the stiffness degradation.

In 2013 Kennedy et al. [14] proposed a method conceptually similar to that of Shokrieh and Lessard [11], based on the 3D analysis of a laminate, whose element properties were gradually degraded according to empirical laws. The element failure, followed by the sudden degradation of the ply properties, was predicted by means of a Puck-like criterion, suitably extended to fatigue loading. They obtained a good correspondence between the simulation results and experimental data on multidirectional laminates concerning the stiffness trend.

Lian and Yao in 2010 [15] proposed a procedure based on 3D FE analyses of a laminate where the strength properties were assigned to each element based on a statistical distribution. The elastic properties of each element were gradually degraded by means of empirical laws. The element final failure was predicted by means of a polynomial criterion similar to that of Hashin [16] coupled with normalised S-N curves for a single lamina under different loading conditions. The properties of a failed element were suddenly degraded. Lian and Yao obtained sound predictions of both the stiffness trends and S-N curves for multidirectional laminates. The main disadvantage of this method, and in general of the models described above, is that they are based on empirical laws both for the prediction of the properties degradation and the element failure. In addition, none of them considers properly the crack propagation phase which can be important for a reliable prediction of the global stiffness degradation, as will be discussed in the following paragraphs.

2) The second type of approaches consists in predicting the evolution of the crack density in the off-axis layers as an input for models capable of linking the crack density to the global elastic properties of a multidirectional laminate. This is based on the fact that the accumulation and propagation of off-axis cracks is the main source of damage in the earlier stages of the fatigue life. In addition, several models can be found in the literature which are able to predict the laminate stiffness as a function of the density of cracks in its layers (see Refs. [17-25] among the others). Recently, a model based on the shear lag method has been proposed by Carraro and Quaresimin, accounting also for the interaction between cracks in different layers [26].

A lower number of contributions have been published concerning the prediction of the crack density evolution, in particular under fatigue loading, and a widely acknowledged procedure is lacking at present. Some very interesting contributions can be found for the static loading case, and they can be grouped into energy-based [18,27,28] and stress-based

[29-31] approaches. Among those, only Vigronadov and Hashin [27] and Huang et al. [30,31] considered the statistical distribution of strength which is essential for an accurate prediction of the crack density evolution.

Concerning the fatigue loading, as mentioned before, two approaches have been identified for the prediction of the crack density evolution: empirical and stress-based models.

2.1. Liu and Lessard [32] proposed a simple empirical rule for a damage variable which is representative of the entity of the crack density and also delaminations. They related the damage variable to the global stiffness by means of relations provided by Talreja [33] and O' Brien [34].

Subramanian and co-authors [35] proposed a cumulative damage model for cross-ply laminates, capable of predicting the stiffness degradation as well as the final failure by means of a *critical element concept*. The crack density evolution was predicted by means of empirical laws and used as an input for a simple shear lag analysis to calculate the stiffness loss.

In 2002 Henaff-Gardin and Lafarie-Frenot [36] developed a method for cross-ply laminates, based on an energetic approach, for the prediction of the cycles spent for the initiation of the first transverse crack, followed by an empirical law to predict the fatigue evolution of a characteristic damage variable proportional to the crack density.

Another interesting contribution for cross-ply laminates was provided by Hoang and co-authors in 2010 [37]. They proposed an approach based on constant-crack density curves against the number of cycles which could be obtained by quasi-static tests.

All the models discussed above provided more or less reliable results when compared to experimental data series presented in the relevant papers. They have the advantage of being simple in their application, but they lack in generality since they are based on empirical laws.

2.2. A stress-based model for the prediction of the crack density evolution under cyclic loading was proposed by Sun and co-authors in 2003, which is valid for a cross-ply laminate [38]. They carried out a Monte Carlo simulation where the 90° layer of a cross-ply laminate was divided into small elements having a strength assigned according to a Weibull distribution. The failure of an element was predicted on the basis of the S-N curve for the 90° UD lamina, of which the input were the ply stresses. These were calculated considering the stress re-distribution after cracking by means of a shear lag analysis. The results of the simulations were in very good agreement with experimental results for the crack density evolution. The propagation phase of the transverse cracks was not taken into account, and this can be justified by the fact the model was verified against experimental results for lay-ups in which the thickness of the 90° plies was high enough to promote the sudden propagation of the nucleated cracks, as also proved by some images of the damaged specimens [38].

Ogi [39] proposed a model for the crack density evolution in cross-ply laminates based on a statistical distribution of micro-sized defects. The initiation of a transverse crack was assumed to occur by the propagation of such defects through the ply thickness, following a Paris-like law. The model was in very good agreement with experimental data reported by the authors. However, it did not consider the through-the-width crack propagation phase and the stress re-distribution in the presence of cracks. In addition, the model required the calibration of several parameters through experimental data.

Within this frame, the present work attempts to move one step further and aims to develop a tool for the prediction of the fatigue crack density evolution for symmetric laminates with a general lay-up, considering both the initiation and the propagation phases, which are, in general, distinct and describable by means of different tools.

The presence of off-axis plies with generic orientation complicates the problem because of the multiaxial stress state, which also changes during fatigue life because of the stress re-distribution after cracking. For this purpose, a crack initiation criterion was proposed by Carraro and Quaresimin [40], based on the experimental observation of the micro-scale damage mechanisms in off-axis plies under a fatigue load (see Chapters 2 and 3 [41,42]). According to this criterion, the S-N curves for the initiation of cracks must be expressed by means an equivalent stress σ_{eq}, accounting for the multiaxial stress state. The equivalent stress was defined on the basis of the damage mechanisms at the microscopic scale bringing to the initiation of a macro-crack. The Local Maximum Principal Stress (LMPS) and the Local Hydrostatic Stress (LHS) should be used as σ_{eq}, depending on the amount of in-plane shear stress σ_6 (see Ref. [40] for the details).

The initiation criterion proposed by Carraro and Quaresimin in [40] is included in the procedure proposed here for the crack density prediction, allowing to deal with cracks initiation in off-axis, and not only transverse, plies.

7.2. Definition of crack density

According to its most common definition, the crack density is meant as the total number of initiated cracks divided by the observation length perpendicularly to the crack faces:

$$\rho = \frac{n}{L \cdot \left|\sin\left(\theta\right)\right|} \tag{7.1}$$

Where n is the total number of initiated cracks, L and θ are defined in Figure 7.1.

It is proven that this definition of the crack density, which can be defined as the *total crack density* ρ, is not a good parameter to correlate with the stiffness degradation. In fact, if the cracks are not completely spanning through the width of a laminate their length becomes a

variable of extreme importance to be considered for a sound estimation of the stiffness degradation [2,19,43]. Accordingly, the weighted crack density, ρ_w, can be defined as the total number of cracks, each of them being weighted by its length c, divided by the observation area, as in Equation (7.2):

$$\rho_w = \frac{\sum_{i=1}^{n} c_i}{w \cdot L} \tag{7.2}$$

where c_i is the length of the i-th crack, n is the number of initiated cracks and w is defined in Figure 7.1.

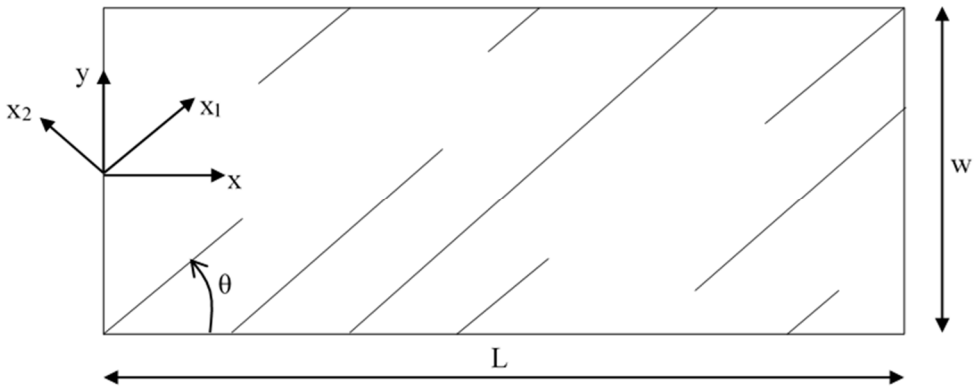

Figure 7.1 – Geometry of a generic cracked layer and reference systems.

According to these observations, it is fundamental to be able to predict the weighted crack density, which depends on both the fatigue crack initiation and propagation phenomena. In paragraphs 7.4 and 7.5 the initiation and propagation phenomena will be treated, respectively.

7.3. Multiscale strategy

In this paragraph, the procedure for the prediction of the weighted crack density is briefly described. Because of the inhomogeneous nature of composite materials, the damage evolution process is always multiscale, as highlighted by Talreja [44]. In addition, "*length scales of damage and their hierarchy are not fixed but are subject to evolution*" [44]. In fact, the fatigue behaviour of a UD laminate is characterised by a progressive damage evolution due to irreversible mechanisms at the microscopic scale, such as fibre-matrix debonding or matrix micro-cracking (see Chapters 2 and 3 and Refs. [2,40-42]. The evolution of these damage mechanisms, consisting for instance in the coalescence of debonds and micro-cracks, leads to the formation of a macroscopic crack, spanning through the thickness of a ply and propagating along the direction of its fibres. Therefore, the length scale changes from the micro-scale (the length scale of the fibre diameter and the inter-fibre spacing) to the macro-scale, related to the crack spacing and the laminate width.

The initiation of a macro-crack is controlled by the evolution of the damage at the microscopic scale. It has been shown by Carraro and Quaresimin that two local parameters, LHS and LMPS, are a sound representation of the driving forces for the micro-damage evolution in the presence of a negligible or high enough in-plane shear stress, respectively [40]. The bridge between the macro-stresses in the material coordinates system (σ_1, σ_2, and σ_6) and the micro-stresses is represented by the stress concentration factors computed by means of a micromechanical analysis, as reported by the authors in Ref. [40]. The LHS and the LMPS can be used as equivalent stress, σ_{eq}, for a successful representation of the crack initiation S-N curves in two single scatter bands, accounting for the influence of multiaxial stress states. The LHS and the LMPS are calculated on the basis of the macro-stresses which can be uniform along the transverse direction of the ply, if the ply is undamaged, or non uniform because of the stress re-distribution due to cracking. The stress re-distribution can be treated as a macro-scale phenomenon, as is commonly done in the literature, and it

can be computed by means of several analytical [17-23-25] and semi-analytical [18] methods or by means of Finite Element (FE) analyses of cracked laminates.

Once the initiation of cracks has been predicted, it is fundamental to describe their through-the-width propagation. It has been shown in the literature [2,3,45-47] that the crack propagation can be successfully described by means of a Paris-like law relating the Crack Growth Rate (CGR) to the Energy Release Rate (ERR) or to the Stress Intensity Factor (SIF).

A schematic of the multiscale procedure for the prediction of the weighted crack density evolution is shown in Figure 7.2, and it consists in the simulation of the fatigue life by progressively increasing the number of cycles by steps ΔN.

For a given step of fatigue cycles ΔN, and for every off-axis layer, the analysis is divided in the following points:

1) Calculation of stresses in each layer, considering the stress re-distribution due to the possible presence of off-axis cracks.

2) Calculation of the micro-stresses (or local stresses) by means of the stress concentration factors calculated as in Ref. [40].

3) Calculation of the parameters LHS and LMPS from the local stresses.

4) Prediction of the initiation of new cracks by means of the LHS or LMPS-based master curves for the considered material. The sequence effect, due to the stress redistribution, and the statistical distribution of the life to crack initiation must be accounted for.

5) Analysis of the propagation phase for the initiated cracks by means of the Paris-like curve of the considered material and length calculation.

6) Calculation of the weighted crack density in each ply and the stiffness degradation.

7) Increase the number of cycles by a further step ΔN and repetition of steps 1-7.

Steps 4 and 5 will be described in detail in the next paragraphs.

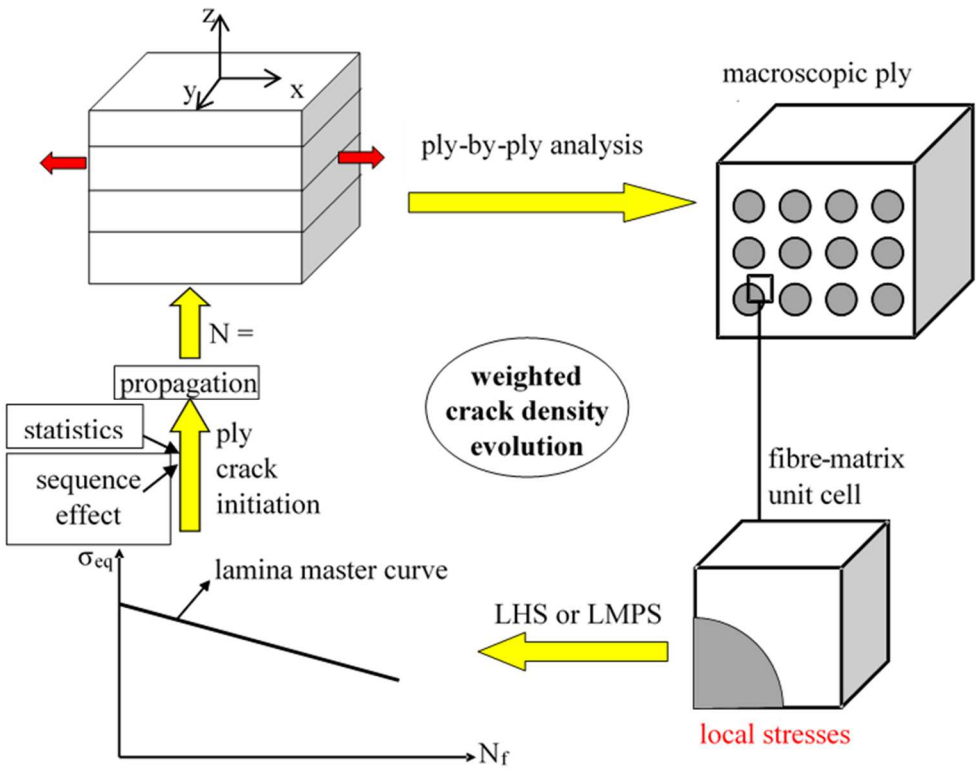

Figure 7.2 – Schematic of the procedure for the prediction of the weighted crack density.

7.4. Prediction of multiple crack initiation

In this paragraph, the procedure for the prediction of the off-axis crack initiation is described in detail. As already mentioned, the initiation of cracks is considered to be controlled by the fatigue resistance of the material, represented by the S-N curves expressed in terms of an equivalent stress σ_{eq} (LHS or LMPS). The S-N curves are expressed by means of the typical power law relating the equivalent stress to the number of cycles to crack initiation N_i:

$$\sigma_{eq} = K \cdot N_i^a \tag{7.3}$$

The exponent *a* is an input of the model and it can be obtained by a series of experimental data on an off-axis lamina with any orientation. More precisely, two values of *a* should be adopted, a_{LHS} and a_{LMPS}, to be used whether the fatigue behaviour is LHS- or LMPS-controlled, respectively. As already explained in Ref. [40], a_{LHS} can be obtained by testing under a fatigue load a UD laminate under pure transverse stress condition ($\theta = 90°$ for instance), while a_{LMPS} can be deduced from experimental tests on a UD laminate under shear-dominated stress states (θ in the range of 10-45° for instance).

As mentioned in the introduction, the statistical distribution of the fatigue strength to crack initiation is a fundamental aspect to account for. In fact, because of the presence of manufacturing defects and, more in general, of the variability of the microstructure, different positions in the same ply are characterised by a different life to crack initiation. This is the reason why the crack density evolves during the fatigue life and the cracks do not form all together at a given number of cycles.

The statistical distribution of the life to crack initiation depends on the multiaxial condition and the load level.

Considering a power law for the S-N curve as in Eq.(7.3), a statistical distribution can be assigned to the parameter K. Considering, for instance, that a Weibull distribution is suitable for the problem under analysis, the cumulative distribution of the parameter K can be expressed as

$$P(K) = 1 - \exp\left[-\left(\frac{K}{K_0} \right)^m \right] \tag{7.4}$$

m and K_0 are respectively the shape and scale parameters of the Weibull distribution. They depend on the material, but also on the manufacturing process, which can affect the fibre

volume fraction, the presence of defects and, in general, the microstructure. Deriving K from equation (7.3) and substituting into equation (7.4), the cumulative distribution of the life to crack initiation, $P(N_i)$, yields

$$P(N_i) = 1 - \exp\left[-\left(\frac{\sigma_{eq}}{K_0 \cdot N_i^a} \right)^m \right] \tag{7.5}$$

The use of the equivalent stress allows the multiaxial stress state to be considered. As for the exponent *a*, also the Weibull parameters *m* and K_0 must be referred to the LHS- or LMPS-driven loading conditions (m_{LHS}, m_{LMPS}, $K_{0,LHS}$, $K_{0,LMPS}$).

Since a statistical strength distribution is involved, it is essential to clarify the volume for which it is defined. In the writer's view, it is a good choice to refer to a volume that is representative of the process zone involved in the crack initiation process. As schematically shown in Figure 7.3, the control volume is chosen to have a length l_0 along the transverse direction, c_0 along the fibres direction and to involve the entire thickness of the ply. The control volume must be big enough to include the phenomena leading to the initiation of a crack and, at the same time, small enough, along the x_2 direction, to consider the stress field uniform within it and to accommodate only one crack, as discussed in [30, 31].

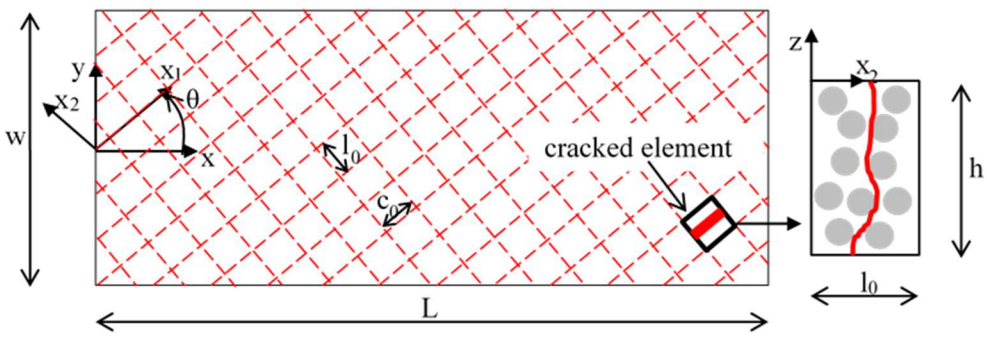

Figure 7.3 – Ply discretisation in elements representative of the crack initiation process zone.

The present model is based on the discretisation of each ply of a laminate into elements as that represented in Figure 7.3. Each element is characterised by a life to crack initiation following the cumulative probability distribution of Eq. (7.5). As a consequence, considering a laminate of dimensions *L*·*w* (Figure 7.3), the total number of cracks, n, in a ply within a uniform stress field, can be calculated, as a function of the number of cycles, as:

$$n(N) = \left[1 - \exp\left(-\left(\frac{\sigma_{eq}}{K_0 \cdot N^a}\right)^m\right)\right] \cdot \frac{L \cdot w}{l_0 \cdot c_0} \tag{7.6}$$

Therefore, the total crack density can be calculated as

$$\rho(N) = \frac{n(N)}{L \cdot |\sin\theta|} = \left[1 - \exp\left(-\left(\frac{\sigma_{eq}}{K_0 \cdot N^a}\right)^m\right)\right] \cdot \frac{w}{l_0 \cdot c_0 \cdot |\sin\theta|} \tag{7.7}$$

Equation (7.7) holds if the stress field in the ply under analysis is uniform in the x_1-x_2 plane and does not change from cycle to cycle. This condition is realistic only at the beginning of the fatigue life, when the laminate is undamaged or when the initiated cracks are far enough and thus non-interacting. This condition is defined as "Non-Interactive regime". After that, the initiated cracks start interacting causing the stress re-distribution, between cracks and between layers. This is defined as "Interactive regime", and it is characterised by the variability of σ_{eq} with the number of cycles and the x_2 coordinate, as schematically shown in Figure 7.4.

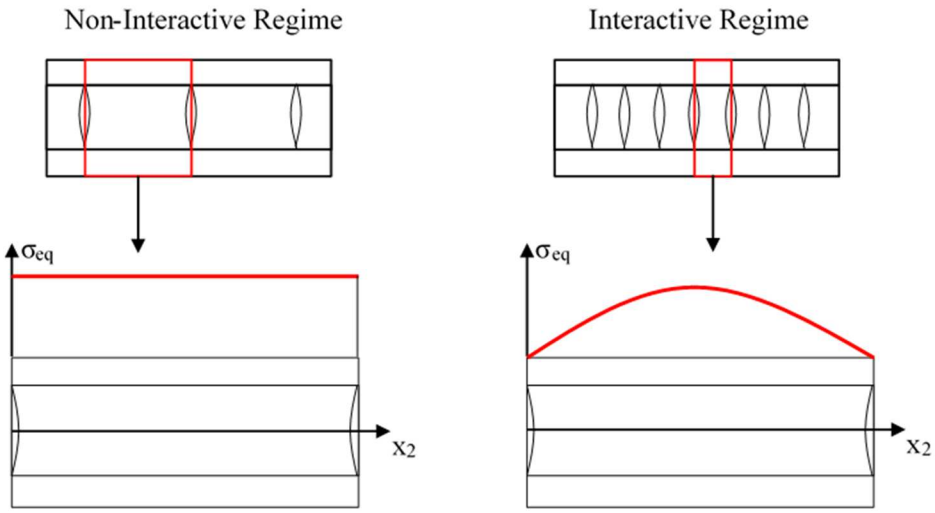

Figure 7.4 – Non-Interactive and Interactive regimes.

Equation (7.7) can be adopted when only the very early stages of damage evolution are of interest. To predict the crack density evolution in the subsequent stages, the stochastic process of crack initiation can be predicted through a Monte Carlo simulation as explained in the following.

7.4.1 Interactive regime

As already mentioned, each ply of a generic laminate can be discretised into elements $l_0 \cdot c_0$, representative of the crack initiation process zone. The dimensions l_0 and c_0 are in principle dependant on the material, in particular on the microstructure, but could also depend on the ply thickness. Each of these elements is assigned a value for the parameter K (K_{LMPS} or K_{LHS}), according to its statistical distribution, as expressed in Eq. (7.4) in the case of a Weibull type.

Once the external laminate loads are known, it is possible to calculate the stresses in the plies (σ_1, σ_2, σ_6), for instance by means of the Classical Laminate Theory (CLT), and therefore the equivalent stress σ_{eq} (LHS or LMPS) which will be the same in all the elements, as the stress field is uniform in the laminate plane. From σ_{eq} it is possible to calculate the number of cycles to crack initiation for the j-th element of the k-th ply as

$$N_i(j,k) = \left(\frac{\sigma_{eq}(j,k)}{K(j,k)} \right)^{1/a} \tag{7.8}$$

The stress state in each element, in general, changes from cycle to cycle, due to the re-distribution of the stresses in the presence of cracks. Therefore, the use of a damage accumulation rule is essential. At the best of the writer's knowledge, neither results or models are available in the literature concerning the sequence effect on the matrix-dominated fatigue behaviour of UD composites. In the present work, the simple and well known Miner's rule is adopted, as done by other authors [38,39], even if its suitability should be checked more carefully by dedicated experimental investigations.

If an initial step of cycles ΔN_1 is applied to a specimen at given external loads, according to Miner's damage accumulation rule the entity of damage in the element is given by

$$D(j,k) = \frac{\Delta N_1}{N_i(j,k)} \tag{7.9}$$

The number of cracks initiated in ΔN_1 is equal to the number of elements for which D(j,k) is higher than or equal to one. When subsequent steps of cycles are applied, the variability of the stresses with the x_2 coordinate and from cycle to cycle must be accounted for.
As a consequence, the damage in the j-th element in the k-ply after s steps of cycles can be calculated as

$$D(j,k,s) = \sum_{p=1}^{s} \frac{\Delta N_p}{\left(\frac{\sigma_{eq}(j,k,p)}{K(j,k)}\right)^{1/a}} \tag{7.10}$$

where $\sigma_{eq}(j,k,p)$ is the equivalent stress in the element during the p-th step of cycles. Again, the number of initiated cracks is equal to the elements for which the damage parameter is higher than or equal to one. When a crack is predicted to initiate, it is considered to involve the entire length of the element, c_0, in agreement with the fact that the element has to be representative of the crack initiation process zone.
It can be shown that the total crack density calculated in this way and with Eq.(7.6) are practically identical in the first stages of the damage evolution, whereas they diverge when the interaction between cracks starts playing an important role. In this latter condition, the stress state in an element placed between two pre-existing cracks can be calculated via several methods. In the present work, the shear lag model proposed by Carraro and Quaresimin [26] is adopted. This model allows the stress re-distribution between plies to be accounted for, considering also the interaction between cracks in different plies, as explained in Appendix 7.A.

At this point the number of cracks and their location is known. The total crack density can be calculated, and the analysis of the propagation phase is now necessary for the computation of the weighted crack density ρ_w.

7.5. Crack propagation

As already mentioned, the propagation of the initiated cracks is assumed to be governed by a Paris-like law, relating the CGR to the maximum cyclic value of the ERR. As the propagation occurs in mixed I + II mode conditions, an equivalent ERR, G_{eq}, must be used, according to Equation (7.11).

$$CGR = C \cdot G_{eq}^{d} \cdot \frac{1-\left(\frac{G_{th}}{G_{eq}}\right)^{n1}}{1-\left(\frac{G_{eq}}{G_{c}}\right)^{n2}} \tag{7.11}$$

where G_{th} and G_c are the threshold value and the static critical value, respectively, for the ERR.

The coefficients *C*, and *d* have to be calibrated with experimental results. The exponents n_1 and n_2 instead control the transition from the power-law behaviour to the threshold and unstable growth regions, respectively.

Several phenomenological expressions have been proposed in the literature for the G_{eq} to be used in Equation (7.11). An experimental investigation carried out by Carraro and Quaresimin [2] revealed that, when the Mode Mixity MM = G_{II}/G_{tot} is low (i.e. the loading condition is mode I dominated) the propagation is controlled by the only mode I contribution G_I. This is because the presence of the fibres does not allow the deviation of the crack propagation direction resulting from the mode II contribution. Conversely, when

the loading condition is mode II dominated, but not pure mode II, it has been found that the Paris-like curves are well collapsed in terms of the total ERR $G_{tot} = G_I + G_{II}$, as can be observed in Figures 7.5a) and b). Those data are related to the propagation of transverse cracks in glass/eposy tubes under combined tension/torsion loadings, with load ratios R (maximum to minimum load ratio) equal to 0.05 and 0.5 [48].

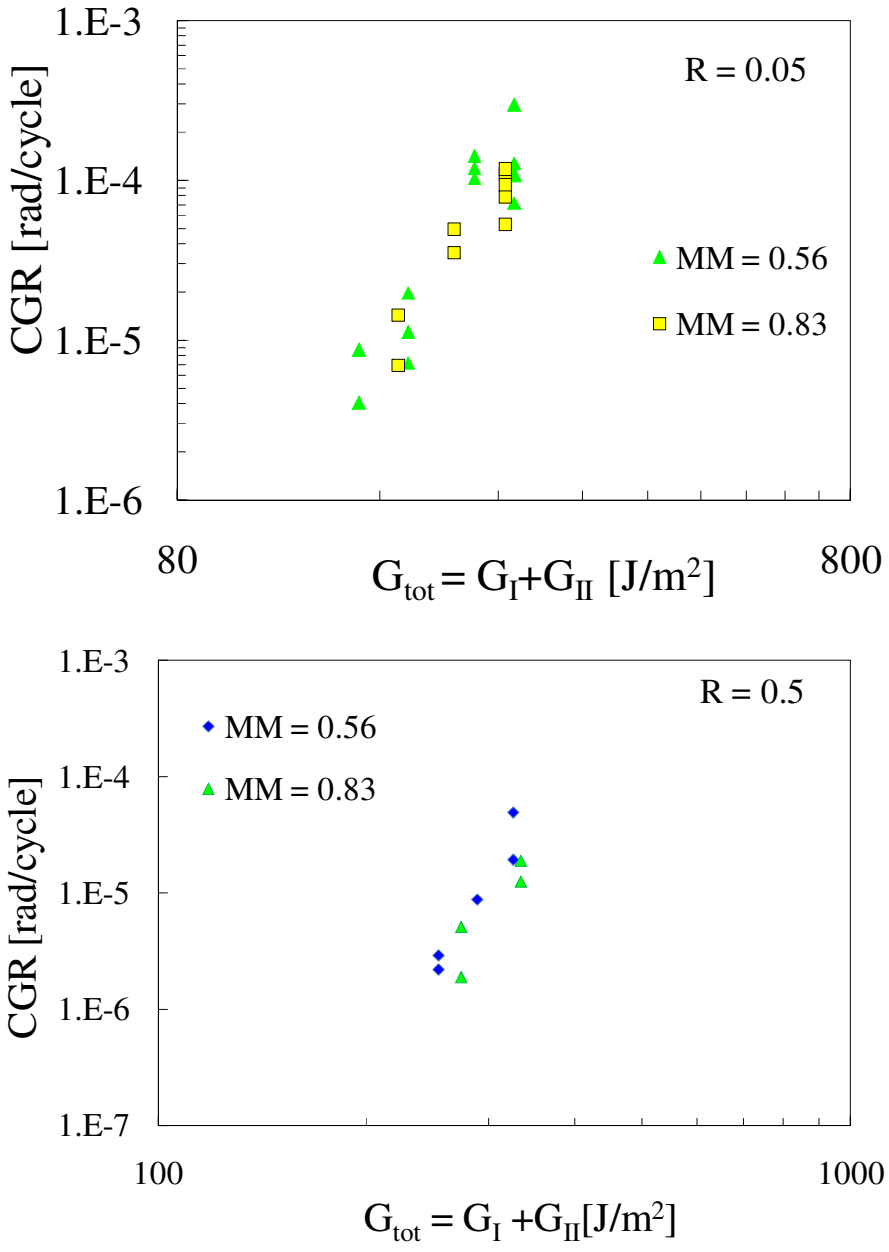

Figure 7.5 – Paris-like curves in terms of G_{tot} for tubes with a) R = 0.05 and b) R = 0.5 [48].

The same conclusion can be drawn, mainly for $0.53 \leq MM \leq 0.82$, considering the fatigue data for mixed mode interlaminar crack propagation presented by Kenane [49], whose data are reported in Figure 7.6.

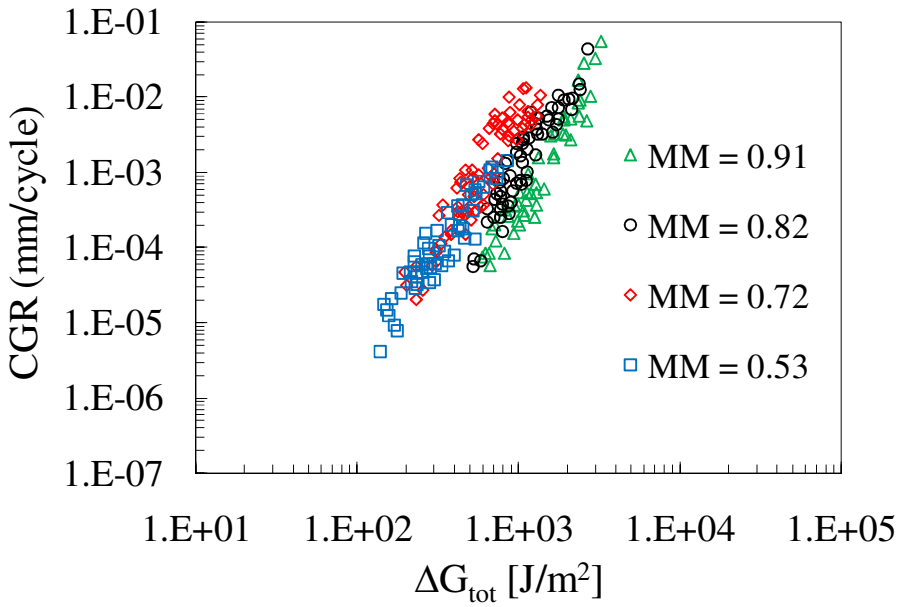

Figure 7.6 – Mixed mode interlaminar crack propagation from Kenane [49].

According to these observations the equivalent ERR can be defined as follows:

$$G_{eq} = \begin{cases} G_I, \ if \ \ MM < MM^* \\ G_{tot}, \ if \ \ MM^* < MM < 1 \end{cases} \tag{7.12}$$

where MM* is the transition point between the G_I and the G_{tot} driven propagation. Therefore, the coefficients of Paris-like curves C_I, d_I and C_{tot}, d_{tot} have to be provided to be used when the propagation is G_I or G_{tot} controlled, respectively.

It is remarked that, however, G_{tot} cannot be used for pure mode II loading. In addition, the use of G_{tot} for MM > MM* is only a phenomenological criterion, whose general validity

should be checked. A damage based criterion for mixed mode crack propagation in bonded joints has been proposed by Carraro and Quaresimin in Ref. [50], which could be adapted to the case of interest. However, also in that case the same observations reported above can be drawn, concerning the use of G_I and G_{tot} for mode I and mode II dominated (but not pure mode II) conditions respectively [51].

A tunnelling crack within an off-axis ply surrounded by tougher layers is characterised by a constant value of the ERR components if the crack length *c* is higher than two times the layer thickness, for edge cracks, and four times the layer thickness for internal cracks [52,53]. This causes a Steady State (SS) propagation of the tunnelling cracks. The steady state values of the ERR components are easy to calculate with several analytical tools or with FE analyses [54]. However, if the length *c* is lower than two or four times the ply thickness, respectively for edge or internal cracks, the transition from zero to the steady state value must be described.

In the present work, the following simple expression is adopted to describe the transition from zero to the steady state ERR, obtained by fitting the FE results for the total G presented in Ref. [54].

$$G = G_{ss} \cdot \left[1 - \exp\left(-2.1 \left(\frac{c}{h'} \right)^{0.6} \right) \right] \tag{7.13}$$

G and G_{ss} can be either the total value or the mode I or mode II component, whereas h' is equal to the ply thickness for edge cracks and two times the ply thickness for internal cracks. This expression was obtained for the particular material system analysed in [54]. However, it is believed that it provides a good approximation even for other materials and

lay-ups, as the main influencing parameter (the ply thickness) is accounted for in the formulation.

As shown in [54], the steady state value of the ERR components depend on the crack density. More precisely, considering a crack propagating between other cracks, the ERR associated to its tips depend upon the distance between its tips and the neighbouring cracks. Let us consider first a condition where a set of equally long cracks propagate in the fibre direction, with a uniform spacing S, as in Figure 7.7a). The ERR components relevant to this condition ($G_{ss}(S)$) can be computed with several analytical methods, as well as with FE analyses. However, this condition is not of interest for studying the propagation of multiple cracks in a laminate. In fact, according to the method proposed to predict crack initiation, at every simulation step, ΔN, new cracks initiate, and then they propagate between longer cracks nucleated in the previous steps. Accordingly, the condition of interest for the calculation of the ERR is relevant to a crack propagating between longer cracks with distances S_1 and S_2 from its tip (Figure 7.7b). Generalising the formulation presented in Ref. [53], the steady state value of each ERR component, named G_{ss} in general, is given by the following relationship, valid for G_I, G_{II} and G_{tot}

$$G_{ss} = 2 \cdot \frac{G_{ss}^{a}(S_1) + G_{ss}^{a}(S_2)}{2} - G_{ss}^{a}(S_1 + S_2) \tag{7.14}$$

where G_{ss}^{a} is relevant to the configuration shown in figure 7.7a).

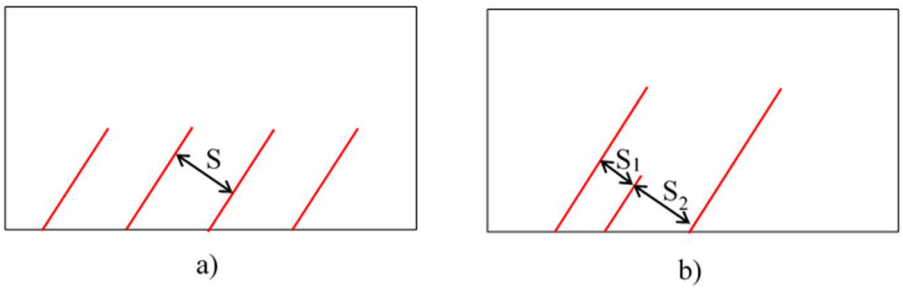

Figure 7.7 – a) Set of equally long cracks and b) Set of short cracks propagating between longer ones.

At every step of the simulation, the location and length of all the cracks is known, so that for each crack tip it is possible to calculate the ERR components through Eqs. (7.13) and (7.14) and then the CGR by means of the Paris-like law in Eq.(7.11). Then, the increment in the length of a given crack during the simulation step is simply given by

$$\Delta c = CGR \cdot \Delta N \tag{7.15}$$

This assumes that the CGR, and therefore the ERR, do not change during the considered step, which is true only if the crack field around the analysed tip remains unvaried. For a suitable prediction, therefore, it is necessary to discretise the fatigue life in steps ΔN that are not too large.

During its propagation, a crack may find another one on its path and merge with it. The possibility of joining of cracks is not included in the present procedure. However, when two crack tips come very close to each other the value of the ERR is so low that the two cracks cannot propagate further. For the sake of the weighted crack density calculation, this condition is equivalent to the joining of the two cracks, which may happen in actual circumstances.

7.6. Implementation of the procedure

The procedure described above was implemented in a Matlab® code for the prediction of the crack density evolution in rectangular flat specimens. The required input data are:

- The elastic properties of a UD ply (E_1, E_2, G_{12}, ν_{12}, G_{23}, G_{13});
- The laminate stacking sequence, width (w) and length (L);
- The external applied loads;
- The slope of the crack initiation S-N curve (a_{LHS}, a_{LMPS});
- The stress concentration factors for the calculation of LHS and LMPS (see Ref. [40]);
- The Weibull distribution parameters m_{LHS}, m_{LMPS}, $K_{0,LHS}$, $K_{0,LMPS}$;
- The coefficients of the Paris-like curve (C_I, d_I and C_{tot}, d_{tot}) and the threshold and static critical values of the ERR;
- The dimensions of the crack initiation process zone (l_0, c_0).

A flowchart of the procedure is shown in Figure 7.8. It is articulated in the following phases:

1) Application of a step of cycles ΔN;
2) For each element of each ply, check if it contains a crack. If so, go to point 3. Otherwise, go to point 4;
3) Calculation of the LHS or LMPS parameters in the element and update of the damage parameter D. If $D \geq 1$, then a crack of initial length c_0 is placed in the element;
4) Calculation of CGR and update the location of each crack tips;
5) Repeat points 2-4 for all the elements in all the laminate plies;
6) Calculation of the weighted crack density;
7) Repeat points 1-6 until the desired number of cycles is reached.

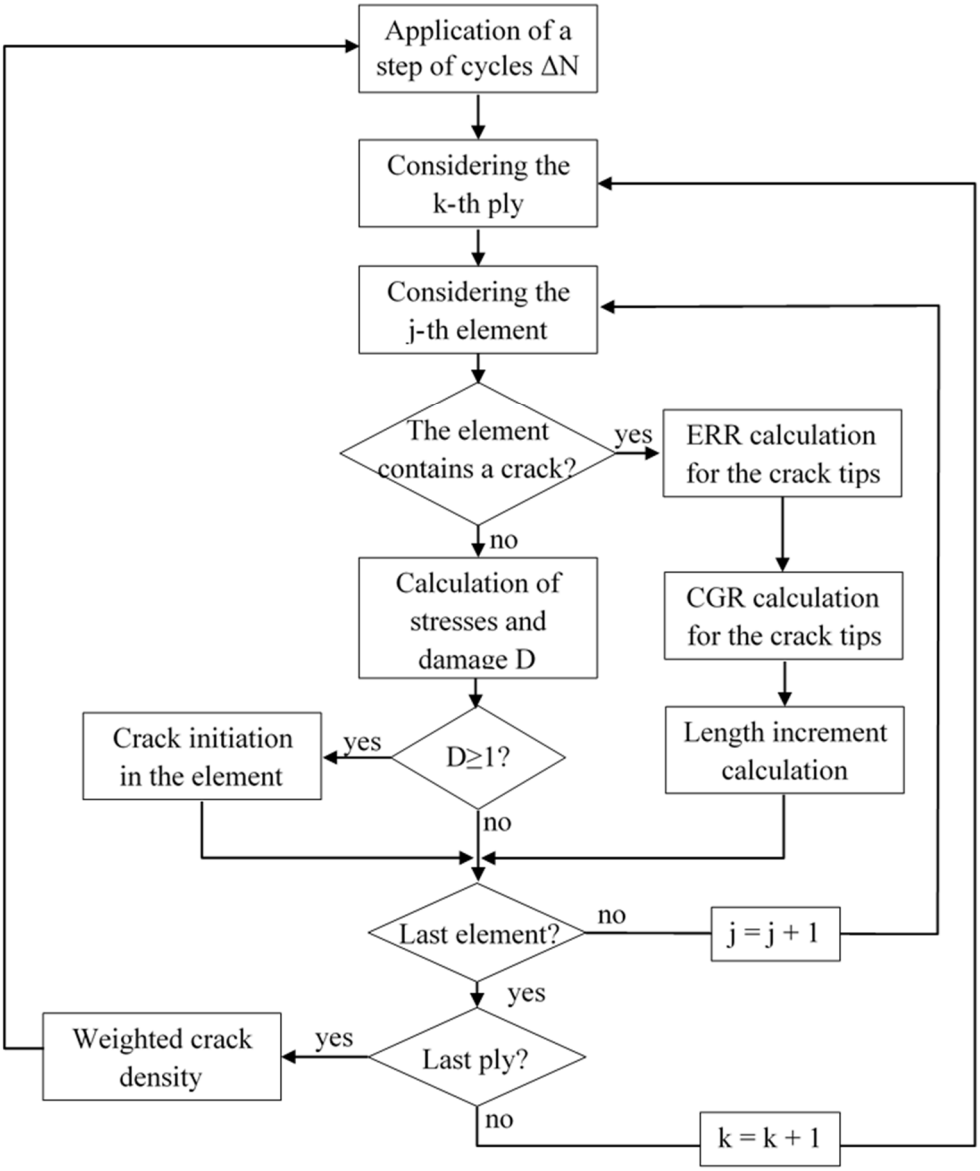

Figure 7.8 – Flow chart for the implementation of the procedure.

7.7. Examples of application

For the sake of validation, the proposed procedure is applied to experimental data for different laminate configurations.

7.7.1 Application to cross-ply laminates

In Chapter 4 [55], an experimental campaign was carried out on $[0/90_2]_s$ glass/epoxy laminates made by vacuum resin infusion. The S-N curve for crack initiation in the 90° ply and the Paris-like curve are reported in Figure 7.9, where also the relevant parameters are shown. As the cracks appeared in the 90° ply, the Paris-like curve is shown as a function of G_I, whereas the S-N curve for crack initiation is here presented in terms of the LHS calculated via the stress concentration factors as reported in [40].

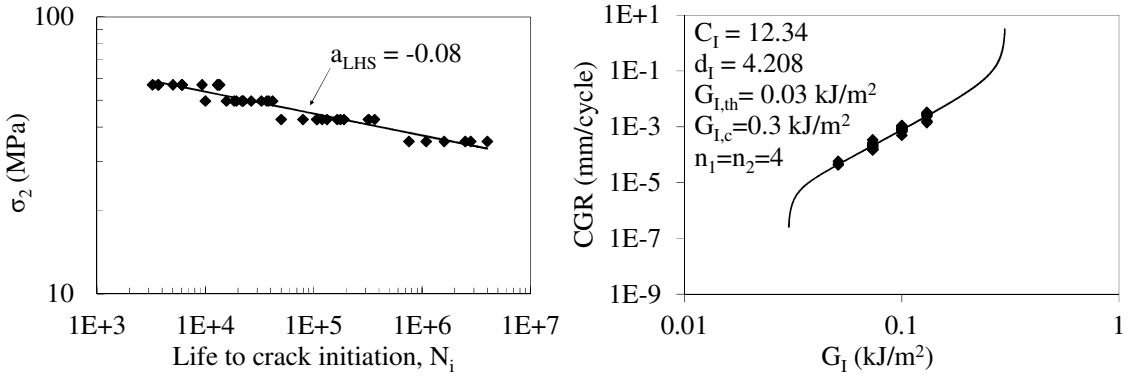

Figure 7.9 – a) S-N curve for crack initiation and b) Paris-like curve for cross-ply laminates (Chapter 4 [55]).

The value of the parameters l_0 and c_0, defining the crack initiation process zone, must be defined for the analysis. Concerning l_0, the guidelines for its choice have already been discussed above. In this work l_0=0.1 mm will be considered. However, the influence of this parameter will be shown later on. The value of c_0 is instead chosen to be equal to 2.7 mm, as an average of experimental observation of the initial crack length.

At this point, the only remaining input data are the parameters of the statistical distribution of the fatigue strength, m_{LHS} and $K_{0,LHS}$. The procedure for their univocal determination is explained in the following.

Consider the specimens tested at a single load level, as for example σ_x = 70 MPa. The total crack density ρ was measured for the two specimens tested at this load level. According to Eqs. (7.5) and (7.7), the cumulative probability of the cycles to crack initiation can be calculated from the experimental measurement of ρ as

$$P(N_i) = \rho \cdot |\sin(\theta)| \frac{c_0 \cdot l_0}{w} \tag{7.16}$$

Now, re-arranging Eq. (7.5) we can write

$$\Psi = -m \cdot Ln\left(N^a\right) + m \cdot Ln\left(\frac{LHS}{K_{0.LHS}}\right) \tag{7.17}$$

where

$$\Psi = Ln\left[Ln\left(\frac{1}{1-P(N)}\right)\right] \tag{7.18}$$

Therefore, when plotting Ψ as a function of $Ln(N^a)$ a straight line is expected, at least in the first stages of the damage evolution, where the cracks are non-interactive. This calculation was performed for the two specimens tested at 70 MPa and the plot is shown in Figure 7.10a). A linear trend is observed only in the first part of the curve, as expected. By fitting the data points in that region with a straight line, the value of m_{LHS} is immediately obtained from the slope of the line (m_{LHS} = 20.4). Then, from the intercept of the line it is possible to calculate $K_{0,LHS}$ = 160.5 MPa. These values are taken as independent of the load level and the loading condition, as far as the crack initiation process is LHS-driven. By

means of the proposed method, the distribution parameters can be simply calculated from the total crack density trend in the non-interactive regime at one load level, thus requiring a very limited experimental effort. With these values of m_{LHS} and $K_{0,LHS}$ three simulations were carried out with the Matlab® code. In Figure 7.10b) the predicted total crack density is plotted together with the experimental measurements (Chapter 4 [55]), showing a good agreement. In addition, it can be seen that the simulation results are almost identical to the prediction obtained with Eq. (7.7) in the early stages. Then, the two solutions diverge when the cracks start to interact, Eq. (7.7) providing highly over-estimated values of the total crack density.

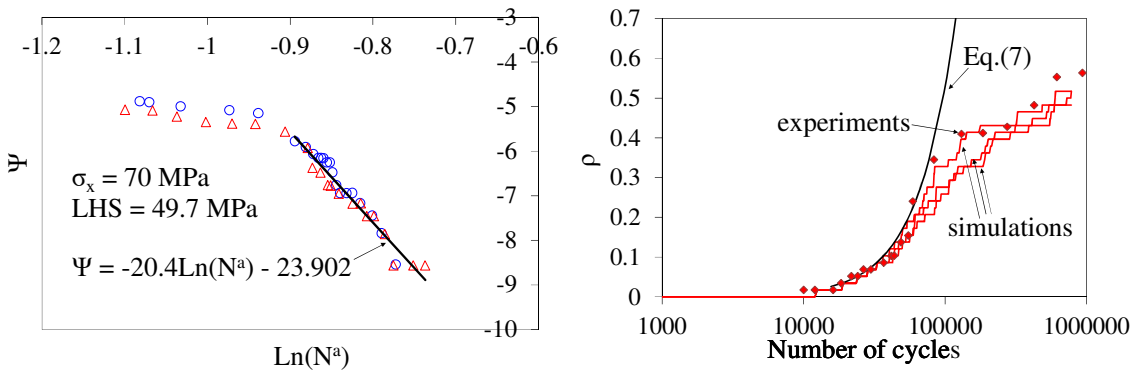

Figure 7.10 – a) Ψ parameter plot and b) Predicted and experimental trends of the total crack density for cross-ply laminates with σ_x=70 MPa.

As highlighted in paragraph 7.2, the most important damage parameter to be used as an input for predicting the stiffness degradation is the weighted crack density. The trends obtained with the simulations for all the load levels are compared to the experimental values in Figure 7.11a). It can be seen that the scatter bands relevant to the simulated and experimental results are compatible, highlighting a very satisfactory agreement. The procedure slightly over-estimates the weighted crack density for the specimens tested at 80 MPa in the later stages. This is not surprising since delaminations were observed to initiate

in the last part of those fatigue tests. The delamination phenomenon and the consequent additional shielding effect are not accounted for in the present procedure at present.

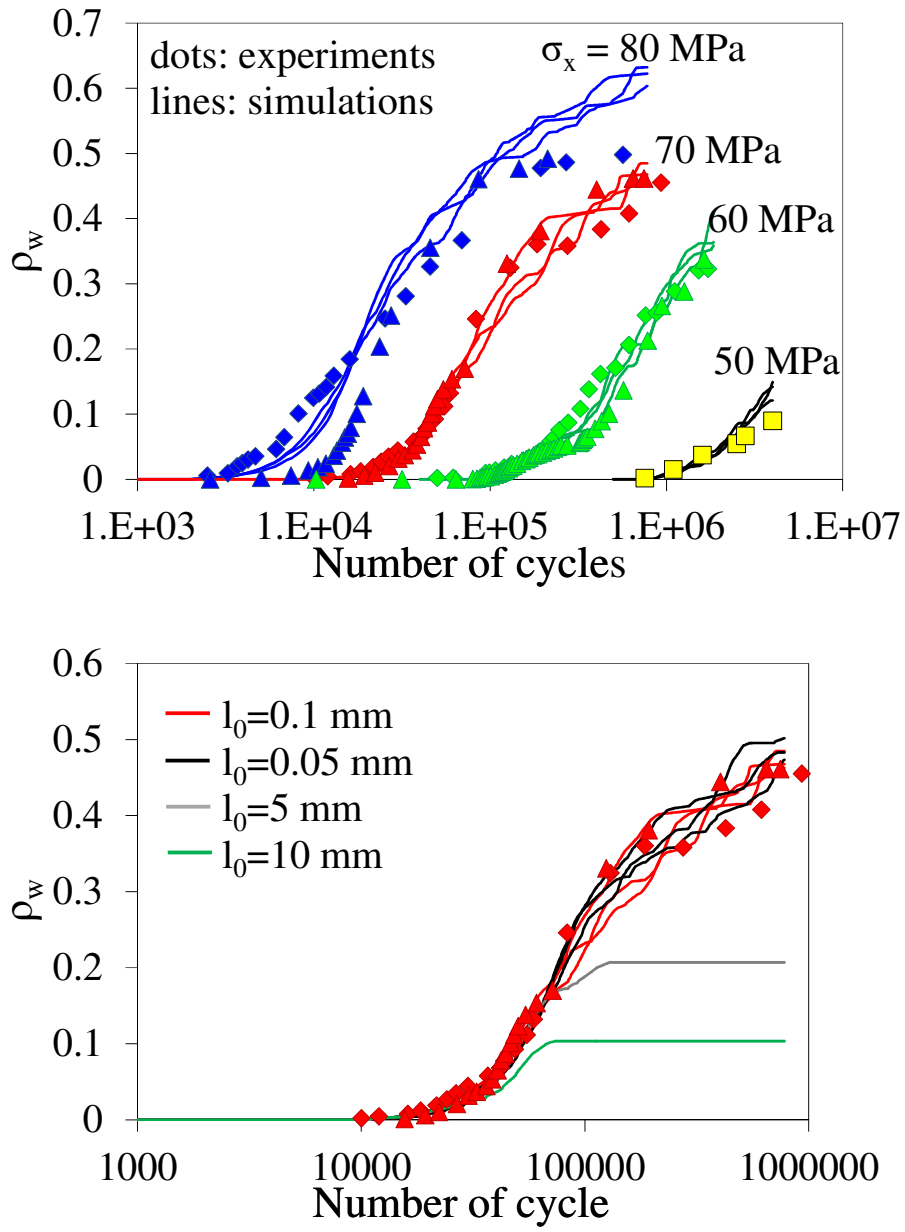

Figure 7.11 – a) Predicted and experimental trends of the weighted crack density and b) Influence of l_0.

For the propagation phase, the trend of the ERR against the crack density in the configuration shown in Figure 7.7a) was calculated with FE analyses as explained in Refs. [2,54] and then fitted with a polynomial expression, both for the cross-ply and the

multidirectional laminates presented later. This was done to achieve the best precision possible. As an alternative, other analytical or semi-analytical models, including the shear-lag model developed by Carraro and Quaresimin [26], can be adopted.

In figure 7.11b) the influence of the value of l_0 is shown. For every value of l_0 the Weibull distribution parameters must be re-calculated according to the proposed procedure. It can be seen that as far as l_0 remains in a range such that the requirements discussed above are respected, the prediction are unvaried. If, instead, l_0 is too large, highly non-conservative predictions are obtained.

7.7.2 Application to multidirectional laminates

In Chapter 4 [55] also the results for glass/epoxy $[0/45_2/0/-45_2]_s$ laminates were reported. The material and geometrical parameters for predicting the crack density evolution in the 45° and -45° plies are listed in Table 7.1 and the results of the simulations in terms of the weighted crack density are shown in Figure 7.12a).

Table 7.1 – Geometrical and material parameters for the simulations for the multidirectional laminates tested in (a) Chapter 4 [55] and (b) [54].

Ply	c_0 mm	l_0 mm	$K_{0,LMPS}$ MPs	m_{LMPS}	a_{LMPS}	C_{eq}	d_{eq}	$n_1=n_2$	G_{th} kJ/m^2	G_c kJ/m^2
45[(a)]	2	0.1	328	14.5	-0.093	0.0115	2.73	4	0.12	1.2
-45[(a)]	2	0.1	345	13.5	-0.093	0.0115	2.73	4	0.12	1.2
50[(b)]	1.5	0.1	515	15	-0.102	0.0411	4.57	4	0.15	1.5
-50[(b)]	1.5	0.1	500	13	-0.102	0.0411	4.57	4	0.15	1.5

Again, a sound agreement between the predictions and the experimental results can be observed, both for the +45° and -45° plies. The calibration of the Weibull parameters was carried out separately for the two plies. In fact, as mentioned above, they can vary with the layer thickness.

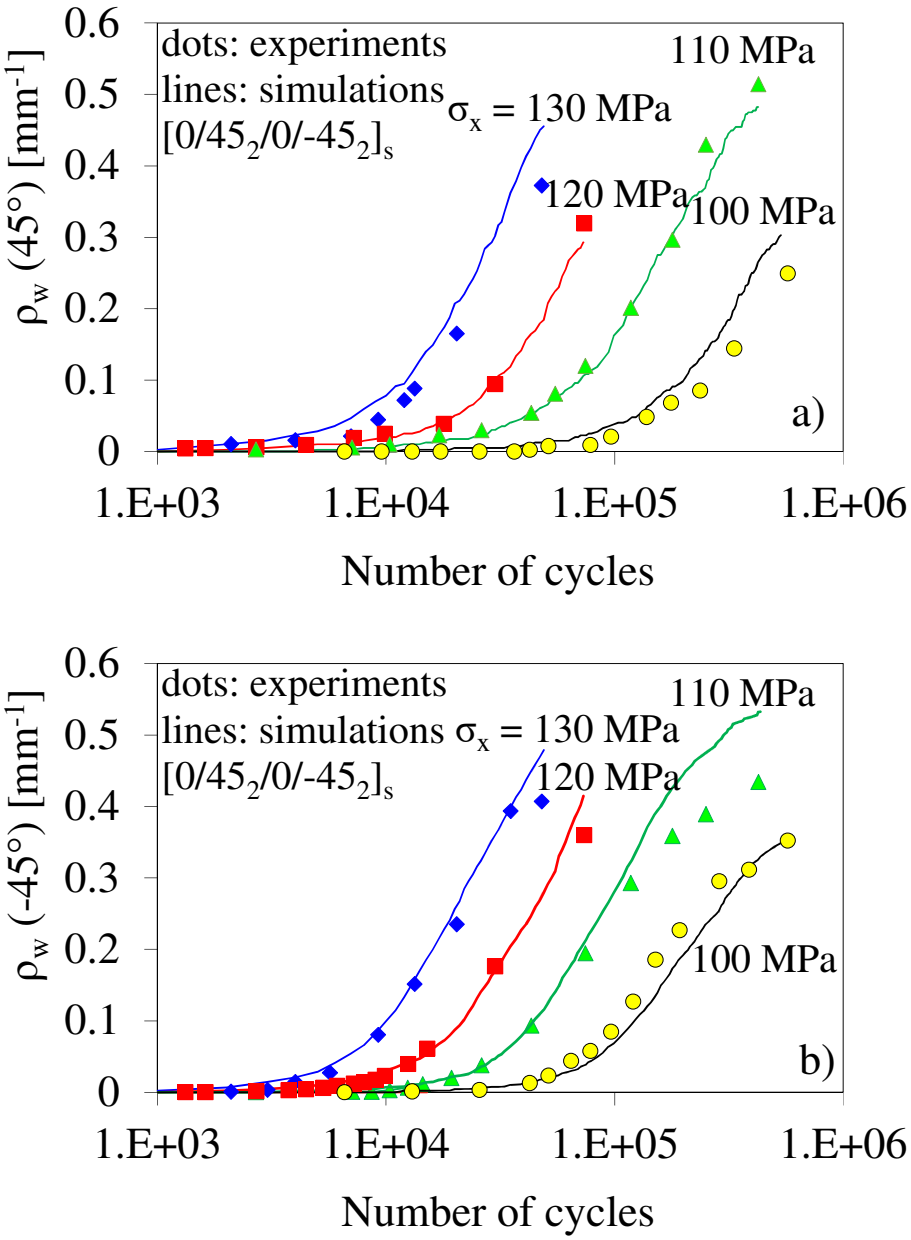

Figure 7.11 – Comparison between simulations and experimental results for the a) 45 and b) -45° plies of $[0/45_2/0/-45_2]_s$ laminates (Chapter 4 [55]).

The same conclusions hold also for the $[0/50_2/0/-50_2]_s$ glass/epoxy laminates tested in [54], whose parameters are reported in Table 7.1 as well (Figure 7.12b). In some specimens some conservative predictions are obtained mainly in the final part of the tests, and this is again attributed to the initiation of delaminations, which were actually observed during the tests.

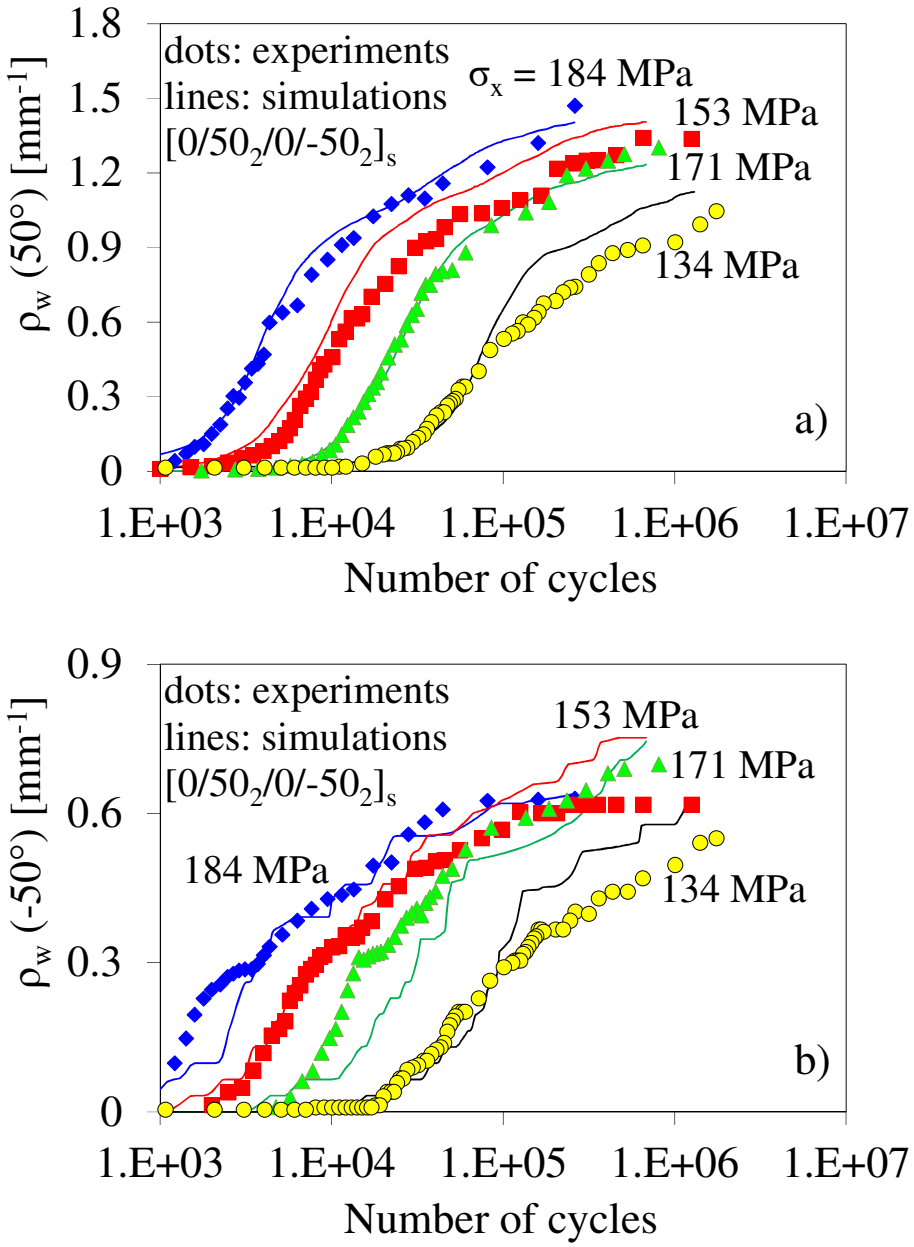

Figure 7.12 – Comparison between simulations and experimental results for the a) 50 and b) -50° plies of $[0/50_2/0/-50_2]_s$ laminates [54].

7.8 Prediction of crack density evolution in the presence of voids

Given the good predictions of the proposed procedure shown in the previous paragraph, it is of interest to explore the possibility of predicting the crack density evolution in the presence of porosity from the behaviour of the void-free material, as done in Chapter 6 for the life to first cracks initiation.

To apply the same principle as in Chapter 6, to predict crack density evolution from the behaviour of the void-free material it is here sufficient to multiply the K_0 parameter of the Weibull distribution of the void-free material times the ratio $LHS^*_{void\text{-}free}/LHS^*_{porous}$ (or $LMPS^*_{void\text{-}free}/LMPS^*_{porous}$, depending on the global stresses acting on the ply). Also the values of the Crack Growth Rate have to be modified, since it was shown to be higher in the presence of voids (see Chapter 4 [55]). The resulting predictions for the $[0/90_2]_S$ laminates produced in Chapter 4, having a void area fraction of Av = 0.34%, are shown in Figure 7.13, where also the 95% Confidence Intervals (CI) are reported, obtained by taking into account the Confidence Interval in the calculation of the Weibull parameter K_0 (Figure 7.10). As can be observed, the experimental trends of crack density in porous specimens are predicted with reasonably good accuracy.

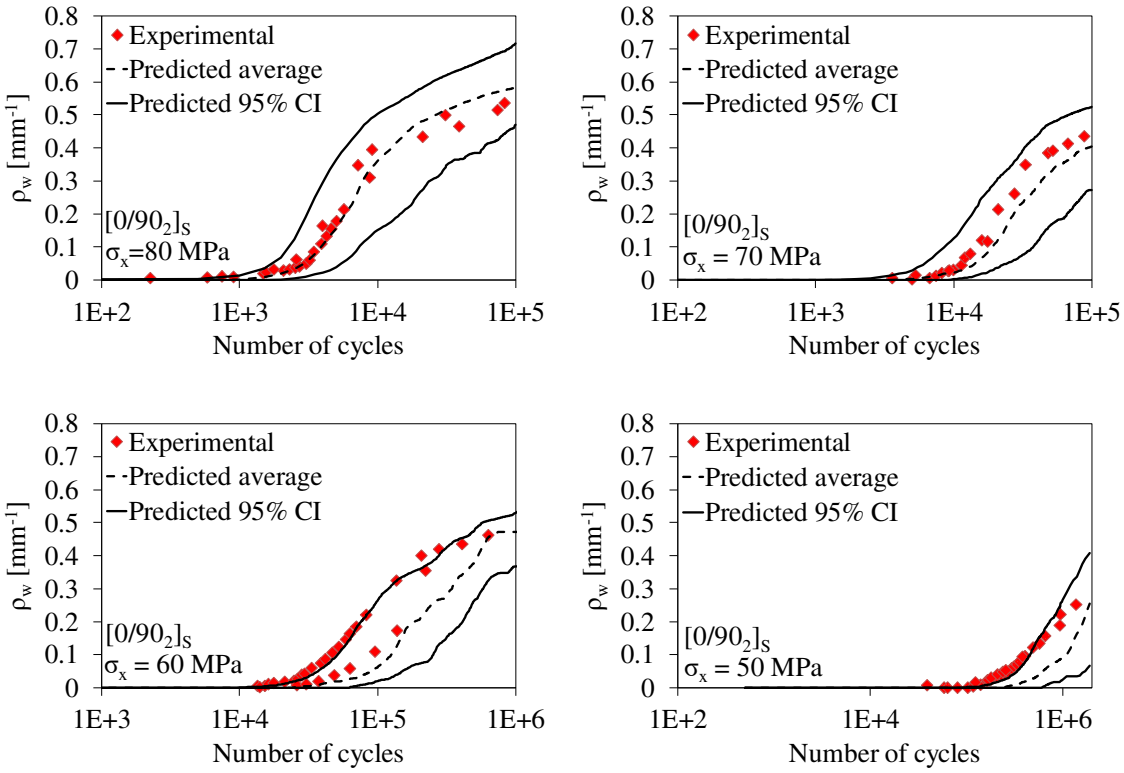

Figure 7.13 – Predicted and experimental trends of the weighted crack density of porous $[0/90_2]_S$ laminates (void area fraction Av = 0.34%).

In Chapter 4 [55], also porous $[0/45_2/0/-45_2]_S$ specimens were produced. However, in those specimens voids were aggregated at regular intervals, resulting in a crack density evolution very similar to the one of the void-free material, with the exception of the early stages. To apply the present procedure to predict such a trend, a possibility could consist of using different Weibull distributions for elements located in different regions, which has not been implemented at present.

7.9. Conclusions

A new procedure has been proposed for the prediction of the weighted crack density evolution in multidirectional laminates subjected to cyclic loadings. The model treats the off-axis crack initiation and propagation phases separately. The multiple cracks initiation

is predicted by means of the S-N curve of the unidirectional lamina expressed in terms of an equivalent stress to account for multiaxial stress states. A Weibull distribution of the fatigue strength has been considered, and a simple and fast way for the determination of the parameters has been proposed. The stress re-distribution between cracks and between layers is accounted for in the procedure. In this case, a shear-lag model previously proposed by Carraro and Quaresimin was adopted, even if, in principle, any other stress analysis tool could be used to this aim.

The propagation phase in treated in terms of Paris-like curve of the lamina, relating the crack growth rate to the equivalent Energy Release Rate, which is a function of the distances between the crack tip and the neighbouring crack faces.

The model is here applied to cross-ply and multidirectional laminates under a uniaxial cyclic load, showing a very satisfactory agreement in predicting the crack density evolution. By making use of the model proposed in Chapter 6, also the crack density evolution in porous specimens could be predicted with reasonable accuracy from the behaviour of the void-free material.

Once coupled with FE analyses for the calculation of the stress fields in the laminates, this procedure can be applied also to components with a more complicated geometry and loading condition.

Appendix 7.A

In this appendix the procedure to account for the influence of cracks in different layers on the stress redistribution is explained. It is based on a model proposed by Carraro and Quaresimin in Ref. [26] for the stiffness degradation of multiply damages laminates. First, an example for a case in which only two layers, *h* and *k*, are cracked is shown for simplicity, and finally the general formula is provided in case of whatever number of cracked layers.

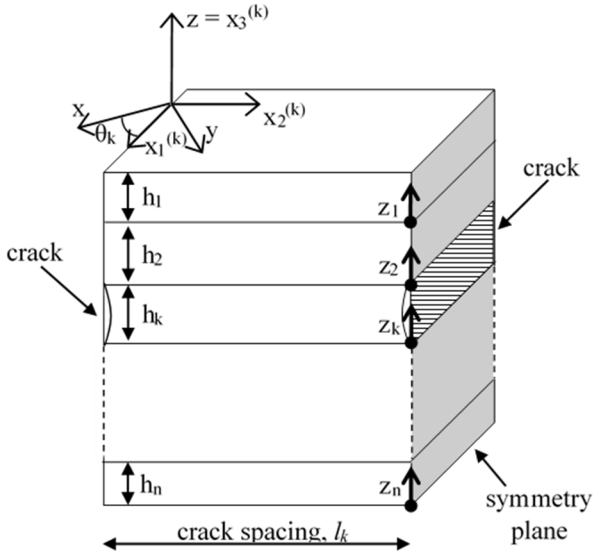

Figure 7.A1 – Laminate with one cracked ply.

By means of the shear lag analysis proposed in [26] the case of a laminate with one cracked ply, *k*, can be addressed (see Figure 7.A1). The in-plane stresses ($\sigma_1^{(k)}(x_2^{(k)})$, $\sigma_2^{(k)}(x_2^{(k)})$, $\sigma_6^{(k)}(x_2^{(k)})$) between the cracks in the cracked layer can be expressed as functions of the transverse coordinate of the *k*-th layer $x_2^{(k)}$, for a general global loading condition $\overset{r}{\sigma}_g = \{\sigma_x, \sigma_y, \sigma_{xy}\}^T$. In addition the in-plane stresses in the reference system of the cracked ply can be calculated, always as function of $x_2^{(k)}$, for every *i*-th non cracked layer ($\sigma_{11}^{(i)}(x_2^{(k)})$, $\sigma_{22}^{(i)}(x_2^{(k)})$, $\sigma_{12}^{(i)}(x_2^{(k)})$). Considering three particular loading conditions ($\overset{r}{\sigma}_g = \{1,0,0\}^T$, $\{0,1,0\}^T$ and $\{0,0,1\}^T$), the stresses in every layer can be averaged over the entire volume of the ply, and the following parameters, function of the crack density on the *k*-th ply ρ_k, can be defined for the *i*-th layer (see Ref. [26] for a more detailed treatise).

$$\gamma_{k,x}^{(i)}(\rho_k) = \frac{1}{l_k}\int_0^{l_k} \sigma_{11}^{(i)}(x_2^{(k)})dx_2^{(k)}\Big|_{\sigma_g=\{1,0,0\}^T},\ \gamma_{k,y}^{(i)}(\rho_k) = \frac{1}{l_k}\int_0^{l_k} \sigma_{11}^{(i)}(x_2^{(k)})dx_2^{(k)}\Big|_{\sigma_g=\{0,1,0\}^T},\ \gamma_{k,xy}^{(i)}(\rho_k) = \frac{1}{l_k}\int_0^{l_k} \sigma_{11}^{(i)}(x_2^{(k)})dx_2^{(k)}\Big|_{\sigma_g=\{0,0,1\}^T} \quad (7.A1)$$

$$\lambda_{k,x}^{(i)}(\rho_k)=\frac{1}{l_k}\int_0^{l_k}\sigma_{22}^{(i)}(x_2^{(k)})dx_2^{(k)}\Big|_{\sigma_g=\{1,0,0\}^T},\ \lambda_{k,y}^{(i)}(\rho_k)=\frac{1}{l_k}\int_0^{l_k}\sigma_{22}^{(i)}(x_2^{(k)})dx_2^{(k)}\Big|_{\sigma_g=\{0,1,0\}^T},\ \lambda_{k,xy}^{(i)}(\rho_k)=\frac{1}{l_k}\int_0^{l_k}\sigma_{22}^{(i)}(x_2^{(k)})dx_2^{(k)}\Big|_{\sigma_g=\{0,0,1\}^T} \quad (7.A2)$$

$$\beta_{k,x}^{(i)}(\rho_k)=\frac{1}{l_k}\int_0^{l_k}\sigma_{12}^{(i)}(x_2^{(k)})dx_2^{(k)}\Big|_{\sigma_g=\{1,0,0\}^T},\ \beta_{k,y}^{(i)}(\rho_k)=\frac{1}{l_k}\int_0^{l_k}\sigma_{12}^{(i)}(x_2^{(k)})dx_2^{(k)}\Big|_{\sigma_g=\{0,1,0\}^T},\ \beta_{k,xy}^{(i)}(\rho_k)=\frac{1}{l_k}\int_0^{l_k}\sigma_{12}^{(i)}(x_2^{(k)})dx_2^{(k)}\Big|_{\sigma_g=\{0,0,1\}^T} \quad (7.A3)$$

Let us consider now a laminate with two cracked plies, *h* and *k*, and subjected to a general external loading condition given by the vector $\underset{\sim}{\sigma}_0=\{\sigma_{x0},\sigma_{y0},\sigma_{xy0}\}^T$. In view of the principle of the superposition of effects, this condition can be decomposed as schematically shown in Figure 7.A2. The reader is referred to Ref. [26] for the detailed explanation.

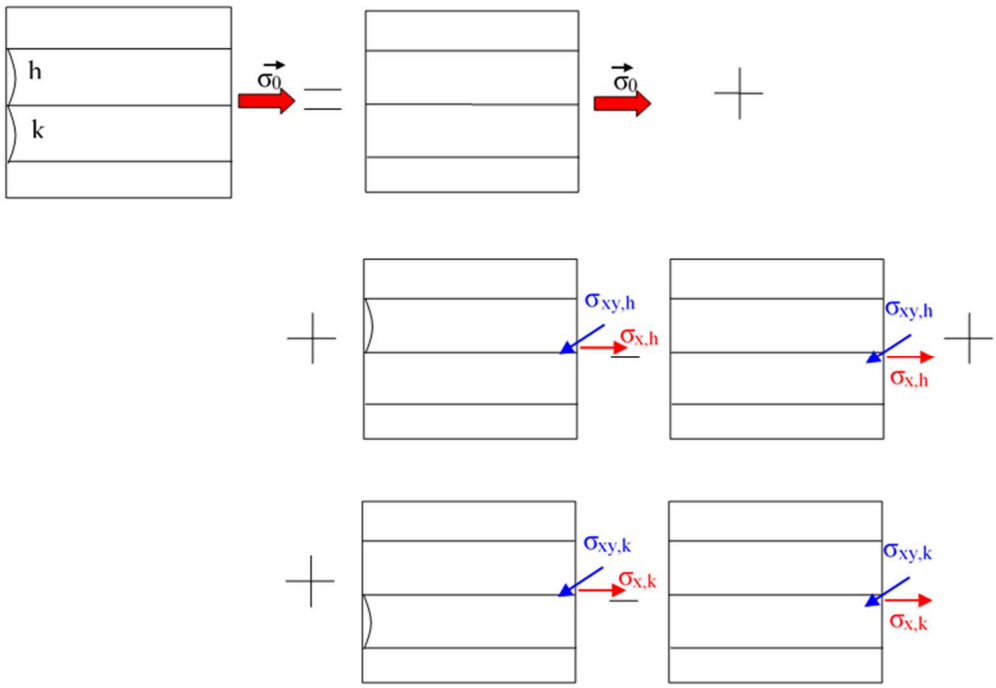

Figure 7.A2 – Decomposition of a laminate with two cracked plies under global load $\underset{\sim}{\sigma}_0$.

The global stresses $\sigma_{x,k}$, $\sigma_{xy,k}$, $\sigma_{x,h}$, $\sigma_{xy,h}$ are unknowns to be calculated as explained in Ref. [26]. The influence of the presence of cracks in the *h*-th layer on the stress distributions in

the *k*-th ply is treated in terms of the increase of the average stress due to the cracks in the *h*-th layer, and vice versa. If only the *k*-th ply was cracked, the average stresses $\sigma_{1av}^{(k)}(\rho_k)$, $\sigma_{2av}^{(k)}(\rho_k)$ and $\sigma_{6av}^{(k)}(\rho_k)$ could be calculated as

$$\begin{Bmatrix} \sigma_{1av}^{(k)}(\rho_k) \\ \sigma_{2av}^{(k)}(\rho_k) \\ \sigma_{6av}^{(k)}(\rho_k) \end{Bmatrix} = \left[\Omega(\rho_k)\right]^{(k)} \{\sigma_0\} \tag{7.A4}$$

where

$$\left[\Omega(\rho_k)\right]^{(k)} = \begin{bmatrix} \gamma_{k,x}^{(k)}(\rho_k) & \gamma_{k,y}^{(k)}(\rho_k) & \gamma_{k,xy}^{(k)}(\rho_k) \\ \lambda_{k,x}^{(k)}(\rho_k) & \lambda_{k,y}^{(k)}(\rho_k) & \lambda_{k,xy}^{(k)}(\rho_k) \\ \beta_{k,x}^{(k)}(\rho_k) & \beta_{k,y}^{(k)}(\rho_k) & \beta_{k,xy}^{(k)}(\rho_k) \end{bmatrix} \tag{7.A5}$$

If, instead, there are cracks also in the *h*-th layer, with density ρ_h, the average stresses in the *k*-th ply can be calculated by summing all the contributions coming from the decomposition shown in figure A2:

$$\begin{Bmatrix} \sigma_{1av}^{(k)} \\ \sigma_{2av}^{(k)} \\ \sigma_{6av}^{(k)} \end{Bmatrix} = [c]^{(k)} \{\sigma_0\} + \left[T(\theta_k - \theta_h)\right]\left[\Omega(\rho_h)\right]^{(k)} \begin{Bmatrix} \sigma_{x,h} \\ 0 \\ \sigma_{xy,h} \end{Bmatrix} - [c]^{(k)} \begin{Bmatrix} \sigma_{x,h} \\ 0 \\ \sigma_{xy,h} \end{Bmatrix} + \left[\Omega(\rho_k)\right]^{(k)} \begin{Bmatrix} \sigma_{x,k} \\ 0 \\ \sigma_{xy,k} \end{Bmatrix} - [c]^{(k)} \begin{Bmatrix} \sigma_{x,k} \\ 0 \\ \sigma_{xy,k} \end{Bmatrix} \tag{7.A6}$$

where

$$[c]^{(k)} = \begin{bmatrix} c_{x,1}^{(k)} & c_{y,1}^{(k)} & c_{xy,1}^{(k)} \\ c_{x,2}^{(k)} & c_{y,2}^{(k)} & c_{xy,2}^{(k)} \\ c_{x,6}^{(k)} & c_{y,6}^{(k)} & c_{xy,6}^{(k)} \end{bmatrix} \tag{7.A7}$$

The coefficients $c_{x,i}^{(k)}$, $c_{y,i}^{(k)}$, $c_{xy,i}^{(k)}$ link the global stresses σ_x, σ_y and σ_{xy}, respectively, to the stress σ_i (i = 1, 2, 6) in the *k*-th layer for an undamaged laminate. Therefore, they can be easily computed with the classical lamination theory.

In the general case of a symmetric laminate with 2*n-1* layers, with cracks in a whatever number plies, the average stresses in the *k*-th lamina can be calculated with the following general formula.

$$\begin{Bmatrix} \sigma_{1av}^{(k)} \\ \sigma_{2av}^{(k)} \\ \sigma_{6av}^{(k)} \end{Bmatrix} = [c]^{(k)} \{\sigma_0\} + \sum_{h=1}^{n} \left\{ \left[T\left(\theta_k - \theta_h\right)\right] \left[\Omega\left(\rho_h\right)\right]^{(k)} \begin{Bmatrix} \sigma_{x,h} \\ 0 \\ \sigma_{xy,h} \end{Bmatrix} - [c]^{(k)} \begin{Bmatrix} \sigma_{x,h} \\ 0 \\ \sigma_{xy,h} \end{Bmatrix} \right\}, \text{ if } \rho_h \neq 0 \quad (7.A8)$$

In the present work it is assumed that the stress distributions $\sigma_1^{(k)}(x_2^{(k)})$, $\sigma_2^{(k)}(x_2^{(k)})$, $\sigma_6^{(k)}(x_2^{(k)})$ in the *k*-th layer should be updated by multiplying them for the ratio between the average stresses calculated accounting for the interaction with other cracked layers ($\sigma_{1av}^{(k)}$, $\sigma_{2av}^{(k)}$ and $\sigma_{6av}^{(k)}$) and those with the only cracked layer *k* ($\sigma_{1av}^{(k)}(\rho_k)$, $\sigma_{2av}^{(k)}(\rho_k)$ and $\sigma_{6av}^{(k)}(\rho_k)$).

Accordingly, the updated stress distributions read

$$\begin{Bmatrix} \sigma_{1,up}^{(k)}\left(x_2^{(k)}\right) \\ \sigma_{2,up}^{(k)}\left(x_2^{(k)}\right) \\ \sigma_{6,up}^{(k)}\left(x_2^{(k)}\right) \end{Bmatrix} = \begin{Bmatrix} \sigma_1^{(k)}\left(x_2^{(k)}\right) \cdot \dfrac{\sigma_{1,av}^{(k)}}{\sigma_{1,av}^{(k)}\left(\rho_k\right)} \\ \sigma_2^{(k)}\left(x_2^{(k)}\right) \cdot \dfrac{\sigma_{2,av}^{(k)}}{\sigma_{2,av}^{(k)}\left(\rho_k\right)} \\ \sigma_6^{(k)}\left(x_2^{(k)}\right) \cdot \dfrac{\sigma_{6,av}^{(k)}}{\sigma_{6,av}^{(k)}\left(\rho_k\right)} \end{Bmatrix} \quad (7.A9)$$

It is worth mentioning that the proposed procedure for crack interaction does not have to be coupled necessary with the shear lag model proposed by Carraro and Quaresimin [26] but also with other stress transfer models available in the literature.

According to this procedure, the effect of crack interaction on the stress fields is treated in an average sense, but it is the best that can be done analytically, in the writer's opinion. Eventually, it is important to mention that, being the cracks in general not fully propagated, the crack densities ρ_h and ρ_k in Equations (7.A8) and (7.A9) are actually the weighted crack densities in the *h*-th and *k*-th layer.

References of Chapter 7

[1] Quaresimin M, Carraro PA. On the investigation of the biaxial fatigue behaviour of unidirectional composites. Composites Part B – Engineering 2013; 54: 200-208.

[2] Quaresimin M, Carraro PA. Damage initiation and evolution in glass/epoxy tubes subjected to combined tension-torsion fatigue loading. International Journal of Fatigue 2014; 63: 25-35.

[3] Tong J, Guild FJ, Ogin SL, Smith PA. On matrix crack growth in quasi isotropic laminates - I. Experimental investigation. Composites Science and Technology 1997; 57: 1527-1535.

[4] Wharmby AW, Ellyin F. Damage growth in constrained angle-ply laminates under cyclic loading. Composites Science and Technology 2002; 62: 1239-1247.

[5] Tohgo K, Nakagawa S, Kageyama K. Fatigue behaviour of CFRP cross-ply laminates under on-axis and off-axis cyclic loading. International Journal of Fatigue 2006; 28: 1254-1262.

[6] Adden S, Horst P. Stiffness degradation under fatigue in multiaxially loaded non-crimped-fabrics. International Journal of Fatigue 2010; 32: 108-122.

[7] Reifsnider KL, Henneke EG, Stinchcomb WW, Duke JC. Damage mechanics and NDE of composite laminates. In: Hashin Z, Herakovich CT, editors. Mechanics of composite materials. Recent advances. New York: Pergamon Press; 1983. p. 399-420.

[8] Wu F, Yao W. A fatigue damage model of composite materials. International Journal of Fatigue 2010; 32: 134-138.

[9] Shokrieh MM, Lessard LB. Multiaxial fatigue behaviour of unidirectional plies based on uniaxial fatigue experiments - I. Modelling. International Journal of Fatigue 1997; 19: 201-207.

[10] Shokrieh MM, Lessard LB. Multiaxial fatigue behaviour of unidirectional plies based on uniaxial fatigue experiments - II. Experimental evaluation. International Journal of Fatigue 1997; 19: 209-217.

[11] Shokrieh MM, Lessard LB. Progressive Fatigue Damage Modeling of Composite Materials, Part I: Modelling. Journal of Composite Materials 2000; 34: 1056-1079.

[12] Shokrieh MM, Lessard LB. Progressive Fatigue Damage Modeling of Composite Materials, Part II: Material Characterization and Model Verification. Journal of Composite Materials 2000; 34: 1081-1115.

[13] M. Naderi M, A. R. Maligno AR. Finite element simulation of fatigue life prediction in carbon/epoxy laminates. Journal of Composite Materials 2013; 47: 475-484.

[14] Kennedy CR, Brádaigh CMO, Leen SB. A multiaxial fatigue damage model for fibre reinforced polymer composites. Composite Structures 2013; 106: 201–210.

[15] Lian W, Yao W. Fatigue life prediction of composite laminates by FEA simulation method. International Journal of Fatigue 2010; 32: 123–133.

[16] Hashin Z, Rotem A. A fatigue failure criterion for fibre-reinforced materials. Journal of Composite Materials 1973; 7: 448-464.

[17] Zhang J, Herrmann KP. Stiffness degradation induced by multilayer intralaminar cracking in composite laminates. Composites: Part A – Applied Science and Manufacturing 1999; 30: 683–706

[18] McCartney LN. Model to predict effects of triaxial loading on ply cracking in general symmetric laminates. Composites Science and Technology 2000; 60: 2255-2279.

[19] Yokozeki T, Aoki T. Overall thermoelastic properties of symmetric laminates containing obliquely crossed matrix cracks. Composites Science and Technology 2005; 65: 1647–1654.

[20] Lundmark P, Varna J. 2005. Constitutive relationships for laminates with ply cracks in in-plane loading. International Journal of Damage Mechanics 2005; 14: 235–259.

[21] Lundmark P, Varna J. Crack face sliding effect on stiffness of laminates with ply cracks. Composites Science and Technology 2006; 66: 1444–1454.

[22] Li S, Singh CV, Talreja R. A representative volume element based on translational symmetries for FE analysis of cracked laminates with two arrays of cracks. International Journal of Solids and Structures 2009; 46: 1793–1804 .

[23] Singh CV, Talreja R. A synergistic damage mechanics approach for composite laminates with matrix cracks in multiple orientations. Mechanics of Materials 2009; 41: 954–968.

[24] Vinogradov V, Hashin Z. Variational analysis of cracked angle-ply laminates. Composites Science and Technology 2010; 70: 638–646.

[25] Cortes DH, Barbero EJ. Stiffness reduction and fracture evolution of oblique matrix cracks in composite laminates. Annals of Solid and Structural Mechanics 2010; 1 29–40.

[26] Carraro PA, Quaresimin M. A stiffness degradation model for cracked multidirectional laminates with cracks in multiple layers. International Journal of Solids and Structures 2015; 58: 34–51.

[27] Vinogradov V, Hashin Z. Probabilistic energy based model for prediction of transverse cracking in cross-ply laminates. International Journal of Solids and Structures 2005; 42: 365–392.

[28] Singh CV, Talreja R. Evolution of ply cracks in multidirectional composite laminates. International Journal of Solids and Structures 2010; 47: 1338–1349.

[29] Lee JW, Daniel IM. Progressive transverse cracking of crossply composite laminates. Journal of Composite Materials 1990; 24: 1225-1243.

[30] Huang Y, Varna J, Talreja R. A statistical approach to evaluate the effect of manufacturing quality on transverse cracking in cross ply laminates. In: Proceedings of ICCM18 Conference, Jeju Island, August, 2011.

[31] Huang Y, Talreja R. Statistical analysis of oblique crack evolution in composite laminates. Composites Part B – Engineering 2014; 65: 34-39.

[32] Liu B, L. Lessard LB. Fatigue and damage-tolerance analysis of composite laminates: stiffness loss, damage modelling, and life prediction. Composites Science and Technology 1994; 51: 43-51.

[33] Talreja R. Fatigue of composite materials. Technometric Publishing Co., Lancaster, PA 1987.

[34] O' Brien TK. Analysis of Local Delaminations and their Influence on Composite Laminate Behaviour, Delamination and Debonding of Materials. ASTM STP 876 (1985) 282-297.

[35] Subramanian S, Reifsneider KL, Stinchcombe WW. A cumulative damage model to predict the fatigue life of composite laminates including the effect of a fibre-matrix interphase. International Journal of Fatigue 1995; 17: 343-351.

[36] Henaff-Gardin C, Lafarie-Frenot MC. The use of a characteristic damage variable in the study of transverse cracking development under fatigue loading in cross-ply laminates. International Journal of Fatigue 2002; 24: 389–395.

[37] Hoang NT, Gamby D, Lafarie-Frenot MC. Predicting fatigue transverse crack growth in cross-ply carbon–epoxy laminates from quasi static strength tests by using iso-damage curves. International Journal of Fatigue 2010; 32: 166–173.

[38] Sun Z, Daniel IM, Luo JJ. Modeling of fatigue damage in a polymer matrix composite. Materials Science and Engineering 2003; A361: 302–311.

[39] Ogi K, Yashiro S, Niimi K. A probabilistic approach for transverse crack evolution in a composite laminate under variable amplitude cyclic loading. Composites Part A – Applied Science and Manufacturing 2010; 41: 383–390.

[40] Carraro PA, Quaresimin M. A damage based model for crack initiation in unidirectional composites under multiaxial cyclic loading. Composites Science and Technology 2014; 99: 154-163.

[41] Quaresimin M, Carraro PA, Maragoni L. Early stage damage in off-axis plies under fatigue loading. Composites Science and Technology 2016; 128: 147-154.

[42] Maragoni L, Carraro PA, Quaresimin M. Effect of voids on the crack formation in a [45/-45/0]s laminate under cyclic axial tension, Composites Part A: Applied Science and Manufacturing 2016, DOI: 10.1016/j.compositesa.2016.02.018

[43] Lafarie-Frenot MC, Hénaff-Gardin C, Formation and Growth of 90° Ply Fatigue Cracks in Carbon/Epoxy Laminates. Composites Science and Technology 1991; 40: 307-324.

[44] Talreja R. Multi-scale modeling in damage mechanics of composite materials. Journal of Materials Science 2006; 41: 6800–6812.

[45] Ogin SL, Smith PA, Beaumont PWR, A Stress Intensity Factor Approach to the Fatigue Growth of Transverse Ply Cracks, Composites Science and Technology 1985; 24: 47-59.

[46] Yokozeki T, Aoki T, Ishikawa T. Fatigue growth of matrix cracks in the transverse direction of CFRP laminates. Composites Science and Technology 2002; 62: 1223–1229.

[47] Hosoi A, Arao Y, Kawada H. Transverse crack growth behavior considering free-edge effect in quasi-isotropic CFRP laminates under high-cycle fatigue loading. Composites Science and Technology 2009; 69: 1388–1393.

[48] Quaresimin M, Carraro PA, Maragoni L. Influence of load ratio on the biaxial fatigue behaviour and damage evolution in glass/epoxy tubes under tension–torsion loading. Composites Part A – Applied Science and Manufacturing 2015; 78: 294–302.

[49] Kenane M, Benzeggagh ML. Mixed-mode delamination fracture toughness of unidirectional glass/epoxy composites under fatigue loading. Composites Science and Technology 1997; 57: 597–605.

[50] Carraro PA, Meneghetti G, Quaresimin M, Ricotta M. Crack propagation analysis in composite bonded joints under mixedmode (I+II) static and fatigue loading: a damage-based model. Journal of Adhesion Science and Technology 2013; 27: 1393-1406.

[51] Carraro PA, Meneghetti G, Quaresimin M, Ricotta M. Crack propagation analysis in composite bonded joints under mixedmode (I+II) static and fatigue loading: experimental investigation and phenomenological modelling. Journal of Adhesion Science and Technology 2013; 27: 1179-1196.

[52] Ho S, Suo Z. Tunneling cracks in constrained layers. Journal of Applied Mechanics 1993; 60: 890-894.

[53] Hutchinson JW, Suo Z. Mixed mode cracking in layered materials. Advances in Applied Mechanics 1991; 29: 63-191.

[54] Quaresimin M, Carraro PA, Pilgaard Mikkelsen L, Lucato N, Vivian L, Brøndsted P, Sørensen BF, Varna J, Talreja R. Damage evolution under internal and external multiaxial cyclic stress state: a comparative analysis. Composites Part B – Engineering 2014; 61: 282–290.

[55] Maragoni L, Carraro PA, Peron M, Quaresimin M. Fatigue behaviour of glass/epoxy laminates in the presence of voids. International Journal of Fatigue 2017; 95: 18-28.

Appendix A

Influence of macro-voids on damage initiation and propagation in carbon/epoxy NCF laminates

Abstract

In this Appendix, two sets of NCF carbon/epoxy laminates have been produced via liquid infusion moulding, with the aim to investigate the influence of some process parameters on the intra- and inter-laminar properties of composite materials. In the first set the resin was degassed before infusion and the bleeding time was large. In the second set the resin was not degassed and the bleeding time was kept very short. Microscopy analyses revealed an evident void content in the second set of panels, whereas no voids were detectable in the first one. Incremental static tests on cross-ply specimens and DCB tests on $[(90/0)_3]_S$ and $[(+45/-45)_3]_S$ laminates obtained with the two processes were carried out, with the aim to characterise the influence of voids on some intra- and inter-laminar properties. Tensile tests revealed that the multiple cracking process in cross-ply laminates was detrimentally affected by the presence of defects. Conversely, DCB tests showed a negligible influence of the presence of defects on the mode I fracture toughness, its propagation value being even higher in the specimens with voids. Damage mechanisms were carefully analysed to deeply understand the role of voids mainly in the crack initiation process. Finite element analyses carried out considering the actual geometry of voids showed that their local shape, and the related stress/strain concentration, are fundamental parameters to properly describe this phenomenon.

A1. Introduction

Due to the intrinsic nature of composites, it is extremely difficult and expensive to obtain defects-free components with such materials; in particular, the presence of microscopic voids is nearly unavoidable in complex structures. In processes where liquid resin is used, like RTM and infusion, voids form when air is entrapped as a result of the different resin flow inside the fibre bundles and in the channels between the bundles. Void content depends on the process parameters and conditions, such as resin degassing, temperatures, pressures, and infusion time (see Refs. [1-4] among the others).

The presence of microscopic voids in a composite component can be detrimental for its mechanical intra-laminar and inter-laminar properties.

The influence of voids on the inter-laminar fracture toughness was investigated by Asp and Brandt [5]. They reported that a small amount of voids (~1% in volume) had a slightly deleterious or no effect, respectively for Mode I and Mixed mode loading, on the critical Energy Release Rate (ERR, or G) at crack growth initiation for a 0°/5° interface. In both cases, an increase of the critical ERR, G_c, was instead found for crack propagation in presence of voids due to the occurrence of ply bridging phenomena under Mode I and multiple crack planes at the main crack tip under Mixed Mode loading. In mode II, instead, voids appeared not to influence the critical ERR. Olivier et al [6] found instead that for a larger amount of voids (5% in volume), the G_c at crack propagation sensibly decreased for a 0°/0° interface under Mode I loading.

The effect of voids on the inter-laminar shear strength (ILSS) has been analysed by several researchers in the literature [6-16]. Some works [7,10,14,15] report a linear relation between the ILSS and void volume fraction. However, clear conclusions regarding the influence of voids on this inter-laminar property are hard to drawn, it being largely dependent on the materials used, and the laminate stacking sequence.

The effect of voids on the in-plane properties of composites has been studied in terms of tensile, compressive and flexural behaviour.

Concerning the tensile behaviour, the experimental results from Olivier et al. [9] highlighted that the fibre-dominated properties were those less affected by the presence of voids, whereas the behaviour in the transverse direction resulted to be more influenced. Varna et al. [17] showed that for larger void content the initiation of the first transverse crack in UD specimens containing a small amount of weft fibres occurred at lower loads and the strain to failure resulted to be larger. However, the influence of voids on tensile modulus and strength was found to depend also on the plies architecture [18]. Huang and co-authors [19] tested autoclave moulded cross-ply laminates obtained with different process parameters resulting in different void contents. They observed a clear dependence of the crack density evolution under static loading on the process parameters, even if this behaviour was not related to the amount or size of voids in the transverse plies.

The compressive strength of composites is also strongly influenced by voids, as shown in [8, 19, 20]. However, the extent of the void influence varied with the material adopted and the laminate lay-up.

The studies carried out on the flexural behaviour in presence of voids [9,15,22-24] did not lead to clear conclusions, with a large variability of the sensitivity of the material performance on the void content. Relating the composite material performance to the global void volume content, as done in the majority of the works, may be too simplistic in presence of bending loads, since in such cases also the voids spatial distribution plays a fundamental role.

Studies on the influence of voids on the fatigue behaviour of composites can be found in [14, 22, 25-28]. S-N curves were found to be shifted towards shorter fatigue life and steeper in presence of voids both for tension-tension and compression-compression loading

conditions [25-27]. The same trend was found in presence of bending loads for unidirectional [22,28] and woven laminates [14]. A linear trend was reported between the fatigue life of $[0/45/-45]_{3S}$ laminates and the size of the largest defect in critical positions by Lambert et al. [29], whereas no clear trend appeared to exist between fatigue life and global void content or the largest defect in the whole specimen. Lambert and co-authors [29] presented an interesting, though qualitative, analysis of fatigue damage evolution, allowing the authors to identify which were the critical plies in which the presence of voids played a deleterious role. In their study of the inter-laminar tensile strength (ILTS) under fatigue, Seon et al. [30] correlated instead the life reduction under cyclic loading to the presence of a single void in critical position. Recently, Sisodia and co-authors [31] analysed the fatigue damage evolution in multidirectional laminates, showing that the density of off-axis cracks, and the subsequent stiffness degradation, were higher in the presence of voids. Several works have been done with the aim to model the influence of voids on the mechanical properties of composite materials. Models based on finite elements method, by far the most used, were proposed to calculate the stress concentration factor in presence of a void and the resulting tensile strength [25], to calculate the ILSS in presence of a single void [11], to analyze the shear strength [32] and to study the decrease of elastic properties as a function of void content [33,34], obtaining good agreement with experimental results through the analysis of a unit cell [33]. Some analytical models too were developed in literature, in particular to justify the larger strain to failure in presence of voids under transverse loading (from a *shear lag* analysis) [17], to predict the ILSS [13] and flexural resistance (through a modification of Mar-Lin criterion) [23] and to study the effect of voids at the interface between plies on the fracture toughness [35]. A statistical model was also developed by Huang et al. [19] to predict crack density evolution in cross-ply laminates. This model can be adopted to obtain the statistical distribution of the transverse strength

for different process parameters, even if the authors did not correlate the so obtained distributions to the amount of voids present in the laminates.

From the analysis of the scientific literature and despite the amount of experimental data, it can be seen that it is still hard to draw quantitative correlations of general validity between the presence of voids and the mechanical properties of composite materials. Concerning the static and fatigue behaviour, the influence of voids has been found to be strongly dependent on the materials adopted and the laminate stacking sequence. Damage evolution in multidirectional laminates is indeed a quite complex phenomenon, characterised by the initiation and propagation of off-axis cracks which then lead to the onset of delamination and final failure. Therefore, both intra-laminar and inter-laminar properties play a fundamental role in the development of damage under static and fatigue loading. As mentioned before, these properties are strongly influenced by the presence of voids. In this scenario, understanding the effect of voids on damage mechanisms leading to the formation and propagation of intra-laminar and inter-laminar cracks is essential. In addition, considering their geometry, size and distribution instead of just their global content could probably bring to an improvement in this direction. In the writer's view, this mechanisms-based approach is fundamental to provide reliable models to predict the effect of the manufacturing process and the induced defects on the static and fatigue performances of composite components.

Within this frame, in this appendix two sets of laminates have been produced using different process parameters to obtain specimens with and without voids. Given the importance of the intra-laminar and inter-laminar properties on damage evolution of laminates, tests have been carried out to characterise the transverse cracking resistance and the mode I fracture toughness, to give a deeper insight of the relation between voids and these fundamental mechanical properties. Particular attention has been paid to the observation of damage

mechanisms during the tests, with the aim to understand the role of manufacturing induced voids on the crack initiation and propagation processes.

A2. Materials

The adopted reinforcement was a commercial ±45° non-crimp fabric (NCF) X-C-218g/m^2-1400mm from Saertex, made of TENAX-J STS40 F13 24K carbon fibres. A low viscosity epoxy resin, EC157 from Elantas, suitable for infusion, was used as matrix. The amminic hardener W152LR allowed a sufficiently long pot life at room temperature (two hours). The matrix-to-hardener ratio, suggested by the manufacturer, was 100:30.

Two sets of laminates were produced: in the first one the resin was degassed after mixing prior to infusion and it was allowed to bleed for a long time; in the second one the resin was not degassed and the bleeding time was much shorter. These conditions led to savings in time and resin waste, but also to the presence of defects, as reported later on.

As already mentioned, both the intra-laminar and inter-laminar properties control damage initiation and evolution in multidirectional laminates, and it is important to characterise and understand how they are affected by the presence of voids.

With this aim, laminates with lay-up $[0/90]_S$ were first produced to characterise the effect of voids on the resistance to the initiation of transverse cracks.

Then, two different lay-ups, namely $[(90/0)_3]_S$ and $[(+45/-45)_3]_S$, were adopted for testing the interlaminar fracture toughness by means of DCB samples. Those two stacking sequences were considered to analyse the possible influence of the orientation of the interface plies (0° and -45°). In the DCB specimens an aluminium film (thickness 10 μm) was placed between layers 6 and 7 to create a pre-crack.

Resin and hardener were mixed for 15 minutes at 300 rpm with a DISPERMAT TU shear blender from VMA-Getzman. For producing the first set of laminates the mixing was

followed by extensive degassing of the resin (at 0.05 mbar for 30 minutes), to consistently reduce the amount of air entrapped in the resin during the mixing. For the second set, the resin was not degassed. The inlet and outlet pressures were, respectively, 1 bar and 0.05 mbar for both sets and the infusion was carried out at room temperature. The bleeding time was measured from the time the resin reached the trap. For the first set, 10 and 15 minutes were allowed for the cross-ply and DCB laminates, respectively, before stopping the infusion. The different time was due to the different thickness of the two laminates. For the second set, a 3 minutes bleeding was maintained to ensure a complete filling of the fibres at a macroscopic level.

De-moulding was performed after 3 days at room temperature. No post-curing was carried out on the laminates.

A3. Static tensile tests on cross-ply laminates

Specimens were cut from the infused $[0/90]_S$ panels and tabs were bonded according to the geometry shown in Figure A1. The specimens were polished on both edges. No voids were found in the degassed specimens, while voids with a very irregular shape between the fibres tows were observed on the edges of the non-degassed ones, in the 90° layers, as shown in Figure A2. The void content, in terms of void area fraction (A_v) measured on the edges, calculated by means of image analysis (carried out on 16 micrographic images), ranged between a minimum value of 1.70 and a maximum value of 4.50%, without any trend with respect to the position of the specimens in the infused panel. The voids were always found in correspondence of the polyester tows used to keep the NCF layers together. This gives reason of the irregular void shapes.

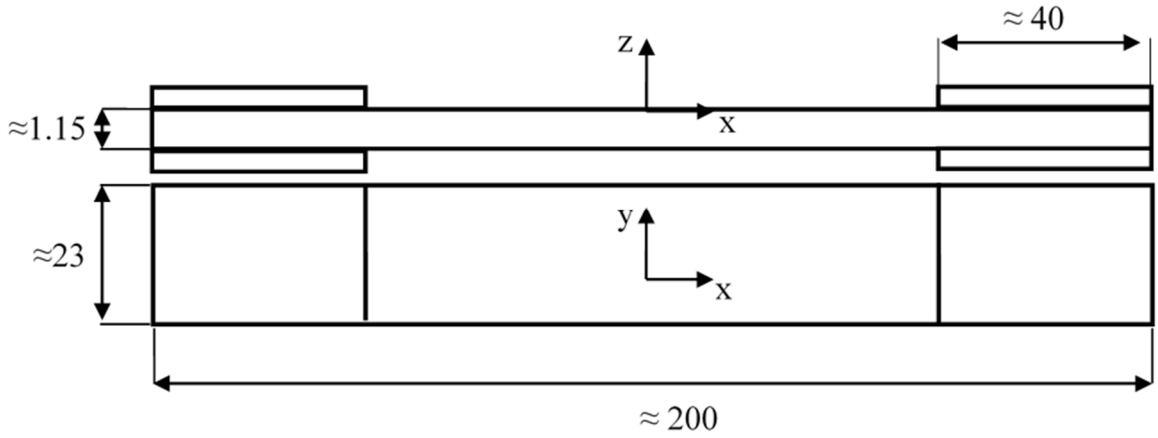

Figure A1 – Geometry of the cross-ply specimens (units in millimetres).

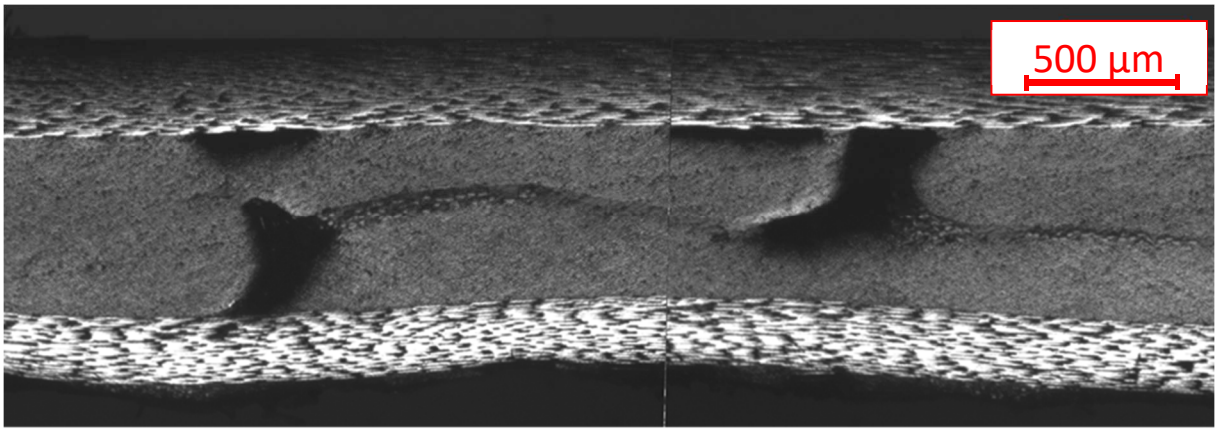

Figure A2 – Example of voids in a non degassed cross-ply laminate.

Static tensile tests were carried out on the cross-ply specimens by means of a MTS 858 MiniBionix hydraulic machine. An axial extensometer MTS632.29F-30 with an initial length of 25 mm was mounted in the central part of the specimens. Load ramps were applied in displacement control in the x-direction until progressively higher values of strain were reached (with strain steps of 0.025%). After each predefined strain level, the specimens were removed from the machine and analysed with an optical microscope, to detect the presence of edge cracks in a zone of 80 mm length centred in the specimen mid-section.

The first event of damage was always represented by the initiation of transverse cracks in the 90° layers. More and more cracks initiated as the strain level was increased. The second damage mode, occurring at higher strain levels, was the onset of macroscopic delaminations which covered tens of millimetres along the specimens length.

Each specimen was observed at both edges. In the non-degassed ones cracks were seen to initiate always in correspondence of the voids. X-Rays analyses revealed that cracks and delaminations did not propagate through the laminates width and stopped after few millimetres from the edges. This is due to the small thickness of the 90° layer, which is therefore highly constrained by the longitudinal plies, thus reducing the crack opening and, as a consequence, the Energy Release Rate (see, for instance Ref [36]). As a consequence, transverse crack initiation was not followed by through the width propagation since the ERR level (even under the maximum applied strain) was too low. For this reason, the two edges of a specimen could be treated as two independent specimens. Three non-degassed and two degassed coupons were tested, and thus results are reported for six and four edges, respectively.

Before analysing the damage initiation and evolution it is important to mention that no influence of the voids was found on the global elastic modulus of the laminates in the loading direction (x-direction). An average Young modulus $E_x \approx 60000$ MPa was found. This is a strongly fibre-dominated property, and therefore not so sensitive to the presence of voids in the matrix [9].

A first basic analysis of the influence of voids on the transverse cracking behaviour may be done by comparing the performance of void-free specimens and specimens containing voids regardless of their individual void content. The strain level after which the first crack and first macroscopic delamination were observed are reported in Figure A3. In spite of the quite high data dispersion, the detrimental effect of the presence of voids is evident for both

phenomena. In fact, the strain to first crack and first delamination initiation are decreased by, respectively, 20 and 14 % in the presence of voids.

As already mentioned, multiple cracking occurred in all the specimens. The density of transverse cracks against the strain level is reported in Figure A4. It is clear that for the same strain level the crack density is much higher in the presence of voids, confirming their detrimental effect on the transverse cracking behaviour.

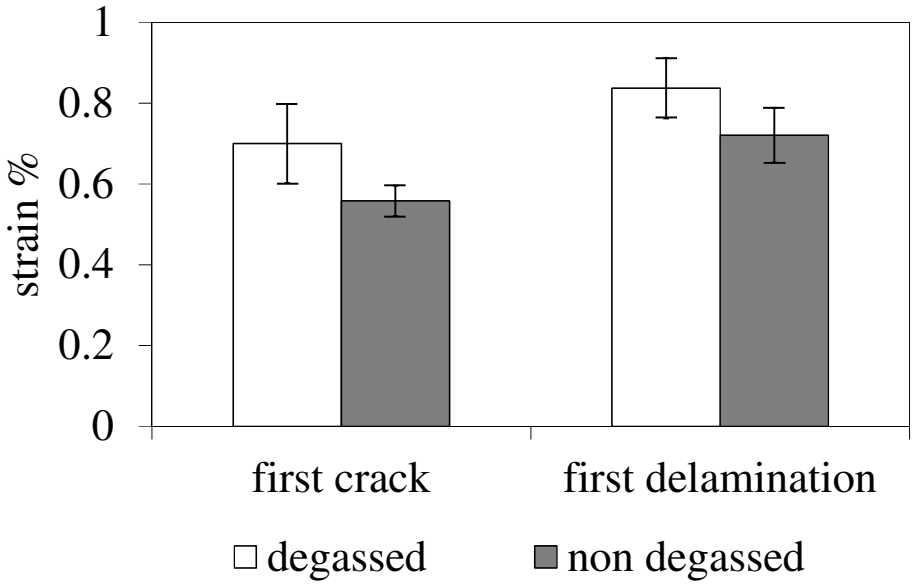

Figure A3 – Strain at initiation of the first crack and first delamination.

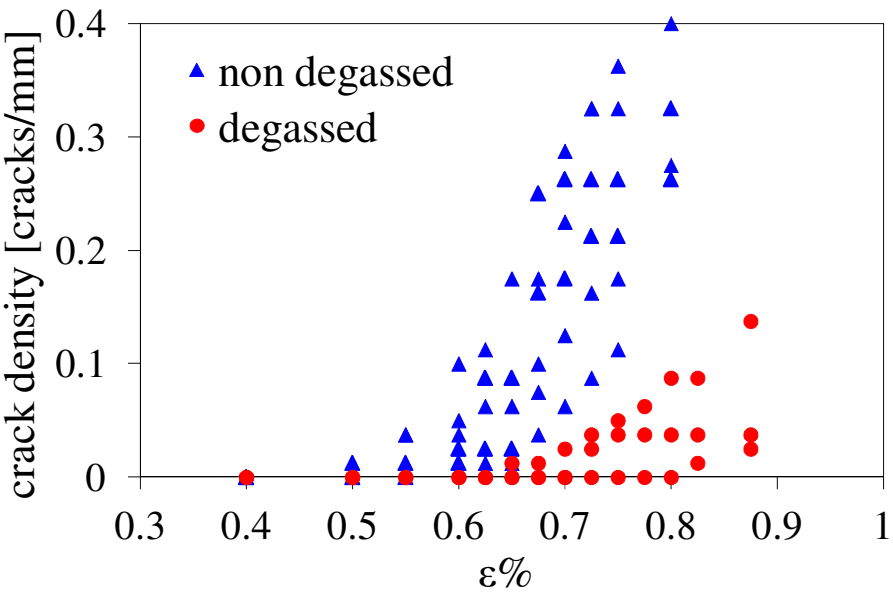

Figure A4 – Crack density evolution against strain level for degassed and non-degassed cross-ply laminates.

A3.1 Statistical distribution of the strain to crack initiation

The influence of the presence of voids on the transverse cracking behaviour can be quantified by means of statistical considerations. If the crack density is low enough to ensure that there is no shielding effect due to the presence of multiple cracks, and if there are no delaminations, the stress and strain fields can be considered, within reason, uniform along the length of the 90° layers, their values being equal to those calculated in absence of damage. In this condition, the initiation of cracks at different strain levels is due to the presence of defects with different criticality (such as voids producing more or less severe stress concentrations) or differences in the local microstructure (such as different local fibre volume fractions, resin rich regions, waviness). From a statistical point of view it can be said that along the length of the 90° layers there is a statistical distribution of the strain to crack initiation, whose cumulative probability function P(ε) is given by

$$P(\varepsilon) = 1 - \exp\left[-\left(\frac{\varepsilon}{\varepsilon_0} \right)^m \right] \tag{A1}$$

in which m and ε_0 are, respectively, the shape and scale parameters of the Weibull distribution.

For the determination of the parameters of the statistical distribution the procedure proposed in Ref. [19] is adopted here.

Let us divide the length of the 90° layers in small elements of length l_0, as shown in Figure A5. At a given value of applied strain, the number of initiated cracks is equal to the number of small elements of which the strain to crack initiation is lower than or equal to the applied strain. Therefore, the crack density $\rho(\varepsilon)$ can be calculated as in Eq. (A2).

$$\rho(\varepsilon) = \frac{1}{l_0}\left(1 - \exp\left[-\left(\frac{\varepsilon}{\varepsilon_0} \right)^m \right] \right) \tag{A2}$$

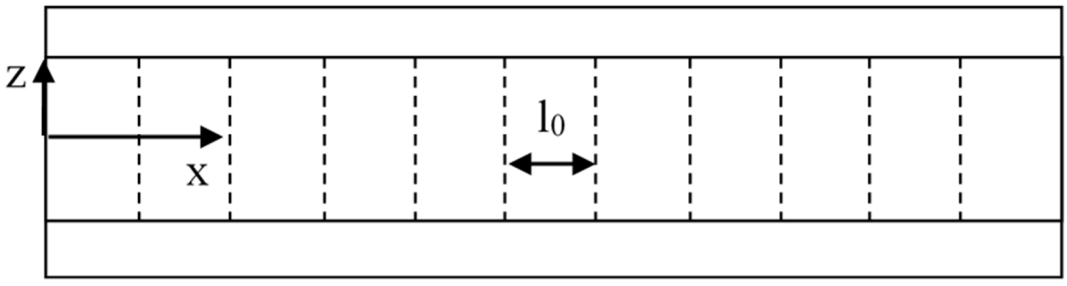

Figure A5 – Subdivision of the 90° layers in elements of length l_0.

With the aim to provide values of the distribution parameters for a unitary length element, let us consider l_0 = 1 mm.

By fitting the crack density data by means of Eq. (A2) it was possible to estimate the parameters ε_0 and *m* for the degassed and non degassed specimens (only cracks initiated before the onset of delamination were considered in the analysis). Once the parameters are calibrated for l_0 = 1 mm and a given ply thickness, if a different value of l_0 or a different ply thickness are used, the cumulative probability function must be corrected to account for the volume effect. Experimental data for each edge and the fitting curves according to Eq. (A2) are shown in Figure A6. Crack density data for the edges of the degassed specimens are fitted all together with a single curve, as they are representative of the void-free condition. For this specimens only two of four edges are reported in Figure A6 since in the other ones delamination occurred contemporary to the initiation of the first transverse cracks and therefore those data are not relevant for the present analysis.

The probability density functions f(ε), expressed in Eq. (A3), are plotted in Figure A7 for all the edges, using the values of m and ε_0 obtained by fitting the crack density curves.

$$f(\varepsilon) = \frac{m}{\varepsilon_0^m}\varepsilon^{m-1} \cdot \exp\left[-\left(\frac{\varepsilon}{\varepsilon_0}\right)^m\right] \tag{A3}$$

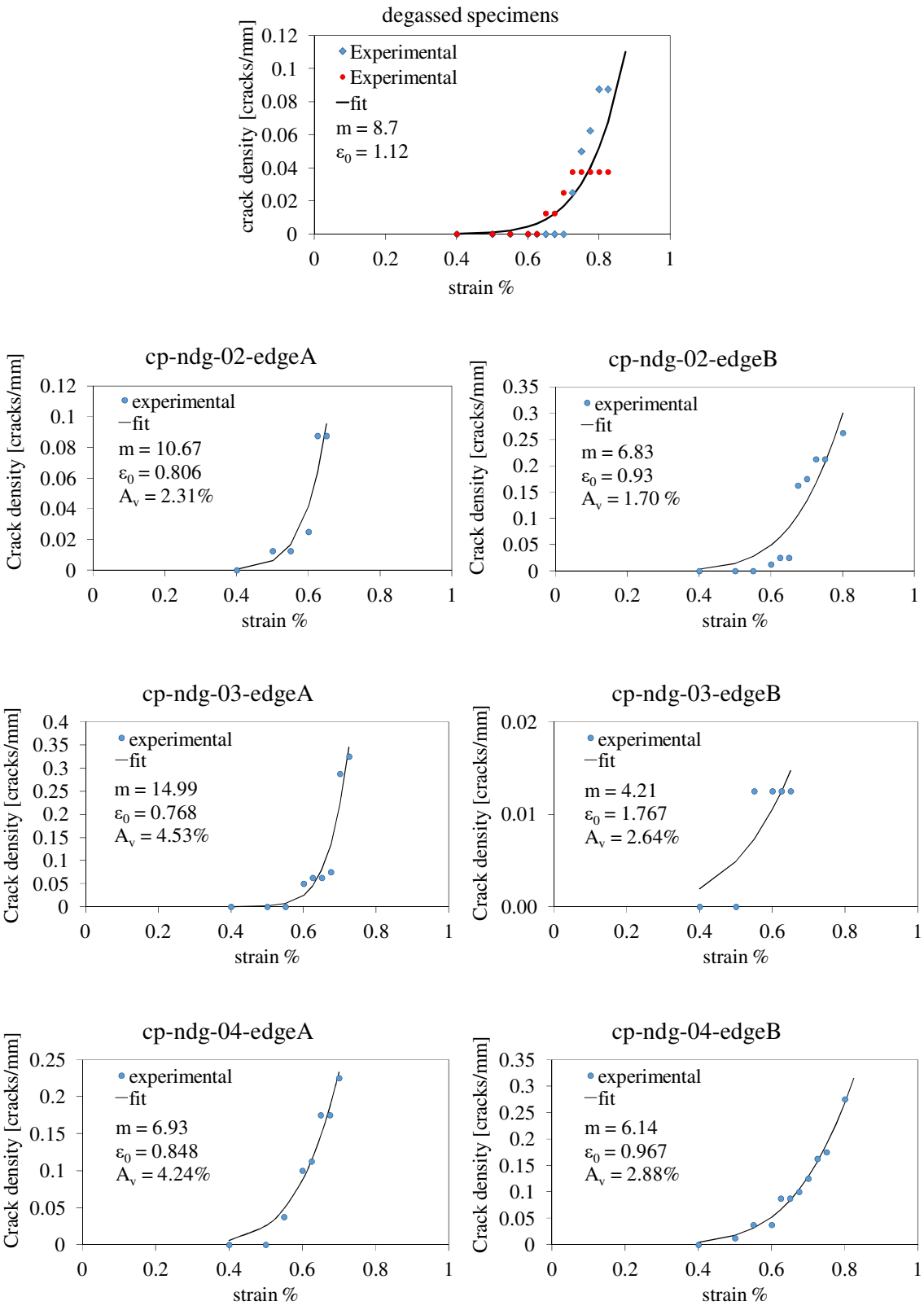

Figure A6 – Crack density evolution before delamination onset and fitting curves for every edge.

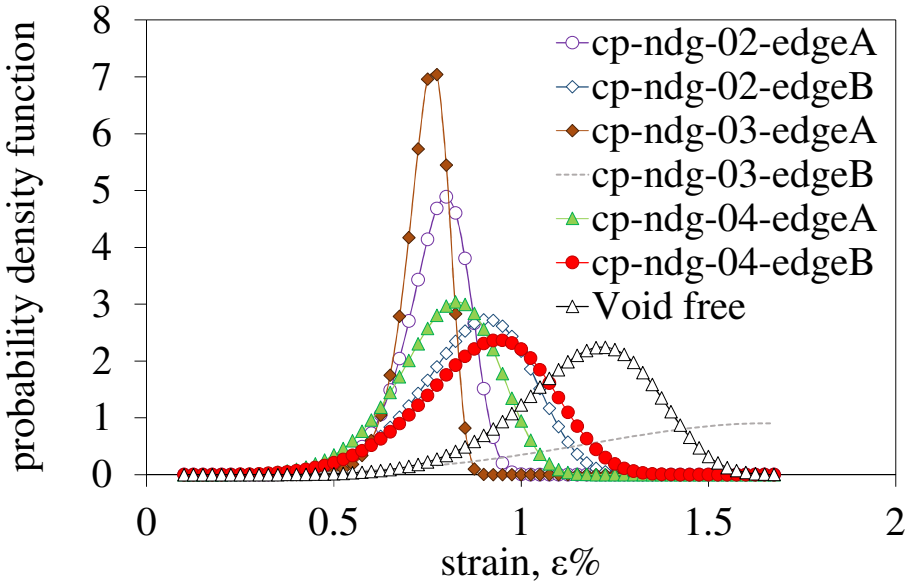

Figure A7 – Probability density function for strain to crack initiation.

The edge B of specimen cp-ndg-03, whose curve is dashed in Figure A7, shows a behaviour not in line with the other specimens. For this edge, however, very limited failure strain data were available, as can be seen in Figure A6. This is due to the fact that in that edge delaminations occurred very early thus affecting the initiation of further transverse cracks. This makes this data set not relevant for the analysis of transverse cracking, and therefore it will not be considered in further analyses in the paper.

As a first attempt to correlate the presence of voids to the statistical distribution of the critical strain to crack initiation, ε_0 and m were related to the void content (A_v) and the linear void density of the individual edges. These two parameters are referred to as "global", since they do not take into account the influence of single voids but just the global effect due to the presence of a certain amount of voids. The linear void density was defined as the ratio between the observed number of voids and the observation length (80 mm for each edge). In Figure A8 the scale and shape parameters are plotted against these two global

parameters. Clearly, no trend is appreciable concerning the influence of the void content on the shape parameter *m*. Conversely, the scale parameter ε_0 is, in general, lower for higher void contents, but it is hard to say that there is a clear and monotonically decreasing trend.

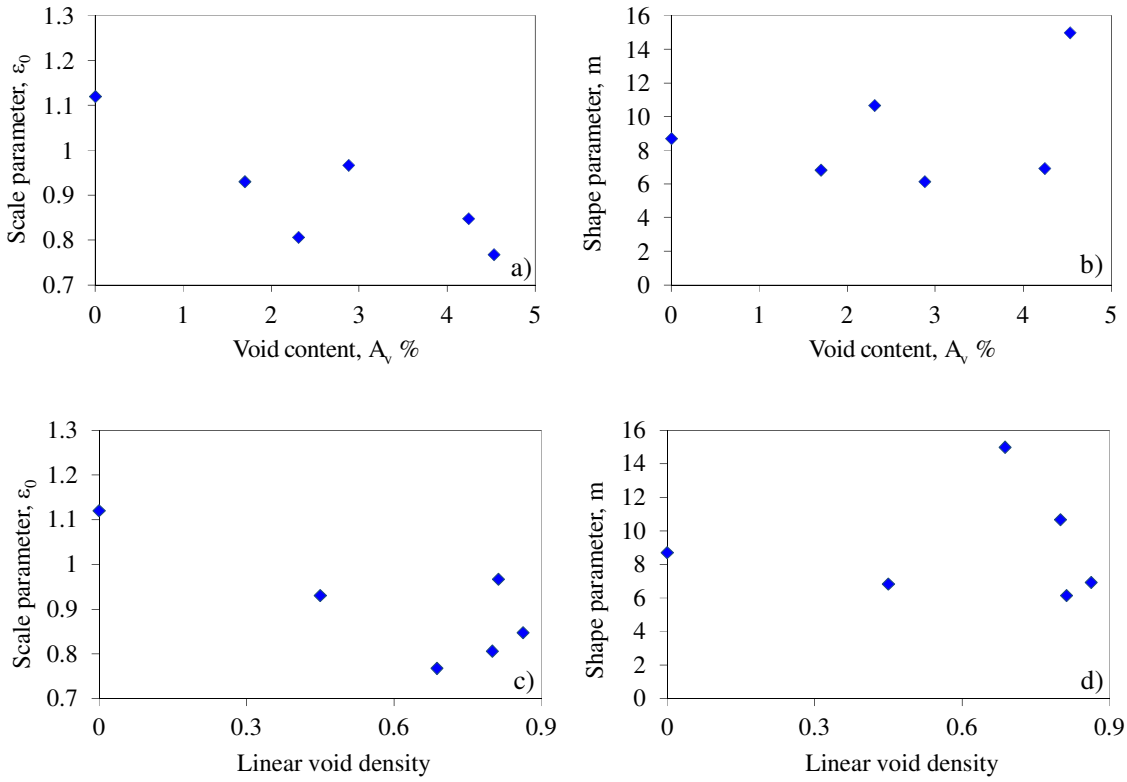

Figure A8 – Weibull scale and shape parameters as a function of void content and linear void density ("global" parameters).

A3.2 Analysis of crack initiation from voids

To better understand the influence of voids on the crack initiation strain and to clarify some discrepancies arisen after the global statistical analysis presented in the previous paragraph, a deeper investigation was carried out at the local level, taking into account some geometric features of the individual voids. In particular, three "local" parameters were considered: the area of the voids from which a crack initiated during the test, the corresponding section reduction of the 90° layer, and the strain concentration due to the actual shape of the voids.

These local parameters were then related to the macroscopic strain at which each crack initiated from single voids.

The void area and the section reduction are plotted against the crack initiation strain in Figure A9a) and b), respectively. No trend at all can be observed in both cases, highlighting that such parameters are not adequate to describe the influence of voids on crack initiation, for the cases analysed.

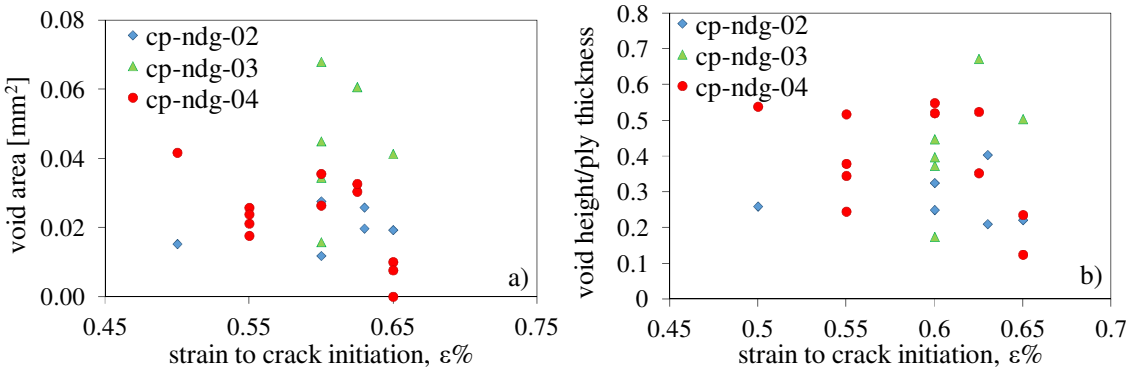

Figure A9 – a) Void area and b) section reduction due to the presence of void plotted against the strain to crack initiation.

A Matlab® code was then developed to extract, via image analysis, the geometry of each void and the surrounding plies from a micrographic image. The code automatically produces an ANSYS APDL file with the geometry to be used for a 2-D stress analysis with the Finite Element code ANSYS 14.0. In the FE analyses the plies were treated as homogeneous and orthotropic, a generalized plain strain condition was assumed and displacement boundary conditions were applied as schematically shown in Figure A10. Eight nodes plane element were used (PLANE 183 in the Ansys library) whose dimension was chosen, after a dedicated convergence analysis, to be about 1/35 of the 90° ply thickness.

As voids are located in the inter-tow regions, it is reasonable to assume that their shape is quite elongated in the fibres direction of the 90° ply. For this reason, a 2-D analysis could be appropriate, even if not exactly representative of the real geometry, mainly considering that this analysis is aimed to understand qualitatively which is the most critical feature of a void that leads to the initiation of a transverse crack.

An example of analysis is reported in Figure A11, where a micrograph and a void reconstruction are shown. The first principal strain field is also shown in the 90° ply, showing an excellent agreement between the crack initiation site and the peak point of the maximum principal strain.

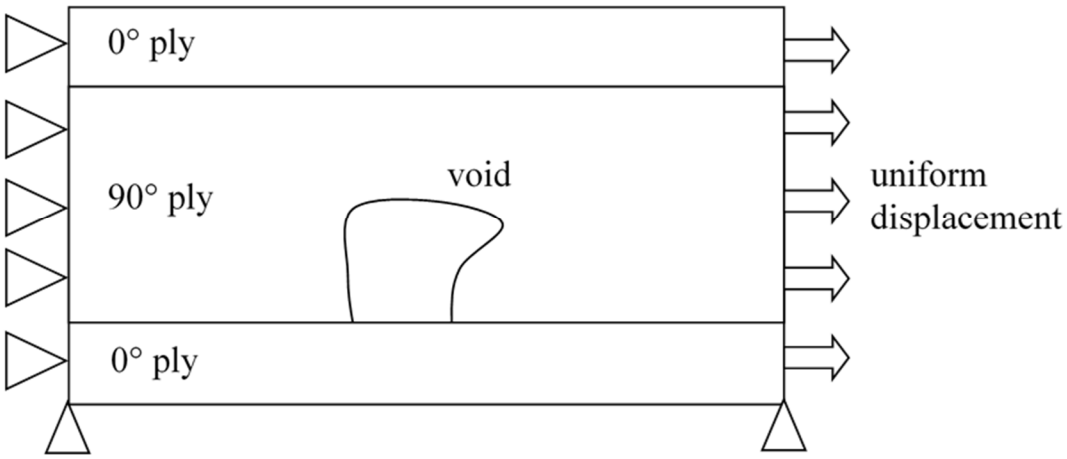

Figure A10 – Schematic of displacement boundary conditions for the FE analysis.

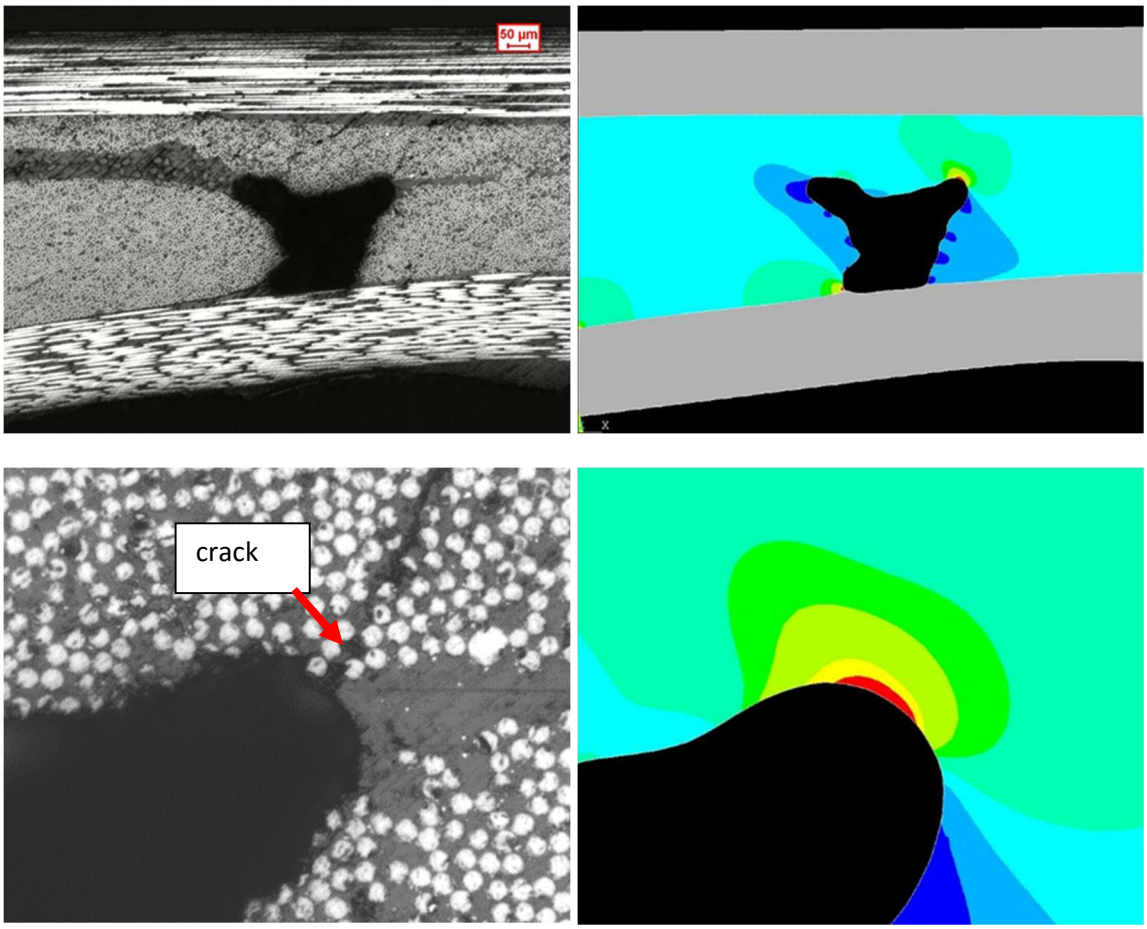

Figure A11 – Example of principal strain plot in a FE analysis carried out on the geometry extracted from a micrographic image.

The calculated strain concentration factors (ratio between the peak strain at the void and the global strain) for all the voids that lead to transverse cracks before the onset of delaminations are plotted in Figure A12 against the global strain to crack initiation. In spite of the considerable data scatter a clear decreasing trend can be observed. An analysis of variance (one-way ANOVA) confirmed that there is a statistically significant influence of the void shape (and the strain concentration it causes) on the global strain level at which cracking occurs, as shown in Table 1. The *null hypothesis*, that consists of assuming no influence of the strain concentration, is rejected as the F value is larger than the critical F value, calculated for a significance level $\alpha = 0.01$ (see Ref. [37] for detailed explanations

of the required calculations). This result means that in the presence of such irregularly shaped inter-tow defects the very local geometry of the voids and the surrounding plies, and the relevant strain concentration, are fundamental to be accounted for to predict the global strain or stress for crack initiation. This explains the results shown in Figures A8a) and c), where a global decreasing trend was highlighted for the scale parameter against the void content (even if some discrepancies were found). In fact, if the void content is higher there is a higher probability to find higher stress or strain concentrations, and this explains the globally degreasing trend. However, a global parameter such as the void content is not enough to describe the phenomenon in a detailed and completely reliable way, since the local shape of the voids has been found to play a fundamental role in the crack initiation phenomenon. Even if this conclusion has been drawn for the initiation of transverse cracks at the edges, the writer believes that it can be qualitatively extended for cracks initiating in other regions of a laminate.

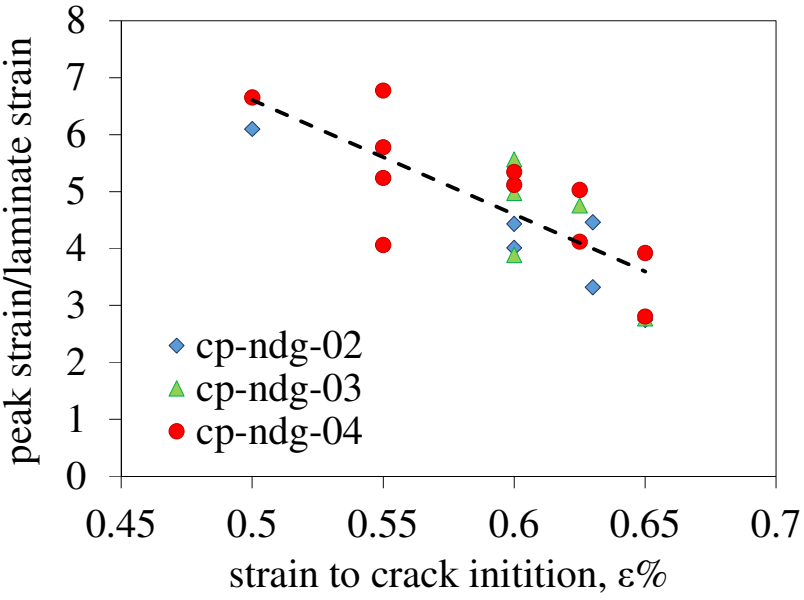

Figure A12 – Peak strain, normalised to laminate strain, plotted against the strain to crack initiation.

Table 1 – One-way ANOVA to assess the influence of the void geometry on the global strain level at which cracking occurred.

Source of variation	Sum of squares (SS)	Degrees of freedom	Mean square (MS)	F	Significance	Critical F ($\alpha = 0.01$)
Between groups	20.09	5	4.018	7.73	0.000595	4.34
Among groups	8.84	17	0.520			
Total	28.93	22				

A4. DCB tests

As mentioned in the introduction and shown in the previous paragraph, transverse cracking is followed by the onset and propagation of delamination. This phenomenon is controlled by the interlaminar fracture toughness, and the presence of voids can have a significant influence on this property.

To understand the effect of the manufacturing process on the mode I interlaminar fracture toughness, static DCB tests were carried out on degassed and non-degassed specimens with two different stacking sequences ($[(90/0)_3]_s$ and $[(\pm45)_3]_s$). This allowed us to analyze also the influence of the orientation of the interface layers (0° or -45°). Test specimens were cut from the infused panels according to the geometry shown in Figure A13.

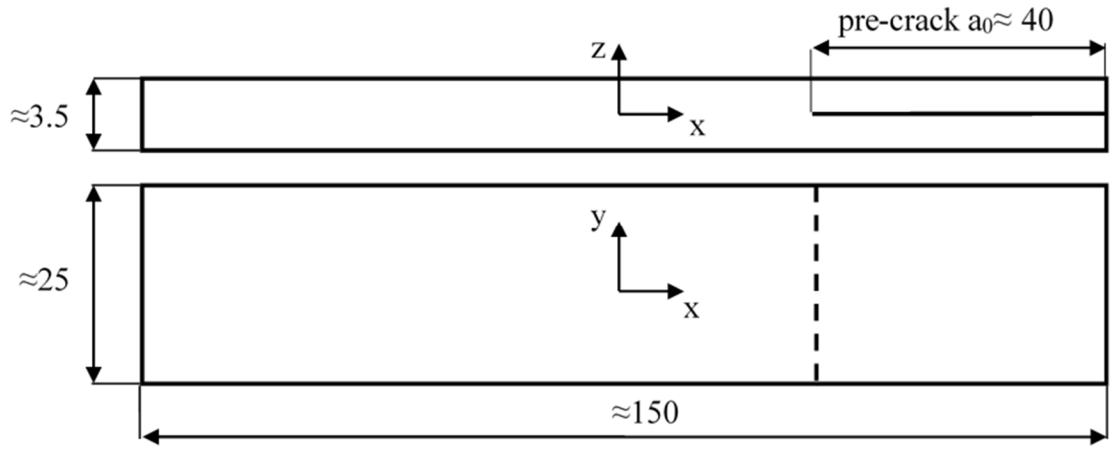

Figure A13 – Geometry of the DCB specimens (units in millimetres).

Tests were carried out with a MTS 858 MiniBionix hydraulic machine in displacement control with a crosshead rate of 2 mm/min. The crack length *a* was measured during the test with the aid of a travelling optical microscope (40x). The applied loads and displacements were recorded during the tests and the mode I Energy Release Rate (ERR), G_I, was calculated by means of the Compliance Calibration method as proposed in the ASTM recommendations [38].

A4.1 0° interface

The edges of the $[(90/0)_3]_s$ DCB specimens were polished and observed under an optical microscope, revealing the presence of voids only in the non-degassed ones, as can be seen in Figure A14 (average void area fraction: 1.9%). In addition to the inter-tow voids some very elongated voids can be observed in the 0° tows, as indicated by the zoom in Figure A14.

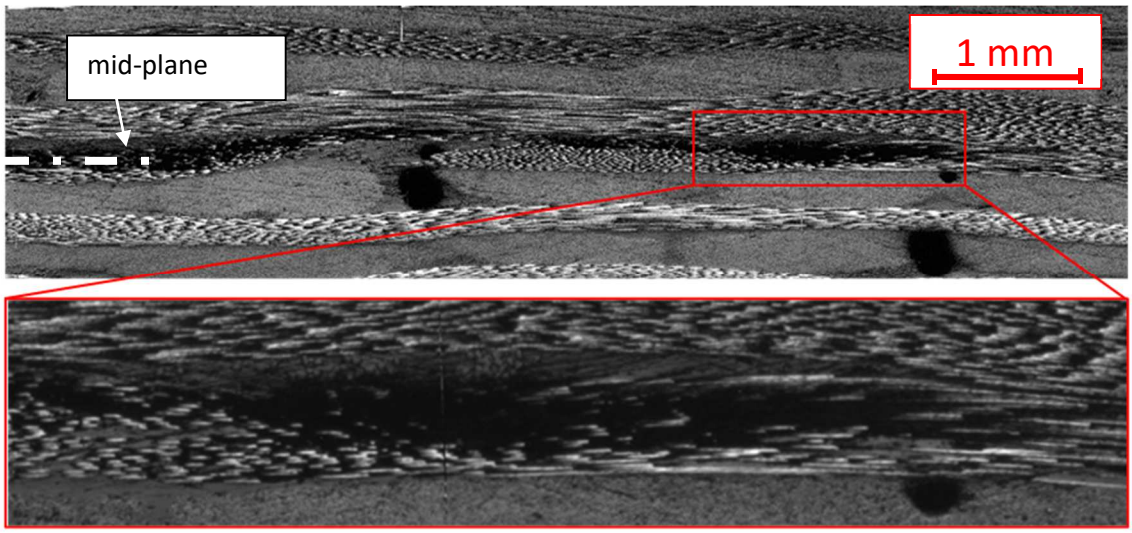

Figure A14 – Voids in a non degassed $[(90/0)_3]_s$ DCB specimen before tests.

The R-curves for the 0° interface specimens are shown in Figure A15. The specimens obtained with degassed and non-degassed resin are indicated, respectively, with the codes DCB-DG and DCB-NDG. The initiation values (for $a\text{-}a_0 = 0$) correspond to the values at which the crack is seen to start propagating from the pre-crack front. The curves exhibit the typical increasing trend in the first part and then a plateau for $a\text{-}a_0 > 10$ - 15 mm. It can be seen that, after the first part in which the curves for degassed and non-degassed specimens are overlapped, the specimens with voids exhibit a slightly higher value of the critical ERR for crack propagation. This beneficial effect of voids is in agreement with the results obtained by Asp and Brandt [5] and is actually due to the fact that the presence of voids gives rise to a more complicated crack path and a more diffused damage, so that a higher energy have to be supplied to make the crack propagate. In particular, in this case, the presence of voids led to a more diffused fibre bridging. In fact, as shown in Figure A16, secondary cracks initiated close to the elongated voids in the 0° plies then promoting the fibre bridging phenomenon as the main crack propagated and joined the void.

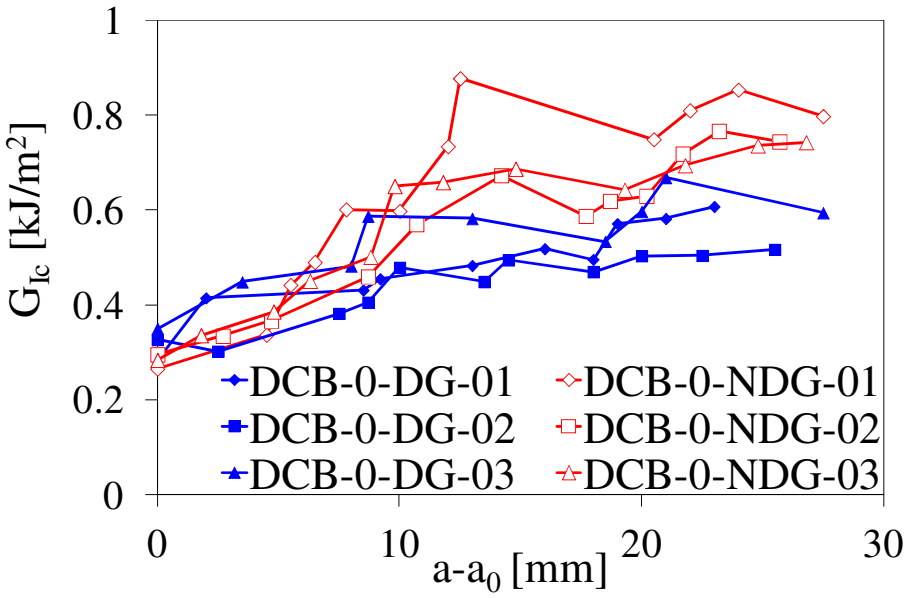

Figure A15 – R-curves for 0° interface DBC specimens.

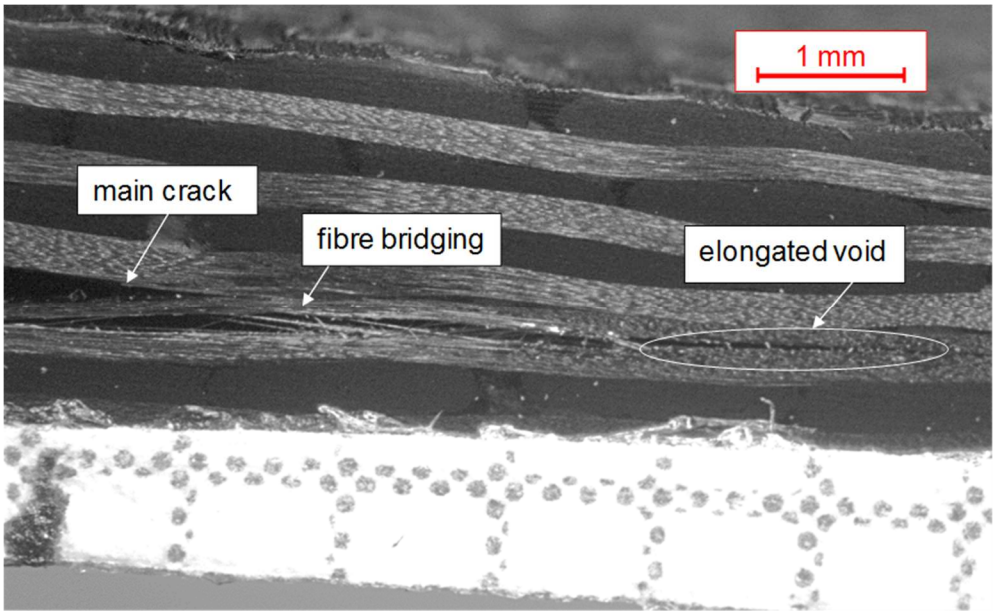

Figure A16 – Secondary cracks and consequent fibre bridging due to the presence of elongated voids.

A4.2 45° interface

Microscopy observation were carried out at the edges of the $[(\pm45)_3]_s$ specimens, revealing, again, the complete absence of voids in the degassed ones. Conversely, an average void area fraction of 1.23% was observed on the edges of the non-degassed specimens. Voids were uniformly distributed along the specimen length and positioned between the tows of the carbon fibre NCF, as shown in Figure A17.

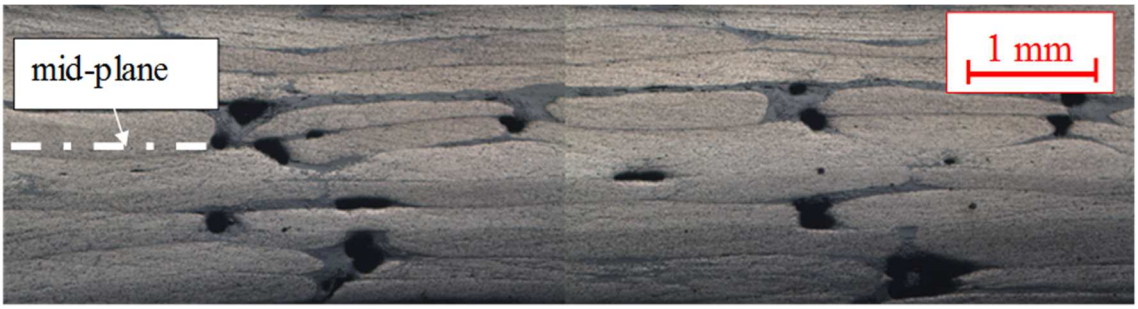

Figure A17 – Voids in a non degassed $[(\pm45)_3]_s$ DCB specimen before test.

The R-curves presenting the critical value of the mode I ERR, G_{Ic}, against the crack increment, are shown in Figure A18. In this case a slightly higher values of the critical ERR has been obtained for non degassed specimen both for crack initiation and propagation. In particular, voids produced deviations of the main crack path as well as secondary cracks initiating from the voids themselves, thus causing a more diffused ply-bridging phenomenon, as shown in Figure A19.

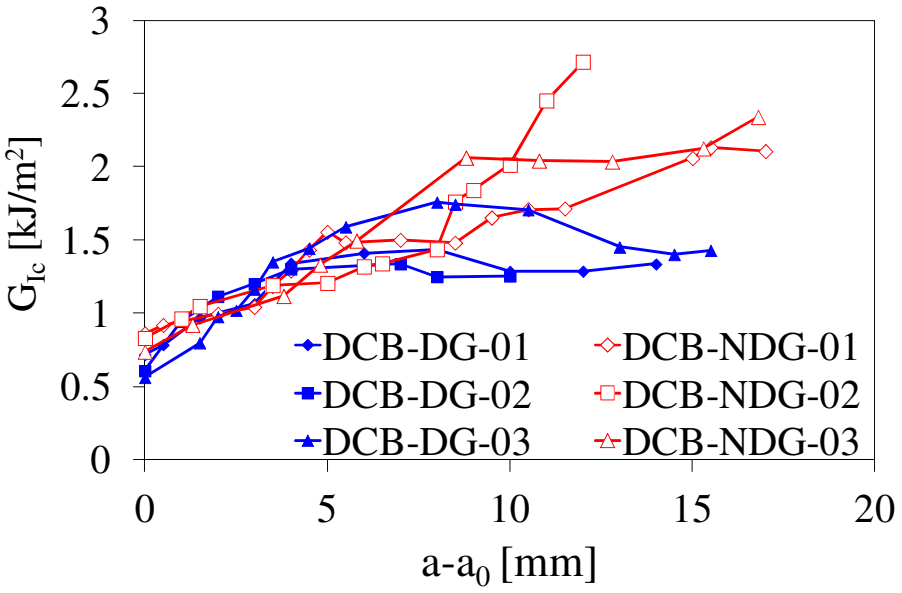

Figure A18 – R-curves for degassed and non-degassed $[(\pm 45)_3]_s$ DCB specimens.

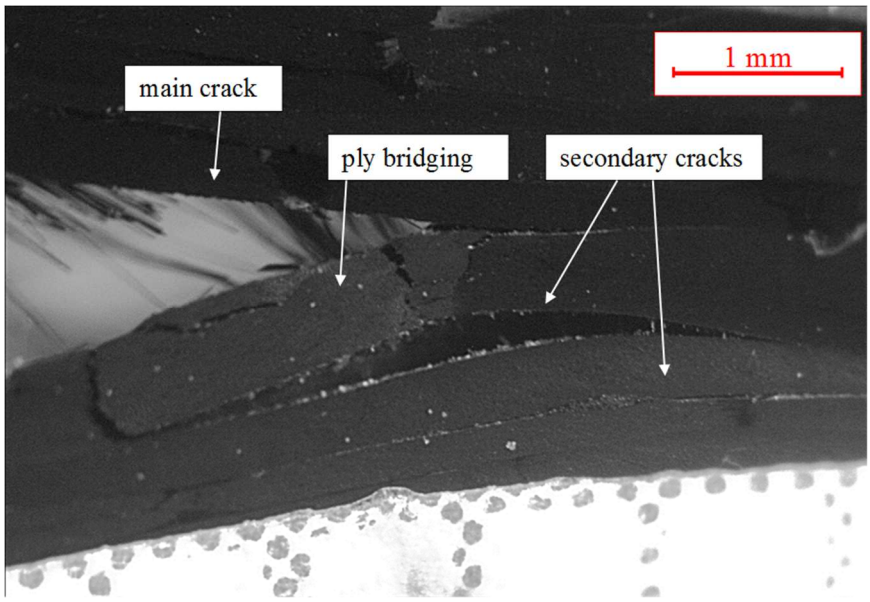

Figure A19 – Secondary crack and ply bridging due to the presence of voids.

A4.3 DCB fatigue tests

For the 0° interface specimens, fatigue tests were also carried out to understand the influence of voids on the Crack Growth Rate (CGR) under mode I loading.

Two void-free specimens and two specimens with 1.9% void area fraction were tested under displacement control with a frequency of 8 Hz and a load ratio (minimum to maximum load ratio) of 0.1. Crack growth data were analysed according to the IPM procedure suggested in the recommendation ASTM E647-00 [39] and presented in Figure A20. The CGR is here plotted against the maximum cyclic value of G_I. Typical S-shaped curves are obtained, and no appreciable difference can be noticed between the degassed and non degassed specimens. The threshold condition is reached for $G_{I,max}$ equal to about 0.08 kJ/m^2, while a rapid increase in the CGR occurs for maximum ERR values around 0.3 kJ/m^2, in good agreement with the static initiation value.

Concerning fatigue loading, the comparable behaviour of specimens with and without voids is consistent with the fact that secondary cracks and fibre bridging were not observed during the tests, as instead happened under static loading.

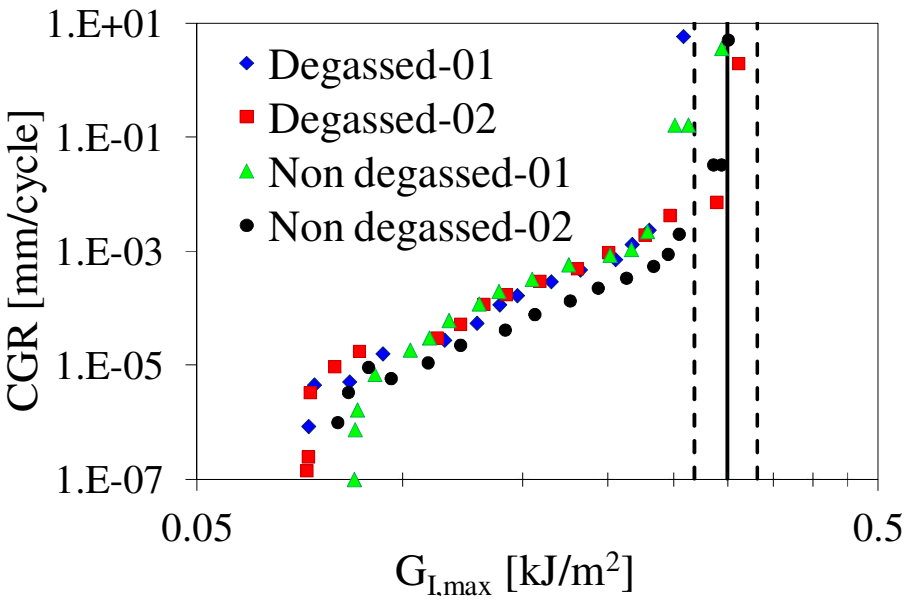

Figure A20 – Paris-like curves for degassed and non degassed DCB specimens.

A5. Conclusions

Infused laminates were produced by a carbon fibre NCF and epoxy matrix adopting two different processes: in the first one the matrix was completely degassed before infusion and a long bleeding time was adopted to optimise the pre-form filling; in the second one the matrix was not degassed and a minimum bleeding time was adopted. The last process led to savings in time and resin waste, but caused the diffuse presence of voids, mainly between the tows of the NCF. Experimental tests were carried out to characterise the influence of voids on some intra- and inter-laminar properties, focusing on the observation of damage mechanisms and their dependence on the presence of voids.

The following main conclusions can be drawn:

- the strain to the initiation of the first transverse crack at the edges and the first delamination, as well as the edge crack density evolution in cross-ply laminates, were found to be detrimentally affected by the presence of voids;
- the statistical distribution of the strain to crack initiation depends on the global void content, but a clear monotonic trend was not observed;
- the very local shape of the voids, and the related strain concentration, are fundamental parameters to describe the influence of such voids on the strain to crack initiation;
- in the cases analysed, the critical value of G_{Ic} for interlaminar crack propagation was slightly higher in the specimens containing voids. In fact, while voids lying on the interface at which crack is propagating are expected to facilitate its propagation, voids away from it are source of more complicated crack paths and more pronounced fibre or ply bridging increasing the apparent fracture toughness.

References of Appendix A

[1] Rohatgi V, Patel N, Lee LJ. Experimental Investigation of Flow-Induced Microvoids During Impregnation of Unidirectional Stitched Fiberglass Mat. Polymer Composites 1996; 17: 161-170.

[2] Kang MK, Lee WI, Hahn KT. Formation of microvoids during resin-transfer molding process. Composites Science and Technology 2000; 60: 2427-2434.

[3] Kuentzer N, Simacek P, Advani SG, Walsh S. Correlation of void distribution to VARTM manufacturing techniques. Composites Part A – Applied Science and Manufacturing 2007; 38: 802-813.

[4] Kedari VR, Farah BI, Hsiao KT. Effects of vacuum pressure, inlet pressure and mold temperature on the void content, volume fraction of polyester/e-glass fiber composites manufactured with VARTM process. Journal of Composite Materials 2011; 45: 2727-2742.

[5] Asp LE, Brandt F. Effects of pores and voids on the interlaminar delamination toughness of a carbon/epoxy composite. In: Proceedings of ICCM11 Conference, Gold Coast, July, 1997.

[6] Olivier PA, Mascaro B, Margueres P, Collombet F. CFRP with voids: ultrasonic characterization of localized porosity, acceptance criteria and mechanical characteristics. In: Proceedings of ICCM16 Conference, Kyoto, July, 2007.

[7] Yoshida H, Ogasa T, Hayashi R. Statistical Approach to the Relationship between ILSS and Void Content of CFRP. Composites Science and Technology 1986; 25: 3-18.

[8] Tang JM, I. Lee WI, Springer GS. Effects of Cure Pressure on Resin Flow, Voids, and Mechanical Properties. Journal of Comopsite Materials 1987; 21: 421-440.

[9] Olivier P, Cottu JP, Ferret B. Effects of cure cycle pressure and voids on some mechanical properties of carbon/epoxy laminates. Composites 1995; 26: 509-515.

[10] Thomason JL. The interface region in glass fibre-reinforced epoxy resin composites: 1. Sample preparation, void content and interfacial strength. Composites, 1995; 26: 467-475.

[11] Wisnom MR, Reynolds T, Gwilliam N. Reduction in interlaminar shear strength by discrete and distributed voids. Composites Science and Technology 1996; 56: 93-101.

[12] Goodwin AA, Howe CA, Paton RJ. The Role of Voids in Reducing the Interlaminar Shear Strength of RTM Laminates. In .Proceedings of ICCM11 Conference , Gold Coast, July, 1997.

[13] Costa ML, de Almeida SFM, Rezende MC. The influence of porosity on the interlaminar shear strength of carbon-epoxy and carbon-bismaleimide fabric laminates. Composites Science and Technology 2001; 61: 2101-2108.

[14] Bureau MN, Denault J. Fatigue resistance of continuous glass fiber-polypropylene composites consolidation dependence. Composites Science and Technology 2004; 64: 1785-1794.

[15] Liu L, Zhang BM, Wang DF, Wu ZJ. Effects of cure cycles on void content and mechanical properties of composite laminates. Composite Structures 2006; 73: 303-309.

[16] Zhu H, Li D, Zhang D, Wu B, Chen Y. Influence of voids on interlaminar shear strength of carbon/epoxy laminates. Transactions of Nonferrous Metals Society of China 2009; 19: 470-475.

[17] Varna J, Joffe R, Berglund A, Lundstrom TS. Effect of voids on failure mechanisms in RTM laminates. Composites Science and Technology 1995; 53: 241-249.

[18] Zhu H, Wu B, Li D, Zhang D, Chen Y. Influence of Voids on the Tensile Performance of Carbon/epoxy Fabric Laminates. Journal of Materials Science and Technology. 2011; 27: 69-73.

[19] Huang Y, Varna J, Talreja R. Statistical methodology for assessing manufacturing quality related to transverse cracking in cross-ply laminates. Composites Science and Technology 2014; 95: 100-106.

[20] Suarez JC, Molleda F, Guemesv A. Void content in carbon fiber/epoxy resin composites and its effects on compressive properties. In: Proceedings of ICCM9 Conference, Madrid, July, 1993.

[21] Cinquin J, Triquenaux V, Rouesne Y. Porosity influence on organic composite material mechanical properties. In: Proceedings of ICCM16, Kyoto, July, 2007.

[22] Chambers AR, Earl JS, Squires CA, Suhot MA. The effect of voids on the flexural fatigue performance of unidirectional carbon fibre composites developed for wind turbine applications. International Journal of Fatigue, 2006; 28: 1389-1398.

[23] de Almeida SFM, Neto ZSN. Effect of void content on the strength of composite laminates. Composite Structures 1994; 28: 139-148.

[24] Hagstrand PO, Bonjour F, Manson JAE. The influence of void content on the structural flexural performance of unidirectional glass fibre reinforced polypropylene composites. Composites Part A – Applied Science and Manufacturing 2005; 36: 705-714.

[25] Dill CW, Tipton SM, Glaessge EH, Branscum KD: 'Fatigue strength reduction imposed by porosity in a fiberglass composite', in 'Damage Detection in Composite Materials', Issue 1128, (ed. by J. E. Masters), 152-162; 1992, Philadelphia, ASTM International.

[26] Schmidt F, Rheinfurth M, Horst P, Busse G. Multiaxial fatigue behaviour of GFRP with evenly distributed or accumulated voids monitored by various NDT methodologies. International Journal of Fatigue, 2012; 43: 207-216.

[27] Gehrig F, Mannov E, Schulte K. Degradation of NCF-epoxy composites containing voids. In: Proceedings of ICCM17 Conference, Edinburgh, July, 2009.

[28] Suhot MA, Chambers AR. The effect of voids on the flexural fatigue performance of unidirectional carbon fibre composites. In: Proceedings of ICCM16 Conference, Kyoto, July, 2007.

[29] Lambert J, Chambers AR, Sinclair I, Spearing SM. 3D damage characterization and the role of voids in the fatigue of wind turbine blade materials. Composites Science and Technology 2012; 72: 337-343.

[30] Seon G, Makeev A, Nikishkov Y, E. Lee E. Effects of defects on interlaminar tensile fatigue behavior of carbon/epoxy composites. Composites Science and Technology 2013; 89: 194-201.

[31] Sisodia SM, Gamstedt EK, Edgren F, Varna J. Effects of voids on quasi-static and tension fatigue behaviour of carbon-fibre composite laminates. Journal of Composite Materials 2015; 49: 2137-2148.

[32] McMillan AJ. Material strength knock-down resulting from multiple randomly positioned voids. Journal of Reinforced Plastics and Composites 2012; 32: 13-28.

[33] Huang H, Talreja R. Effects of void geometry on elastic properties of unidirectional fiber reinforced composites. Composites Science and Technology 2005; 65: 1964-1981.

[34] Van Den Broucke B, Hegemann J, R. Das R, R. Oster R, K. Hackl K, R. Stößel R. Modelling of textile composites using finite element tools and investigation of the influence of porosity on mechanical properties. In: Proceedings of Symposium

'Finite Element Modelling of Textiles and Textile Composites', St Petersburg, September, 2007.

[35] Ricotta M, Quaresimin M, Talreja R. Mode I Strain Energy Release Rate in composite laminates in the presence of voids. Composites Science and Technology 2008; 68: 2616-2623.

[36] Quaresimin M, Carraro PA, Mikkelsen LP, Lucato N, Vivian L, Brøndsted P, Sørensen BF, Varna J, Talreja R. Damage evolution under internal and external multiaxial cyclic stress state: a comparative analysis between glass/epoxy laminates and tubes. Composites Part B – Engineering 2014; 61: 282–290.

[37] Montgomery DC. Design and Analysis of Experiments, 8th edn, 2012, John Wiley & Sons, Inc.

[38] Standard test method for mode I interlaminar fracture toughness of unidirectional fiber-reinforced polymer matrix composites, ASTMD 5528-01.

[39] Standard Test method for measurement of fatigue crack growth rates, ASTM E647-00.

Appendix B

Prediction of transverse crack initiation in unidirectional plies by means of a percolation concept

Abstract

In this Appendix, a novel approach to predict transverse cracks in a composite ply is proposed. By carrying out Finite Element Analyses on Representative Volume Elements, a transverse crack is predicted to initiate when the applied strain is sufficient to induce local failure at the fibre-matrix interface in a certain percentage of fibres (percolation threshold), neglecting the actual damage initiation and propagation along the thickness of the ply. The influence of temperature gradient, fibre volume fraction and fibre material on the percolation threshold is analysed, and the applicability of the model to different systems is discussed. The present study was carried out in collaboration with Texas A&M University.

B1. Introduction

The need for lighter structures to reduce fuel consumption, greenhouse gas emissions, and increase green energy production lead in the last decades to an exponential growth in the use of composite materials in fields such as aerospace, automotive and wind power.

Despite their wide use, the knowledge of the mechanical behaviour of such materials under general loading conditions is not complete yet. Composites are indeed characterised by a more complex damage scenario compared to traditional materials. In a composite laminate

subjected to a static tensile load, the first visible damage event consists of the initiation of multiple cracks in the plies with the least favourable fibre orientation in comparison with the loading directions. As these cracks propagate in the fibres direction, new cracks initiate, until a saturation condition is reached. From this point on, the main damage mechanism consists on delamination initiation and growth, followed by fibre breakage in the most favourably oriented plies, which finally leads to the separation of the laminate.

The process of crack multiplication and growth causes a decrease in the stiffness of a laminate. Also, it influences the following damage evolution leading to the final failure of the laminate. For design purposes, it is therefore essential to predict the occurrence of such cracks. Models like the ones proposed by Hashin [1], Tsai and Hill [2], Tsai-Wu [3] and Puck [4] can be used to predict crack formation once the strength of the material is known. Therefore, experimental tests on the material of interest are needed to find such properties. In this sense, it would be convenient to predict the strength of a composite ply from the properties of the constituents and the microstructure. Several models were proposed in this direction, mostly based on non-linear Finite Element (FE) analyses of models in which fibre and matrix are separately modelled [5-8]. Such simulations, however, require a relatively large computational effort and the mechanical properties of the fibre-matrix interface as an input. A simplified model that overcomes these issues, offering nonetheless interesting insights on the crack formation process, may then be useful.

In 1996, Asp and co-authors [9] proposed a model to predict the strain to transverse crack initiation in unidirectional plies, based on the dilatational energy density in the matrix at the fibre-matrix interface, obtaining good predictions of experimental data for different fibre volume fractions. In their work, the dilatational energy density was calculated by means of linear elastic FE analyses on a unit cell. Clearly, by assuming a regular fibre

distribution, according to that model a crack involving the whole thickness of a ply would form as soon as damage is induced in a unit cell.

The present Appendix aims at developing a model, based on Asp and co-author's failure criterion [9], to analyse more in depth the crack formation process from the first local damage initiation in real composite plies, characterised by an irregular fibre distribution.

B2. Model development

The fundamental idea at the basis of the present model is the application of the percolation concept to the transverse crack initiation process. The formation of a crack is assumed to form through a series of independent local damage initiation along the thickness of the composite ply. This means that both the propagation of the local damage and the stress redistribution due to them are neglected, keeping the analysis extremely simple. The local damages occur in the form of fibre-matrix debonding, driven by the local value of the dilatational energy density, as proposed by Asp and co-authors [9]. In Figure B.1 are reported experimental evidences showing that in the process of crack formation local debondings often appear not to be interconnected, thus supporting the proposed concept.

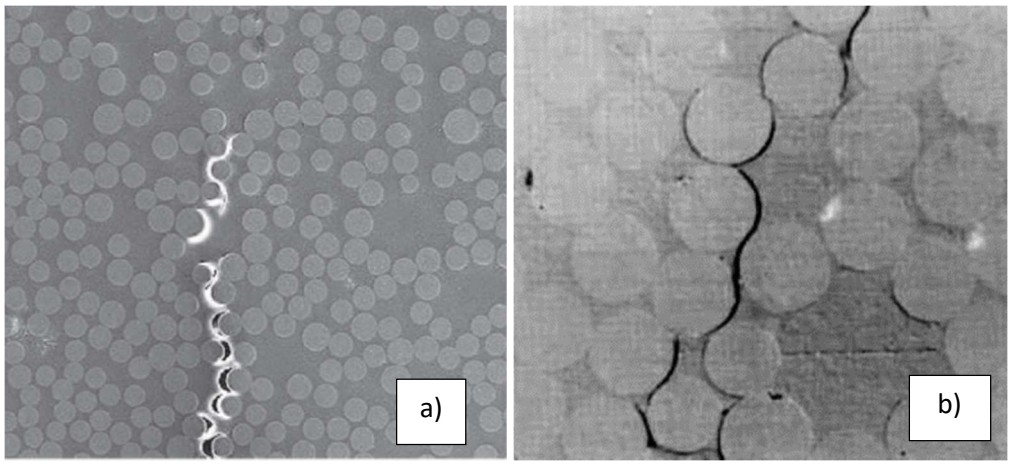

Figure B.1 – Experimental evidences showing non-interconnected local damage in the crack formation process, adapted from a) Ref. [5] and b) Ref. [10].

The stress state at the fibre-matrix interfaces must be calculated by Finite Element analyses on Representative Volume Elements of the composite ply. The same procedure developed in Chapter 5 was used to build RVEs. Since a crack form along the thickness of the ply, the stress analysis is focussed on a vertical strip of material (see also Chapter 6). In contrast with the procedure proposed in Chapter 5, the material outside a central strip was homogeneised, and transverse displacement was applied directly on the sides of the RVE. A dedicated study showed that the stresses at the fibre-matrix interface are influenced for the largest part from the location of the neighbouring fibres within a circle of diameter around three times the diameter of the fibre. Therefore, fibre and matrix were separately modelled in a region having a width of 8 times the fibre diameter, and the stress analysis is restricted to a central strip that was 2 fibre diameters wide to ensure negligible stress perturbations from the border with the homogeneised material (Figure B.2). Local failure at the fibre-matrix interface was assumed to occur when the dilatational energy density in the matrix is larger than 0.2 MPa, as suggested for epoxy resins in [11].

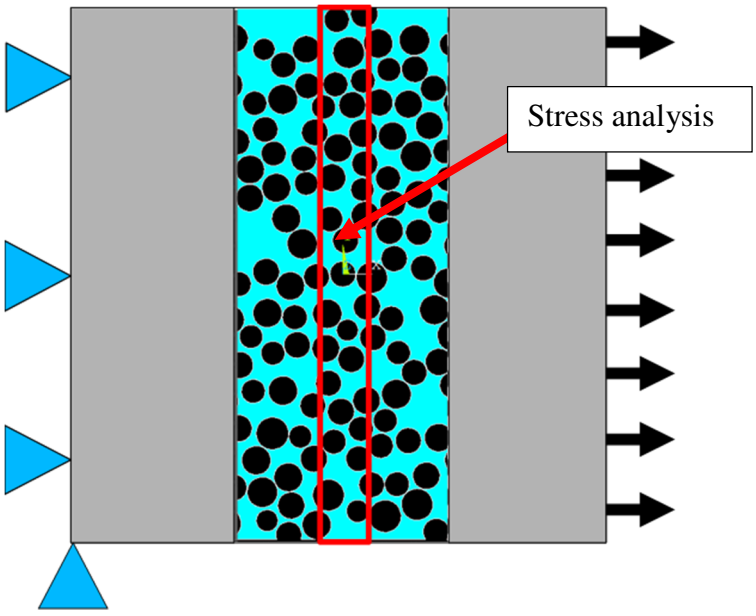

Figure B.2 – Example of RVE used in the analysis.

By neglecting the propagation phase and the stress redistributions due to the initiation of local damages, it is sufficient to carry out a single linear elastic FE analysis on a RVE. From this analysis it is indeed possible to calculate, for each fibre, the strain to be applied to the material to initiate damage at its fibre-matrix interface. A crack involving the whole ply thickness will form when a strain is applied to the material high enough to induce local damage in a sufficiently large percentage of fibres in a vertical strip of material. In Figure B.3 it is shown an example of the increase in *locally debonded fibres* with higher applied transverse strain.

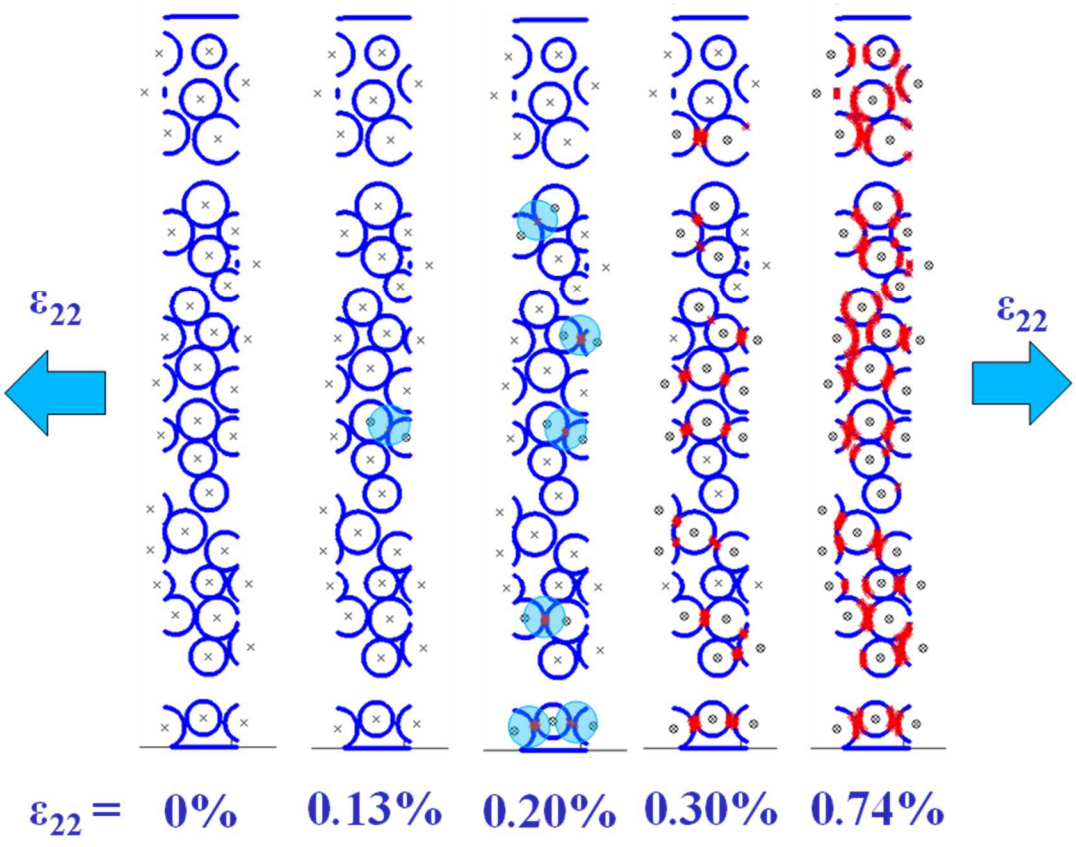

Figure B.3 – Example of the increase in fibres having local debonding (red spots) as a function of the transverse strain.

Once the trend of *locally debonded fibres* against the applied transverse strain is known, a percolation threshold must be defined, corresponding to a certain percentage of lo*cally debonded fibres* along a strip of material. The strain that leads to reaching such a defined percolation threshold will be the strain to transverse crack initiation.

Since the trend of locally debonded fibres against the transverse strain depends on temperature gradient, fibre volume fraction and fibre type (as shown in the following paragraphs), and the present model need to be validated against experimental data, let us refer to a work by de Kok and Meijer [12]. In that work, the authors carried out transverse tensile tests on unidirectional glass/epoxy plies containing different fibre volume fractions. The laminates were cured for 4 hours at 80°C. By assuming a ΔT of 60 K, the trend of locally debonded fibres against the transverse strain for different fibre volume fractions can be calculated (Figure B.4). The material properties used in the FE analyses are reported in Table B.1.

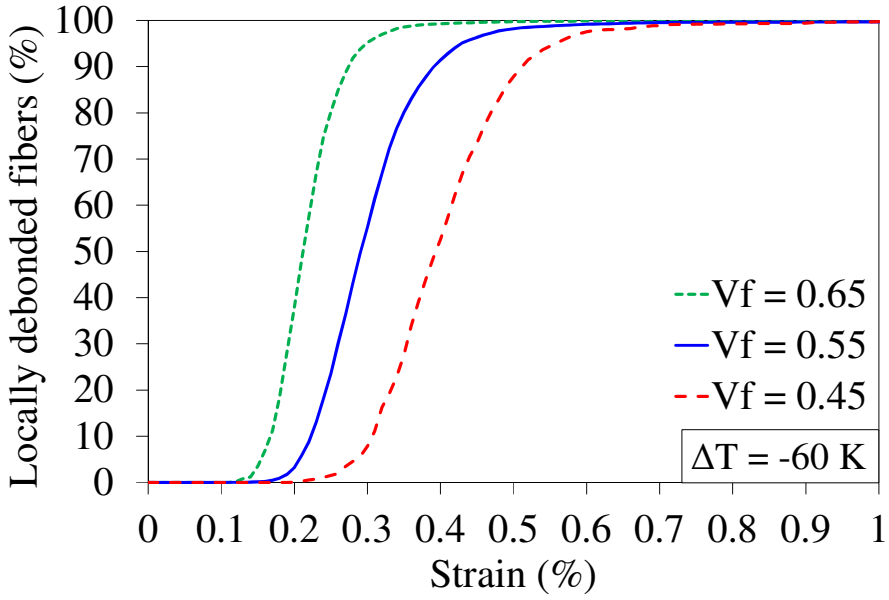

Figure B.4 – Trend of locally debonded fibres against the transverse strain for the material produced in Ref. [12].

Table B.1 – Material properties used in the FE analyses of a glass/epoxy system.

Material	Young's modulus (GPa)	Poisson's ratio	CTE
Epoxy resin	3.1	0.38	$6.75 \cdot 10^{-5}$
Glass fibre	74	0.25	$7 \cdot 10^{-6}$

From the curves in Figure B.4, it is possible to define as percolation threshold the presence of 80-90% of *locally debonded fibres* in a vertical strip of material, where the trends clearly change their slope. This slope change appears to be more evident and to occur at higher percentages of *locally debonded fibres* for higher fibre volume fractions, as will be more discussed in the next paragraph. The strains needed to reach such percolation thresholds are compared to the experimental data of Ref. [12] in Figure B.5, where a satisfactory agreement can be observed. In particular, although reasonably good predictions are made if a constant percolation threshold of 85% is taken for all the fibre volume fractions, to take into account a variation in the percolation threshold as a function of the fibre volume fraction, as highlighted in Figure B.4, appears to lead to a better agreement with the experimental data.

An interesting comparison can be made with the prediction of damage initiation made in Ref. [9] with the use of a unit cell (Figure B.6). It is possible to observe that the first local damage occurs at lower strains in RVEs, as expected given the dependence of the stress concentrations in the matrix on the fibre orientation and fibre distances. At the same time, the strain needed to reach a percolation threshold (~85%) is in line with the strain needed to induce damage in a square or hexagonal unit cell, implying that the stress state at fibre-matrix interface of the late-debonded fibres is comparable to the one of a unit cell. A diagonal-square unit cell predicts larger strains to transverse crack initiation because fibres

are not aligned in the loading direction, thus generating smaller stress concentrations in the matrix.

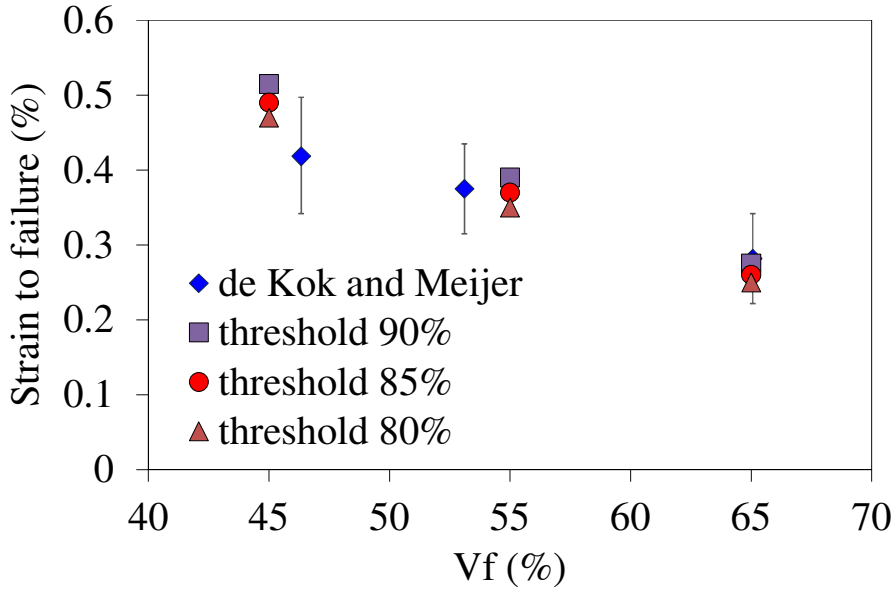

Figure B.5 – Comparison between predicted and experimental strain to transverse crack initiation.

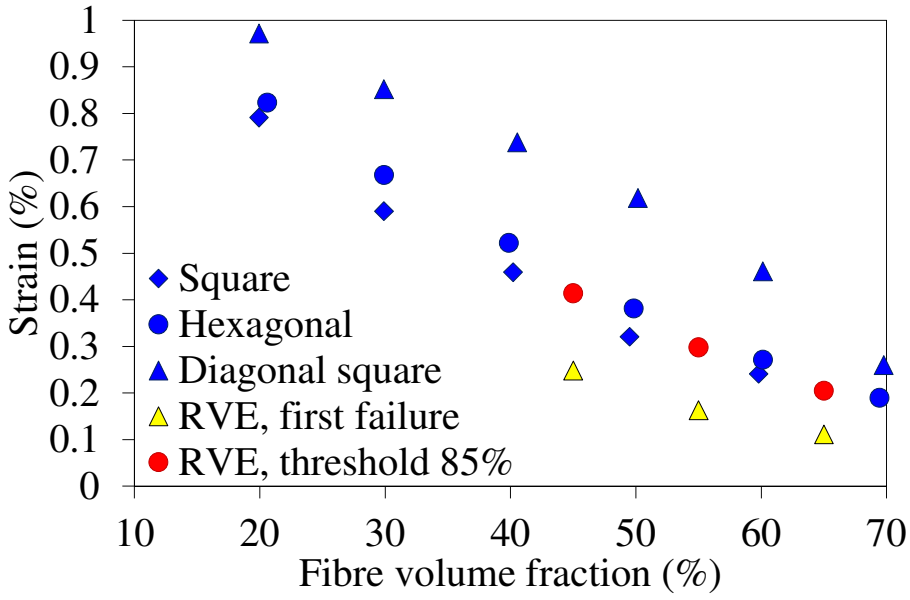

Figure B.6 – Comparison between strains to transverse crack initiation predicted with the present percolation concept and with the analysis of a unit cell [9].

Thanks to the easiness of application of the proposed model, it is extremely simple to study the influence of different parameters on the crack formation process. In particular, the effect of the cooling down, fibre volume fraction and fibre material were investigated, as reported in the following paragraphs.

B3. Influence of cooling down

To analyse the influence of cooling down, a glass/epoxy system having a fibre volume fraction of 55% was chosen. As shown later on, the effect of ΔT is qualitatively the same for the other analysed materials. The trend of locally debonded fibres against the applied strain in the presence of different ΔT is reported in Figure B.7. Since the influence of the temperature gradient was found to be complex, the figure was split in two.

To explain such a complex trend, it is necessary to analyse the influence of ΔT on local stresses. In Figure B.8 the hydrostatic stress, directly related to the dilatational energy density, is shown in the same region of a RVE subjected to a transverse strain of 1% (Figure B.8a) and a cooling down of -1 K (Figure B.8b). In the presence of pure transverse strain, the most critical locations are the inter-fibre regions between very close fibres aligned along the loading direction, while inter-fibre regions between close fibres perpendicular to the loading direction tend to be in compression. A negative temperature gradient instead causes inter-fibre regions between close fibres to be in compression regardless of their orientation; at the same time, higher stresses rise in regions that were not critical under pure transverse strain. Consequently, a cooling down reduces the stress concentration in the locations that under pure transverse strain are the most critical. At the same time, the criticality of other (formerly less critical) locations increase. This explains the trends in Figure B.7a: As ΔT increases (in absolute value), the first damages initiate later, but the trend of *locally*

debonded fibres against the applied strain is steeper due to a general increase in the hydrostatic stress in the matrix.

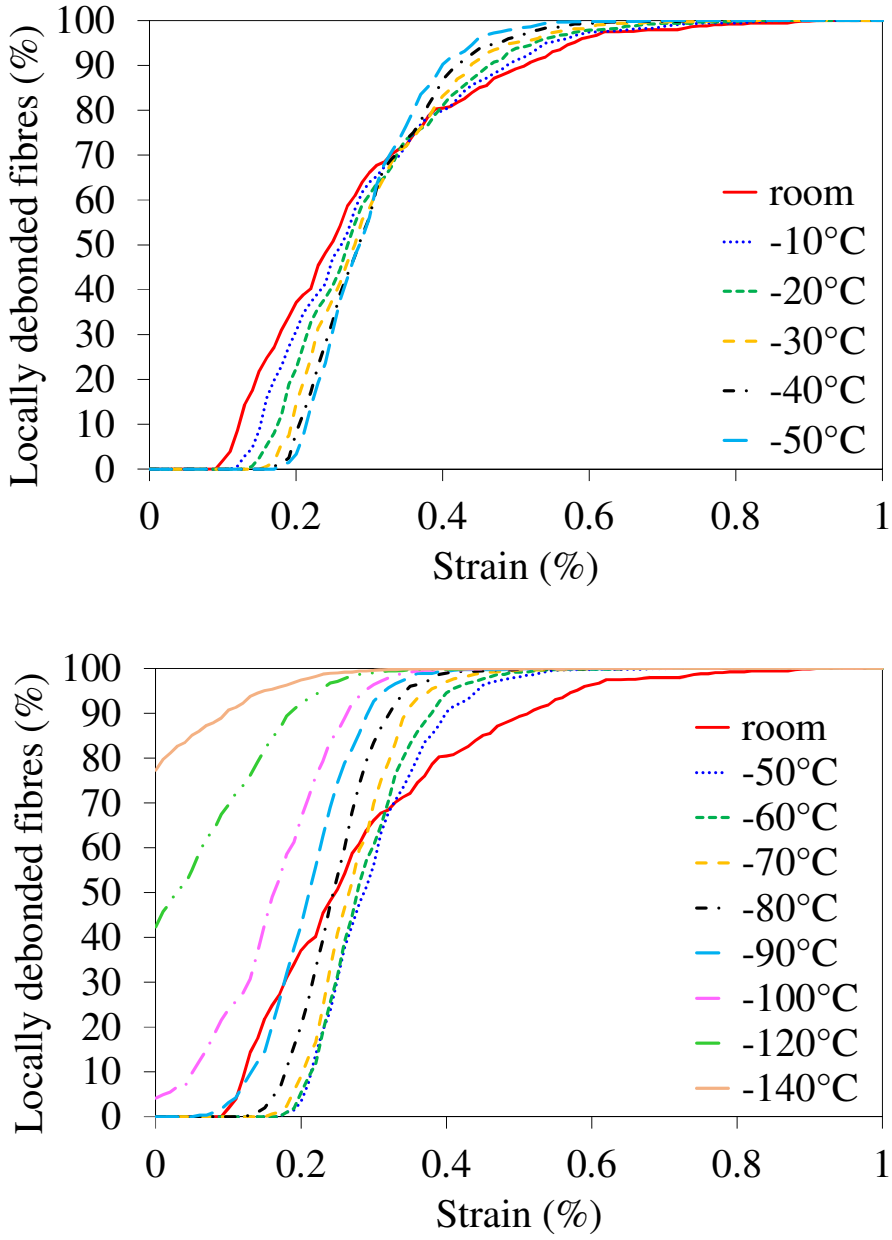

Figure B.7 – Locally debonded fibres as a function of the applied strain in the presence of different temperature gradients.

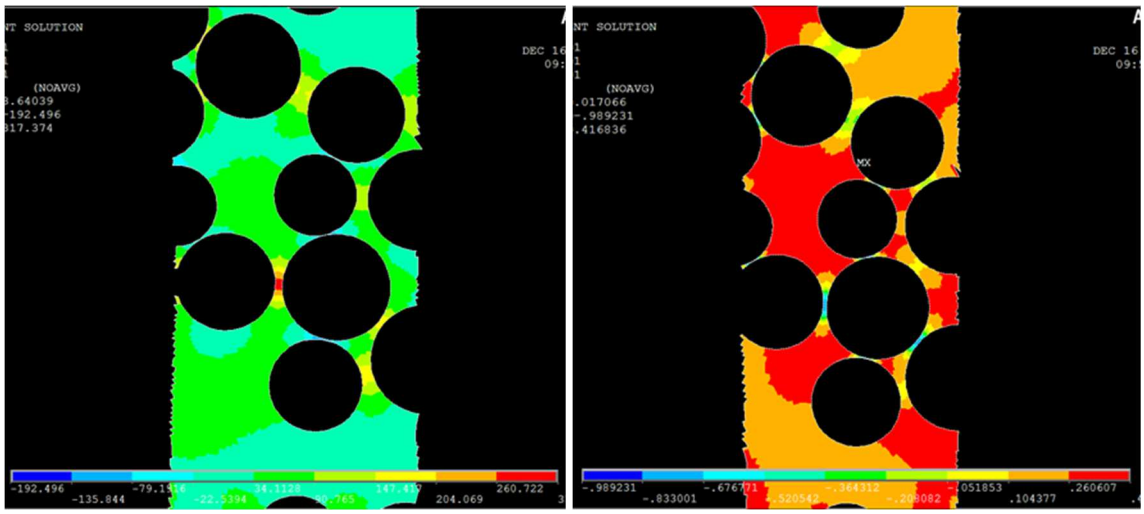

Figure B.8 – Example of hydrostatic stress in the matrix under (a) pure transverse strain of 1%, and (b) temperature gradient of -1 K.

This trend holds up to a temperature gradient of -50 K. Up to this point, the locations in which the first damages occur are the ones that are most critical under pure transverse strain, although shielded by ΔT. For larger temperature gradients, the regions where the first damages take place shift towards the ones that are most critical under pure ΔT. Therefore, an increase in ΔT (in absolute value) will lead to a shift of the whole curve of *locally debonded fibres* towards smaller strains (Figure B.7b).

It can be observed that for sufficiently high temperature gradients it is possible to have local damages, and even the formation of a full crack, as soon as a unidirectional ply cools down from manufacturing.

One more thing to note is that the trend of *locally debonded fibres* against the transverse strain tends not to show a clear change in slope at high strains in the presence of small temperature gradients, suggesting that the validity of a percolation threshold in such conditions should be verified.

B4. Influence of fibre volume fraction and fibre material

In addition to a temperature gradient, other factors that deeply influence the local stresses in the matrix are the fibre volume fraction V_f and the fibre material.

In Figure B.9, the *locally debonded fibres* against the transverse strain are shown for a glass/epoxy system and a carbon/epoxy system having V_f of 0.45, 0.55 and 0.65, both without cooling down and with ΔT = -60 K. The material properties used in the FE analyses of carbon fibres are taken from Ref. [13] and reported in Table B.2.

As already noticed in the paragraph B2, smaller fibre volume fractions lead to a later damage evolution. This could be expected since the highest stress concentrations occur where fibres are close to each other, and smaller fibre volume fraction imply a smaller number of fibres, hence smaller probability of having higher local criticality.

When glass fibres are replaced by carbon fibres, damage is found to occur later. This can be attributed to a smaller modulus mismatch between fibre and matrix in the plane perpendicular to the fibres direction, which generates smaller stress concentrations in the matrix. In the same plane, also the difference between coefficients of thermal expansions is smaller with carbon fibres.

Finally, the influence of both fibre type and fibre volume fraction appears to be qualitatively similar in the absence and presence of a temperature gradient.

Table B.2 – Material properties used for carbon fibres in the FE analyses.

E_{11} (GPa)	E_{22} (GPa)	E_{33} (GPa)	ν_{12}	ν_{23}	ν_{31}	G_{12} (GPa)	G_{23} (GPa)	G_{13} (GPa)	CTE_{11} ($\cdot 10^{-6}$)	CTE_{22} ($\cdot 10^{-6}$)	CTE_{33} ($\cdot 10^{-6}$)
28	28	235	0.33	0.02	0.28	7.2	24	24	10	10	-0.1

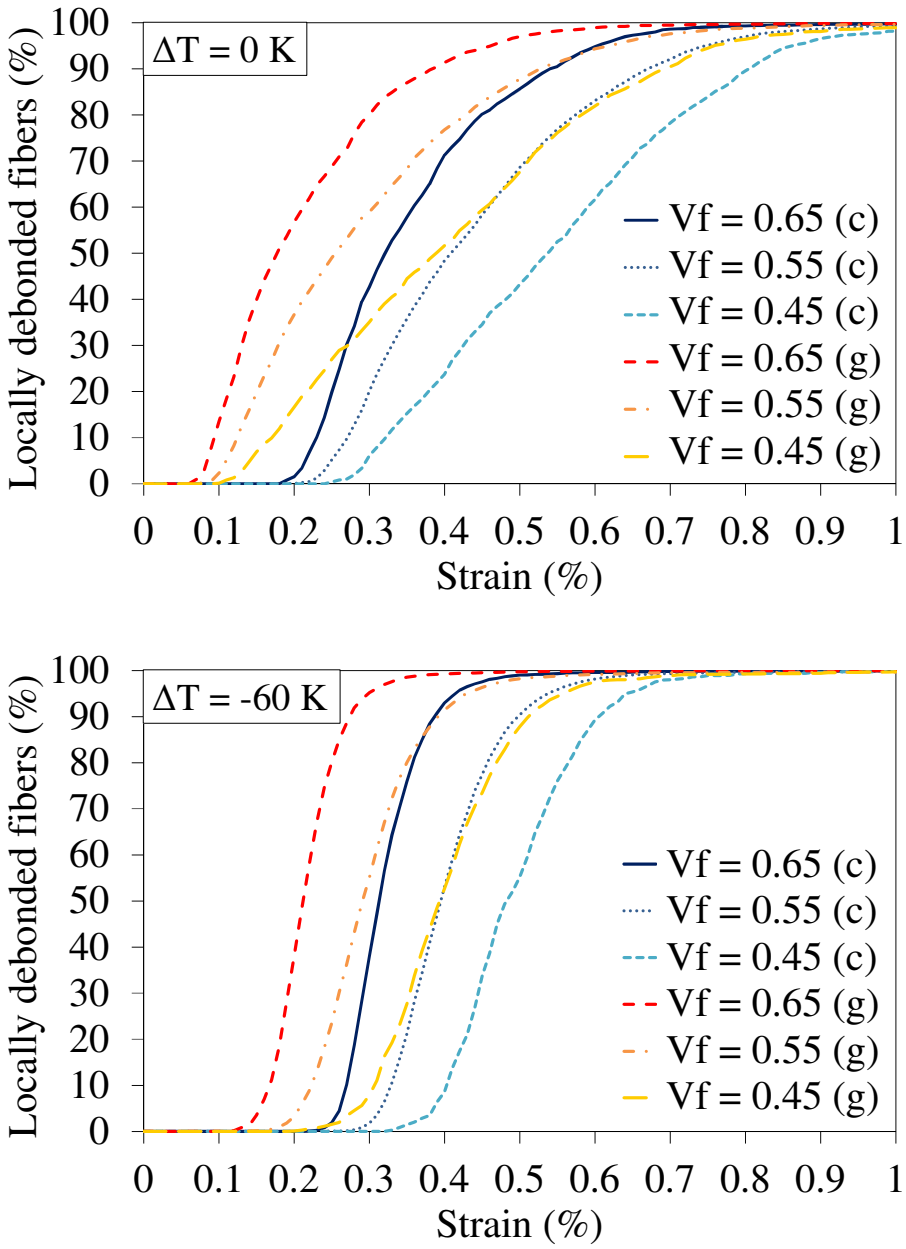

Figure B.9 – Influence of fibre volume fraction and fibre type (c=carbon, g=glass) on the trend of *locally debonded fibres* against transverse strain.

As observed in the previous paragraphs, low fibre volume fractions and temperature gradients may lead to an unclear identification of a percolation threshold from the trend of *locally debonded fibres*. In addition to this, is possible that for small values of fibre volume fraction other damage mechanisms take place, and also the damage propagation in matrix-

rich regions could play an important role in the crack formation process. Hence, care should be taken in the application of the present model for such material and process conditions.

B5. Conclusions

In the present Appendix, a novel concept was developed to predict the transverse strain to crack initiation in unidirectional composite plies. The proposed model assumes that a crack forms through the initiation of independent local damages in the form of fibre-matrix debonding, driven by the dilatational energy density in the matrix calculated via Finite Element analyses on RVEs. The trend of locally debonded fibres against the transverse strain allowed the identification of a *percolation threshold* in correspondence of a change in the slope (~85% of *locally debonded fibres*). A transverse crack is proposed to initiate at the strain that reaches such a threshold, obtaining good agreement with experimental data for different fibre volume fractions.

The influence of cooling down, fibre volume fraction and fibre type on the crack formation process was analysed. The effect of a temperature gradient was observed to have a complex influence on the trend of locally debonded fibres due to the different influence of on the local stresses in the matrix compared to a condition of pure transverse strain.

Lower stress concentrations take place in the matrix for smaller fibre volume fractions and smaller mismatch between elastic properties of matrix and fibres. Therefore, larger strains to crack initiation were predicted.

Lastly, in the presence of low fibre volume fraction and small temperature gradient, a percolation could not be clearly identified from the trend of *locally debonded fibres* against the applied strain, other damage mechanisms could take place, and the damage propagation phase along the thickness could play an important role in the crack formation. Hence, care should be taken when applying the proposed model in such conditions.

Although the present model was developed for static loadings, the same percolation concept could be transferred to predict fatigue crack initiation, as a potential alternative to the model developed in Chapter 6 based on the local stresses in a process zone of the matrix.

References of Appendix B

[1] Hashin Z. Failure criteria for unidirectional fiber composites. Journal of Applied Mechanics 1980; 47: 329-34.

[2] Tsai SW. Strength characteristics of composite materials. NASA CR-224, 1965.

[3] Tsai SW, Wu EM. A general theory of strength for anisotropic materials. Journal of Composite Materials 1971; 5: 58-80.

[4] Puck A, Schurmann H. Failure analysis of FRP laminates by means of physically based phenomenological models. Composites Science and Technology 1998; 58: 1045-67.

[5] Canal LP, Gonzalez C, Segurado J, Llorca J. Intraply fracture of fibre-reinforced composites: Microscopic mechanicms and modelling. Composites Science and Technology 2012; 72: 1223-32.

[6] Vajari DA, Gonzalez C, Llorca J, Legarth BN. A numerical study of the influence of microvoids in the transverse mechanical response of unidirectional composites. Composites Science and Technology 2014; 97: 46-54.

[7] Herraez M, Mora D, Naya F, Lopes CS, Gonzalez C, Llorca J. ransverse cracking of cross-pliy laminates: A computational micromechanics perspective. Composites Science and Technology 2015; 110: 196-204.

[8] Han G, Guan Z, Li Z, Zhang M, Bian T, Du Shanyi. Multi-scale modeling and damage analysis of composite with thermal residual stress. Applied Composite Materials 2015; 22: 289-305.

[9] Asp LE, Berglund LA, Talreja R. Prediction of matrix initiated transverse failure in polymer composites, Compos Sci Technol 1996;56:1089-1097.

[10] París F, Correa E, Cañas J. Micromechanical view of failure of the matrix in fibrous composite materials. Composites Science and Technology 2003; 63: 1041-1052.

[11] Asp LE, Berglund LA, Gudmundson P. Effects of composite-like stress state on the fracture of epoxies. Composites Science and Technology 1995; 53: 27-37.

[12] De Kok JMM, Meijer HEH. Deformation, yield and fracture of unidirectional composites in transverse loading: 1. Influence of fibre volume fraction and test-temperature. Composites Part A – Applied Science and Manufacturing 1999; 30: 905-916.

[13] Hojo M, Mizuno M, Hobbiebrunken T, Adachi T, Tanaka M, Ha SK. Effect of fiber array irregularities on microscopic interfacial normal stress states of transversely loaded UD-CFRP from viewpoint of failure initiation. Composites Science and Technology 2009; 29: 1726-1734.

Concluding remarks

The use of composite materials for load-bearing structures experienced an extremely rapid growth since the 1950s, thanks to their appealing combination of high mechanical properties and low weight, and to the possibility to tailor the material for specific parts by a suitable fibre orientation.

In spite of their currently wide employment, the diffusion of such materials is still limited due to their high cost, that can be attributed to the manufacturing process (labour-intensive and with elevated price of raw materials), and also to the current lack of general and reliable design criteria and guidelines, in particular under fatigue loadings, that forces companies in expensive and time-consuming experimental campaigns.

Both these aspects are influenced by the presence of manufacturing-induced defects. Such defects cause a premature damage initiation and evolution, and to keep their content as low as possible costly process conditions are used. The most common manufacturing-induced defect in composite laminate is the presence of porosity, that is also the most difficult to avoid due to the materials and processes involved.

The objective of the present work was to quantitatively study the influence of porosity on the fatigue behaviour of composite materials, with the aim to draw advanced design procedures and to move a step closer to a *cost-effective* production of composite parts.

As a first step, a specimen was designed and carefully prepared to observe fatigue damage evolution in off-axis plies at the micro-scale prior to the formation of a visible crack. Multiple micro-cracks were observed in the inter-fibre regions, inclined with respect to the fibre direction. A visible crack was seen to form by the coalescence of such micro-cracks, and its propagation in the fibre direction involved the initiation and coalescence of micro-cracks ahead of its tip. These first-of-their-kind observations provide a strong support to a damage-based model proposed by Carraro and Quaresimin to predict fatigue crack

initiation in unidirectional plies, as the direction of the micro-cracks was found to be in good agreement with the orientation of the plane perpendicular to the calculated *Local Maximum Principal Stress* in the matrix.

To understand if the same damage-based criterion could be applied in the presence of porosity, specimens with the same configuration but containing voids were prepared and tested under fatigue. Before the formation of a visible crack, micro-cracks in the inter-fibre regions were observed also in this case, mainly ahead of void tips and above voids that lied beneath the observed surface, both regions being characterized by the highest stress concentrations. The inclination of the micro-cracks was found again to be in good agreement with the direction of the Local Maximum Principal Stress, but the number of regions showing micro-cracks was much higher compared to the void-free scenario, resulting in an earlier visible crack formation. These findings indicate that the same damage-based criterion may be applied in absence and presence of voids, provided that the influence of voids on the local stress state is suitably accounted for.

Given the earlier damage formation observed in the presence of porosity, an experimental campaign was carried out to extensively quantify the effect of voids on the fatigue performances of composite materials. Two series of glass/epoxy laminates were produced by VARTM, changing process parameters to explore possible ways to reduce the manufacturing costs, obtaining both void-free and porous laminates (characterized by the void area fraction A_v). Two stacking sequences were adopted, namely $[0/90_2]_S$ and $[0/45_2/0/-45_2]_S$, characterized by a damage driven in the off-axis plies by the *Local Hydrostatic Stress* and the *Local Maximum Principal Stress*, respectively. A large detrimental effect of voids was found on the fatigue performances of both lay-ups. In $[0/90_2]_S$ specimens with $A_v = 0.34\%$, the life to crack initiation was reduced by 80% and the crack growth rate increased by 75% compared to the void-free condition. In $[0/45_2/0/-$

$45_2]_S$ specimens with A_v = 1.07%, the reduction in life to crack initiation was of 65% and the increase in crack growth rate of 60%. In $[0/90_2]_S$ laminates, voids were homogeneously distributed and the crack density evolution, and therefore also the stiffness drop, was much faster in porous specimens. In $[0/45_2/0/-45_2]_S$ laminates instead, voids were rather aggregated at regular intervals, and they influenced the crack density evolution and stiffness drop only in the first stages.

The experimental results highlighted the need of properly accounting for the presence of voids in the design of a composite part. In particular, a model should be developed capable of including the effect of void content, size and distribution on the local stresses in the matrix, that are responsible for the formation of fatigue cracks. As a first step in this direction, a tool was developed to build Representative Volume Elements (RVEs) of a unidirectional composite lamina. The procedure is based on altering an initially regular fibre distribution, and was validated against real microstructures in terms of morphology and stress distributions. In particular, the distribution of the *Local Hydrostatic Stress* and the *Local Maximum Principal Stress* in the matrix were analysed.

Once a tool to calculate the local stresses in the matrix was available, a model was proposed to predict fatigue crack initiation in porous unidirectional plies, by suitably extending Carraro and Quaresimin's criterion to account for the actual microstructure and the presence of voids. In particular, the *Local Hydrostatic Stress* and the *Local Maximum Principal Stress* in a process zone of the matrix, calculated by means of Finite Element analyses on RVEs and referred to as LHS* and LMPS*, were proposed as driving forces to fatigue crack formation. The procedure to generate RVEs was then slightly modified to include homogeneously distributed *cigar-like* voids. The S-N curves for void-free and porous laminates fall into the same scatter band when plotted in terms of the proposed driving forces for both $[0/90_2]_S$ and $[0/45_2/0/-45_2]_S$ stacking sequences, suggesting that the

life to first cracks initiation in the presence of voids can be estimated with reasonably good accuracy from the behaviour of the void-free material. The criterion could potentially be applied also to other void distributions and shape once they have been properly included in a RVE.

The proposed model can be useful for components where no damage is allowed. However, in many cases the design of a composite parts is stiffness-driven, meaning that a certain amount of cracks can be tolerated. To proceed along this line, a procedure was developed to predict crack density evolution in multidirectional laminates subjected to fatigue loadings, capable also to include the presence of voids. The procedure is based on Monte Carlo simulations, in which the composite part is divided in small elements and a fatigue strength is assigned to each of them based on an experimental statistical distribution. As the number of cycles increases, new cracks initiate where elements fail and previously initiated cracks propagate. Both for the initiation and propagation phases, the stress redistribution caused by the presence of already initiated cracks is accounted for. The predictions of crack density evolution of the proposed procedure are in good agreement with the experimental data for cross-ply and multidirectional void-free specimens. By suitably modifying the fatigue strength distribution based on the proposed driving forces to fatigue crack initiation (LHS* or LMPS*) calculated in absence and presence of voids, the crack density of porous specimens could also be predicted with reasonable accuracy from the behaviour of the void-free material.

The experimental data and the models developed in this work can provide useful tools for the advanced design of composite parts where porosity has to be tolerated, and move a step forward in the definition of guidelines for *cost-effective* manufacturing processes.

List of publications

(a) INTERNATIONAL JOURNALS

[1] Quaresimin M, Carraro PA, Maragoni L. Influence of the load ratio on the biaxial fatigue behavior and damage evolution in glass/epoxy tubes under tension-torsion loading. Composites Part A – Applied Science and Manufacturing 2015; 78: 294-302;

[2] Carraro PA, Maragoni L, Quaresimin M. Influence of manufacturing-induced defects on damage initiation and propagation in carbon/epoxy NCF laminates. Advanced Manufacturing: Polymer and Composite Science 2015; 1; 44-53;

[3] Quaresimin M, Carraro PA, Maragoni L. Early stage damage in off-axis plies under fatigue loading. Composite Science and Technology 2016; 128, 147-154;

[4] Maragoni L, Carraro PA, Quaresimin M. Effect of voids on the crack formation in $[45/-45/0]_S$ laminate under cyclic axial tension. Composites Part A – Applied Science and Manufacturing 2016; doi: http://dx.doi.org/10.1016/j.compositesa.2016.02.018;

[5] Maragoni L, Carraro PA, Peron M, Quaresimin M. Fatigue behaviour of glass/epoxy laminates in the presence of voids. International Journal of Fatigue 2017; 95: 18-28;

[6] Maragoni L, Carraro PA, Quaresimin M. Development, validation and analysis of representative volume elements for unidirectional composites. To appear;

[7] Maragoni L, Carraro PA, Quaresimin M. Prediction of life to crack initiation in unidirectional plies containing voids. To appear;

[8] .Carraro PA, Maragoni L, Qauresimin M. Prediction of crack density evolution in multidirectional laminates under fatigeu loading. To appear.

(b) INTERNATIONAL CONFERENCES

[9] Carraro PA, Maragoni L, Quaresimin M. Influence of the stress ratio on the multiaxial fatigue behaviour of glass/epoxy tubes. In: Proceedings of ECCM15, the 15th European Conference on Composite Materials, Venice, Italy, 24-28 June, 2012;

[10] Carraro PA, Maragoni L, Quaresimin M. A tool for the simulation of fatigue damage evolution in multidirectional laminates. In: Proceedings of ECCM 16, the 16th European Conference on Composite Materials, Seville, Spain, 22-26 June 2014;

[11] Maragoni L, P. A. Carraro, Quaresimin M. Fatigue behaviour of composite laminates in the presence of micro-sized voids. In: Proceedings of ICCM 20, the 20th International Conference on Composite Materials, Copenhagen, Denmark, 19-24 July 2015;

[12] Carraro PA, Quaresimin M, Maragoni L. Influence of manufacturing-induced defects on intra- and inter-laminar properties of carbon/epoxy NCF laminates. In: Proceedings of ICCM 20, the 20th International Conference on Composite Materials, Copenhagen, Denmark, 19-24 July 2015;

[13] Quaresimin M, Maragoni L, Carraro PA. Microscopic damage evolution in off-axis plies under fatigue loading. In: Proceedings of ICCM 20, the 20th International Conference on Composite Materials, Copenhagen, Denmark, 19-24 July 2015;

[14] Quaresmin M, Carraro PA, Maragoni L. Micro-scale damage initiation and evolution in off-axis plies under fatigue loading. In: Proceedings of CompTest 2015, the 7th International Conference on Composite Testing and Model Identification, Madrid, Spain, 8-10 April 2015;

[15] Maragoni L, Carraro PA, Quaresimin M. Influence of Micro-voids on the fatigue behaviour of glass/epoxy laminates. In: Proceedings of ECCM 17, the 17th

European Conference on Composite Materials, Munich, Germany, 26-30 June 2016.

(c) NATIONAL CONFERENCES

[16] Maragoni L, Carraro PA, Dallavia A, Quaresimin M. Influence of manufacturing-induced voids on the mechanical properties of carbon/epoxy laminates. In: Proceedings of the 43rd AIAS National Conference, Rimini, Italy, 9-12 September 2014;

[17] Maragoni L, Carraro PA. Influenza della porosità sul comportamento a fatica di alminati in composito vero/epossidica. In: Proceedings of the 44th AIAS National Conference, Messina, Italy, 2-5 September 2015;

[18] Quaresimin M, Carraro PA, Maragoni L. Evoluzione del danno su scala microscopica in laminate in composito. In: Proceedings of the 44th AIAS National Conference, Messina, Italy, 2-5 September 2015;

[19] Maragoni L, Carraro PA, Quaresimin M. Effetto di micro-vuoti sul comportamento a fatica di laminati multidirezionali in vetro/epossidica. In: Proceedings of the 45th AIAS National Conference, Trieste, Italy, 7-10 September 2016.